Solid-state N.M.R. studies of platinum and tin compounds

Patrick William Reams

SOLID-STATE N.M.R. STUDIES OF PLATINUM AND TIN COMPOUNDS

by

Patrick William Reams, B.Sc.(Hons.)

(Collingwood College)

A thesis submitted

for the Degree of Doctor of Philosophy

to the University of Durham

1986

To my Parents

MEMORANDUM

The work reported in this thesis was carried out in the Chemistry Laboratories of the University of East Anglia between September 1982 and August 1984 and the University of Durham between September 1984 and September 1985. This work has not been submitted for any other degree and is the original work of the author except where acknowledged by references.

Partsof this work have been the subject of the following publications:

1. High-resolution Solid-state ^{31}P N.M.R. Spectrum of $Pt(PPh_3)_2(P(mesityl)C=Ph_2)$
   H.W. Kroto, S.I. Klein, Mohamed F. Meidine, J.F. Nixon, R.K. Harris, K.J. Packer and P.Reams,
   J.Organomet.Chem., 1985 (280), 281.
2. High-resolution Tin-119 N.M.R. of solid trimethyltin hydroxide,
   R.K. Harris, K.J. Packer and P. Reams,
   J.Mag.Res., 1985 (61, 564.
3. High-resolution Tin-119 N.M.R. of solid tributyltin fluoride,
   R.K. Harris, K.J. Packer and P. Reams,
   Chem.Phys.Letts., 1985 (115), 16.
4. Aspects of High-resolution multinuclear magnetic resonance of solid organometallic compounds,
   R.K.Harris, K.J. Packer and P. Reams,
   J.Mol.Struct., 1986 (141), 13.
5. High-resolution Solid-state platinum-195 nuclear magnetic resonance,
   R.K.Harris, K.J.Packer and P. Reams,
   J.Chem.Soc., Dalton Trans., 1986, 1015.

Aspects of this work were presented as a lecture, given by the author, at the Royal Society of Chemistry, Seventh International Meeting of N.M.R. Spectroscopy, entitled:

"Solid-state N.M.R. Studies of Platinum and Tin Compounds"
University of Cambridge, July 1985.

ACKNOWLEDGEMENTS

I am indebted to many people and would like to express my thanks to:

Professors Robin K. Harris and Ken J. Packer for their guidance, interest and enthusiasm throughout the period of my research.

The NMR groups at the Universities of East Anglia and Durham for providing stimulating (or at least amusing) conversations, especially Steven, Pete, Alan and Andy (UEA); also Larry, Phil and Pete (Durham), without forgetting the brilliant minds of Ian (what does it all mean?) and Geoff (Multisports).

I would also like to thank Prof. Terry Mitchell (University of Dortmund) for interesting discussions concerning ^{119}Sn NMR, Helen Davis (Queen Mary College) for the X-ray crystal structure determination, Dr. John F. Nixon for providing the phosphaalkene sample and Mrs. Marion Wilson for her patience in typing this manuscript.

I gratefully acknowledge financial support from SERC and Johnson Matthey and Dr. Chris Barnard (JMRC) for providing the platinum compounds and for many useful discussions.

I thank the following for their perennial encouragement during the writing of this thesis:

Debbie, Nick, Dale, Alan, Wendy and, of course, my family.

Finally, I am very grateful to Felix Bloch and Edward Purcell, without whom none of this work would have been possible.

SOLID-STATE N.M.R. STUDIES OF PLATINUM AND TIN COMPOUNDS

by

PATRICK WILLIAM REAMS

ABSTRACT

High-resolution solid-state N.M.R. studies of dilute spins are now possible using cross-polarisation and MAS techniques. A systematic evaluation has been undertaken to determine their applicability to spin-½ metal nuclei, in particular ^{195}Pt and ^{119}Sn. In addition, an extensive ^{13}C and ^{31}P solid-state N.M.R. study has been carried out on a selection of Pt(II) complexes, supplying information on isotropic (scalar) coupling constants and shielding anisotropy. The majority of ^{119}Sn and ^{195}Pt spectra exhibit a multitude of spinning sidebands due to the large shielding anisotropy present. The tin systems under study have been of type R_3SnX (where R = Alkyl, phenyl and X = F, OH, Cl); some are shown to be polymeric in the solid-state with penta-coordinate tin present. Where possible, correlations with X-ray crystallographic data and solution-state N.M.R. studies are given. The interactions present in Pt(IV) compounds containing directly bonded quadrupolar nuclei have been studied and imply motional activity present in the solid-state. A more comprehensive study of these effects is given for two tin systems (Ph_3SnCl and $(NH_4)_2SnCl_6$), whereby observed splittings can be accounted for by a combination of ^{119}Sn-Cl dipolar and scalar coupling. The interplay of tensor properties between spin-½ nuclei, namely (i) dipolar coupling, (ii) indirect (scalar) coupling and (iii) shielding anisotropy is explored in solid-state ^{195}Pt-^{31}P and ^{119}Sn-^{19}F systems. The theory for such tensorial interplay is given for an AX_2 system.

SYMBOLS AND ABBREVIATIONS

These lists contain the symbols and abbreviations most frequently used in this work. Some specialized notations are defined in the relevant chapter.

Symbols

B_o Static magnetic field (components, B_x, B_y, B_x)

B_1 rf magnetic, associated with ν_1 (components (B_{1x}, B_{1y}, B_{1z})

D Dipolar coupling constant $(\frac{\mu_o}{4\pi}.\gamma_1\gamma_2(\frac{\hbar}{2\pi})r^{-3})$

D^C Nuclear receptivity relative to that of carbon-13

$\mathfrak{D}$ Wigner rotation matrix

$\hat{\mathcal{H}}$ Hamiltonian operator (in energy units), subscripts indicate the nature of the operator.

$\hat{I}_j$ Nuclear spin operator for nucleus; (components $\hat{I}_{jx}$, $\hat{I}_{jy}$, $\hat{I}_{jz}$)

$\hat{I}_{j+}$, $\hat{I}_{j-}$ 'Raising' and 'lowering' spin operators for nucleus;

I_j Nuclear spin quantum number associated with $\hat{I}_j$

$^nJ_{AX}$ Nuclear spin-spin coupling constant through n bonds (in Hz) between nuclei A and X.

m_j eigenvalue of $\hat{I}_{jz}$ (Nuclear spin component quantum No.)

m_T total magnetic quantum No. for a spin system (eigenvalue of $\Sigma_j\hat{I}_{jz}$)

M_o equilibrium macroscopic magnetization of a spin system in the presence of B_o

M_n moment of spectrum (M_2 = second moment, *etc.*)

N Total number of nuclei of a given type in the sample

S (i) Signal Height
(ii) Nuclear spin quantum number/type of nucleus.

T_1 Spin-lattice relaxation time

T_2 Spin-Spin relaxation time

$T_{1\rho}$ Spin-lattice relaxation time in the rotating frame

T_{IS} Cross-relaxation time between I and S spins

T_X Spin temperature of nucleus X.

α/β Nuclear spin wave functions (eigenfunction of $\hat{I}_z$) for spin $+\frac{1}{2}/-\frac{1}{2}$ states respectively

γ_X magnetogyric ratio of nucleus X

δ Chemical shielding anisotropy ($\delta=\sigma_{33}-\sigma_{iso}$)

δ_X Chemical shift of nucleus of element X, in ppm

$\Delta\nu_{HH}$ homogeneous proton line width.

Δ Static linewidth

$\Delta\nu$ Full width (in Hz) of a resonance line at half-height

$\Delta\sigma$ Shielding anisotropy $(\Delta\sigma=\sigma_{//} - \sigma_{\perp})$

η_o Asymmetry in shielding

μ_o permeability of a vacuum

ν_c carrier frequency of radiation

ν_j Larmor precession frequency of nucleus j (in Hz)

ν_L (i) frequency of local field
(ii) Larmor frequency (general)

ν_Q quadrupole resonance frequency

$\nu_{r/R}$ Rotation speed (Hz)

ρ spherical tensor component in PAS

σ_j shielding constant of nucleus j

σ_{jj} principal component of shielding tensor

τ_c correlation time

χ nuclear quadrupole coupling constant $(=e^2q\ Q/h)$

ω (general) As for ν terms but in rad s^{-1}

ABBREVIATIONS

acac	acetyl acetonato
AI	absolute intensity mode
COD	1,5-cyclooctadiene
CP	cross-polarisation
efg	electric field gradient
en	ethylenediamine
FID	Free Induction Decay
FT	Fourier transform
HPD	High-power decoupling
MAS	Magic-Angle spinning
NMR	Nuclear magnetic resonance
NQR	Nuclear quadrupole resonance
NQS	Non-quaternary suppression
PAS	Principal Axis system
PCTFE	Poly(chlorotrifluoroethylene)
ppm	parts per million
rf	radiofrequency
S/N	Signal to Noise ratio
SSB	Spinning sideband
SP	Single pulse only
TMS	Tetramethylsilane

CONTENTS

Page No.

CHAPTER ONE

INTRODUCTION

Solution-state N.M.R. has long established itself as one of the most powerful and informative analytical tools for the elucidation of structure and dynamics in chemistry.[1] The advent of superconducting magnets along with powerful computer hardware and software[2] is forever increasing the high resolution capabilities of N.M.R., with even the scarcest of nuclei becoming accessible.[3] However, the use of N.M.R. is not limited to the solution-state. Low resolution N.M.R. of the solid-state has been achievable for a considerable number of years, albeit applied to the abundant nuclei (*i.e.* ^{1}H, ^{19}F and ^{31}P). The major problem encountered when studying solids is the broadening factor caused by interactions usually averaged by rapid motional fluctuations in solutions. In order to obtain sharp N.M.R. lines for solids, where the motions are more constrained, this kind of averaging must be brought about artificially by specific line-narrowing techniques. The successful application of magic-angle spinning[4] (MAS) and high-power decoupling[5] (HPD) has led to the availability of "high-resolution" solid-state N.M.R. The other major advance is cross-polarization (CP), which increases the sensitivity for dilute spin systems and can considerably reduce the recycle time between pulses.[2] Schaefer and Stejskal[6] were the first to report on utilizing the combination of CP/HPD/MAS to obtain high-resolution solid-state N.M.R. spectra of a dilute spin system (^{13}C). Although the above suite of techniques has been used to obtain high-resolution solid-state spectra for a decade, it has mainly been applied to ^{13}C, ^{29}Si

and ^{31}P nuclei.[7] However, the potential of solid-state N.M.R. to probe the structures of inorganic and organometallic systems *via* metal spin-½ nuclei is vast. To date, there has been only two previous publications of high resolution ^{119}Sn and ^{195}Pt N.M.R.,[8] which is surprising given the wealth of information available from solid-state studies. As well as being invaluable for compounds which are insoluble, or whose chemical structures are altered by dissolution, solid-state spectra have the advantage over those in solution in that they yield information on the anisotropy of N.M.R. parameters (particularly the shielding tensor). Correlations with single-crystal X-ray data are useful, but in cases of compounds which are amorphous or otherwise unsuitable for X-ray work, solid-state N.M.R. can still provide structural and even some crystallographic information. It is the above advantages of studying spin-½ metal nuclei (along with the more abundant ^{13}C and ^{31}P nuclei) that form the basis for this work.

REFERENCES - Chapter One

1. R.K. Harris, 'Nuclear Magnetic Resonance', Pittman, London, 1983, J.A.Pople, W.G. Schneider, H.J. Bernstein, 'High-Resolution Nuclear Magnetic Resonance', McGraw-Hill, New York, 1959.

2. E. Fukushima and S.B.W. Roeder, 'Experimental Pulse NMR: A Nuts and Bolts Approach', Addison-Wesley Publishing Co., 1981, T.C. Farrar and E.D. Becker, 'Pulse and Fourier Transform NMR', Academic Press, New York, 1971.

3. 'NMR and the Periodic Table', Eds. R.K. Harris and B.E. Mann, Academic Press, New York, 1978.

4. E.R. Andrew, Prog.NMR.Spectrosc., 1971 (8), 1.

5. A. Pines, M.G. Gibby and J.S. Waugh, J.Chem.Phys., 1973, (59), 569.

6. J. Schaefer and E.O. Stejskal, J.Am.Chem.Soc., 1976, (98), 1031.

7. C.A. Fyfe, 'Solid-State NMR for Chemist', CFC.Press, 1984.

8. E.T. Lippmaa, M.A. Alla, T.J. Pehk and G. Engelhardt, J.Am.Chem.Soc., 1978, (100), 1929.
D.M. Doddrell, P.F. Barron, D.E. Clegg and C. Bowie, J.C.S.Chem.Comm., 1982, 57.

CHAPTER TWO

THEORY

2.1 Introduction

This chapter contains a brief résumé of general theory which is applicable to solution and solid-state NMR. The main differences between the two forms of NMR are covered, with particular attention paid to the broadening mechanisms in solid-state NMR. The main interactions for spin-½ nuclei are dealt with by use of Hamiltonian expressions, derived using spherical tensor calculus. The theory initially covers both axial and non-axial shielding AX systems and is then extended for the AX_2 system. Crystallographic effects and factors governing linewidths are also discussed.

2.2 General Theory

The basic theory of NMR has been outlined in many books and reviews. All nuclei with odd atomic mass or odd atomic number possess spin angular momentum (SAM). The magnitude of the nuclear SAM(P) is given by

$$P = \hbar[I(I+1)]^{\frac{1}{2}}$$

where I is the nuclear spin quantum number. Nuclei with $I \geqslant 1$ possess electric quadrupole moments as a result of a non-spherical distribution of charge. These nuclei can interact with electric field gradients in the environments causing efficient relaxation.[1]

The nuclear magnetic moment $\underline{\mu}$, arising from the motion (spinning) of a charged particle is usually expressed in terms of the magnetogyric ratio, γ, such that

$$\underline{\mu} = \gamma \underline{P}$$

The values of nuclear magnetic dipole moments, and magnetogyric ratios for selected nuclei (relevant to this work) are given in Table 2.1.

TABLE 2.1 NMR PROPERTIES OF SELECTED NUCLEI[a]

ISOTOPE	SPIN	NATURAL ABUNDANCE %	MAGNETIC MOMENT (μ/μ_n)	MAGNETOGYRIC RATIO $\gamma/10^7 radT^{-1}s^{-1}$	QUADRUPOLE MOMENT $10^{28}Q/m^2$	RELATIVE RECEPTIVITY[c] D^P
^{1}H	1/2	99.985	4.837	26.752	-	1.000
^{13}C	1/2	1.108	1.217	6.728	-	1.76×10^{-4}
^{14}N	1	99.63	0.571	1.934	1×10^{-2}	1.00×10^{-3}
^{19}F	1/2	100	4.553	25.181	-	0.834
^{23}Na	3/2	100	2.863	7.080	0.10	9.27×10^{-2}
^{31}P	1/2	100	1.960	10.841	-	0.0665
^{35}Cl[d]	3/2	75.53	1.061	2.624	-0.10	3.56×10^{-3}
^{39}K[d]	3/2	93.1	0.505	1.250	4.9×10^{12}	4.75×10^{-4}
^{79}Br[d]	3/2	50.54	2.718	6.723	0.37	4.01×10^{-2}
^{119}Sn[d]	1/2	8.58	-1.812	-10.021	-	4.51×10^{-3}
^{195}Pt	1/2	33.8	1.043	5.768	-	3.39×10^{-3}

(a) Reference 2.

(b) Nuclear magneton, $\mu_n = eh/4\pi M_p$ (M_p = mass of a proton)

(c) Relative receptivity (to ^{1}H) = $\left|\frac{\gamma_X^3}{\gamma_P^3}\right| \frac{N_X I_X (I_X+1)}{N_P I_P (I_P+1)}$

(d) Most abundant isotope selected.

2.3 Solid-State NMR

There are a number of contributions to NMR spectra, including Zeeman, dipolar, electron shielding, scalar coupling and quadrupole interactions whose relative importance depends on the nucleus under study. The critical feature

of the latter four interactions is that they are anisotropic (*i.e.* orientation dependent) and thereby produce major differences between the appearance of solid and solution-state NMR spectra. The cause of this primary difference between these interactions affecting solids and those in solution is the motional averaging of orientation dependence in isotropically tumbling molecules of the solution-state. In solids, where such motion is generally inhibited, anisotropic interactions are at most incompletely averaged, and the width of the lines tends to be much greater (several kHz). Furthermore, sensitivity in these spectra is severely reduced by such large linewidths and by the long spin-lattice relaxation times.

The most common and often dominant interaction present in solids is the magnetic dipole-dipole coupling. This interaction involves the direct coupling of magnetic moments through their magnetic fields. Nuclear electric quadrupole coupling, for nuclei $I>1$, involves the coupling of the electric quadrupole moment, arising from an ellipsoidal charge distribution, with the electric field gradient component of local electromagnetic fields. Two forms of spectroscopy are available for observing a quadrupole nucleus, NMR or NQR, depending on the relative magnitude of the Zeeman and quadrupolar energy terms. Magnetic shielding, which produces chemical shifts, is caused by the screening of the nucleus from the applied B_o by surrounding electrons. The resonance frequency of a nucleus in a non-cubic site of a molecule depends on the orientation of the molecule relative

to B_o. In general, it is found that three independent numbers are required to specify the magnitude in three molecule-fixed directions, although relative to the laboratory frame three more numbers are required to specify the orientation. Scalar or 'J' coupling is indirect and is transmitted *via* the electrons in the system. As with the dipolar coupling, J coupling also contains an anisotropic term causing orientation dependence.

In solutions, the anisotropic interactions are averaged by rapid, molecular tumbling (although in solution-state NMR of quadrupolar nuclei averaging may not be enough to completely reduce broadening)[2] which leaves only isotropic contributions (*i.e.* chemical shift and J coupling constant). However, in solids no such averaging takes place and for powdered samples all possible orientations are equally probable giving a large spread of frequencies (see Table 2.2).

TABLE 2.2 APPROXIMATE SIZE OF NMR INTERACTIONS FOR SOLIDS AND LIQUIDS (in Hz)

	Solids	Liquids
Zeeman	$10^6 - 10^9$	$10^6 - 10^9$
Dipolar	$0 - 5\times10^4$	0
Chemical shift	$0 - 10^6$	$0 - 10^6$
J coupling	$0 - 4\times10^4$	$0 - 4\times10^4$
Quadrupolar	$0 - 10^9$	$0^{(a)}$

(a) In principle, but linewidth can be as large as tens of kHz.[2]

2.4 The nuclear Spin Hamiltonian

The nuclear spin Hamiltonian consists of a number of terms that represent the interactions of a nucleus with a magnetic moment. For a spin-½ nucleus the general Hamilton ($\hat{\mathcal{H}}_T$) can be expressed in the following way: (in angular frequency terms).

	TERM	DESCRIPTION OF INTERACTION
$\hat{\mathcal{H}}_T$ =	$\hat{\mathcal{H}}_Z$	Zeeman interaction with the magnetic field.
+	$\hat{\mathcal{H}}_{RF}$	Interaction with Radio-frequency magnetic fields.
+	$\hat{\mathcal{H}}_S$	Magnetic shielding of nucleus by surrounding electrons.
+	$\hat{\mathcal{H}}_D$	Direct dipole-dipole interactions with other nuclei.
+	$\hat{\mathcal{H}}_J$	Indirect spin-spin coupling to other nuclei.
+	$\hat{\mathcal{H}}_Q$	Quadrupolar interaction with electric field gradients.

The first two terms, $\hat{\mathcal{H}}_Z$ and $\hat{\mathcal{H}}_{RF}$, may be called external Hamiltonians because they depend, apart from specific nuclear properties (γ_n^i), on external parameters, (B_Z, $B_1(t)$, $B_2(t)$ *etc.*) which can be experimentally controlled. The remaining terms supply information of chemical interest and are independent of experimental conditions and can thus be called internal Hamiltonians.

Each of the Hamiltonian terms, given in Table 2.2, represents a Cartesian tensor linking two vectors (eqn. 2.1).

$$\hbar^{-1}\hat{\mathcal{H}} = \underline{I}.\underline{\underline{R}}.\underline{Y} = (I_x, I_y, I_z) \begin{pmatrix} R_{xx} & R_{xy} & R_{xz} \\ R_{yx} & R_{yy} & R_{yz} \\ R_{zx} & R_{zy} & R_{zz} \end{pmatrix} \begin{pmatrix} Y_x \\ Y_y \\ Y_z \end{pmatrix} \quad (2.1)$$

where $\underline{I}$ and $\underline{Y}$ are row and column vectors respectively and $\underline{\underline{R}}$ is a 2nd rank Cartesian tensor (3x3 matrix).

The product written in full is -

$$I_x R_{xx} Y_x + I_x R_{xy} Y_y + \ldots\ldots I_y R_{yz} Y_z + I_z R_{zz} Y_z \qquad (2.2)$$

or $$\sum_{\alpha,\beta} I_\alpha R_{\alpha\beta} Y_\beta \quad (\alpha,\beta = x,y,z) \qquad (2.3)$$

2.4.1 External Hamiltonian

The external Hamiltonian ($\hat{\mathcal{H}}ext$) is the sum of the Zeeman and Radio-frequency terms (eqn. 2.4)

$$\hat{\mathcal{H}}ext = \hat{\mathcal{H}}_Z + \hat{\mathcal{H}}_{RF} \qquad (2.4)$$

where $$\hbar^{-1}\hat{\mathcal{H}}_Z = \underline{I}.\underline{\underline{Z}}.\underline{B}_o \qquad (2.5)$$

where $$B_o = (B_x, B_y, B_z) \text{ and } \underline{\underline{Z}} = -\gamma^j \underline{\underline{1}} \qquad (2.6$$

(γ^i is the magnetogyric ratio for the i^{th} nucleus)

with the unit matrix $$\underline{\underline{1}} = \begin{pmatrix} 1 & 0 & 0 \\ 0 & 1 & 0 \\ 0 & 0 & 1 \end{pmatrix} \qquad (2.7)$$

The z direction in the laboratory frame is chosen to be parallel to the static applied field (B_o), *i.e.* $B_o = (0,0,B_z)$. Therefore, it can be shown by matrix multiplication that only the term $I_z B_z$ is non-zero.

Hence, $$\hbar^{-1}\hat{\mathcal{H}}_Z = -\sum_j \gamma^j I_z B_z = -\sum_j \omega_o^j I_z^j \qquad (2.8)$$

The radio-frequency Hamiltonian ($\hat{\mathcal{H}}_{RF}$) may be expressed similarly as

$$\hbar^{-1}\hat{\mathcal{H}}_{RF} = \underline{I}.\underline{\underline{Z}}.\underline{B}_1 \qquad (2.9)$$

where $$B_1(t) = 2(B_{1x}(t), B_{1y}(t), B_{1z}(t)) \cos \omega t. \qquad (2.10)$$

The rf field is usually applied perpendicular to the static field and is chosen to be parallel to the x axis. Therefore, eqn. (2.9) becomes -

$$\hbar^{-1}\hat{H}_{RF} = -2\, B_{1x}(t)\, \cos \omega t \sum_j \gamma^j\, I_x^j \qquad (2.11)$$

In the type of NMR experiment carried out in this work the rf Hamiltonian does not directly affect the NMR spectrum and so will not be considered further.

2.4.2 The Internal Hamiltonians

The internal Hamiltonians all have a common structure and can be given by eqn. (2.12)

$$\hbar^{-1}\hat{H}_\lambda = k^\lambda \underline{I}\, \underline{\underline{R}}^\lambda\, \underline{Y}^\lambda \qquad (2.12)$$

where k^λ is a scalar constant, $\underline{I}$ is a vector representing a nuclear spin, $\underline{\underline{R}}^\lambda$ is the tensor of the interaction and $\underline{Y}^\lambda$ is another vector property, which can be another nuclear spin vector (λ=J,D) or the external magnetic field (λ=S). The values for k, $\underline{\underline{R}}$ and $\underline{Y}$ for each interaction (λ) are listed in Table 2. . The quadrupolar term $\hat{H}_Q$ has been excluded as only spin-½ nuclei are directly studied in this work.

TABLE 2.3

HAMILTONIAN TERM

$\hbar^{-1}\hat{H}_\lambda$	k_λ	$\underline{\underline{R}}^\lambda$	$\underline{Y}^\lambda$	Units of $\underline{\underline{R}}$
$\hbar^{-1}\hat{H}_S$	γ_i	$\underline{\underline{\sigma}}$	$\underline{B}_o$	None
$\hbar^{-1}\hat{H}_D$	$(\frac{\mu_o}{4\pi})\gamma^i\gamma^k\hbar r^{-3}$	$\underline{\underline{D}}$	$\underline{I}^k$	None
$\hbar^{-1}\hat{H}_J$	2π	$\underline{\underline{J}}$	$\underline{I}^k$	Hz

Equation (2.12) may be expressed as a sum (*c.f.*eqn. 2.3)

$$\hbar^{-1}\hat{H}_\lambda = k^\lambda \sum_{\alpha,\beta} I_\alpha R^\lambda_{\alpha\beta} Y^\lambda_\beta = k^\lambda \sum_{\alpha\beta} R^\lambda_{\alpha\beta} T^\lambda_{\beta\alpha} \qquad (2.13)$$

where $T^\lambda_{\beta\alpha}$ is the dyadic product of the vectors I_α and Y^λ_β.

All $\underline{\underline{R}}^\lambda$ are tensors of rank two, orientation dependent and can be represented by a (3x3) matrix of nine

components. All the tensors are molecular properties and are therefore best described in a molecule-fixed axis system. An axis system can be chosen for each, such that the $\underline{\underline{R}}^{\lambda}$ tensors become diagonalized. This coordinate system is called the principal axes system (PAS) - in principle different for all $\underline{\underline{R}}^{\lambda}$ - and is fixed in the molecular frame. The diagonalization of $\underline{\underline{R}}^{\lambda}$ reduces the relevant tensor to three diagonal components (eqn. 2.14).

$$\underline{\underline{R}} = \begin{bmatrix} R_{xx} & R_{xy} & R_{xz} \\ R_{yx} & R_{yy} & R_{yz} \\ R_{zx} & R_{zy} & R_{zz} \end{bmatrix} \xrightarrow[\text{(choice of appropriate coordinate system)}]{\text{'Diagonalization'}} \begin{bmatrix} R_{XX} & 0 & 0 \\ 0 & R_{YY} & 0 \\ 0 & 0 & R_{ZZ} \end{bmatrix}$$

where R_{XX}, R_{YY} and R_{ZZ} are the diagonal elements in the PAS and are called the principal components (may also be defined as R_{11}, R_{22} and R_{33} respectively).

The following conventions may be used to label the axes:

$$|R_{ZZ}-R_{iso}| \geq |R_{XX}-R_{iso}| \geq |R_{YY}-R_{iso}|^{4} \qquad (2.15)$$

or $$R_{XX} > R_{YY} > R_{ZZ}.^{5} \qquad (2.16)$$

The former convention, chosen by Haeberlen,[4] will be used in this work. It is often convenient to use three alternative parameters instead of $R_{\alpha\alpha}$ one of which is the isotropic value of R given by

$$R_{iso} = \frac{1}{3} \text{Tr } \underline{\underline{R}} = \frac{1}{3} (R_{XX} + R_{YY} + R_{ZZ}) \qquad (2.17)$$

The other two, the anisotropy (δ) and the asymmetry (η), are defined by

$$\delta = R_{ZZ} - R_{iso} = \{2R_{ZZ} - (R_{YY} + R_{XX})\}/3 \qquad (2.18)$$

$$\eta = \frac{R_{YY} - R_{XX}}{R_{ZZ} - \frac{1}{3}\ \mathrm{Tr}\underset{\sim}{R}} = \frac{R_{YY} - R_{XX}}{\delta} \qquad (2.19)$$

The asymmetry (η) has a value between 0 and 1. If η=0, the tensor $\underset{\sim}{R}$ is axially symmetric, where $R_{XX}=R_{YY}=R_{\perp}$ and $R_{ZZ} = R_{//}$. Using the new parameters R_{iso}, δ and η, the $\underset{\sim}{R}^{\lambda}$ tensor can be expressed as

$$\underset{\sim}{R}(PAS) = \begin{bmatrix} R_{XX} & & \\ & R_{YY} & \\ & & R_{ZZ} \end{bmatrix} = R_{iso}\underset{\sim}{1} + \delta \begin{bmatrix} -\frac{1}{2}(1+\eta) & & \\ & -\frac{1}{2}(1-\eta) & \\ & & 1 \end{bmatrix} \qquad (2.20)$$

2.4.3 Rotations of the Internal Hamiltonians

A tensor is defined by its transformation properties under changes of a coordinate system. When dealing with NMR interactions these changes are rotations. The dyadic product $T^{\lambda}_{\beta\alpha}$ (eqn.2.13) is derived from the vectors I_{α} and Y^{λ}_{β}, and so is expressed in the laboratory frame; therefore $R^{\lambda}_{\alpha\beta}$ must also be expressed in this frame of reference. This is carried out by a transformation of $\underset{\sim}{R}$ by rotation of PAS Frame into the Laboratory frame. This can be achieved by using direction cosines, *e.g.* $R'_{jk} = \sum_{\alpha,\beta} C_{\alpha j}C_{\beta k}R_{\alpha\beta}$ (2.21)

where $R_{\alpha\beta}$ are tensor components in axes x,y,z

and R'_{jk} are tensor components in axes x′,y′,z′

However, it is more convenient to express the tensors in a spherical basis, when rotations are involved.[6] The Cartesian tensor of second rank ($\underset{\sim}{R}$) is in a reducible form and the nine components $R_{\alpha\beta}(\alpha,\beta=x,y,z)$ can be readily reduced to form a scalar ($R^{(o)}$)

$$R^{(o)} = (\frac{1}{3}\ \mathrm{Tr}\underset{\sim}{R})\ \underset{\sim}{1} = R\underset{\sim}{1} \qquad (2.22)$$

which has one component, an antisymmetric tensor ($R^{(1)}$)

$$R^{(1)} = (\underline{\underline{R}} - \underline{\underline{R}}^{*})/2, \text{ (where } R^{*} \text{ is the transpose of } \underline{\underline{R}}) \tag{2.23}$$

having three components and a symmetric tensor $R^{(2)}$ which has five components.

$$R^{(2)} = (\underline{\underline{R}} + \underline{\underline{R}}^{*})/2 - R\underline{\underline{1}} \tag{2.24}$$

This leads to a sum of three irreducible tensors:

$$\underline{\underline{R}} = R^{(o)} + R^{(1)} + R^{(2)} \tag{2.25}$$

The components of the three quantities $R^{(o)}$, $R^{(1)}$ and $R^{(2)}$ transform in the same way as the spherical harmonics of order zero, one and two respectively. $R^{(l)}$ (l=0,1 and 2) can therefore be expressed as spherical tensors of the type $R_{l,m}$ where l is the rank and $m(=-l,-l+1, \ldots, l)$ is the component.[6] The equivalent of eqn.(2.13) can be expressed in irreducible spherical tensor terms[6] as

$$\hbar^{-1}\hat{H}_{\lambda} = k^{\lambda}\sum_{l}\sum_{m=-l}(-1)^{m} R^{\lambda}_{l,-m} T^{\lambda}_{lm} \tag{2.26}$$

where the $R^{\lambda}_{l,-m}$ derive from the $R^{\lambda}_{\alpha,\beta}$ and T^{λ}_{lm} from the $T^{\lambda}_{\alpha\beta}$. The three NMR tensors $\underline{\underline{R}}^{\lambda}$ (λ=D,J,S) can contain, in principle, the three constituents $R^{(o)}$, $R^{(1)}$ and $R^{(2)}$. However, only the isotropic and traceless symmetric parts are readily measurable by spectroscopic techniques.[4] [Note: the Dipolar tensor, $\underline{\underline{D}}$, is traceless and symmetric by its very nature]. The anti-symmetric constituents ($R^{(1)}$) may usually therefore be ignored, and so all $\underline{\underline{R}}^{\lambda}$ may be treated as symmetric tensors. For a symmetric 2nd rank Cartesian tensor $R^{\lambda}_{\alpha\beta}$, only R^{λ}_{lm} with l=0,2 will be non-zero. The general Hamiltonian can therefore be re-defined as

$$\hbar^{-1}\hat{H}_{\lambda} = k^{\lambda}[(-1)^{o}R^{\lambda}_{oo}T^{\lambda}_{oo} + \sum_{m=-2}^{2}(-1)^{m}R^{\lambda}_{2,-m}T^{\lambda}_{2m}] \tag{2.27}$$

The components of the irreducible spherical tensor operators R_{lm} in their respective PASs are denoted by $\rho_{l\ m}$ and their values are given in Table 2.4.

TABLE 2.4 RELATIONS BETWEEN SPHERICAL TENSOR COMPONENTS ρ_{lm} AND THE CARTESIAN TENSOR COMPONENTS $R_{\alpha\alpha}$ IN THE PRINCIPAL AXES SYSTEM[4]

l	m	
0	0	$\rho_{00} = {}^{1}/_{3}\ \mathrm{Tr}\ \underline{\underline{R}} = R$
2	0	$\rho_{20} = \sqrt{3}/2\ (R_{ZZ} - {}^{1}/_{3}\ \mathrm{Tr}\ R) = \sqrt{\frac{3}{2}}\ \delta$
2	1	$\rho_{2\pm1} = 0$
2	2	$\rho_{2\pm2} = (R_{YY} - R_{XX}) = \frac{1}{2}\ \eta\ \delta$

The spherical tensor components may be expressed in the laboratory frame by the use of Wigner rotation matrices $\mathfrak{D}_{m',m}\ (\alpha^{\lambda}, \beta^{\lambda}, \gamma^{\lambda})$.

$$R^{\lambda}_{lm} = \sum_{m'} \mathfrak{D}_{m'm}\ \rho^{\lambda}_{lm'} \qquad (2.28)$$

where α^{λ}, β^{λ}, γ^{λ} are the Euler angles by which the λ^{th} PAS may be aligned with the laboratory frame (see Figure 2.8).

FIGURE 2.8 Orientation of the principal axis system (X,Y,Z) with respect to the laboratory frame (B_1 is taken to be in plane perpendicular to B_o), where α, β and γ are the Euler Angles.[7]

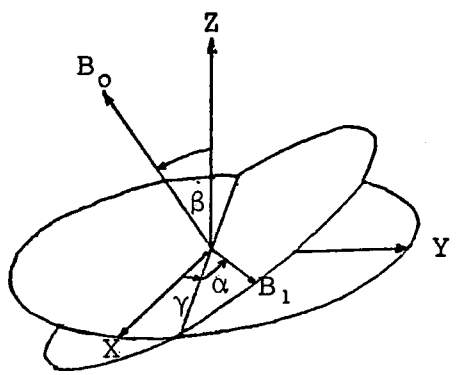

[*N.B.* - Some authors use (ψ, θ, ϕ) instead of α,β,γ]

The value of ρ_{oo} is a scalar constant (Table 2.4) and therefore transforms in the same way as a spherical harmonic of 0 (*i.e.*, a sphere), thus $\mathfrak{D}^{(o)}_{o,o}$ is a constant (unity). Therefore, the only Wigner rotation matrices required are of the type $\mathfrak{D}^{(2)}_{m',m}$ which are given in Table 2.5.

The elements of the dyadic product $T^{\lambda}_{\beta\alpha} = I_{\alpha}Y^{\lambda}_{\beta}$ form a reducible representation which can be reduced to form irreducible components in spherical coordinates $T^{\lambda}_{\ell m}$. The constituents of $T^{\lambda}_{\ell m}$ for the J, D and S interactions are given in Table 2.6.

The spin vector $\underline{I}$ has 3 components in spherical coordinates, I_m (m=1,0,-1) and can be related to the vector in Cartesian coordinates in the following way.[6]

$$\underline{I} = \begin{bmatrix} I_1 \\ I_o \\ I_{-1} \end{bmatrix}, \quad I_{\pm 1} = \frac{1}{\sqrt{2}}(I_x \pm iI_y), \quad I_o = I_z \tag{2.29}$$

As, $$I\pm = I_x \pm iI_y \tag{2.30}$$

therefore $$I_{+1} = -\frac{1}{\sqrt{2}}I_+ \quad \text{and} \quad I_{-1} = +\frac{1}{\sqrt{2}}I_- \tag{2.31}$$

The equations (2.26) - (2.31) and Tables 2.3 - 2.6 can now be used to determine the values for each internal Hamiltonian in terms of scalar constants.

TABLE 2.5 WIGNER ROTATION MATRIX $\mathcal{D}^{(2)}_{m'm}(\alpha,\beta,\gamma)$

$$\mathcal{D}^{(2)}_{m'm} = f(\beta)\ \exp\left[i(m\alpha+m'\gamma)\right]$$

$f(\beta)$	$m=2$	$m=1$	$m=0$	$m=-1$	$m=-2$
$m'=2$	$\frac{1}{4}(1+\cos\beta)^2$	$\frac{1}{2}(1+\cos\beta)\sin\beta$	$\sqrt{\frac{3}{8}}\sin^2\beta$	$\frac{1}{2}(1-\cos\beta)\sin\beta$	$\frac{1}{4}(1-\cos\beta)^2$
$m'=1$	$-\frac{1}{2}(1+\cos\beta)\sin\beta$	$\cos^2\beta-\frac{1}{2}(1-\cos\beta)$	$\sqrt{\frac{3}{8}}\sin 2\beta$	$\frac{1}{2}(1+\cos\beta)-\cos^2\beta$	$\frac{1}{2}(1-\cos\beta)\sin\beta$
$m'=0$	$\sqrt{\frac{3}{8}}\sin^2\beta$	$-\sqrt{\frac{3}{8}}\sin 2\beta$	$\frac{1}{2}(3\cos^2\beta-1)$	$\sqrt{\frac{3}{8}}\sin 2\beta$	$\sqrt{\frac{3}{8}}\sin^2\beta$
$m'=-1$	$-\frac{1}{2}(1-\cos\beta)\sin\beta$	$\frac{1}{2}(1+\cos\beta)-\cos^2\beta$	$-\sqrt{\frac{3}{8}}\sin 2\beta$	$\sqrt{\frac{3}{8}}\sin 2\beta$	$\frac{1}{2}(1+\cos\beta)\sin\beta$
$m'=-2$	$\frac{1}{4}(1-\cos\beta)^2$	$-\frac{1}{2}(1-\cos\beta)\sin\beta$	$\sqrt{\frac{3}{8}}\sin^2\beta$	$-\frac{1}{2}(1+\cos\beta)\sin\beta$	$\frac{1}{4}(1+\cos\beta)^2$

TABLE 2.6 REDUCIBLE REPRESENTATIONS OF DYADIC PRODUCTS T^{λ}_{lm}

INTERACTION (λ)	T_{00}	T_{20}	$T_{2\pm1}$	$T_{2\pm2}$
S	$I^j_o B_o$	$\sqrt{\frac{2}{3}} I^j_o$	$\frac{1}{\sqrt{2}} I^j_{\pm1} B_o$	0
$D_J\}$	$\underline{I}^j \underline{I}^k$	$\sqrt{\frac{1}{6}}(3I^j_o I^k_o - \underline{I}^j \underline{I}^k)$	$\frac{1}{\sqrt{2}}(I^j_{\pm1} I^k_o + I^j_o I^k_{\pm1})$	$I^j_{\pm1} I^k_{\pm1}$

2.5 Chemical Shielding

The chemical shift arises from the electronic shielding of the nucleus by the surrounding electrons. Since this shielding is a three-dimensional quantity, it can be represented by a 2nd rank tensor $\underline{\underline{\sigma}}$. In solutions, molecular tumbling averages the shielding to a single isotropic consant, σ_{iso}. However, in solids the chemical shift will be anisotropic in any non-cubic environment due to the orientation dependence in the magnetic field. The complete three-dimensional shielding of the nucleus may be determined, giving in principle much more information regarding structure and bonding than can be obtained in solution.

The general equation for shielding Hamiltonian may be derived from eqn. (2.12) and Table 2.1.

$$\hbar^{-1}\hat{\mathcal{H}}_s = \gamma\hat{\underline{I}}.\underline{\underline{\sigma}}.\underline{B}_o \tag{2.32}$$

where $\underline{I} = (I_x, I_y, I_z)$ and $B_o = (0, 0, B_z)$ (x,y,z refer to Lab. frame). Hence,

$$\hbar^{-1}\hat{\mathcal{H}}_s = \gamma[\sigma_{xz}\hat{I}_x B_z + \sigma_{yz}\hat{I}_y B_z + \sigma_{zz}\hat{I}_z B_z] \tag{2.33}$$

The first two terms in parenthesis are non-secular and cause negigibly small second order shifts.[4,5] The chemical shielding is then given by

$$\hbar^{-1}\hat{\mathcal{H}}_s = \gamma\sigma_{zz}\hat{I}_z B_z = \omega_o\sigma_{zz}\hat{I}_z \tag{2.34}$$

where σ_{zz} (the zz shielding component in the laboratory frame) is the observed shielding constant.

The shielding tensor σ may be diagonalized in its PAS to reduce the number of constituents to three principal components, σ_{11}, σ_{22} and σ_{33}.

$$\underline{\underline{\sigma}}_{PAS} = \begin{pmatrix} \sigma_{11} & 0 & 0 \\ 0 & \sigma_{22} & 0 \\ 0 & 0 & \sigma_{33} \end{pmatrix} \qquad (2.35)$$

where σ_{11}, σ_{22} and σ_{33} are the shielding components in the $\underline{X}\underline{X}$, $\underline{Y}\underline{Y}$, ZZ directions of the PAS respectively. The shielding anisotropy δ is given by

$$\delta = \sigma_{33} - \sigma_{iso}$$

where $\sigma_{iso} = {}^{1}/3\ (\sigma_{11} + \sigma_{22} + \sigma_{33})$. The asymmetry η may be expressed as

$$\eta = \frac{\sigma_{22} - \sigma_{11}}{\delta}$$

The use of spherical tensor calculus can yield an expression for σ_{zz} (Lab. frame) in terms of the above two PAS parameters. From eqn. (2.27) the shielding Hamiltonian may be expressed as

$$\hbar^{-1}\hat{H}_s = k^S[(-1)^0 R^S_{oo} T^S_{oo} + \sum_{m=-2}^{2} (-1)^m R^S_{2,-m} T^S_{2m}] \qquad (2.36)$$

where $R^S_{2,-m}$ is given by

$$R_{2,-m} = \sum_{m'} \mathcal{D}_{m',-m}\, \rho_{2m'}$$

Hence from Table 2.2.

$$R_{2,-m} = \mathcal{D}_{o,-m}\sqrt{\frac{3}{2}}\ \delta + (\mathcal{D}_{2,-m} + \mathcal{D}_{-2,-m})\ \tfrac{1}{2}\ \eta\ \delta \qquad (2.37)$$

It therefore follows from equations (2.36) and (2.37) that the complete shielding Hamiltonian may be expressed as

$$\hbar^{-1}\hat{\mathcal{H}}_s = k^s\Big[\frac{1}{3}\,\mathrm{Tr.}\,\underline{\underline{R}}\,T_{00}\Big] \qquad l=0,\ m=0$$

$$+\ (-1)^0\{D^{(2)}_{0,0}\sqrt{\tfrac{3}{2}}\,\delta + (D^{(2)}_{2,0}+D^{(2),}_{-2,0})\tfrac{1}{2}\,\eta\,\delta\}\,T_{20} \qquad l=2,\ m=0$$

$$+\ (-1)^{+1}\{D_{0-1}\sqrt{\tfrac{3}{2}}\,\delta + (D^{(2)}_{2,-1}+D^{(2)}_{-2,-1})\tfrac{1}{2}\,\eta\,\delta\}\,T_{2,1} \qquad l=2,\ m=+1$$

$$+\ (-1)^{-1}\{D^{(2)}_{0,1}\sqrt{\tfrac{3}{2}}\,\delta + (D^{(2)}_{2,1}+D^{(2)}_{-2,1})\tfrac{1}{2}\,\eta\,\delta\}\,T_{2,-1} \qquad l=2,\ m=-1$$

(2.38)

There are no terms $l=2$, $m=\pm2$, because the $T_{2,\pm2}$ involved are zero. Equation (2.38) may be truncated by considering only the $m=0$ terms as they are the secular terms giving rise to 1st order effects (involving I_o, see Table 2.4).

$$\hbar^{-1}\hat{\mathcal{H}}_s = k^s[\sigma_{iso}\hat{I}^j_o B_o + \delta\{\sqrt{\tfrac{3}{2}}(\tfrac{1}{2})(3\cos^2\beta-1) + \tfrac{\eta}{2}(\sqrt{\tfrac{3}{8}}\sin^2\beta)(e^{2i\gamma}+e^{-2i\gamma})\}\sqrt{\tfrac{2}{3}}\hat{I}^j_o B_o]$$

$$= \gamma[\sigma_{iso}\hat{I}^j_z B_o + \delta\{\tfrac{1}{2}(\cos^2\beta-1) + \tfrac{\eta}{4}\sin^2\beta\,(2\cos2\gamma)\}\hat{I}^j_z B_z]$$

$$\hbar^{-1}\hat{\mathcal{H}}_s = \omega_o\hat{I}^j_z\{\sigma_{iso} + \delta[\tfrac{1}{2}(3\cos^2\beta-1) + \tfrac{\eta}{2}\sin^2\beta\cos2\gamma]\} \qquad (2.39)$$

From equation (2.34) it can be seen that σ_{zz} can be given by

$$\sigma_{zz} = \sigma_{iso} + \delta[\tfrac{1}{2}(3\cos^2\beta-1) + \tfrac{\eta}{2}\sin^2\beta\cos2\gamma] \qquad (2.40)$$

Equation (2.34) may be combined with the Zeeman Hamiltonian term (eqn. 2.8). Thus, for a single spin only

$$\hbar^{-1}\hat{\mathcal{H}}_{z,s} = -\omega_o(1-\sigma_{zz})\hat{I}_z \qquad (2.41)$$

The total Zeeman and chemical shielding Hamiltonian for one spin species present is

$$\hbar^{-1}\hat{\mathcal{H}}_{z,cs} = -\omega_o[1-\sigma_{iso}-\delta\{\tfrac{1}{2}(3\cos^2\beta-1)+\tfrac{\eta}{2}\sin^2\beta\cos2\gamma\}]\hat{I}_z \qquad (2.42)$$

For a single crystal, in a fixed orientation to the magnetic field, a single sharp line will be observed for each magnetically unique orientation of the nucleus to the field direction, and the position of these lines will alter as the

orientation of the crystal is changed. For a powdered sample all orientations are equally probable and a broad line will result, the shape of which will depend on the principal elements of the shielding tensor.

The two common types of powder pattern are shown in Figure 2.9. The general case (A) has all three principal elements with different values giving rise to a non-axially symmetric shielding pattern. A second common situation is an axially symmetric environment where two of the principal elements are averaged to a single value (or are equal) and are perpendicular to the axis of symmetry and therefore designated $\sigma_{\perp}$. The remaining component is aligned in the direction of the axis of symmetry and called $\sigma_{//}$.

FIGURE 2.9

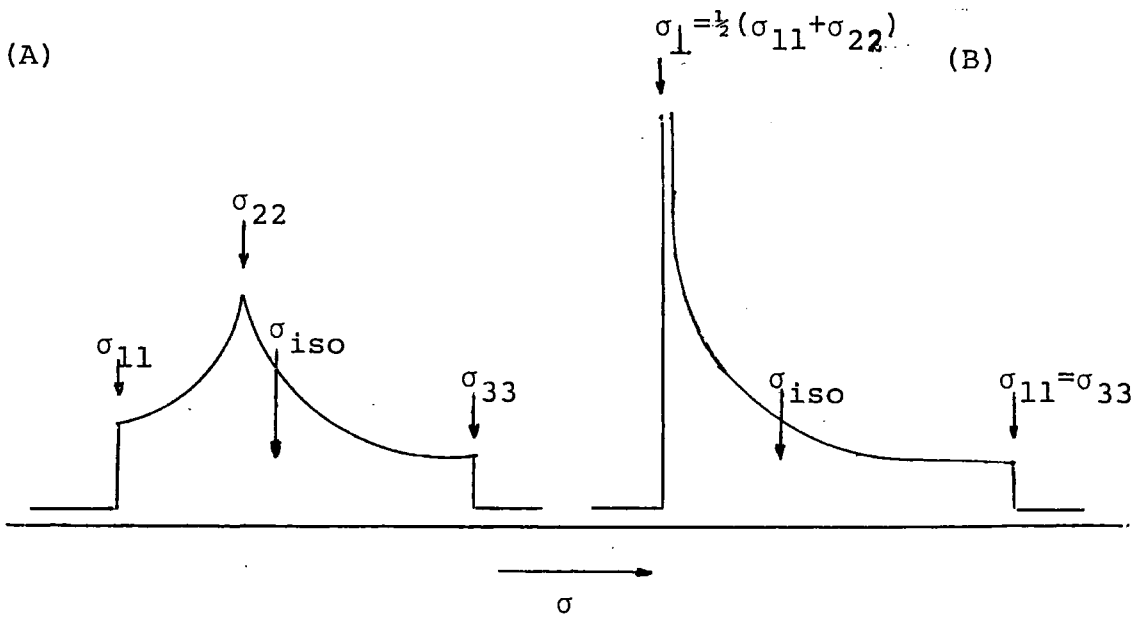

Schematic representation of theoretical powder line shapes for the chemical shift tensor. (A) Asymmetric tensor ($\eta \neq 0$), (B) Axially symmetric tensor ($\eta = 0$).

The asymmetry η is always positive and can have values $0 \rightarrow 1$; for the axially symmetric case, $\eta=0$. The sign of the anisotropy δ is given by the relationship between $\sigma_{//}$ and $\sigma_{\perp}$ where $\sigma_{//} > \sigma_{\perp}$ for a positive sense of anisotropy, or, $\sigma_{33} > \sigma_{22} \geq \sigma_{11}$.

The isotropic averages are given by

$$\sigma_{iso} = {}^{1}/_{3}(\sigma_{11} + \sigma_{22} + \sigma_{33}) \text{ for non-axial symmetry}$$

and $\sigma_{iso} = {}^{1}/_{3}(\sigma_{//} + 2\sigma_{\perp})$ for axial symmetry.

The shielding tensor components σ_{11}, σ_{22}, σ_{33} and the trace σ_{iso} have values expressed in ppm relative to a reference standard and is given by

$$\sigma_{jj} = -10^{6} \frac{(\nu_{jj} - \nu_{ref})}{\nu_{ref}} \quad \text{(ppm)} \tag{2.43}$$

where σ_{jj} is the tensor component (or σ_{iso}), ν_{ref} and ν_{jj} are the absolute frequency of the reference standard and tensor component respectively. The isotropic, absolute frequency is given by

$$\begin{aligned} \nu_{iso} &= \left|\frac{\gamma}{2\pi}\right| B_{o}(1-\sigma_{iso}) \quad \text{(In Hz)} \\ &\doteq \nu_{o}(1-\sigma_{iso}) \end{aligned} \tag{2.44}$$

For solutions and solids the isotropic chemical shift δ_{iso}/ppm is usually quoted, whereby, $\delta_{iso} = -\sigma_{iso}$ (2.45)

The principal values of the shielding tensor may be obtained from the spectra of simple polycrystalline systems (as indicated in Figure 2.9). However, it is in general not possible to relate these values to the molecular axis system without single crystal NMR data. The use of multiple-pulse techniques for line narrowing of powder spectra by removal

of dipolar interactions provides a direct way of measuring shift anisotropy patterns and parameters, although only the very abundant spin-½ nuclei (*e.g.* ^{1}H, ^{19}F, ^{31}P) are suitable candidates for this technique.[4,5]

2.6 Dipolar Coupling

The dipolar coupling between the magnetic moments of two spin-½ nuclei is entirely analogous to the classical dipolar coupling between two bar magnets. The classical interaction E between two magnetic moments $\underline{\mu}_1$ and $\underline{\mu}_2$ is given by

$$E = \left[\frac{\underline{\mu}_1 \underline{\mu}_2}{r^3} - 3\frac{(\underline{\mu}_1 \cdot \underline{r}_{12})(\underline{\mu}_2 \cdot \underline{r}_{12})}{r^5} \right] \frac{\mu_o}{4\pi} \qquad (2.46)$$

where r_{12} is the radius vector from μ_1 to μ_2 and r is the distance between the moments. The quantum mechanical version of eqn.(2.46) is obtained by substituting

$$\hat{\underline{\mu}} = \gamma \hat{\underline{I}} \hbar \qquad (2.47)$$

which yields the dipolar interaction Hamiltonian

$$\hbar^{-1}\hat{H}_D = \frac{\mu_o}{4\pi} \frac{\gamma_1 \gamma_2}{r^3} \cdot \hbar \left\{ \hat{\underline{I}}_1 \cdot \hat{\underline{I}}_2 - 3\frac{(\hat{\underline{I}}_1 \cdot \underline{r}_{12})(\hat{\underline{I}}_2 \cdot \underline{r}_{12})}{r_{12}^2} \right\} \qquad (2.48)$$

By expanding the various scalar products $\hat{\underline{I}}_1 \cdot \hat{\underline{I}}_2$, $\hat{\underline{I}}_1 \cdot \underline{r}_{12}$ and $\underline{I}_2 \cdot \underline{r}_{12}$, eqn.(2.48) may be rewritten in matrix form as

$$\hbar^{-1}\hat{H}_D = \left(\frac{\mu_o}{4\pi} \gamma_1 \gamma_2 \hbar\right) [\hat{I}_{1x}, \hat{I}_{1y}, \hat{I}_{1z}] \begin{bmatrix} (r^2-3x^2)/r^5 & -3xy/r^5 & -3xz/r^5 \\ -3xy/r^5 & (r^2-3y^2)/r^5 & -3yz/r^5 \\ -3xz/r^5 & -3yz/r^5 & (r^2-3z^2)/r^5 \end{bmatrix} \begin{bmatrix} \hat{I}_{2x} \\ \hat{I}_{2y} \\ \hat{I}_{2z} \end{bmatrix} \qquad (2.49)$$

which can be expressed in an abbreviated form

$$\hbar^{-1}\hat{H}_D = (\frac{\mu_o}{4\pi}\ \gamma_1\gamma_2\hbar)\ \hat{\underline{I}}_1 \cdot \underline{\underline{D}} \cdot \hat{\underline{I}}_2 \qquad (2.50)$$

where $\underline{\underline{D}}$ is the dipolar coupling tensor. If the orientation of the x,y,z axes with respect to r in the laboratory frame is chosen, as shown in Figure 2.10, then $\underline{\underline{D}}$ is clearly not diagonal. However, a coordinate system may be chosen so that the direction of internuclear axis is also the z axis, thereby diagonalising the symmetric $\underline{\underline{D}}$ tensor.

FIGURE 2.10 Orientation of dipolar vector in laboratory frame

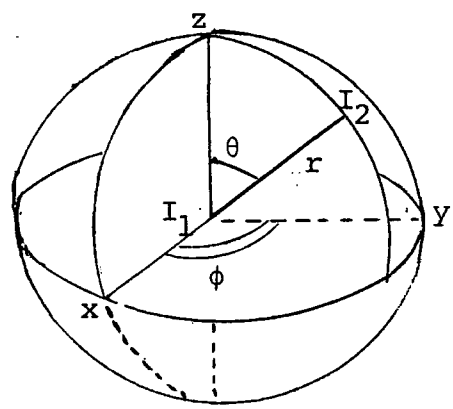

If $\underline{r}$ points along the z axis then x=y=xz=xy=zx=0 and r=z. Therefore, equation 2.49 becomes

$$\hbar^{-1}\hat{H}_D = (\frac{\mu_o}{4\pi}\gamma_1\gamma_2\hbar)\,[\hat{I}_{1x},\hat{I}_{1y},\hat{I}_{1z}] \begin{bmatrix} 1/r^3 & 0 & 0 \\ 0 & 1/r^3 & 0 \\ 0 & 0 & -2/r^3 \end{bmatrix} \begin{bmatrix} \hat{I}_{2x} \\ \hat{I}_{2y} \\ \hat{I}_{2z} \end{bmatrix} \qquad (2.51)$$

which can be abbreviated as

$$\hbar^{-1}H_D = (2\pi)D\ \hat{\underline{I}}_1 \cdot \underline{\underline{D}} \cdot \hat{\underline{I}}_2 \qquad (2.52)$$

where $D = (\frac{\mu_o}{4\pi})\frac{\gamma_1\gamma_2\hbar}{r^3(2\pi)}$ (in Hz) and $\underline{\underline{D}} = \begin{pmatrix} 1 & 0 & 0 \\ 0 & 1 & 0 \\ 0 & 0 & -2 \end{pmatrix}$ which is the dipolar tensor in the principal axis frame. The anisotropy of $\underline{\underline{D}}$ is $\delta = -2$, and the asymmetry, $\eta = 0$. Equation (2.52) may be expressed in the laboratory frame by the use of spherical tensors.

$$\hbar^{-1}\hat{H}_D = k^D[(-1)^0 R^D_{00}\, T^D_{00} + \sum_{m=-2}^{2} (-1)^m\, R^D_{2,-m} T^D_{2m}] \qquad (2.53)$$

where $R^D_{2,-m} = \mathfrak{D}_{0,-m}\sqrt{3}/2\ \delta$ (as $\eta=0$), and $R^D_{00} = 1/3\ \mathrm{Tr}\ \underline{\underline{D}} = 0$

Therefore, $\hbar\hat{H}_D = k\sqrt{3}/2\ \delta \left[\sum_{m=-2}^{2} (-1)^m\, T^{(2)}_m\ \mathfrak{D}_{0,-m} \right]$ (2.54)

Using Tables 2.3 and 2.4, equation (2.54) is given in this expanded form as

$$\begin{aligned}\hbar^{-1}\hat{H}_D = k^D\sqrt{3}/2\ \delta\Big[&(-1)^0 \tfrac{1}{\sqrt{6}}(3I^j_0I^k_0 - \underline{I}^j.\underline{I}^k)\tfrac{1}{2}(3\cos^2\beta - 1) \\ &+ (-1)^1 \tfrac{1}{\sqrt{2}}\,(I^j_{+1}I^k_0 + I^j_0I^k_{+1})\sqrt{3}/8\ \sin 2\beta\ \exp -i\alpha \\ &+ (-1)^{-1} \tfrac{1}{\sqrt{2}}\,(I^j_{-1}I^k_0 + I^j_0I^k_{-1}) - \sqrt{3}/8\ \sin 2\beta\ \exp i\alpha \\ &+ (-1)^2 (I^j_{+1}I^k_{+1})\sqrt{3}/8\ \sin^2\beta\ \exp -2i\alpha \\ &+ (-1)^{-2}\ (I^j_{-1}I^k_{-1})\sqrt{3}/8\ \sin^2\beta\ \exp 2i\alpha\ \Big] \end{aligned} \qquad (2.55)$$

By substituting $\delta = -2$ and equations (2.29→31) the dipolar Hamiltonian may be expressed in terms of a dipolar alphabet.[3]

$$\hbar^{-1}\hat{H}_D = k^D\ [A + B + C + D + E + F] \qquad (2.56)$$

where $k^D = (\frac{\mu_o}{4\pi})\frac{\gamma_1\gamma_2 h}{r^3}$. From equations (2.29)→(2.31) the scalar product $\underline{I}^j.\underline{I}^k$ is

$$\underline{I}^j.\underline{I}^k = \tfrac{1}{2}(I^j_+I^k_- + I^j_-I^k_+) + I^j_zI^k_z. \qquad (2.57)$$

The 1st terms (A+B) are then given by

$$A+B = -\sqrt{6}\frac{1}{2\sqrt{6}} [2I_z^j I_z^k + (-\tfrac{1}{2})(I_+^j I_-^k + I_-^j I_+^k)] \ (3\cos^2\beta - 1)$$

$$A = -I_z^j I_z^k \ (3\cos^2\beta - 1) \qquad (2.58)$$

$$B = {}^1/_4 (I_+^j I_-^k + I_-^j I_+^k) \ (3\cos^2\beta - 1) \qquad (2.59)$$

By simple substitution of $I_{+1} = \frac{-1}{\sqrt{2}} I_+$ and $I_{-1} = +\frac{1}{\sqrt{2}} I_-$ the remaining terms are

$$C = -\frac{3}{2} (I_+^j I_z^k + I_z^j I_+^k) \cos\beta \sin\beta \exp(-i\alpha) \qquad (2.60$$

$$D = -\frac{3}{2} (I_-^j I_z^k + I_z^j I_-^k) \cos\beta \sin\beta \exp(i\alpha) \qquad (2.61$$

$$E = -\frac{3}{4} (I_+^j I_+^k) \sin^2\beta \exp(-2i\alpha) \qquad (2.62)$$

$$F = -\frac{3}{4} (I_-^j I_-^k) \sin^2\beta \exp(2i\alpha) \qquad (2.63)$$

Note, the Euler angles α and β, used in equations (2.58 - (2.63), are equivalent respectively to the polar angles ϕ and θ of the internuclear vector $\underline{r}_{12}$ in the laboratory frame[4] (Figure 2.10).

Each of the terms A→F of the dipolar Hamiltonian affects the component nuclear spin quantum number m_I in a particular way *via* the shift operators. A causes no change, B alters both the nuclear states by ±1 simultaneously. The mixing of the basis states by $\hat{H}_D$ is shown below in a matrix representation (Table 2.7).

TABLE 2.7

SPIN STATE	/αα>	/αβ>	/βα>	/ββ>
<αα/	A	C	C	E
<αβ/	D	A	B	C
<βα/	D	B	A	C
<ββ/	F	D	D	A

The C, D, E and F terms are all off-diagonal, having non-zero integrals between non-degenerate basis states. By considering the dipolar Hamiltonian as a 1st order perturbation of the Zeeman interaction, then by 1st order perturbation theory, the C, D, E and F terms are of negligible importance. For a homonuclear two-spin system B couples degenerate basis states ($\alpha\beta$ and $\beta\alpha$) causing 'flip-flop' transitions. In order to make the B term diagonal, $/\alpha\beta>$ and $/\beta\alpha>$ can be combined into two new functions $\frac{1}{\sqrt{2}}$ $(/\alpha\beta>+/\beta\alpha>)$ and $\frac{1}{\sqrt{2}}$ $(/\alpha\beta>-/\beta\alpha>)$. However, for heteronuclear systems term B can be neglected. The theory applicable to this work concerns heteronuclear interactions, *i.e.* isolated spin systems of the AX type. For two heteronuclear spins the dipolar Hamiltonian may be truncated to include the 'A' term only, equation (2.56) becomes

$$\hbar^{-1}\hat{H}_D = \left(\frac{\mu_o}{4\pi}\right) \frac{\gamma_A\gamma_X}{r^3} \hbar \, (3\cos^2\beta-1) \, I_{Z_A} I_{Z_X} \qquad (2.64)$$

Dipolar powder patterns were first observed for a homonuclear two spin system by Pake.[9] Although the splitting observed is different, a heteronuclear powder pattern has exactly the same shape.[7] In considering theoretical powder patterns summing over all interacting spins is necessary. However, since analytical solutions to many-bonded quantum mechanical problems are virtually impossible, and the internuclear interactions are considered to decrease greatly with distance, isolated spin pairs may be treated as a reasonable approximation.

If heteronuclear dipolar coupling is considered in the absence of chemical shielding anisotropy, the total Hamiltonian

including Zeeman, dipolar and chemical shift terms becomes (observing the A nucleus only)

$$h^{-1}\hat{H}_T = -\nu_o(1-\sigma_{zz})\hat{I}_{Z_A} - D(3\cos^2\beta-1)\,\hat{I}_{Z_A}\hat{I}_{Z_X} \qquad (2.65)$$

where $D=(\frac{\mu_o}{4\pi})\,\frac{\gamma_A\gamma_X}{r_{AX}^3}\,\frac{\hbar}{2\pi}$ (in Hz) and the σ_{zz} term reduces to σ_{iso} since $\delta = \eta = 0$ in the absence of any shielding anisotropy. This Hamiltonian gives rise to four energy levels due to the possible A and X spin states.

$$\begin{aligned}
\alpha\alpha &= E(1) = -\tfrac{1}{2}\,\nu_o\,(1-\sigma_{iso}) - \tfrac{1}{4}D\,(3\cos^2\beta-1)\\
\alpha\beta &= E(2) = -\tfrac{1}{2}\,\nu_o\,(1-\sigma_{iso}) + \tfrac{1}{4}D\,(3\cos^2\beta-1)\\
\beta\alpha &= E(3) = \tfrac{1}{2}\,\nu_o\,(1-\sigma_{iso}) + \tfrac{1}{4}D\,(3\cos^2\beta-1)\\
\beta\beta &= E(4) = \tfrac{1}{2}\,\nu_o\,(1-\sigma_{iso}) - \tfrac{1}{4}D\,(3\cos^2\beta-1)
\end{aligned} \qquad (2.66)$$

Due to the selection rule $\Delta m_I = \pm 1$, transitions are allowed between these four energy levels, E(4)-E(2) and E(3)-E(1), which can be designated "minus" and "plus" respectively in accord with the X spin state which remains constant during the 'A' transitions.

$$\begin{aligned}
\nu_- &= E(4) - E(2) = \nu_o(1-\sigma_{iso}) - \tfrac{1}{2}D(3\cos^2\beta-1)\\
\nu_+ &= E(3) - E(1) = \nu_o(1-\sigma_{iso}) + \tfrac{1}{2}D(3\cos^2\beta-1)
\end{aligned} \qquad (2.67)$$

Since $\nu_o(1-\sigma_{iso}) = \nu_{iso}$, shifts from the isotropic value equal $\Delta\nu = \nu\pm-\nu_{iso}$. This then produces two equations which determine the intra dipolar lineshape for a two (AX) spin system (Figure 2.11).

$$\begin{aligned}
\Delta\nu_- &= -\tfrac{1}{2}D(3\cos^2\beta-1)\\
\Delta\nu_+ &= +\tfrac{1}{2}D(3\cos^2\beta-1)
\end{aligned} \qquad (2.68)$$

FIGURE 2.11 Schematic dipolar powder pattern for A spins of an AX system (Pake Doublet) - no shielding anisotropy present

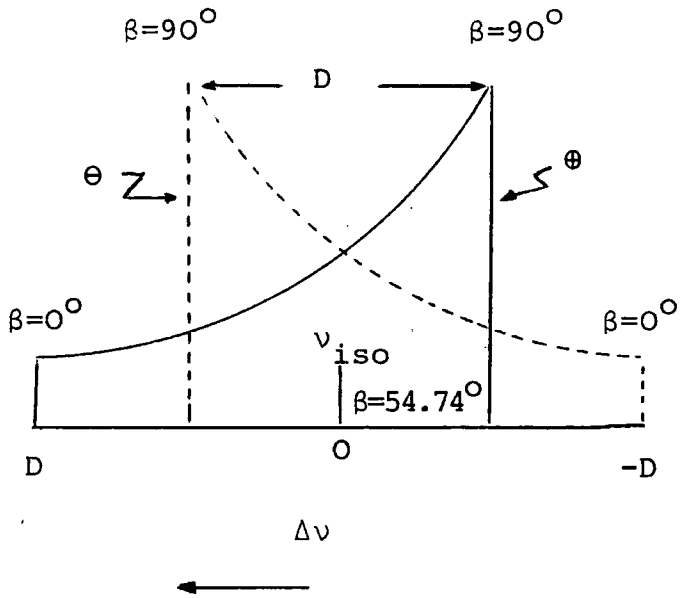

The separation between the divergences is the dipolar coupling constant D, and is a measure of the dipolar interaction strength. If this separation D can be measured from a "Pake doublet" in a static spectrum, then the internuclear distance r may be calculated.[9] As shown in Figure 2.11, the isotropic resonance ν_{iso} appears when the two nuclei in question are orientated at 54.74° to the static field B_o, this is the so-called "magic-angle".

A heteronuclear AX spin pair with shielding anisotropy present will give rise to a powder pattern of similar shape although the divergences and shoulders will appear at different frequencies. As with the dipolar-only case, there are two allowed transitions when the axially symmetric shielding term (η=0) is included:

$$\nu_+ = \nu_o\,[1-\sigma_{iso}-{}^{\delta}/_{2}(3\cos^2\beta-1)] + \tfrac{1}{2}D(3\cos^2\beta-1)$$
$$\nu_- = \nu_o\,[1-\sigma_{iso}-{}^{\delta}/_{2}(3\cos^2\beta-1)] - \tfrac{1}{2}D(3\cos^2\beta-1) \qquad (2.69)$$

The two equations for $\nu\pm$ can be expressed in terms of shifts from ν_{iso} (eqn.2.70). The combination of dipolar and shielding terms assumes that the axis of symmetry is coincident with the internuclear vector thus making β the same for both axis systems.

$$\Delta\nu_+ = (D-\nu_o\delta)\tfrac{1}{2}(3\cos^2\beta-1)$$
$$\Delta\nu_- = -(D+\nu_o\delta)\tfrac{1}{2}(3\cos^2\beta-1) \qquad (2.70)$$

FIGURE 2.12 Heteronuclear dipolar doublet with axially symmetric shielding tensor

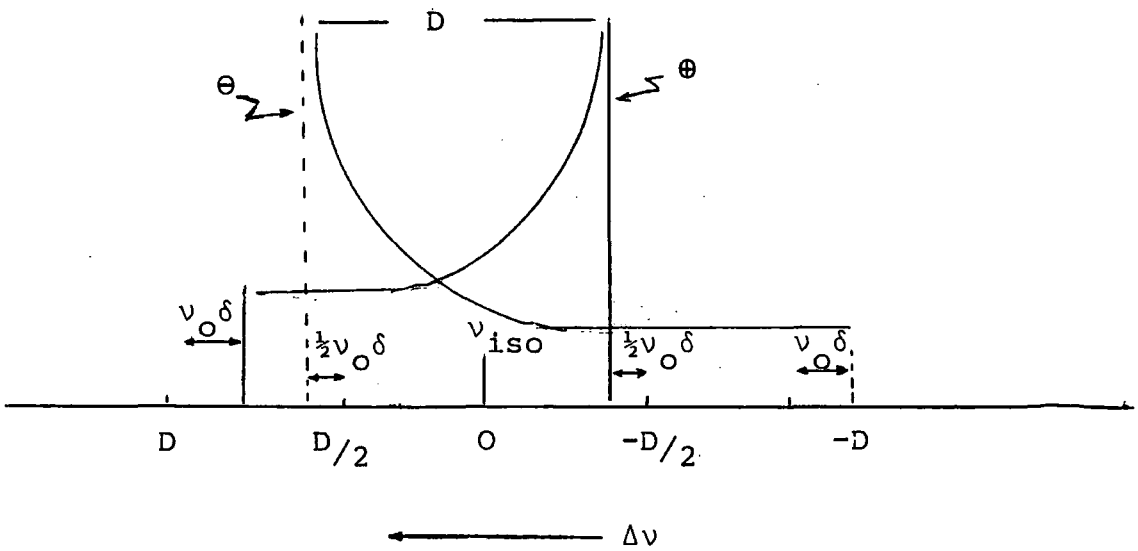

If $\nu_o\delta$ is positive, then for axial symmetry (η=0), $\sigma_{//} > \sigma_{\perp}$, since $\delta = {}^{2}/_{3}(\sigma_{//} - \sigma_{\perp})$, therefore $\Delta\nu_+$ has negative anisotropy and $\Delta\nu_-$ has positive anisotropy. As can be seen in Figure 2.12 the $\Delta\nu_+$ subspectrum is "squeezed" while that of $\Delta\nu_-$ is "stretched", relative to the lineshapes in Figure 2.11, caused by the effects of shielding anisotropy.

A combination of shielding and dipolar anisotropic interactions has been observed in the ^{31}P NMR of $BaFPO_3$[10] where axial symmetry is assumed. In such a case the shielding term may be separated from any spin-spin coupling terms by the use of 2nd moment analysis,[2,3,8] For a powder spectrum with chemical shielding and dipolar interactions present, the rigid lattice second moment is given by[10]

$$\Delta\nu^2 = \langle(\nu-\nu_o)^2\rangle = \Delta\nu_o^2 + \Delta\nu_\sigma^2$$

where the term $\Delta\nu_o^2$ represents the direct and indirect dipolar contributions; the intramolecular contribution, following Vanderhart *et al*, can be expressed as

$$\Delta\nu_o^2 = \frac{1}{5}(D')^2 + \frac{1}{4}J^2$$

where D' is the effective dipolar coupling constant (see on). The shielding contribution is given by

$$\Delta\nu_\sigma^2 = \frac{4}{5}(\sigma_{//}-\sigma_\perp)^2$$

Therefore the only term dependent on the magnetic field is $\Delta\nu_\sigma^2$, thus by plotting $\Delta\nu^2$ against ν_o^2 (from a multifield study) a linear graph may be obtained giving rise to $(\sigma_{//}-\sigma_\perp)$.

The shielding anisotropy has also been studied for solid nitrogen using ^{15}N NMR.[11] In this case homonuclear dipolar interactionsare present and the observed powder pattern consists of a Pake doublet superimposed on the chemical shift. As with the above case a multi-field study was used to obtain the shielding anisotropy except using lineshape simulation analysis. With increasing field the shape of the subspectra change with one widening and the other contracting, eventually reversing its sense with increasing applied field.

2.7 Indirect spin-spin coupling (J coupling)

In addition to the direct magnetic interaction between two nuclear spins in a molecule, the nuclei can have an effective mutual interaction as a result of the coupling between the nuclear magnetic moments and the bonding electrons. Such a coupling is indirect, unlike dipolar coupling, and is often called J coupling. The theory governing the relationship between J coupling and molecular electron distribution was derived by Ramsey,[12] and can be divided into four mechanisms[13] - (i) nuclear moments interacting with the electronic orbital motion, (ii) a dipole interaction between the magnetic moment of the nucleus and the electron spin angular momentum, (iii) interactions between the electron spins and nuclear spins in the S-orbital, as the electronic wavefunction has a finite value at the nucleus. (This is known as the Fermi contact term) and (iv) the Fermi contact - spin dipolar cross term whereby the nucleus interacts with the electron distribution by one mechanism, and the electrons to the second nucleus by the other.

As with the shielding and dipolar terms, the J coupling interaction is an anisotropic tensor quantity ($\underline{\underline{J}}$) and the Hamiltonian can be given by

$$\hbar^{-1}\hat{H}_J = 2\pi \hat{\underline{I}}_1 \cdot \underline{\underline{J}} \cdot \hat{\underline{I}}_2 \qquad (2.71)$$

The tensor $\underline{\underline{J}}$ is not necessarily symmetric and in general has nine components. However, symmetry can reduce this number. From the four coupling mechanisms,[13] the Fermi contact is purely isotropic and therefore only contributes to the scalar, isotropic value of $\underline{\underline{J}}$. The cross-contribution term is traceless

and symmetric and so therefore does not contribute to the isotropic value. The orbital and spin dipolar terms are non symmetric and contribute to all $\underline{\underline{J}}$ components.

The isotropic value of $\underline{\underline{J}}$ is given by (in the PAS)

$$J = {}^{1}/_{3}(J_{11} + J_{22} + J_{33}) \text{ for non-axial symmetry}$$
$$J = {}^{1}/_{3}(J_{//} + 2J_{\perp}) \text{ for axial symmetry} \qquad (2.72)$$

and the anisotropy δ_J and asymmetry η_J are given by[4]

$$\delta_J = J_{33} - J \qquad \eta_J = (J_{22} - J_{11})/\delta_J \text{ for non-axial symmetry} \qquad (2.73)$$

(Note, alternative definition of asymmetry parameter $\eta_J = (J_{22} - J_{11})/J_{33}$ [14,15])

$$\delta_J = \frac{2}{3}(J_{//} - J_{\perp}) = \frac{2}{3}\Delta J, \ \eta_J = 0 \text{ for axial symmetry} \qquad (2.74)$$

(ΔJ is most commonly used to describe the $\underline{\underline{J}}$ anisotropy and will be used onwards in this work).

In dealing with AX_n (1st order) spin systems, the antisymmetric terms of $\underline{\underline{J}}$ play only a small role in the determination of the A spectrum.[17] Therefore, $\underline{\underline{J}}$ may be considered to consist of a scalar and a symmetric 2nd rank tensor. The Hamiltonian expression for the J coupling can be deduced from equations (2.26)-(2.28) and Table 2.2, which gives the following:

$$
\begin{aligned}
\hbar^{-1}\hat{H}_J = k^J[&\tfrac{1}{3}\mathrm{Tr}\,\underline{J}\,T_{00} && l=0,\ m=0\\
&+(-1)^0\{\sqrt{\tfrac{3}{2}}\delta\mathfrak{D}^{(2)}_{00}+(\mathfrak{D}^{(2)}_{2,0}+\mathfrak{D}_{-2,0})\tfrac{1}{2}\eta\delta\}T_{2,0} && l=2,\ m=0\\
&+(-1)^{+1}\{\sqrt{\tfrac{3}{2}}\delta\mathfrak{D}^{(2)}_{0,-1}+(\mathfrak{D}_{2,-1}+\mathfrak{D}_{-2,-1})\tfrac{1}{2}\eta\delta\}T_{2,1} && l=2,\ m=+1\\
&+(-1)^{-1}\{\sqrt{\tfrac{3}{2}}\delta\mathfrak{D}_{0,1}+(\mathfrak{D}_{2,1}+\mathfrak{D}_{-2,1})\tfrac{1}{2}\eta\delta\}T_{2,-1} && l=2,\ m=-1\\
&+(-1)^{+2}\{\sqrt{\tfrac{3}{2}}\delta\mathfrak{D}_{0,-2}+(\mathfrak{D}_{2,-2}+\mathfrak{D}_{2,-2})\tfrac{1}{2}\eta\delta\}T_{2,2} && l=2,\ m=+2\\
&+(-1)^{-2}\{\sqrt{\tfrac{3}{2}}\delta\mathfrak{D}_{0,2}+(\mathfrak{D}_{2,2}+\mathfrak{D}_{-2,2})\tfrac{1}{2}\eta\delta\}T_{2,-2} && l=2,\ m=-2
\end{aligned}
\qquad (2.75)
$$

For a two spin system it can be assumed that J coupling is dominated by electrons which directly take part in the chemical bond between two coupled nuclei. If these electrons reside in an electron-pair sigma single bond, the J-tensor should possess axial symmetry along the internuclear axis, *i.e.* $\eta_J=0$.[15] The general expression for the J-coupling Hamiltonian (eqn.(2.75)) can be recast in the following way for an axially symmetric ($\eta_J=0$) AX spin system by substituting values from Tables 2.3 and 2.4:

$$
\begin{aligned}
\hbar^{-1}\hat{H}_J = 2\pi[&J\,\underline{I}^j\underline{I}^k\\
&+\delta_J\sqrt{\tfrac{3}{2}}\{\tfrac{1}{2}(3\cos^2\beta-1)\,\tfrac{1}{\sqrt{6}}\,[3I^j_0I^k_0-\underline{I}^j.\underline{I}^k]\\
&-(\sqrt{\tfrac{3}{8}}\sin2\beta\exp(-i\alpha)\,\tfrac{1}{\sqrt{2}}\,[I^j_{+1}I^k_0+I^j_0I^k_{+1}])\\
&-(-\sqrt{\tfrac{3}{8}}\sin2\beta\exp(i\alpha)\,\tfrac{1}{\sqrt{2}}\,[I^j_{-1}I^k_0+I^j_0I^k_{-1}])\\
&+(\sqrt{\tfrac{3}{8}}\sin^2\beta\exp(-2i\alpha)[I^j_{+1}I^k_{+1}])\\
&+(\sqrt{\tfrac{3}{8}}\sin^2\beta\exp(2i\alpha)[I^j_{-1}I^k_{-1}]\}]
\end{aligned}
\qquad (2.76)
$$

As can be seen from equation (2.76) the J coupling Hamiltonian consists of an isotropic scalar part and an

anisotropic part dependent on orientation. The latter part is identical in form to the dipolar coupling term and may be expressed similarly in terms of a J coupling alphabet:

$$\hbar^{-1}\mathcal{H}_J = 2\pi[J\ \underline{I}^i.I^k + \delta_J(A + B + C + D + E + F) \qquad (2.77)$$

where terms A→F are the same as for the dipolar case (see eqns. 2.58-2.63) except divided by a factor of -2 (which comes from the anisotropy of $\underline{D}$). For a heteronuclear AX spin system, terms B, C, D, E and F give a negligible contribution and may be ignored leaving the following expression for $\hat{\mathcal{H}}_J$;

$$\hbar^{-1}\hat{\mathcal{H}}_J = 2\pi[J\ I_z^j I_z^k + {}^{\delta_J}/_2\ (3\cos^2\beta - 1)\ I_z^j I_z^k] \qquad (2.78)$$

In solutions, only the scalar contribution is observed since the isotropic average of $\cos^2\beta_{ij}$ is $\frac{1}{3}$.[14] This scalar coupling plays a very important role in high resolution solution-state NMR experiments for molecular structure determination. On the other hand, in solids, multiplets arising from the spin-spin interaction are almost always masked by competing interactions, most notably the dipole-dipole interaction. The few reported cases involving solid-state J coupling have included ^{203}Tl and ^{205}Tl NMR studies of Thallium and Thallic oxide in which the reported linewidth is *c a.* lOX that of the theoretical dipolar width, found to be due to homonuclear J coupling.[18] The large linewidths found for the NMR spectrum of metallic silver were accounted for by the J interaction of the nuclei *via* conduction electrons.[19] Vanderhert *et al* have studied the ^{19}F and ^{31}P NMR spectra of $BaFPO_3$ which show the presence of shielding anisotropy, and direct and indirect coupling between the ^{31}P and ^{19}F nuclei.[10] The ^{19}F NMR study of $KBiF_6$ by Fukushira showed that the observed spectral pattern was due to the J coupling of the

fluorines to the quadrupolar ^{209}Bi nucleus, the dipolar interactions being reduced by the hindered rotation of the BiF_6^- ions.[20] A more recent example has dealt with ^{125}Te NMR studies of polycrystalline CdTe, HgTe and PbTe.[21] The solid-state spectra show the structure accountable to direct and indirect coupling. The two contributions were separated by the use of theoretical lineshapes and values for D, J, $J_\perp$ and $J_{//}$ are given. These experiments have tended to be successful because of the use of relatively heavy nuclei, as one of a pair or both. J-coupling is found to play a major role in the NMR of heavy isotopes due to greater electron density[18] producing large contributions from the nuclear-electron spin terms (direct magnetic moment interaction and Fermi contact terms).[12] This is found to be most notable in the latter ^{125}Te NMR experiment[21] where the dipolar coupling constant was found to be small due to small magnetogyric ratios, yet the J values were relatively large.

Further data on indirect coupling in the solid-state is available from magic-angle spinning experiments by which the shielding and dipolar interactions are averaged out.[14,22] However, this method has the disadvantage of also reducing the anisotropic contribution of the indirect spin-spin coupling. The exception to this is when the total static band width is greater than the experimental spinning speed (see Chapter Six). As J-coupling is a probe of molecular structure, knowledge of J coupling tensors will undoubtedly lead to better correlations between NMR and structure than J_{iso} has done previously.

The full Hamiltonian for a heteronuclear, axially symmetric, AX spin system (for the A spin only) can now be derived as follows: (in Hz)

from eqn.(2.42) $\hbar^{-1}\hat{H}_{Z,S} = -\nu_o[1-\sigma_{iso} - {}^{\delta}/_2\ (3\cos^2\beta-1)]\hat{I}_{z_A}$ (2.79)

from eqn.(2.64) $\hbar^{-1}\hat{H}_D = -D(3\cos^2\beta-1)\hat{I}_{z_A}\hat{I}_{z_x}$ (2.80)

from eqn.(2.78) $\hbar^{-1}\hat{H}_J = [J + {}^{\Delta J}/_3\ (3\cos^2\beta-1)]\hat{I}_{z_A}\hat{I}_{z_x}$ (2.81)

Combining all three equations gives

$$\hbar^{-1}\hat{H}_T = -\nu_o[1-\sigma_{iso}-\delta(3\cos^2\beta-1)/2]\hat{I}_{z_A} + [J-D'(3\cos^2\beta-1)]\hat{I}_{z_A}\hat{I}_{z_x} \quad (2.82)$$

where it is assumed that the symmetry axis of shielding is along the internuclear vector, $D' = D-{}^{\Delta J}/_3$ where $\Delta J=J_{//}-J_{\perp}$, $J_{//}$ being parallel to the symmetry axis and $J_{\perp}$ perpendicular to the axis. As can be seen from equation (2.82), the anisotropy in $\underset{\sim}{J}$ cannot be distinguished from $\underset{\sim}{D}$ experimentally unless the internuclear distance (r_{AX}) is known.

2.8 Non-axially symmetric AX system

In molecular systems where there are non-axially symmetric $\underset{\sim}{J}$ and $\underset{\sim}{\sigma}$ tensors present, complexities can arise in obtaining the total Hamiltonians. If the non-secular terms are ignored from equation (2.75), by substituting values from Tables 2.3 and 2.4, the J Hamiltonian for a hetero-nuclear AX system is now given by

$$\hbar^{-1}\hat{H}_J = [J+{}^{\Delta J}/_3(3\cos^2\beta-1) + {}^{\Delta J}/_3\ \eta\ \sin^2\beta\cos2\gamma]\hat{I}_{z_A}\hat{I}_{z_x} \quad (2.83)$$

The asymmetric shielding and axially symmetric dipolar terms are given by equations (2.42) and (2.64)

$$h^{-1}\hat{H}_{Z,S} = -\nu_o[1-\sigma_{iso}- {}^{\delta}/_{2}\{(3\cos^2\beta-1) + \eta\sin^2\beta\cos2\gamma\}]\hat{I}_{z_A}$$

$$h^{-1}\hat{H}_{D} = -D(3\cos^2\beta-1)\hat{I}_{z_A}\hat{I}_{z_x}$$

The total Hamiltonian for non-axial symmetry is given by the sum of the above three equations. However the three terms cannot be combined as each of the tensors involved has its own unique principal axis system.[4] Thus, much simplification can only occur on assumption of the coincidence of frames.

If the asymmetry in $\underline{J}$ is considered to be small enough to assume axial symmetry (as is the case for most two spin sigma-bonded systems[15]) then $\underline{J}$ and $\underline{D}$ tensors can be assumed to have coincident frames. The AX spectrum then depends upon the mutual orientation of the shielding and dipolar tensors (see Figure 2.13)

FIGURE 2.13 Orientation of the dipolar vector in the PAS of $\underline{\sigma}$

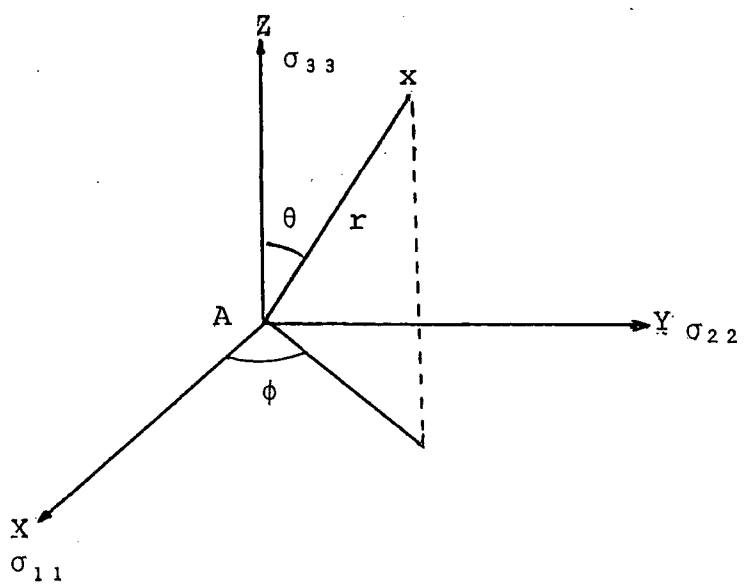

An analysis has been made by Zilm and Grant for a non-axially symmetric AX system in which one of the shielding axes is not along the dipole vector[23] although certain conditions are enforced concerning the angle θ.

Some assumptions can be made from knowledge of the molecular symmetry as to the designation of the principal shielding axes. For example, the D_{2h} molecular symmetry of ethylene is sufficient to assign the shielding axes parallel to the three C_2 rotation axes.[24] In a more general case, if both spins are contained in a reflection plane then symmetry arguments require one of the shielding tensor components to be perpendicular to the plane.[23] Since the dipolar vector is contained in this plane then it is also perpendicular to the component of $\underline{g}$. If ν_{33} is the component, and θ is the angle between the dipolar vector and ν_{33}, *i.e.* 90°, (see Figure 2.13) then the following equations of Zilm and Grant hold:

$$T_3^{\pm} = \nu_{33}^{\pm} \pm \tfrac{1}{2}D \qquad (2.84)$$

$$T_1^{\pm} = \frac{\nu_{11}^{\pm} + \nu_{22}^{\pm} \mp \tfrac{1}{2}D}{2} + \tfrac{1}{2}\alpha^{\pm} \qquad (2.85)$$

$$T_2^{\pm} = \frac{\nu_{11}^{\pm} + \nu_{22}^{\pm} \pm \tfrac{1}{2}D}{2} - \tfrac{1}{2}\alpha^{\pm} \qquad (2.86)$$

where $T_{ii}^{\pm}$ are the shoulders and divergences of the two sub-spectra, $\nu_{ii}^{\pm}$ are the principal shielding tensor components (on a resonance scale) and are defined by

$$\nu_{ii}^{\pm} = \nu_{ii} \pm \tfrac{1}{2} J_{ii} \qquad (2.87)$$

$$\alpha^{\pm} = [(\nu_{11}^{\pm} + \nu_{22}^{\pm} \mp \tfrac{1}{2}D)^2 - 4(\nu_{11}^{\pm}\nu_{22}^{\pm} - \tfrac{1}{2}D^2 \pm \nu_{11}^{\pm} \tfrac{1}{2}D(1-3\sin^2\phi)$$

$$\pm \nu_{22}^{\pm} \tfrac{1}{2}D(1-3\cos^2\phi))]^{\frac{1}{2}} \qquad (2.88)$$

(It should be noted that the designation of T^+ and T^- is the same as that used by Zilm and Grant,[24] although this is the reverse of the convention introduced previously, *i.e.*, the designation of $^+/-$ according to the sign of the X (unobserved) nucleus).

If $\underline{\underline{J}}$ is assumed to be axially symmetric ($\eta_J=0$), $J_{//}=J_{11}$, $J_{\perp}=J_{22}=J_{33}$ and $\Delta J=J_{//}-J_{\perp}$. Equations (2.84-2.86) can now be recast as follows:[25]

$$T_3^{\pm} = \nu_{33} \pm (J_{\perp}/2) \pm \tfrac{1}{2}D$$

$$= \nu_{33} \pm (J+D') \qquad (2.89)$$

where $D'=D-\Delta J/3$

$$T_1^{\pm} = [\nu_{11} + \nu_{22} \pm J_{11}/2 \pm J_{22}/2 \mp (D/2)+\alpha^{\pm}]/2$$

$$= [\nu_B \pm J \mp (D'/2) + \alpha^{\pm}]/2 \qquad (2.90)$$

$$T_2^{\pm} = [\nu_B \pm J \mp (D'/2)-\alpha^{\pm}]/2 \qquad (2.91)$$

where $\nu_B = \nu_{22} + \nu_{11}$, $\alpha^{\pm}$ may be simplified from equation (2.88) by temporarily excluding J_{ii}

$$\alpha^{\pm} = [(\nu_{11}+\nu_{22}\mp\tfrac{1}{2}D)^2 - 4(\nu_{11}\nu_{22}-\tfrac{1}{2}D^2\pm\tfrac{1}{2}\nu_{11}D(1-3\sin^2\phi)$$

$$\pm\tfrac{1}{2}\nu_{22}D(1-3\cos^2\phi))]^{\frac{1}{2}}$$

$$= [\nu_{11}^2+\nu_{22}^2+2\nu_{11}\nu_{22} \mp D\nu_{11} \mp D\nu_{22}+\tfrac{1}{4}D^2-4\nu_{11}\nu_{22}+2D^2$$

$$\mp 2\nu_{11}D(1-3\sin^2\phi) \mp 2\nu_{22}D(1-3\cos^2\phi)]^{\frac{1}{2}}$$

$$= [(\nu_{22}-\nu_{11})^2 + 9/4D^2 \mp D(\nu_{11}+\nu_{22}) \mp 2D(\nu_{22}-\nu_{11})$$

$$\mp 2D\{-3\cos^2\phi(\nu_{22}-\nu_{11})\}]^{\frac{1}{2}}$$

(If $\nu_A = \nu_{22} - \nu_{11}$),

$$\alpha^{\pm} = [\nu_A^2 + {}^9/_4D^2 \mp D(\nu_{11}+\nu_{22}) \mp 2D\{\nu_A - \tfrac{1}{2}(\nu_B - \nu_A)\} \pm 6D\nu_A\cos^2\phi]^{\frac{1}{2}}$$

$$\alpha^{\pm} = [\nu_A^2 + {}^9/_4D^2 \pm 3D\nu_A(2\cos^2\phi - 1)]^{\frac{1}{2}} \qquad (2.92)$$

Equation (2.92) can be expanded to include the indirect spin-spin coupling term as the anisotropic secular parts of $\underline{\underline{J}}$ and $\underline{\underline{D}}$ cannot be separated experimentally. Thus, only the effective dipolar coupling constant D' is observed and eqn. 2.92 becomes:

$$\alpha^{\pm} = [\nu_A^2 + {}^9/_4(D')^2 \pm 3D'\nu_A(2\cos^2\phi - 1)]^{\frac{1}{2}} \qquad (2.93)$$

At the limit, $\phi = 0^o$, $\alpha^{\pm}$ may be expressed as

$$\alpha^{\pm} = [\nu_A^2 + {}^9/_4(D')^2 \pm 3\nu_A D']^{\frac{1}{2}} \qquad (2.94)$$

The values of $\alpha^{\pm}$ given by the square roots of the above equation are positive by definition. According to the appropriate conditions the order $T_1^- > T_2^- > T_3^-$ and $T_1^+ > T_2^+ > T_3^+$ is always preserved.[25] The shielding tensor components are defined such that $\nu_{33} \leq \nu_{22} \leq \nu_{11}$ (*i.e.*, $\sigma_{33} \geq \sigma_{22} \geq \sigma_{11}$).

From equations (2.89) to (2.92) the relevant NMR parameters may be derived from the $T_{ii}^{+/-}$ extrema as follows:[25]

$$D' = T_3^+ - T_3^- - J = (T_1^- + T_2^-) - (T_1^+ + T_2^+) + 2J \qquad (2.95)$$

$$= (T_1^- + T_2^-) + (T_1^+ + T_2^+) \qquad (2.96)$$

$$T_1^+ - T_2^+ = \alpha^+ \qquad (2.97)$$

$$T_1^- - T_2^- = \alpha^- \qquad (2.98)$$

$$2\nu_{33} = T_3^+ + T_3^- \qquad (2.99)$$

These results can now be substituted to give the remaining parameters

$$(\alpha^{+})^2 + (\alpha^{-})^2 = 2\nu_A^2 + \tfrac{9}{2}(D')^2 \qquad (2.100)$$

$$(\alpha^{+})^2 - (\alpha^{-})^2 = 6\nu_A D'(2\cos^2\phi-1) \qquad (2.101)$$

Zilm and Grant[23] have obtained the above NMR parameters for matrix isolated nuclear species in A_2, AB and AX spin systems. An alternative to the use of matrix isolation is slow MAS experiments whereby the extrema $T_{ii}^{+/-}$ can be obtained from spinning sideband analysis.[27,28] The tensorial interplay for an AX system has been analysed in such a way from the ^{13}C CP/MAS spectrum of $[Me_2Ph_2P]^+I^-$.[25]

2.9 The AX_2 Spin System

2.9.1 Axially Symmetric System

The theory described in Section 2.7 and 2.8 may be extended for an AX_2 system although further assumptions are required. As noted previously the Hamiltonian for an AX system is given by

$$\hbar^{-1}\hat{\mathcal{H}}_T = -\nu_o[1-\sigma_{iso}-\delta(3\cos^2\beta-1)/2]\hat{I}_{z_A} + [J-D'(3\cos^2\beta-1)]\hat{I}_{z_A}\hat{I}_{z_X}$$

This equation may be used for an AX_2 system given the following assumptions: (1) the molecular system is linear and therefore contains only a single dipolar vector, (2) any asymmetry in $\underset{\sim}{J}$ is negligible and $J_{//}$ is parallel to the internuclear axis, and (3) the shielding tensor is axially symmetric with the axis of symmetry along the internuclear axis.

The energy of the 'A' transition in an AX_2 spin system depends upon the sum of the spin components of the two equivalent X nuclei ($\sum m_x$). Since $m_I = \pm\frac{1}{2}$, this sum can take the values 1, 0, -1. The eight eigenstates may be given as follows:

TABLE 2.6 ENERGIES OF AN AXIALLY SYMMETRIC AX_2 SPIN SYSTEM

SPIN STATE	$\sum m_x$	
ααα	+1	$E(1) = -\frac{1}{2}\nu_o(1-\sigma_{zz}) + \frac{1}{2}[J-D'(3\cos^2\beta-1)]$
ααβ	0	$E(2) = -\frac{1}{2}\nu_o(1-\sigma_{zz})$
αβα	0	$E(3) = -\frac{1}{2}\nu_o(1-\sigma_{zz})$
αββ	-1	$E(4) = -\frac{1}{2}\nu_o(1-\sigma_{zz}) - \frac{1}{2}[J-D'(3\cos^2\beta-1)]$
βαα	+1	$E(5) = \frac{1}{2}\nu_o(1-\sigma_{zz} - \frac{1}{2}[J-D'(3\cos^2\beta-1)]$
βαβ	0	$E(6) = \frac{1}{2}\nu_o(1-\sigma_{zz})$
ββα	0	$E(7) = \frac{1}{2}\nu_o(1-\sigma_{zz})$
βββ	-1	$E(8) = \frac{1}{2}\nu_o(1-\sigma_{zz}) + \frac{1}{2}[J-D'(3\cos^2\beta-1)]$

(2.102)

According to the selection rule $\Delta m_I = \pm 1$, four transitions are allowed between the eight energy levels which are designated "minus" and "plus" depending on the constant spin-state during the A transitions.

$$\nu^+ = E(5)-E(1) = \nu_o[1-\sigma_{iso}-\delta(3\cos^2\beta-1)/2] - (J-D'(3\cos^2\beta-1)]$$

$$\nu^o = E(6)-E(2) = E(7)-E(3) = \nu_o[1-\sigma_{iso}-\delta(3\cos^2\beta-1)/2]$$

$$\nu^- = E(8)-E(4) = \nu_o[1-\sigma_{iso}-\delta(3\cos^2\beta-1)/2 + [J-D'(3\cos^2\beta-1)]$$

(2.103)

Hence, there are only three transitions with the NMR transition due to the zero total X spin state having twice the intensity of the $\nu^{+/-}$ transitions, giving rise to the characteristic 'triplet' pattern. The transition frequencies can now be expressed relative to the isotropic shift ν_{iso}

$$\Delta\nu^{+} = -\tfrac{1}{2}\nu_{o}\delta(3\cos^{2}\beta-1) - [J-D'(3\cos^{2}\beta-1)] \qquad (2.104)$$

$$\Delta\nu^{o} = -\tfrac{1}{2}\nu_{o}\delta(3\cos^{2}\beta-1) \qquad (2.105)$$

$$\Delta\nu^{-} = -\tfrac{1}{2}\nu_{o}\delta(3\cos^{2}\beta-1) + [J-D'(3\cos^{2}\beta-1)] \qquad (2.106)$$

Equations (2.104) and (2.106) can be rearranged to give

$$\Delta\nu^{+} = (D' - \tfrac{1}{2}\nu_{o}\delta)(3\cos^{2}\beta-1) - J \qquad (2.107)$$

$$\Delta\nu^{-} = -(D' + \tfrac{1}{2}\nu_{o}\delta)(3\cos^{2}\beta-1) + J$$

From these equations it can be seen that the AX_2 spin system behaves rather like an uncoupled 'A' plus an $(AX)_{eff}$ with $D_{(eff)}$ and $J_{(eff)}$ equal to twice the proper values of D and J between A and one of the X spins.

Figure 2.14 shows the three subspectra arising from the three spin-states of the X nuclei. The study of an AX_2 system has advantages over the AX system in that the middle subspectrum gives information concerning only the shielding tensor characteristics. However, overlaps of the subspectra plus broadening due to magnetic susceptibility effects[22,26] complicate matters unless matrix isolation techniques are used.[24]

FIGURE 2.14

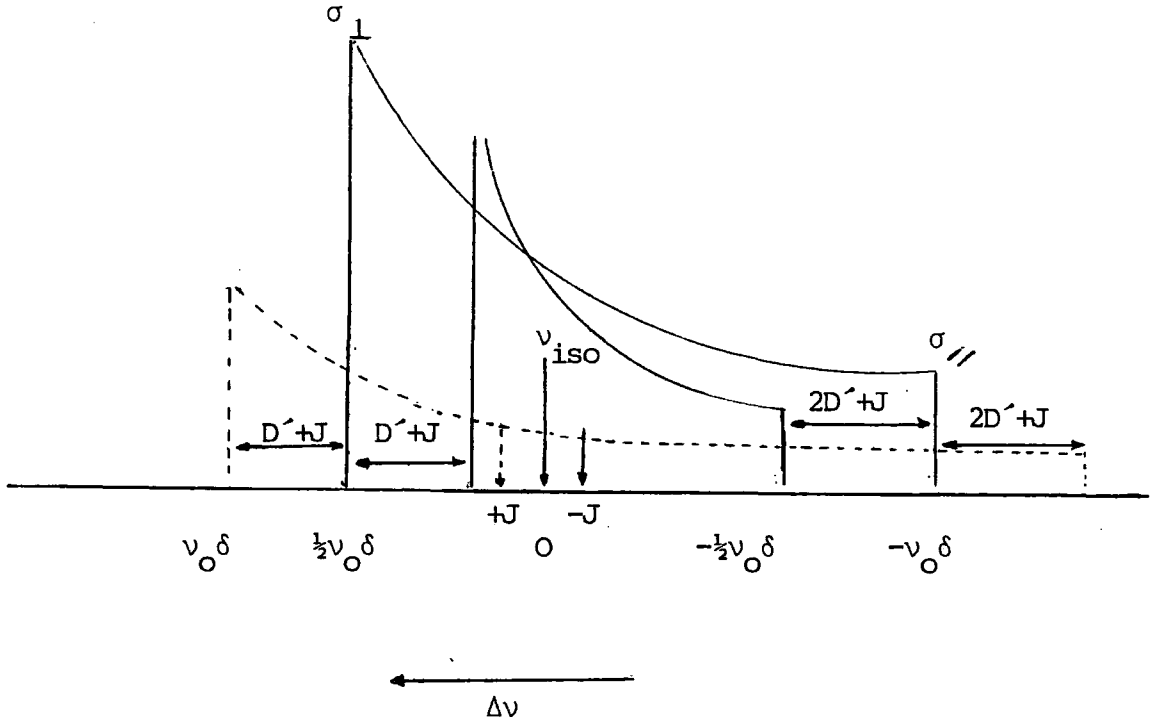

NMR solid-state powder pattern for the A spins of an AX_2 system influenced by axially symmetric shielding anisotropy by direct and indirect spin-spin coupling. The dashed line represents the subspectrum due to the -1 spin state of the X nuclei, the solid lines representing the subspectra due to the 0 and +1 spin states. The isotropic positions ($\beta=54.7^{o}$) of the subspectra are indicated by vertical arrows. δ, D' and J are positive and $\nu_o\delta >> D' \,\&\, J$ so that it is the shielding tensor characteristics which influence the shape of the spectrum.

2.9.2 Non-Axially Symmetric AX_2 System

For an AX_2 system with a non-axially symmetric shielding tensor and an axially symmetric $\underset{\sim}{J}$ tensor, the equations of Zilm and Grant[23] can be extended to give a similar

analysis to that shown in Section 2.8. The shielding term remains the same, and the spin-spin coupling terms change due to the consideration of the total spin component numbers of the X nuclei (*cf.* eqn. 2.102). The equations for the powder pattern extrema $T_{ii}^{+/-}$ are thus as follows:

$$T_1^{\pm} = [\nu_B \mp D' + \alpha^{\pm} \pm 2J]/2 \qquad (2.108)$$

$$T_2^{\pm} = [\nu_B \mp D' - \alpha^{\pm} \pm 2J]/2 \qquad (2.109)$$

$$T_3^{\pm} = \nu_{33} \pm (D'+J) \qquad (2.110)$$

where,

$$\alpha^{\pm} = [\nu_A^2 + 9(D')^2 \pm 6\nu_A D'(2\cos^2\phi-1)] \qquad (2.111)$$

$$D' = D - (J_{//}-J_{\perp})/3$$

$$\nu_A = \nu_{22} - \nu_{11}$$

$$\nu_B = \nu_{22} + \nu_{11}$$

and ϕ is the angle between ν_{11} and the internuclear axis. As was previously assumed for the non-axial AX case, these equations will only hold if one of the shielding tensor components is perpendicular to the internuclear vector, such that $\theta=90^{\circ}$ (see Figure 2.13). However, the only clear reason to make this assumption is if the molecule possesses certain appropriate symmetry elements (*e.g.* reflection plane) and further, that the molecular symmetry is not destroyed by crystalline packing effects.

From the above equations the relevant NMR parameters may be deduced:

$$2D' = T_3^+ - T_3^- - 2J = (T_1^- + T_2^-) - (T_1^+ + T_2^+) + 4J \quad (2.112)$$

$$2\nu_B = (T_1^- + T_2^-) + (T_1^+ + T_2^+) \quad (2.113)$$

$$\alpha^+ = T_1^+ - T_2^+ \quad (2.114)$$

$$\alpha^- = T_1^- - T_2^- \quad (2.115)$$

$$(\alpha^+)^2 + (\alpha^-)^2 = 2\nu_A^2 + 18(D')^2 \quad (2.116)$$

$$(\alpha^+)^2 + (\alpha^-)^2 = 12\nu_A D'(2\cos^2\phi - 1) \quad (2.117)$$

$$2\nu_{33} = T_3^+ + T_3^- \quad (2.118)$$

Thus, the shielding tensor parameters along with J, D and ϕ may be determined. However, there is ambiguity concerning the assignment of the 'plus' and 'minus' subspectra. At the limit $\phi=0^o$, equation (2.111) becomes:

$$\alpha^{\pm} = [\nu_A^2 + 9(D')^2 \pm 6\nu_A D']^{\frac{1}{2}} \quad (2.119)$$

A positive value is always taken for the square root in the definition of $\alpha^{\pm}$. Thus, $\alpha^{\pm}$ becomes $3D \pm \nu_A$ when $3D' > |\nu_A|$ and $-\nu_A \mp (3D')$ when $-\nu_A > 3D'$. If the shielding tensor components are defined such that $\nu_{11} \geq \nu_{22} \geq \nu_{33}$ (*i.e.* $\sigma_{33} \geq \sigma_{22} \geq \sigma_{11}$), this implies that ν_A is negative. With the above definitions, the order $T_1^+ > T_2^+ > T_3^+$ and $T_1^- > T_2^- > T_3^-$ is maintained providing $\nu_{11} - \nu_{33} > 3D'$. At the limit $\phi=90^o$, the order also holds if $\nu_{22} - \nu_{33} > 3D'$.

The total width of the subspectra $\Delta T^{\pm}$ is given by

$$\Delta T^{\pm} = T_1^{\pm} - T_3^{\pm} \quad (2.120)$$

At the limit $\phi=0^o$, the difference in subspectral width, $\Delta T^- - \Delta T^+$, is equal to $3D' - \nu_A$ when $3D' > |\nu_A|$ and equal to $6D'$ when $-\nu_A > |3D'|$. At the limit $\phi=90^o$, this difference, $\Delta T^- - \Delta T^+$, becomes $\nu_A + 3D'$ when $3D' > |\nu_A|$ and zero when $-\nu_A > |3D'|$.

With the exception of the last limit, inspection of the two subspectra can reveal which is "minus" and which "plus". However, it should be noted that from equation (2.112) D′ and J can be calculated to be positive or negative depending on the assignment of the "plus" and "minus" spectra. In some cases the ambiguity can be solved by knowledge of D and the size of ΔJ.

The rapid MAS spectrum of an AX_2 system will give rise to an isotropic averaged spectrum containing a triplet. If the spinning speed is considerably less than the total static linewidth then three spinning sideband manifolds will be observed. The middle manifold can be analysed by sideband analysis[27,28] to determine the shielding tensor components for the 'A' nucleus, whilst the outer sideband manifolds can be analysed to give D′ and ϕ. The isotropic scalar coupling constant is, of course, available from the centre peaks. An example of such a spectrum is given in Chapter Six.

2.10 High Resolution Solid-State NMR

The characteristically broad lines of solid-state NMR may be considerably narrowed by two techniques: magic-angle spinning (MAS) and high-power decoupling (HPD). MAS involves the rapid rotation of a solid sample about an axis making an angle 54.7^{o} with the static applied field Bo.[14] (see Chapter Three). This technique can be used to average the shielding anisotropy and in principle to eliminate dipolar interactions and anisotropic indirect coupling. This is true providing the spinning speed exceeds the size of the

interaction (or the combined effects from the interplay of two or more interactions). However, in some cases the size of dipolar interactions well exceeds the attainable spinning speed.[29] High-power decoupling has solved this problem for heteronuclear dipolar coupling involving protons.[30] Elimination of homonuclear dipolar broadening in the solid-state is clearly not possible by such a technique. The use of multiple-pulse sequences,[4,5] overcomes this problem, and manipulates the proton spins in such a way as to give a zero average of the ^{1}H-^{1}H dipolar interactions.

In NMR studies of the solution-state, 'high-resolution' may be defined as where the dispersion of chemical shifts and the magnitude of indirect (J) spin-spin coupling constants are considerably larger than the natural width of the resonances. For solid samples, the linewidths that are normally attainable with available techniques (MAS, HPD) usually obscure the small J couplings that are so useful in solution-state NMR, hence, the usual criterion for high resolution in the solid-state is the ability to distinguish resonances with reasonably different chemical shifts.

2.11 Magnetic Equivalence in Solid-state NMR

In high resolution NMR of liquids two nuclei are magnetically equivalent when they have identical chemical shifts and they couple equally to every other nucleus in the molecule,[3] *e.g.* CH_2CF_2 (see Figure 2.8)

FIGURE 2.8

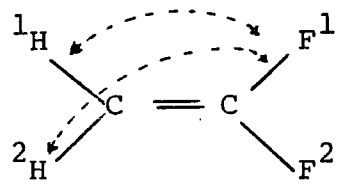

Although F1 and F2 are chemically equivalent (*i.e.* they have the same chemical shift) they are magnetically non-equivalent as $J_{cis} \neq J_{trans}$

J_{1H^1F} = "J_{cis}" J_{2H^1F} = "J_{trans}"

Taking scalar coupling into account, equivalence of nuclei in liquids is defined with respect to molecular symmetry alone. In crystals, nuclei are called 'magnetically equivalent', if they are related by translation and/or inversion elements of the space group. On the other hand, nuclei are called 'crystallographically equivalent' if they are related by one of the symmetry elements of the space group.[4] The difference between these two terms experimentally is that the shielding tensor elements of magnetically equivalent nuclei are identical, whereas nuclei which are crystallographically equivalent can have different shielding tensor parameters in the laboratory frame (though the principal values will be identical).

If there are Nm magnetically non-equivalent but crystallographically equivalent sites for a spin-½ nucleus in a static single crystal, the NMR spectrum will consist of Nm sharp lines. (Although in some special orientations of the crystal with respect to Bo some of the lines will coalesce). This is because each of these sites, although related by some symmetry operation, (*e.g.* rotation, reflection) is orientated differently in the static field, giving rise to

different shielding magnitudes and overall different tensor components in the laboratory frame. However, it is impossible *a priori* to know which of the lines arises from which crystallographically equivalent site.[4]

The use of magic-angle spinning (at a rate greater than the difference between the shielding extremities) causes all crystallographically equivalent molecules to appear at the same average orientation to Bo. Therefore, the single-crystal case with Nm sites, there would only be a single peak present in the spectrum, with a relative intensity of Nm, occuring at the isotropic chemical shift.

A powder sample with Nm sites would in principle give rise to a line for each different orientation present. The impossible resolution of these lines leads to the observation of the characteristic shielding powder pattern described earlier. The MAS spectrum of such a powder would show a single peak at the isotropic chemical shift. Hence the NMR of powders, with only equivalent crystallographic sites present, cannot distinguish between the magnetically non-equivalent sites. However, if a powder sample contained Nn crystallographically non-equivalent sites, then the static bandshape would contain an overlap of Nn shielding patterns, whereas the averaging MAS technique would produce, in principle, a spectrum containing Nn lines.

Crystallographically non-equivalent sites can arise from two possibilities, either (i) *intermolecular effects*, where there are independent molecules in the unit cell not related by any symmetry elements of the space group, or (ii) *intramolecular effects* where the site symmetry is lower than the

molecular symmetry. Consider a molecule containing two spin-½ nuclei of the same species in chemically equivalent positions; then if a MAS spectrum of the nucleus in question exhibited two peaks, it would be impossible to assign these resonances to *inter* or *intra*molecular effects.

2.12 Factors Affecting Resolution in CP/MAS NMR

In principle, the CP/MAS technique used to obtain high-resolution solid-state NMR spectra should give rise to solution-type linewidths. However, the linewidths observed in solids tend to be roughly 10 to 100 times those observed in the liquid phase.[11] The reasons for this lack of resolution are the residual interactions (*i.e.* those not averaged by MAS), motional and relaxation effects. A summary of the more important sources of broadening is given below, although the external (instrumental) factors will be discussed in Chapter Three.

(i) Chemical Shift Effects

The chemical shift distribution reflects a fundamental difference between the solid and solution states. In solids there can be a distribution of chemical shifts arising from small variations in environment or lattice defects which would normally be removed in solution by dynamic averaging by the molecules. This distribution can generate a linewidth which would be proportional to Bo. (In theory, a high enough Bo would resolve such splittings since a truly continuous distribution is unlikely).

(ii) Intermolecular J-Coupling

In the solid-state molecules are fixed in a particular orientation by the close packed system, this then allows the possibility of static intermolecular scalar coupling, implying some electronic overlap between molecules. In the solution-state, random molecular motion would remove this effect. Such a distribution of J couplings would be independent of the Bo field strength.

(iii) Antisymmetric Tensor Interactions

In the theory section outlining the various Hamiltonian interactions, the $\underset{\sim}{J}$ tensor was considered to be symmetric as the effect of the antisymmetric components of $\underset{\sim}{J}$ on the NMR spectrum should be small.[4,17] However, their effects should be borne in mind for spectra with narrow lines when $J \gtrsim \nu_o \delta_{AB}$,[17] as MAS does not remove them.

(iv) Quadrupolar Effects

Magic-angle spinning does not remove dipolar broadening if one of the interacting spins is not quantized along the magnetic field. Such a situation can arise if one spin belongs to a quadrupolar nucleus subjected to both quadrupole and Zeeman interactions whereby $\nu_Q \simeq \nu_L$. Such an effect can cause broadening for mobile systems[31] and also asymmetric splitting in rigid systems.[32] A combination of J coupling and dipolar coupling of a spin-½ nucleus to a quadrupolar nucleus has also been observed, where the influence of each interaction depends upon the strength of the applied field.[33] The quadrupole dipole effects are found to significantly diminish at higher applied fields.

(v) Random Molecular Motion

Many of the interactions responsible for line-broadening in solid-state NMR can be removed by molecular motions. However, such a blessing can sometimes be seen as a bane if extra narrowing is attempted by magic-angle spinning. Molecular motions, which reduce the inherent linewidth, can be divided into two classes: (i) fast restricted motion and (ii) moderate isotropic motion. In the first case magic-angle spinning can reduce the residual linewidth further as the time-average Hamiltonian for the anisotropic interactions averages to zero.[22] The second class of motion achieves narrowing similarly to liquids whereby all degrees of freedom are mobilised. In such a case, MAS is only effective if the rotation rate is greater than the internal motion (correlation frequency),[22,34] which in some cases is impossible.

(vi) Relaxation Effects in Mobile Systems

Molecular motion in solids can cause broadening by providing relaxation pathways for the transverse magnetization of the observed nucleus. One mechanism is motional modulation of the dipolar coupling. This can arise when molecular motion occurs at the frequency corresponding to the proton decoupling field. The amount of broadening can be considerable, especially for some organic polymers.[26]

The second mechanism arises from a loss of phase coherence in the transverse magnetization of the observed nucleus, because of random motional modulation of the resonance frequency *via* shielding anisotropy.[26] This type of

broadening is proportional to the anisotropy and the strength of the applied field. In cases of slow motion, broadening can be reduced by rapid MAS.[26,35]

(vii) Anisotropic Bulk Magnetic Susceptibility (Rigid Systems)

In general bulk magnetic susceptibility broadening (BMS) occurs because of non-uniform shielding effects caused by samples of irregular shapes. The linebroadening from a single particle of arbitrary shape or arbitrary configuration of irregularly shaped particles will be removed by MAS.[26] However, this condition will only be true for isotropic BMS. If the BMS of a polycrystalline solid is anisotropic this produces a dispersion of chemical shifts attributable to dipolar fields. These dipolar fields arise from orientation dependent dipoles with their strength depending on the orientation of the susceptibility tensor with respect to Bo. This effect is not completely spun out by MAS and is thought to be significant for anisotropic molecules.[26]

2.13 Spinning Sidebands

2.13.1 Rotational Echoes

It is a recognized phenomenon that powder patterns associated with anisotropic shielding break up, at spinning speeds much below the static powder linewidth, into sharp spinning sidebands. These sidebands appear as satellites about each peak, with separations between the main peaks and sidebands equal to the rotation frequency (ν_r). Sidebands of significant intensity cover a frequency range comparable to the static linewidth Δ, and accordingly there will be *c a.* Δ/ν_r of them. Rapid sample magic-angle rotation may be considered as a modulation of the spin interactions manifesting itself in the form of sidebands. Maricq and Waugh[27] have developed the concept of 'Rotational echoes' to explain this phenomenon.

As a rotation period proceeds, the magnetization vectors get out of phase with each other, and the net transverse magnetization decays to zero. However, after one complete revolution these magnetization vectors return to their original phases, reinforcing each other (assuming they were in phase at the end of a 90° pulse). The resulting refocussed magnetization is called a rotational echo. As the rotation continues, the above process is repeated producing a train of rotational echoes.[36] Fourier transformation of the echo train transforms the modulation in the time domain, at the rotor period ν_r^{-1}, into sidebands in the frequency domain, with splittings equal to ν_r.

The spinning sideband intensities in the FT spectrum depend on the size of the shielding anisotropy and

asymmetry relative to the spinning speed. For $\Delta\sigma >> \nu_r$, the decay of the individual echoes is pronounced, and an extensive spinning sideband pattern is produced in the frequency spectrum. In the case of $\Delta\sigma << \nu_r$, the decay of individual echoes is much less pronounced, and little sideband intensity, if any, is observed in the FT spectrum.

The loss of sensitivity at low spinning speeds arises from the fact that rotational echoes become more widely spaced in time, and fewer of them are available for construction of the envelope. When $\nu_r >> \Delta$, the echoes merge into a continuous decay, corresponding to the collapse of the sideband pattern into a single line. The number of spinning sidebands increases when the field strength, B_o, is increased and decreases as the sample rotation speed increases. Hence, the most reliable way to eliminate sidebands is by a manipulation of the two parameters B_o and ν_r.

The concepts of modulation and rotational echoes have been applied above exclusively only to the shielding anisotropy. However, these ideas equally apply to the other spin anisotropic interactions that can be modulated by simple rotation, *i.e.* heterogeneous dipole-dipole interactions and nuclear electric quadrupole interactions.

2.13.2 Spinning Sideband Analysis

It is interesting to note that as ν_r is made small, the envelope of sidebands approaches its static powder pattern whose maximum intensity typically lies quite far from the isotropic Larmor frequency. Thus, location of

the isotropic centreband by inspection of the sideband is often difficult. However, if the experiment is repeated using a different spinning speed (ν_r'), the Nth sideband will shift by $N(\nu_r' - \nu_r)$, the true centreband is the one which remains at the same absolute frequency. Alternatively, another method is possible, without any additional experiments, by using the first moments of the spectra. The lth moment is given by[27]

$$M_l = \nu_r^l \sum_{N=N^-}^{N^+} N^l A_N / \sum_N A_N$$

where N = No. of the sideband, A_N = Amplitude of the Nth sideband and ν_r is the spinning speed in Hz. The first moment is therefore,

$$M_1 = \nu_r \sum_{N=N^-}^{N^+} NA_N / \sum_N A_N = 0 \text{ about } \nu_{iso}$$

It follows that

$$\sum_{N=N^-}^{N^+} = A_N . N = 0.$$

Thus, a straightforward summation of sideband intensities leads to the correct isotropic shift. However, unless the signal to noise is good, there may be some ambiguity in the result from this simple procedure.

Maricq and Waugh[27] have shown that the second and third moments of N.M.R. spectra are related to the chemical shift properties and can, in principle, be used to extract the chemical shift anisotropy from the sideband intensities. The second and third moments can be calculated from a spinning sideband pattern by the use of the above general equation (M_l). Their relation to the shielding anisotropy parameters[27] is given by:

$$M_2 = (\delta^2/15)(3 + \eta^2)$$

$$M_3 = (2\delta^3/35)(1 - \eta^2)$$

Thence, δ may be solved from the following cubic equation

$$4\delta^3 - 15M_2\delta - \frac{35}{2} M_3 = 0$$

The principal shielding components may be then deduced:

$$\sigma_{33} = \sigma_{iso} + \delta$$

$$\sigma_{22} = \sigma_{iso} - \tfrac{1}{2}\delta(1-\eta)$$

$$\sigma_{11} = \sigma_{iso} - \tfrac{1}{2}\delta(1+\eta)$$

where $\eta = \frac{\sigma_{22}-\sigma_{11}}{\delta}$

The above method of Maricq and Waugh requires accurate measurements of all sideband intensities, which may not always be possible. In some instances sidebands may overlap with those of another. In other cases poor signal to noise can create ambiguity over the intensities of sidebands, especially those from the outer wings of the envelope, which nevertheless have a profound influence on M_2 and (particularly) M_3.

Herzfield and Berger[28] have derived general integral and series expressions for the intensities of sidebands observed in MAS spectra of inhomogeneously broadened $I=\frac{1}{2}$ systems. The results have been used to construct a graphical method for the extraction of the principal values of chemical shift tensors. A series of contour plots is given for each ratio of I_N/I_o, where I_N is the intensity of the Nth sideband ($N=\pm1\rightarrow\pm5$) and I_o is the intensity of the isotropic centreband. By calculating the I_N/I_o ratios from the spectrum and tracing around the corresponding contour lines, a necessary intersection point may be obtained which

is used to extract the values of μ and ρ, as displayed on the x and y axes respectively. These quantities are related to the chemical shielding parameters by the following:

$$\mu = \frac{\nu_o}{\nu_r} (\sigma_{33} - \sigma_{11})$$

$$\rho = \left(\frac{\sigma_{11} + \sigma_{33} - 2\sigma_{22}}{\sigma_{33} - \sigma_{11}}\right)$$

where $-1 \leq \rho \leq 1$ and $\mu \geq 0$.

Of course the advantage in using the graphical method of Herzfield and Berger[28] is that only a few selected sideband intensities are required (contrary to the Maricq and Waugh method[27]) but in such cases the information in the other sidebands is not used.

Thus, the technique was found to give inconsistent results, mainly due to the ambiguity of the real intersection point of the graphical contours. Hence, the Maricq and Waugh method has been favoured for sideband analysis in this work.

REFERENCES (Chapter 2)

1. J.A. Pople, W.G. Schneider and J. Bernstein, 'High-Resolution Nuclear Magnetic Resonance', McGraw-Hill, Inc. 1959.

2. R.K. Harris, 'NMR Spectroscopy. A Physicochemical View', Pitman, 1983.

3. A. Abragam, 'The Principles of Nuclear Magnetism', Clarendon Press, Oxford, 1961.

4. U. Haeberlen, 'High-Resolution NMR in Solids - Selective Averaging', Suppl. 1, Adv.Mag.Res., 1976, Academic Press.

5. M. Mehring, 'Principles of High-Resolution NMR in Solids', 2nd Edition, Springer-Verlag, 1976.

6. M.E. Rose, 'Elementary Theory of Angular Momentum', J.Wiley and Sons, 1957.

7. P.C. Taylor, J.F. Baugher, and H.H. Kriz, Chem.Revs., 1975, (75), 203.

8. C.P. Slichter, 'Principles of Magnetic Resonance', 2nd Edition, Springer-Verlag, Berlin, (1980).

9. G.E. Pake, J.Chem.Phys., 1948, (16), 327.

10. D.L. Vanderhart, H.S. Gutowsky and T.C. Farrar, J.Chem. Phys., 1969, (50), 1058.

11. L.M. Ishol and T.A. Scott, J.Mag.Res., 1977, (27), 23.

12. N.F. Ramsey, Phys.Rev., 1953, (91), 303.

13. A.D. Buckingham and I. Love, J.Mag.Res., 1970, (2), 338.

14. E.R. Andrew, Prog.NMR Spec., 1972, (8), 1.

15. P.N. Tutunjian and J.S. Waugh, J.Chem.Phys., 1982,(76),1223

16. R. Balz, M. Haller, W.E. Hertler, O. Lutz, A. Nolle and R. Schafitel, J.Mag.Res., 1980 (40), 9.

17. E.R. Andrew and L.F. Farnell, Mol.Phys., 1968,(15), 157.

18. N. Bloembergen and T.J. Rowland, Phys.Rev., 1955, (97),1679

19. M.A. Rudermann and C. Kitel, Phys.Rev., 1954, (96), 99.

20. E. Fukushima, J.Chem.Phys., 1971, (55), 2463.

21. R. Balz, M. Haller, W.E. Hertler, O, Lutz, A. Nolle and R. Schafitel, J.Mag.Res., 1980, (40), 9.

22. E.R. Andrew, Int.Rev.Phys.Chem., 1981, (1), 195.

23. K.W. Zilm and D.M. Grant, J.Am.Chem.Soc., 1981, (103),2913.

24. K.W. Zilm, R.T. Conlin, D.M.Grant and J. Michl, J.Am.Chem. Soc., 1980, (102), 6672.

25. R.K. Harris, K.J. Packer and A.M. Thayer, J.Mag.Res., 1985, (62), 284.

26. D.L. Vanderhart, W.L. Earl and A.N. Garroway, J.Mag.Res., 1981, (44), 361.

27. M.M. Maricq and J.S. Waugh, J.Chem.Phys., 1979, (70),3300.

28. J. Herzfield and A.E. Berger, J.Chem.Phys., (1980),(73),6021

29. C.S. Yannoni, Acc.Chem.Res., 1982, (15), 201.

30. A. Pines, M.G. Gibby, and J.S. Walsh, J.Chem.Phys., 1973, (59), 569.

31. C.A. Fyfe, J.R. Lyerla, W. Volksen and C.S. Yannoni, Macromol., 1979, (12), 757.

32. C.J. Groombridge, R.K. Harris, K.J.Packer, B.J. Say, and S.F. Tanner, J.Chem.Soc.Chem.Comm., 1980, 174.

33. E.M. Menger and W.S. Veeman, J.Mag.Res., 1982, (46), 257.

34. J.S. Waugh, "NMR and Biochemistry", Eds. S.J. Opella and P.Lu, 1979.

35. D. Svwelak, W.P. Rothwell and J.S. Waugh, J.Chem.Phys., 1980, (73), 2559.

CHAPTER THREE

EXPERIMENTAL

3.1 Introduction

This chapter is concerned with descriptions of techniques utilized to obtain high resolution solid-state N.M.R. To date, there is no reported work describing the tuning procedures applicable for CP/MAS ^{119}Sn and ^{195}Pt spectra. The methods by which such spectra are obtained are discussed in detail, incorporating descriptions of cross-polarisation, high-power decoupling and magic-angle spinning techniques.

3.2 The Spectrometers

3.2.1 The CXP200 Spectrometer

All multinuclear solution and solid-state spectra in this work (excluding ^{13}C solid-state N.M.R., *vide infra*) were obtained using a Bruker CXP200 spectrometer, operating at 4.7T (^{1}H=200MHz). Solid-state experiments were performed using broad-band MAS probes incorporating the Andrew Beams type of rotor (see on). Two probes were utilized for nuclei directly studied in this work: a "silicon" CP/MAS probe operational at *ca.* 30-60MHz and a "phosphorus" CP/MAS probe (60-90MHz) - so-called because of their optimized performances at the N.M.R. frequencies of the ^{29}Si and ^{31}P nuclei respectively. Both probes could be used for single-pulse excitation, high-power decoupling and CP experiments. In general, solution-state experiments were performed using a high-resolution broad-band probe. However, to avoid unnecessary time delays, satisfactory results could be obtained from the solid-state probes by employing vials of solution (in place of the rotor).

3.2.2 Home-built ^{13}C Spectrometers

The ^{13}C solid-state spectra in this work were acquired using two home-built spectrometers based at UEA. High-field studies were performed using a high-power double resonance spectrometer (the 'UEA 200') which included an Oxford Instruments superconducting magnet operating at 4.7T (^{1}H=200MHz, ^{13}C=50.29MHz). The spectrometer operation is largely under computer control using a suite of automated written software running on a Nicolet 1180 computer. Solid-state studies were conducted using a commercial Bruker ^{13}C CP/MAS probe employing the Andrew-Beams type of rotors.

Low-field ^{13}C spectra were obtained from the 'Nic 90" spectrometer operating at 2.11T (^{1}H=90.0MHz, ^{13}C=22.6MHz). The MAS system used cylindrical glass rotors (8x12mm) driven by a gas turbine. More detailed and comprehensive descriptions of the CXP200 spectrometer and home-built ^{13}C systems can be found in previous works.[1,2,3]

3.2.3 Shimming

The inhomogeneity of the magnetic field was kept minimal by the correct adjustment to the shim gradients. The shimming of the magnet was achieved by the observation of the proton FID from a cross-linked "silicone gun", containing mobile protons. The spectra were obtained under conditions of MAS and single-pulse excitation. The magnet was considered well-shimmed when linewidths of 20-30Hz were obtained.

3.2.4 Detection

All N.M.R. experiments were performed with the use of quadrative detection.[2] Quadrature phase routing was used to eliminate quadrature images in single-pulse experiments. The spin temperature inversion sequence was used to eliminate any such artifacts present in FIDS from cross-polarization.

3.2.5 Acquisition Conditions

The spectra presented in this work were obtained at the spectrometer operating frequencies quoted in Table 3.1 for the various nuclei. For individual spectra of the same nucleus, the carrier frequency is not necessarily constant, with the variation denoted by the offset, O1. Other variable conditions quoted for each spectrum are as follows:

NT = No. of transients

SW = Spectral Width (kHz)

AQ = Acquisition time (ms)

DO = Recycle delay (s)

D2 = Contact time (ms)

D3 = Decoupler time (ms)

SF = Spectrometer operating frequency (MHz)

O1 = Frequency offset (kHz)

SS = Spinning Speed (Hz)

DR* = Digitization Resolution (Hz/pt.)

* This is calculated after cosmetic improvements to the FID. The actual experimental DR = $\frac{1}{AQ}$

where AQ = $\frac{\text{Memory Size (pts)}}{2 \times SW}$

3.3 Chemical Shift Measurements

The chemical shift, δ, for nucleus i, is reported on a dimensionless scale and defined as[4]

$$\delta_i = \frac{\nu_i - \nu_R}{\nu_R} \times 10^6 = \frac{\sigma_R - \sigma_i}{1-\sigma_R} \approx (\sigma_R - \sigma_i) \times 10^6$$

where R refers to a reference standard, and δ is measured in ppm. Ideally, it would be desirable to reference all isotropic chemical shifts with respect to that of the bare nucleus. An absolute frequency has been used on several occasions for platinum, but this relies on a homogeneous applied field as well as standard experimental conditions. Tetramethyl silane is the accepted reference standard for ^{1}H and ^{13}C N.M.R., and in analogy with this, tetramethyl stannane is used for ^{119}Sn N.M.R. . All ^{31}P N.M.R. data in this work are referenced to the widely used standard, 85% H_3PO_4/D_2O. For ^{195}Pt N.M.R. there is no universally accepted reference, although by far the most commonly used is the anion $PtCl_6^{2-}$. The advantages of using the sodium salt, Na_2PtCl_6 are that it is readily available and is stable in solution over relatively long periods of time.[5] However, it does have disadvantages ; the signal is not very sharp and indeed as shown by Ismail *et al*[6] is the composite of various $Pt^{35}Cl^{3}$ Cl isotopomers. Furthermore, the shift is reported to have a large temperature dependence.[7] Although the CXP "probe" or "ambient" temperature can be considered to be fairly constant, temperatures will vary from instrument to instrument and should be borne in mind for any future investigations.

The errors involved in chemical shift analysis can be indicated by the reproducibility of spectral data.

TABLE 3.1 Experimental conditions of observed nuclei

Nucleus	Spectrometer Operating Freq.[e]	Reference	Exptl. Linewidths[a] of References (Hz)
^{13}C	50.29	Adamantane[b]	10
^{23}Na	52.94	3M NaCl[c]	50
^{31}P	81.01	85% H_3PO_4[c]	20
^{119}Sn	74.63	$SnMe_4$[c]	100
^{195}Pt	43.02	Na_2PtCl_6/D_2O[c,d]	100

(a) Linewidths are defined as the total width of the line at half-height (obtained using high power decoupling).

(b) ^{13}C solid-state spectra were initially calibrated to Adamantane (^{13}C CP/MAS) by the replacement method and then referenced to TMS using a +37.7 p.p.m. conversion factor.

(c) Glass ampoules used, (Note, MAS eliminates the need to correct for bulk magnetic susceptibility differences; however the references were run without MAS. Thus, shifts between solid samples may be more accurate than those with respect to the reference.)

(d) Saturated solution.

(e) The chemical shift obtained from the CXP spectrometer was calculated using:

$$\delta = \frac{\nu - \nu_R}{S.F.} \times 10^6 \text{ p.p.m.}$$

where ν is the absolute frequency of the sample, ν_R is the absolute frequency of the reference and S.F. is the absolute spectrometer operating frequency. So therefore, the value of S.F. was set as close as possible to the reference frequency ν_R.

For ^{195}Pt solid-state spectra this was found to be within ±2 p.p.m., as measured at different times (excluding experimental resolution effects). This error limit was also found to be the case for ^{119}Sn N.M.R., although for ^{31}P N.M.R. results a limit of less than ±0.5 p.p.m. could be expected. The experimental conditions of the reference standards used for nuclei studied in this work are given in Table 3.1 (*N.B.* For spectra containing several spinning sidebands, centrebands are indicated by arrows on the figures).

3.4 Magic-Angle Spinning (MAS)

Rapid sample rotation about an axis inclined at an angle to the direction of the applied magnetic field (Figure 3.1) will affect the anisotropic N.M.R. interactions containing the term $(3\cos^2\theta-1)$.[8] For these orientation-dependent terms the average value $\langle 3\cos^2\theta-1\rangle$ must be considered. It can be shown that[9]

$$\langle 3\cos^2\theta-1\rangle = \tfrac{1}{2}(3\cos^2\beta-1)\ (3\cos^2\chi-1)$$

Thus, under rapid rotation (all values of χ allowed), the powder spectrum is scaled by factor $\frac{1}{2}(3\cos^2\beta-1)$. If the angle of rotation is chosen such that $(3\cos^2\beta-1)=0$, *i.e.* $\beta=54.7^{\circ}$ (the "magic-angle"), the reduction factor is zero and averaging of the anisotropic interactions may be accomplished.

Since the major nuclei studied in this work were usually contained in an environment with a large shielding anisotropy, the accuracy of setting the magic-angle played a crucial role in obtaining high resolution spectra. The effect on the linewidth of mis-setting the angle θ between the rotation axis and Bo is given by[10]

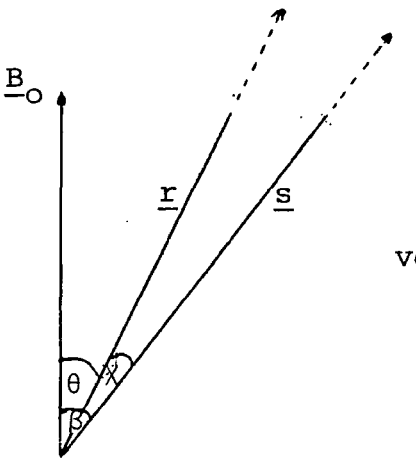

vector r rotating about axis s

FIGURE 3.1 Macroscopic sample rotation at an angle β to the magnetic field Bo

---

$$\Delta\nu_{\frac{1}{2}} \text{ (mis-set)} \simeq 0.5\ (3\cos^2\theta - 1)\Delta\nu_{\frac{1}{2}} \text{ (static)}$$

where $\Delta\nu_{\frac{1}{2}}$(static) is the static linewidth. For example, if the angle was mis-set by 1^{o}, and the static linewidth was 20kHz, (which would correspond to being 465 p.p.m. at 43MHz) then the linewidth would increase by *ca.* 500Hz.

The observation of spinning sidebands in the ^{79}Br N.M.R. (at 50.14MHz) of solid KBr was used for angle adjustments.[11] The extensive sideband manifold that is seen when the axis is very near the magic angle arises from the spinning modulation of $-\frac{3}{2} \leftrightarrow -\frac{1}{2}$ and $\frac{1}{2} \leftrightarrow \frac{3}{2}$ transitions. Such first order quadrupolar interactions exist because of imperfections in crystal lattice[11] (*i.e.* a non-cubic environment resulting in the presence of an electric field gradient). For sufficiently accurate setting of the magic angle (that is, to obtain minimum linewidths) as much as half a rotor of KBr is required; this of course decreases the sensitivity for the observation of the N.M.R. signal of interest. Fine adjustments of the

angle were made by a slight alteration of the spinning speed while observing the ^{79}Br free-induction decay (FID). When the optimum speed is obtained, small sharp spikes appear superimposed on the regular cosine decay of the FID. An alternative approach consisted of adding a small quantity of brushite ($CaHPO_4.2H_2O$) to the rotor. By observing the ^{31}P CP N.M.R. signal, the proximity to the magic-angle can be clearly seen by an increase in the time domain of the FID. This method was found to be most beneficial in obtaining high resolution ^{119}Sn spectra.

The Bruker CP/MAS probes incorporate an Andrew type stator[12], which drives an Andrew/Beams fluked rotor (composed of delrin; inner volume $\sim 0.4 cm^3$) by gas outlets. However, this MAS system was found to be prone to angular instability whereby the rotor may wander, wobble, precess or nutate significantly from its correct orientation. The uniform packing of the solid sample in the rotor was found to play a major role in producing rotational stability. Furthermore, insufficient spinning speeds (*i.e.* <2kHz) were found to have a broadening effect reflecting a lower stability at low rotation rates. (Theory suggests that lines should narrow in proportion to ω_r^{-2}, although experiment shows only a linear dependence [13]). In addition, it was found that changing the sample or spinning speed resulted in a change of the average angle for an Andrew-Beams rotor.

3.5 High Power Decoupling

The large size of the nuclear moment of a proton and the generally high abundance in organometallic samples leads to

"flip-flop" transitions of protons with anti-parallel moments.[14] This spin diffusion process is uniquely easy for coupled nuclei with the same precession frequency (see Figure 3.2).

Figure 3.2

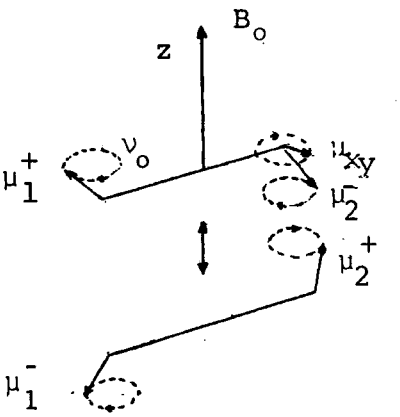

FIGURE 3.2 Spin-Diffusion for Dipolar Coupled Protons

The rotating component of the spin (xy plane) which is in the higher energy state (μ_2^-), precessing at a frequency ν_o, acts like a resonant rf field at the site of μ_1^+, which is also precessing at ν_o.

The exchange of spin energy limits the lifetime of the spin state leading to uncertainty broadening of the proton resonance. The homogeneous proton linewidth ($\Delta\nu_{HH}$) is approximately equal to the flip-flop rate, which can be as large as 50kHz for some solids.[15]

Heteronuclear proton dipolar coupling has the same kind of angular dependence as shielding anisotropy and therefore should be averaged to zero if $\nu_r >> D$ (heteronuclear dipolar coupling constant). However, proton spin diffusion limits the lifetime of a nuclear moment coupled to a proton to $\Delta\nu_{HH}^{-1}$s, which disrupts the coherent averaging of the dipolar

coupling by MAS. Therefore, unless $\nu_r >> \Delta\nu_{HH}$, ^{1}H-X dipolar coupling will surviveunder MAS conditions.[15]

Elimination of linebroadening effects due to dipolar interactions with protons can be obtained by high-power ^{1}H decoupling (HPD)[16]. This is completely analogous to the low power ^{1}H decoupling used routinely in solution-state N.M.R. to remove the effects of heteronuclear indirect (J) coupling with protons. The important difference from decoupling in liquids is based on the fact that dipolar couplings of up to tens of kHz must be overcome which requires very high power for the decoupling field (*ca.* 100W). The process can be viewed as stimulating rapid transitions of ^{1}H spin states, so that the average ^{1}H dipolar effect on the observed nucleus vanishes.

In the cross-polarisation sequence (*vide infra*), proton decoupling is attained by spin-locking the proton moments.[17] This process is most easily visualized in the rotating frame (at a frequency $\nu_o = (\gamma_H/2\pi)Bo$). The application of a 90^o pulse followed by a 90^o phase change of the B_{1H} field results in the spin-locking of the protons in this state. Packets of proton moments execute a precession around B_{IH}, and the Z components oscillate at a frequency ν_{1H}. The observed nuclei will now experience a field from a coherently averaged Z component of the proton moment, *i.e.* $\langle \mu_z^H \rangle = 0$, resulting in decoupling.

If $\nu_{1H} >> \Delta\nu_{HH}$, proton spin diffusion will not affect the decoupling.[16] To meet such a requirement decoupling fields of >40kHz must be used. The maximum decoupling field strength that could be applied was limited by the ability of the probe

circuit to sustain the power levels, without arcing, rather than by the performance of the rf amplifier. In practice, decoupling fields of 40-60kHz could be used on the CXP200 spectrometer, corresponding to proton 90^{o} pulse lengths of 4-6μs. For most samples analysed, a 50kHz decoupling field strength was used (proton pulse length 5μs, measured for a sample of silicone gum).

The effect of off-resonance proton decoupling on the ^{119}Sn N.M.R. linewidth of Ph_3SnMe has been investigated under CP/MAS conditions (see Figure 3.3). In the case when the decoupling field strength (ν_{1H}) and the local field in a static sample resulting from proton-proton dipolar interactions (ν_L) are in the regime where $\nu_{1H} >> \nu_L$, then the line-broadening due to off-resonance proton decoupling irradiation ($\Delta\nu$ORPI) is given by[10]

$$\Delta\nu(\text{ORPI}) \alpha (\Delta\nu_H)^2$$

where $\Delta\nu_H$ is the frequency offset from proton resonance. Figure 3.3a illustrates that the relationship between the irradiation frequency and the linewidth is approximately quadratic, for the sample and acquisition conditions considered.

3.6 Cross-Polarization

High-power decoupling can be utilized in solid-state N.M.R. in conjunction with cross-polarization (CP), in which abundant, I spin magnetization is transferred to less abundant S nuclear spins on a millisecond time scale.[16] This is accomplished by preparing the I spin system in a state of low spin temperature as performed by a spin-locking pulse. The

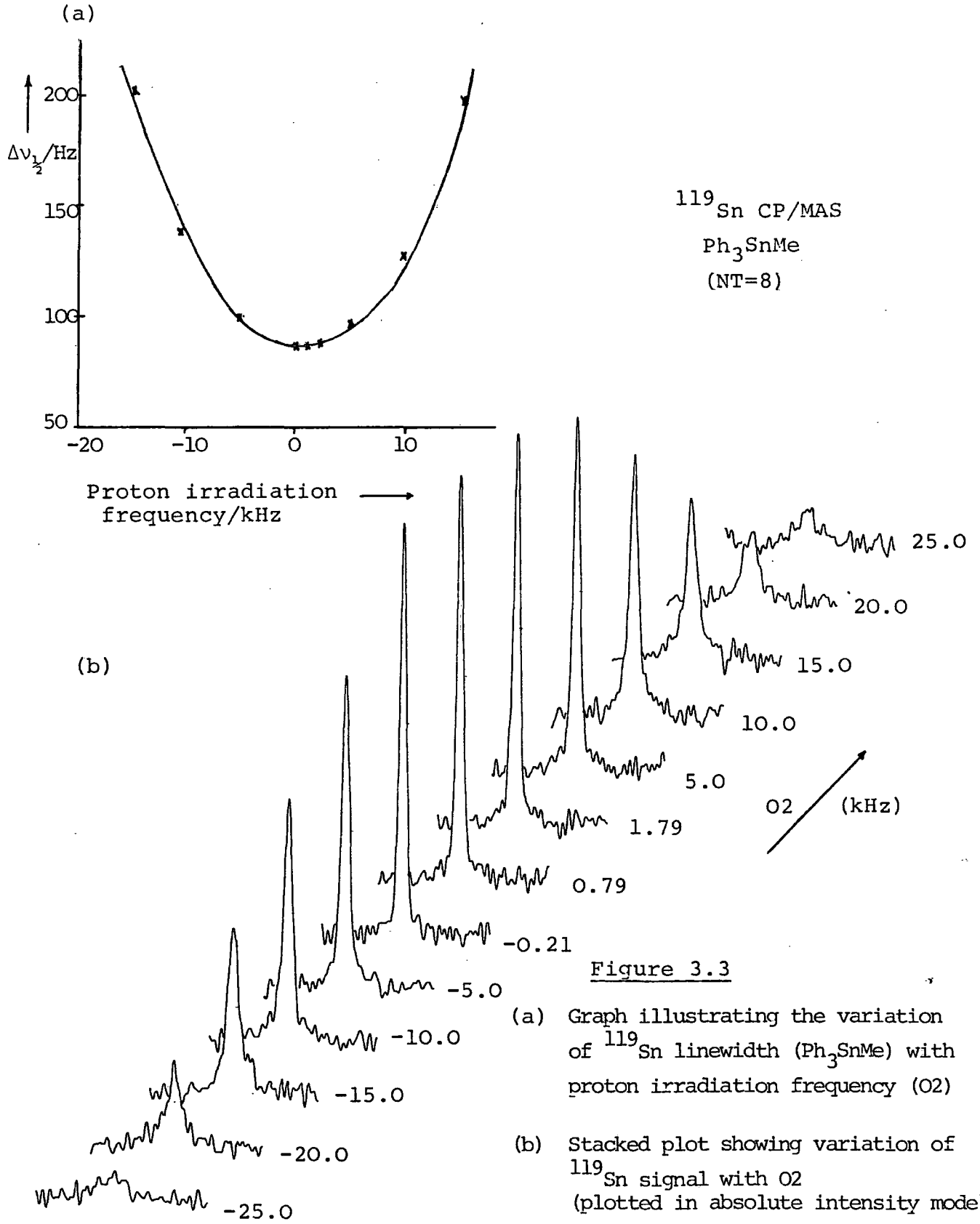

Figure 3.3

(a) Graph illustrating the variation of ^{119}Sn linewidth (Ph_3SnMe) with proton irradiation frequency (O2)

(b) Stacked plot showing variation of ^{119}Sn signal with O2 (plotted in absolute intensity mode)

less abundant S spins are then set in thermal contact with the I spins by applying a RF field under the Hartmann-Hahn condition[17]:

$$(\gamma/2\pi)B_{1S} = \nu_{1S} = \nu_{1I} = (\gamma_I/2\pi)B_{1I}$$

Under this condition, the I and S spins have Z components of their respective magnetic moments oscillating at the same frequency, and thereby experience a resonant perturbation. Thus, the two types of spins can cross-relax by energy conserving spin flips, with the cross-relaxation time T_{IS} dependent on the strength of the I-S dipolar coupling. This exchange of energy brings about a decrease in spin temperature and a consequent generation of S magnetization along B_{1C}. A S-spin FID follows the termination of the S-spin contact pulse, and is stored on a computer. During the acquisition time, the I spins are continually decoupled by the spin-locking field (see Figure 3.4). The CP sequence may then be repeated by waiting a period of *ca.* 5 T_{1I}. This time may be reduced by the use of a "flip-back" pulse sequence.[18] If the $T_{1\rho}$ of the I-spin is long compared to the CP time plus the acquisition time of the S-spin FID, then a substantial fraction of I-spin polarization remains at the end of each observation period. A 90°_{-x} pulse (reversed in phase with respect to the initial preparation pulse 90°_{x}) can be applied at the end of the spin-locking pulse. The I-spin magnetization remaining at the end of t_3 is flipped back along the static field, B_o. A small time-delay is then required for a full recovery of Mo_I along B_o before the process is repeated. (In this work, this was found to be $\sim T_{1H}$, although the delay

significantly depends on the rate of spin-locked ^{1}H magnetization, *i.e.* $T_{1\rho}^{-1}$). In any case, the use of flip-back will never decrease the S/N ratio, compared with the single contact experiment.

The S-spin magnetization established in the rotating frame after a single CP contact with Hartmann-Hahn matching, compared with that observable in the applied static field B_o after $\sim 5 \times T_{IS}$, is approximately (γ_I/γ_S).[16]

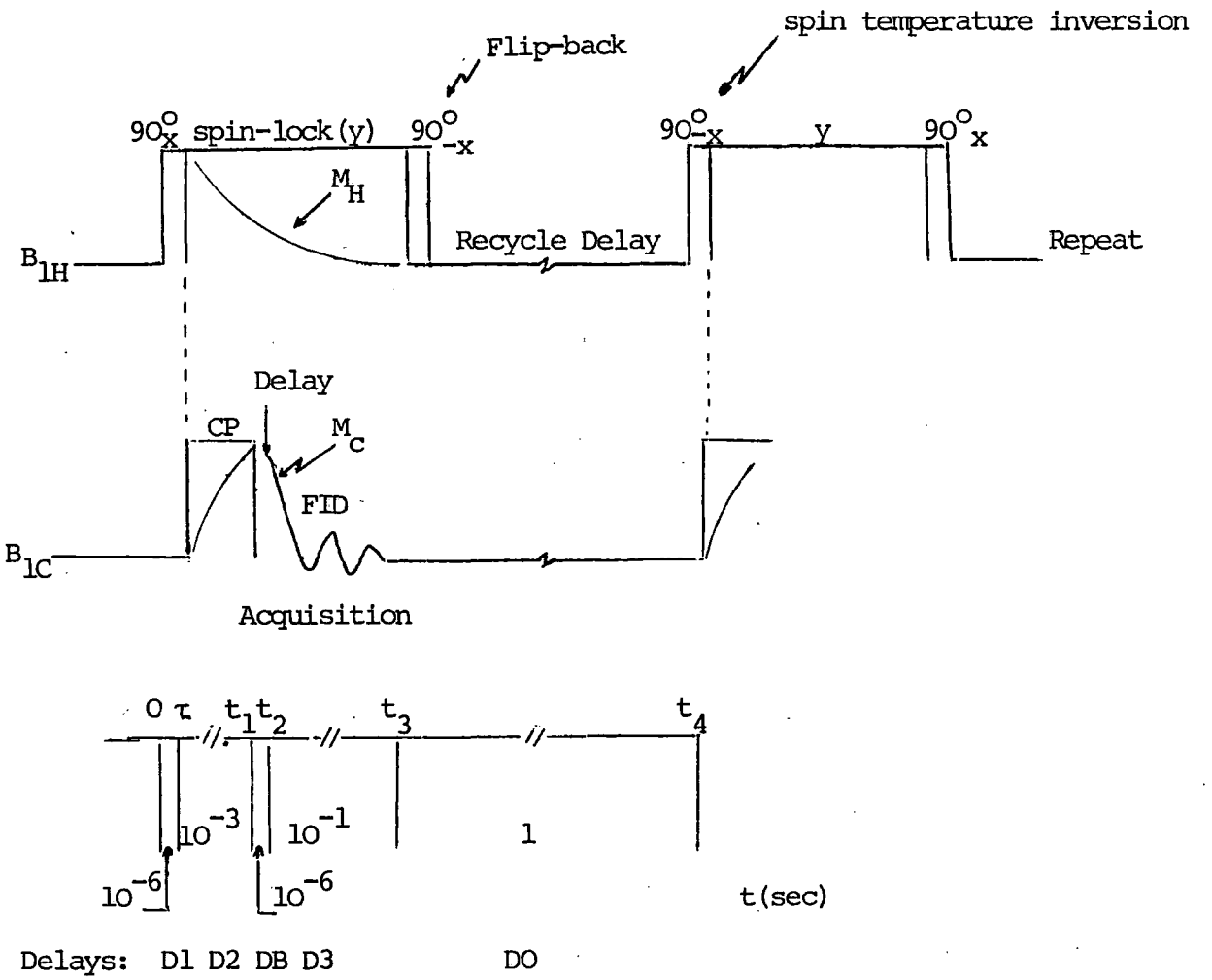

FIGURE 3.4 Single-contact cross-polarization (illustrated between carbon and hydrogen) RF pulse sequence incorporating flip-back and spin-temperature inversion, showing the time scales for parts of the sequence

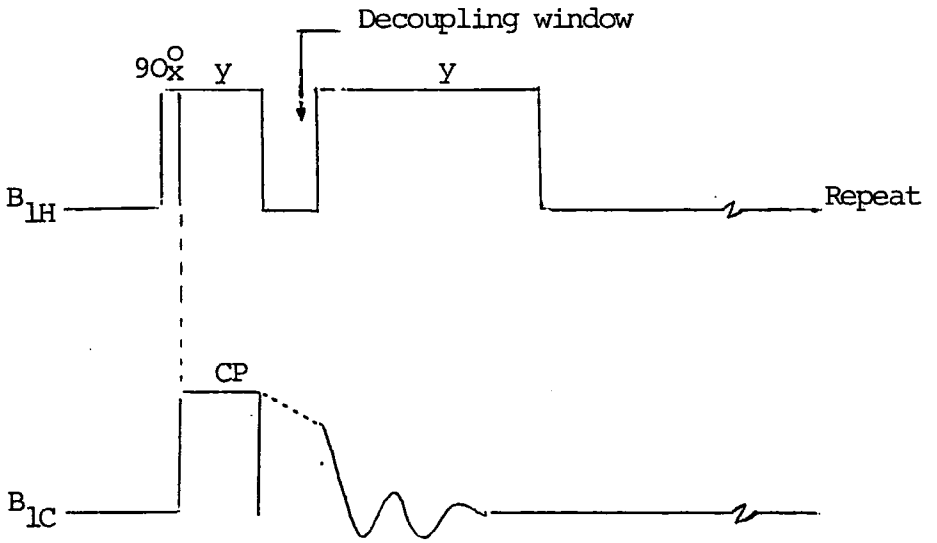

FIGURE 3.5 Non-quaternary suppression[20]

This CP pulse sequence incorporates a "window" (of *ca.* 40μs duration) in the proton decoupling before acquisition of the carbon FID commences. As a result, the spectrum retains only peaks due to quaternary carbons, by virtue of protonated carbons having strong (C,H) dipolar interactions, giving rise to a rapid decay of transverse magnetization. Quaternary carbons by the same token give relatively long T_2 relaxation. Methyl carbons also appear due to motion producing narrow lines.

A further gain in sensitivity (relative to the single pulse experiment) may be obtained by repeating the contact and observation period of the S-spins before re-establishing the I-spin polarization (if $T_{1\rho}$ is long enough). This method of multiple-contacts was generally not used because it required B_{1H} to be on for excessive lengths of time. Assignment of ^{13}C spectra may be assisted considerably by using a simple pulse sequence, non-quaternary suppression[20] (see Figure 3.5). In general this sequence will discriminate against S-spins with relatively short I-S distances.

The presence of artifacts in the FID, arising from the long rf pulse in the observed channel, can cause severe baseline problems, or even give rise to spurious peaks in the CP spectrum. Suppression of such unwanted signals can be obtained by spin temperature inversion.[19] If the phase of the 90^{o} pulse on the protons is shifted by 180^{o} during every other spin-lock sequence, then M_{o}^{H} will be spin-locked alternately parallel and anti-parallel to B_{1H}, making the corresponding proton spin temperature (T_{H}) positive and negative respectively (*cf.* usual situation of spins aligned with B_{o}). Then the S-spin temperature, which follows T_{H}, is also reversed every CP sequence; *i.e.* S-spin magnetization grows alternately parallel or antiparallel to B_{1C} in the S rotating frame. This shifts the phase of the ^{13}C FID by 180^{o} every CP sequence, even though the S-spin RF field retains the same phase. By alternately adding and subtracting the S-spin FID, RF transients are subtracted out, while the S-spin FIDS are coherently added.

In this work, cross-polarization was successfully applied to protonated systems containing the less abundant nuclei of ^{13}C, ^{31}P, ^{119}Sn and ^{195}Pt, utilizing flip-back (FB) and spin-temperature inversion (STI) techniques (see Figure 3.4). An important advantage of cross-polarization is that it allows one to use recycle times of the order of T_{1}^{H} instead of T_{1}^{S}, as in practice T_{1}^{S} is generally much longer than T_{1}^{H}. However, it has been found (see Chapter Five) that proton-containing platinum IV compounds, with directly bonded quadrupolar nuclei (*e.g.* Cl or N) attached, offer no such advantage.

The use of CP to obtain ^{13}C and ^{31}P spectra is well documented, as are the tuning techniques that apply. However, this is not the case for ^{195}Pt and ^{119}Sn CP/MAS N.M.R. The

major problem with studying such nuclei is the large shielding anisotropy present. Clearly a symmetrical molecule with an abundance of protons is desired. For ^{119}Sn CP/MAS N.M.R., the tuning compound chosen was Ph_3SnMe. A recycle delay time of 30s and a contact time of 1ms was found to be optimum, producing a single peak of reasonable S/N after a single scan. Figure 3.6a illustrates the variation of signal intensity against the contact time. The resultant graph (Figure 3.7a) shows the rapidity of both the decay of ^{1}H spin-locked magnetization and the cross-polarization rate.

The application of CP to ^{195}Pt MAS N.M.R. was found to be successful using $K_2[Pt(OH)_6]$. At first sight, this compound would appear to possess the necessary criteria to be suitable for tuning. However, the spectrum exhibits spinning sidebands, necessitating at least ten scans before any signal can be observed. The lack of a "single scan" compound drastically increases the duration of the Hartmann-Hahn matching procedure. The optimum contact time was found to be in the order of 1-2ms as shown by Figure 3.8. The conditions used for $K_2[Pt(OH)_6]$ in tuning the CXP spectrometer for ^{195}Pt CP/MAS NMR were a recycle delay of 2s and a contact time of 1ms. Although the slow decay of the ^{1}H magnetization (see Figure 3.7b) suggests more advantageous conditions could be applied, technical problems were often encountered (*e.g.* arcing) in using long contact times or multiple-contact pulse sequences.

The tuning procedures for a particular nucleus could be significantly reduced in time by noting the power outputs of the low frequency (RF) and high-power decoupling amplifiers when the Hartmann-Hahn condition was met. The criticalness

FIGURE 3.6

(a) Variation of ^{119}Sn signal (Ph_3SnMe) with contact time (ms)

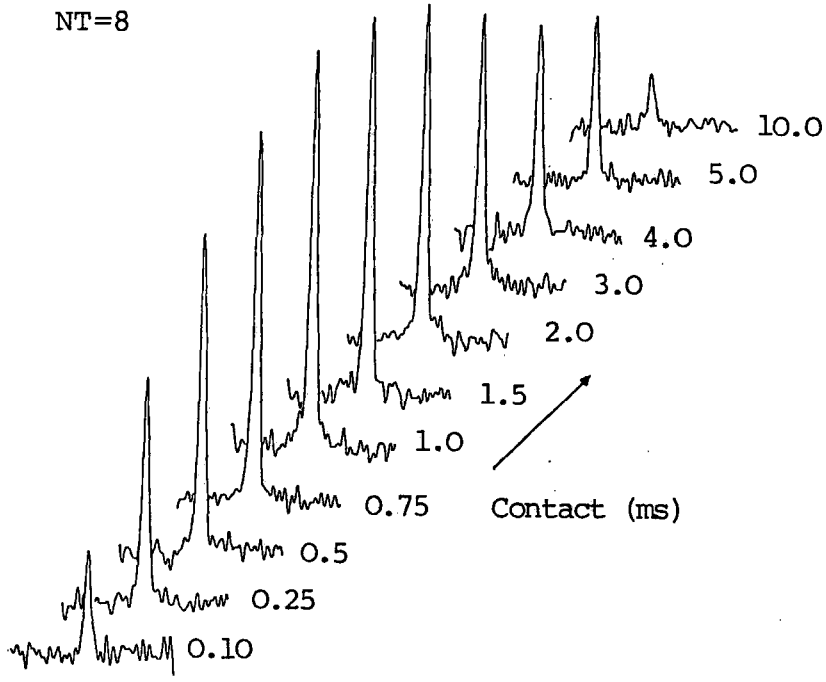

(b) Variation of ^{119}Sn signal (Ph_3SnMe) with rf gain

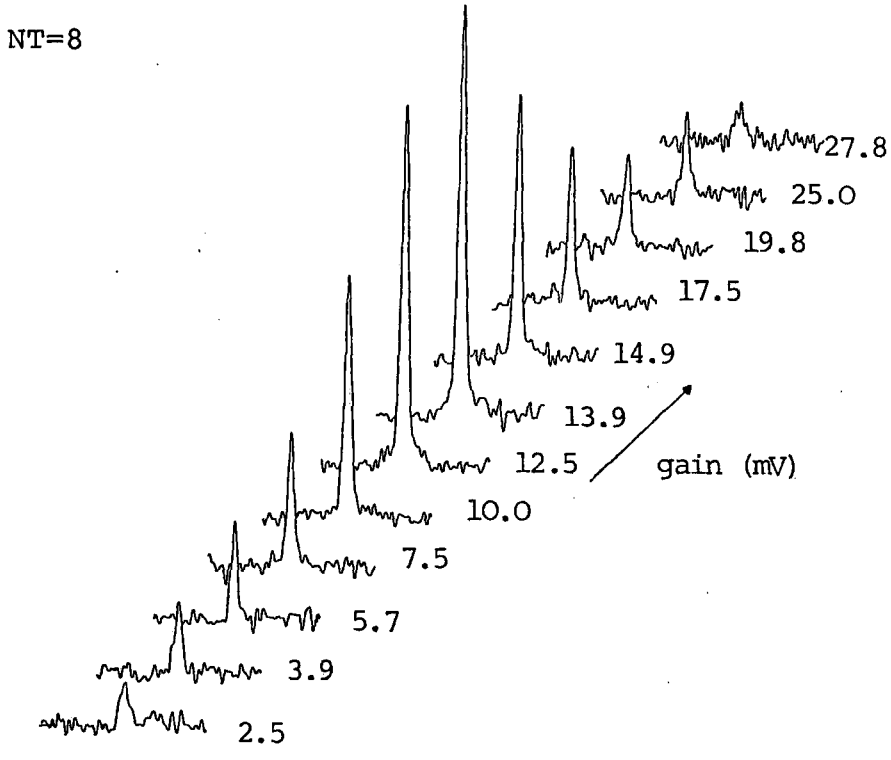

FIGURE 3.7 Graphical Illustrations of CP Signal Intensity with Contact Time

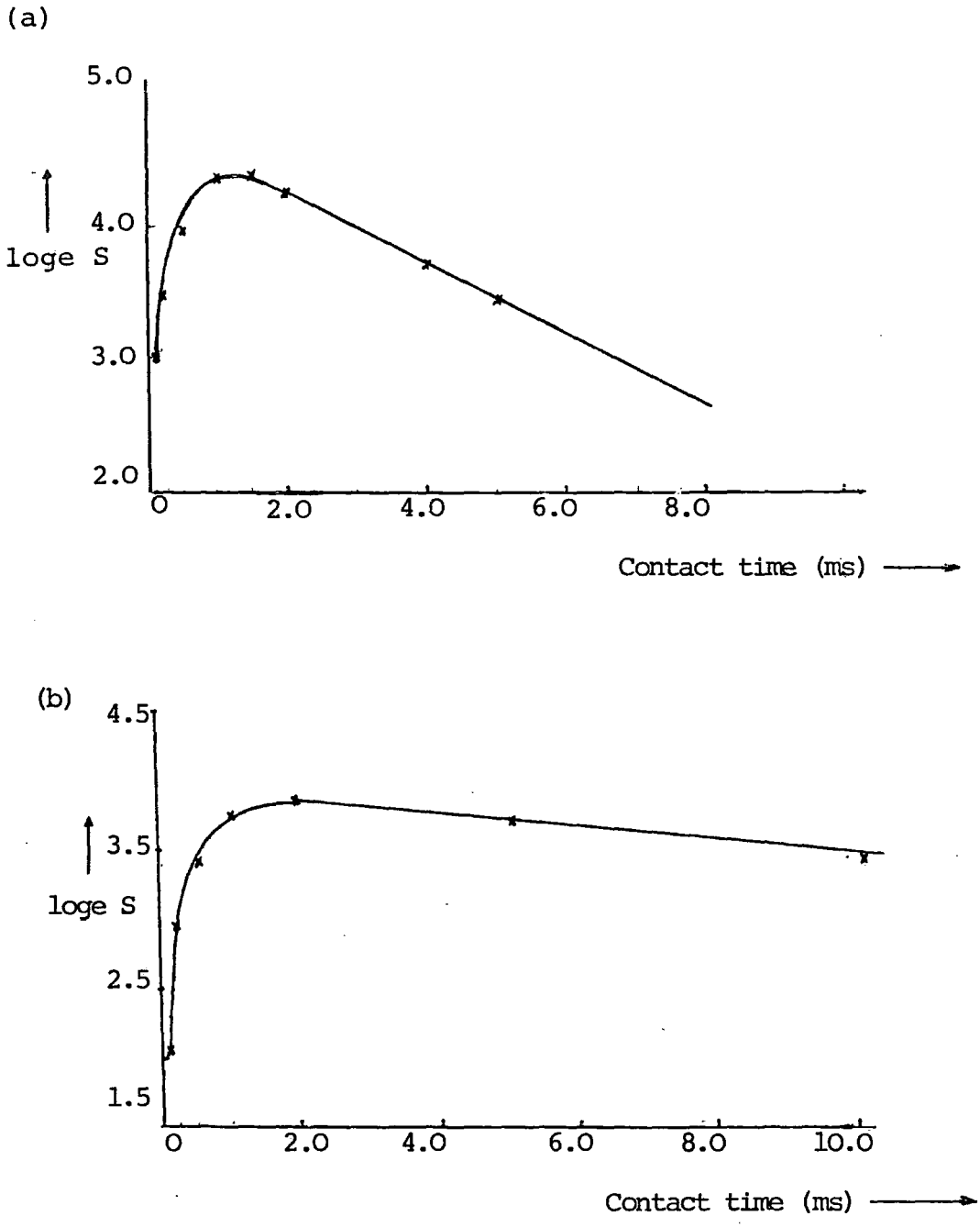

(a) ^{119}Sn CP/MAS spectra of Ph_3SnMe

(b) ^{195}Pt CP/MAS spectra of $K_2[Pt(OH)_6]$

FIGURE 3.8

^{195}Pt CP/MAS spectra of $K_2[Pt(OH)_6]$

Variation of signal intensity with contact time (ms)

NT=100

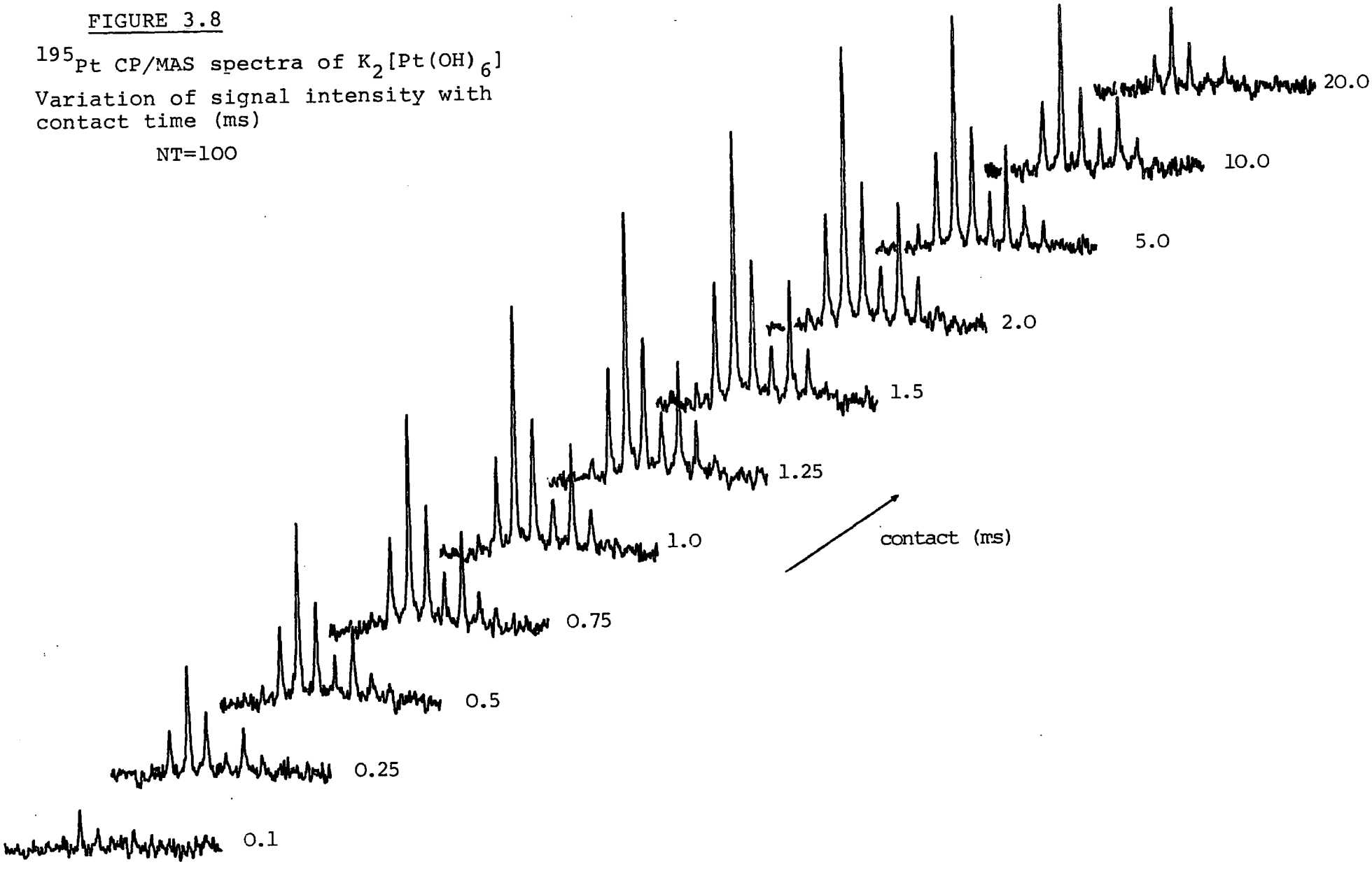

of the matching of the power levels is exemplified in Figure 3.6(b). It can be seen from this that a signal is still observed even with a substantial mismatch. However, the sensitivity of the signal intensity to the match tends to be crucial within 2mV of the low-frequency RF output, which corresponds to only a slight alteration in the RF gain control.

3.7 Sample Origins

The following samples were obtained from Johnson-Matthey Research Centre and used without further purification:

Pt(IV) compounds

$K_2[PtCl_6]$

$K_2[Pt(OH)_6]$

$Na_2[PtCl_6].6H_2O$

$[Pt(en)_3]Cl_4.2H_2O$ (en=ethylenediamine)

cis $[PtCl_4(NH_3)_2]$

trans $[PtCl_4(NH_3)_2]$

Pt(II) compounds

cis $[PtMe_2(PEt_3)_2]$

cis $[PtMe_2(PPh_3)_2]$

cis $[PtPh_2(PPh_3)_2]$

cis $[Pt(c\text{-}C_3H_5)_2(PPh_3)_2]$

$[PtCl_2(COD)]$

cis $[PtCl_2(nBu_3P)_2]$

trans $[PtCl_2(nBu_3P)_2]$

trans $[PtCl_2(PEt_3)_2]$

cis $[PtCl_2(PPh_3)_2]$

trans $[PtCl_2(PPh_3)_2]$

$[Pt(CBDCA)(NH_3)_2]$

The sample of *cis*-$[PtCl(SnCl_3)(PPh_3)_2]$ was prepared at Johnson-Matthey Research Centre during an industrial training period using a synthesis devised by Baird.[21]

The phosphaalkene, $[(Ph_3P)_2Pt(mesP{=}CPh_2)]$ was prepared and characterized by J.F. Nixon of Sussex University.

The following Tin compounds were received from P.Granger (Université de Rouen):

Ph_3SnCl

Ph_3SnMe

Ph_3SnBu^n

Ph_3SnEt

Me_3SnF

Other tin samples used in this work were supplied by the below-mentioned chemical companies:

Me_3SnOH)
) ALFA INORGANICS
Ph_3SnOH)

$(NH_4)_2SnCl_6$)
)
$(NH_4)_2SnF_6$) PILKINGTON BROTHERS LTD.
)
$(nBu)_3SnF$)

The sample of nBu_2SnCl_2 was kindly supplied by S. Matlin of City University.

REFERENCES - Chapter Three

1. I.J. Cox, Ph.D. Thesis, University of East Anglia, 1984.
2. C.J. Groombridge, Ph.D. Thesis, University of East Anglia,1983.
3. A. Kenwright, Ph.D. Thesis, University of East Anglia, 1985.
4. F.H.A. Rummens, Org.Mag.Res., 1970, (21), 209.
5. P.S. Pregosin, Coord.Chem.Rev., 1982, (44), 247.
6. I.M. Ismail, S.J.S. Kerrison and P.J. Sadler, Chem.Commun. (1980), 1175.
7. R.G.Kidd and R.J. Goodfellow, "NMR and the Periodic Table", Eds.R.K.Harris & B.E.Mann, Academic Press,New York,1978,p.250.
8. E.R. Andrew, Prog.N R Spectrosc. 1971 (8), 1.
9. R.K.Harris, "Nuclear Magnetic Resonance", Pitman, Longon,1983
10. D.L. Vanderhart, W.L. Earl and A.N. Garroway, J.Mag.Res. 1981, (44), 367.
11. J.S.Frye and G.E. Maciel, J.Mag.Res., 1982, (48), 125.
12. E.R. Andrew, A. Bradbury and R.G. Eades, Nature 1958 (182), 1659.
13. H. Kessemeier and R.E. Norberg, Phys.Rev., 1967, (155), 321.
14. A.Abragam, "The Principles of Nuclear Magnetism", Oxford University Press, London, 1967, p.98.
15. C.S. Yannoni, Acc.Chem.Res., 1982, (15), 201.
16. A. Pines, M.G. Gibby and J.S. Waugh, J.Chem.Phys., 1973, (59), 569.
17. S.R. Hartmann and E.L. Hahn, Phys.Rev., 1962, (128), 2042.
18. J. Tegenfeldt and U. Haeberlen, J.Mag.Res., 1979, (36), 453.
19. E.O. Stejskal and J. Schaefer, J.Mag.Res., 1975, (18), 560.
20. S.J. Opella and M.H. Frey, J.Amer.Chem.Soc., 1979, (101), 5854.
21. M.C. Baird, J.Inorg.Nucl.Chem., 1967, (29), 367.

CHAPTER FOUR

CARBON-13 AND PHOSPHORUS-31 CP/MAS NMR OF ORGANOPLATINUM COMPLEXES

4.1 Introduction

4.1.1 Carbon-13 Solid-State NMR

Since the development of cross-polarization and magic-angle spinning, first combined experimentally by Schaefer and Stejskal,[1] high-resolution solid-state ^{13}C NMR is rapidly becoming a routine and powerful analytical tool. The range of materials studied is vast and has been well documented by recent reviews.[2-8] Along with proton NMR, ^{13}C is the most common nucleus studied by solution and solid-state NMR spectroscopy due to its favourable properties.

However, the potential of ^{13}C solid-state NMR to probe organometallic complexes has yet to receive much attention. So far, a large amount of NMR studies concerning this type of compound has involved ^{31}P CP/MAS NMR (see below). However, valuable information can come from the investigation of ^{13}C solid-state spectra of attached organic ligands. This was first made evident by Maricq, Waugh and co-workers by the ^{13}C NMR study of two chromium (0) complexes.[9] In other work, Waddington and Jennings[10] have investigated the reaction of Zeise's dimer with compounds which all contain cyclopropane rings using ^{13}C CP/MAS NMR (see on).

This chapter is mainly concerned with the study of organo-Pt(II) complexes in which ^{13}C NMR has provided extra structural information regarding the geometry of the organic sites unobtainable from ^{31}P or ^{195}Pt NMR. The large number of carbon sites present in some compounds can lead to complexity in the spectra, although this can be reduced by the non-quaternary suppression technique (NQS - see Chapter Three) at

the expense of some loss of sensitivity. However, even with NQS, aromatic carbons may still appear broad due to motional modulation of the resonance frequency *via* the anisotropic chemical shift.[7] It is therefore non-aromatic carbons which tend to produce the most structural information through chemical shifts and ^{13}C-^{31}P/^{195}Pt scalar couplings.

4.1.2 Phosphorus-31 Solid-State NMR

Due to the attractive properties of the phosphorus-31 nucleus, (Natural abundance = 100%, spin-½, D^C = 377) ^{31}P solid-state NMR is becoming widely used to study a vast area of chemistry, biochemistry and medicinal problems.[11] There are few phosphorus environments in a molecule generally, rendering solid-state spectra easily interpretable. The chemical shift range is *c a.* 250 ppm. on the high frequency side to *c a.* 450 ppm. on the low frequency side of H_3PO_4, a total range of 700 ppm.[3] In addition to crystallographic and geometric information, anisotropic shielding tensor data is available for most phosphorus compounds. If the shielding anisotropy of the ^{31}P nucleus is considerably greater than the spinning rate, as tends to be the case at high fields, the anisotropy will not be averaged by MAR giving rise to significantly intense sidebands. A substantial amount of information regarding chemical shielding parameters has been obtained for solid calcium phosphates.[13-15] However, there have been no reports of shielding tensor data obtained for phosphorus-containing transition metal complexes.

^{31}P CP/MAS spectra have been obtained for a variety of triphenyl phosphine transition metal complexes.[18] The large chemical shift and large scalar couplings together with a sensitivity to electronic, steric and geometric arrangements makes it an ideal probe of the molecular and electronic structure of transition metal complexes. The compounds studied have included phosphine complexes containing Rhodium, Copper, Gold, Nickel, Palladium and Platinum.[16-20] As well as large solid-state scalar couplings being reported; dipolar coupling to the quadrupolar copper nucleus has also been observed.[16] Fyfe and co-workers have investigated a number of ^{31}P spectra of phosphorus-containing platinum(II) complexes,[18-20] and report on phosphorus-platinum coupling constants as well as non-equivalences only present in the solid-state.

The scope of this chapter will consider a ^{31}P NMR study of a series of square planar platinum(II) complexes including a discussion of shielding tensor parameters of which there has been no previous study for transition-metal complexes. A comparison between ^{31}P solution and solid-state results is also given. The possible change in structure on going from solid to solution-state is outlined by a study of a phospha-alkene where ^{31}P CP/MAS bridges the data from ^{31}P solution-state NMR and X-ray crystallographic data.

4.2 Indirect (Scalar) and Direct (Dipolar) Coupling

Platinum has four isotopes, one of which has a spin-½ nucleus (^{195}Pt) with a natural abundance of 33.8%; the other three isotopes have zero spin (I=0) nuclei. ^{13}C and ^{31}P NMR spectra of organoplatinum complexes should, in theory, exhibit "platinum satellites". These satellites are caused by a spin-½ nucleus (*e.g.* ^{31}P) coupling to the ^{195}P nucleus producing a doublet of separation $J_{^{31}P,\ ^{195}Pt}$. In addition, there will be a central peak arising from ^{31}P nuclei adjacent to the other 66.2% of platinum nuclei with zero spin, *i.e.*, no coupling takes place producing a single phosphorus resonance. The ratio of the lines in this characteristic pseudo triplet is therefore 1:3.9:1. The scalar coupling of Carbon-13 and Phosphorus-31 to Platinum-195 in the solution-state has been well documented by several authors.[21,22] In the solid-state, to date, there has only been a single report of ^{13}C-^{195}Pt 'J' coupling[11] and four cases of ^{31}P-^{195}Pt coupling.[18-20] In some cases, platinum satellites which would normally show up in solution-state spectra can be concealed under broad peaks or spinning side bands present in the spectrum. The magnitude of 'J' (^{195}Pt, ^{31}P) is known to be very sensitive to the nature of the *trans* ligand in square planar platinum(II) complexes,[21] and thus can provide a useful probe of the geometry of possible isomers present. Although not as widely studied as the ^{31}P, ^{195}Pt case, ^{13}C, ^{31}P coupling can be of similar use, with *trans*-^{2}J ^{13}C, ^{31}P across a platinum nucleus being around an order of magnitude greater than the *cis*-^{2}J ^{13}C, ^{31}P coupling constant.[21]

Dipolar coupling will also be present between spin-½ species present in these phosphorus-containing organoplatinum complexes. Calculations based on known magnetogyric ratios and internuclear distances indicate that ^{31}P, ^{195}Pt and ^{13}C, ^{195}Pt dipolar couplings are less than 1 kHz. For *cis*-(bisphosphine)platinum(II) complexes, ^{31}P-^{31}P dipolar couplings are around 0.5 kHz and *c a*. 2kHz for the ^{13}C, ^{31}P interaction. Therefore, spinning the solid samples at *c a*. 3kHz at the magic-angle effectively eliminates all these dipolar interactions unless there is interplay with larger interactions such as shielding anisotropy.

4.3 Solid-State ^{13}C NMR Characterization of the Anti-Tumour Drug: Platinum(II) Diammine 1,1-Cyclobutane-Dicarboxylate

Platinum-containing compounds are of considerable importance to the Johnson-Matthey Research Centre, and current interest centres in their potential as anti-tumour drugs. In the pharmaceutical area, full characterization is vital and is required by the DHSS for licences for clinical trials.

In the preparation of Platinum(II)Diammine 1,1-Cyclobutane-dicarboxylate ([Pt(CBDCA)$(NH_3)_2$]) an insoluble impurity was found to be associated with it. Elemental analysis of the impurity was consistent with the formulation [Pt(CBDCA)$(NH_3)_2]_n$ but due to its extreme insolubility further characterization proved difficult. The analysis and insolubility of this compound does, however, suggest the presence of a polymeric form

of [Pt(CBDCA)$(NH_3)_2$]. Solid-state ^{13}C NMR data has a high potential for characterizing such compounds; information on crystal structure, solid-state conformation and polymorphism, for example, is available.

A ^{13}C CP/MAS NMR spectrum has been previously obtained at low field (Bo = 2.1T) of pure [Pt(CBDCA)$(NH_3)_2$][11] and exhibits five peaks (see Table 4.1). This compound contains a cyclobutane ring and two carboxyl groups as shown below (Figure 4.1).

Fig. 4.1 [Pt(CBDCA)$(NH_3)_2$]

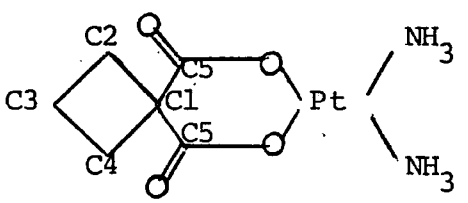

TABLE 4.1 ^{13}C CHEMICAL SHIFT DATA FOR PLATINUM(II) DIAMMINE 1,1-CYCLOBUTANECARBOXYLATE AND ASSOCIATED IMPURITY

Solid Shift (Bo = 2.1T) $\delta^{13}C$/ppm[a,d]	Solution Shift $\delta^{13}C$/Ppm.[b]	Solid Shift (Bo = 4.7T) $\delta^{13}C$/ppm[a,c]	Peak No. (Fig.4.3)
182.1	182.8	180.1	1
56.6	57.0	53.9	2
35.7	31.9	29.4	3
28.4			
16.8	16.8	14.2	4

a, Relative to TMS.

b, Relative to TMS, converted from dioxan reference using δ=67.4 ppm. for dioxan on TMS scale (Ref.23).

c, Chemical shifts of impurity [Pt(CBDCA)$(NH_3)_2]_n$

d, Reference 11.

The two carboxyl groups are crystallographically equivalent and give rise to a single peak at 182.1 ppm. which compares well with the solution-state value. The solid-state ^{13}C resonances of the C1 and C3 atoms (56.6 and 16.8 ppm.) also agree well with their solution-state values, however, C2 and C4 are crystallographically non-equivalent as shown by the two peaks at 35.7 and 28.4 ppm.

A full X-ray crystallographic analysis has been carried out on the pure compound[23] and shows that $Pt(NH_3)_2(CBDCA)$ is a square planar complex with the dicarboxylate chelate ring in the boat conformation and a planar cyclobutane ring (see Figure 4.2).

Figure 4.2 X-RAY CRYSTAL STRUCTURE OF PLATINUM DIAMMINE 1,1-CYCLOBUTANE DICARBOXYLATE[23]

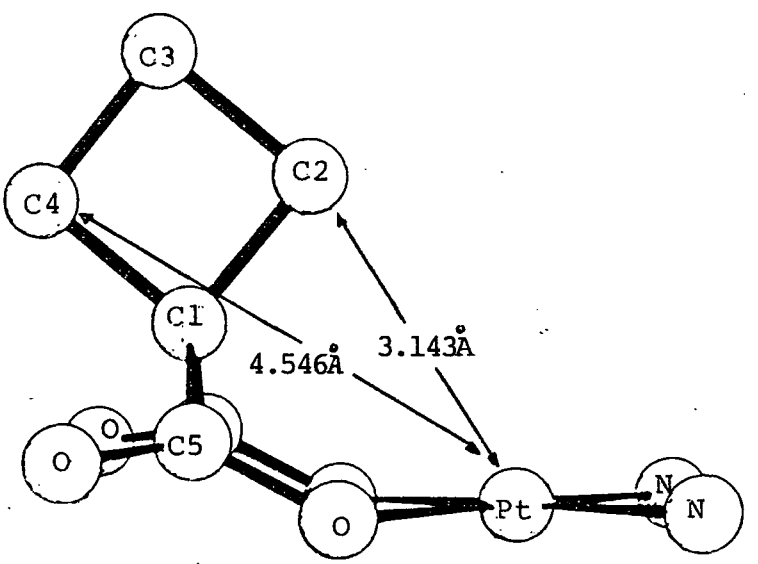

The molecule has all four cyclobutane atoms and the platinum atom placed on a mirror plane with the cyclobutane ring planar. The six-membered ring adopts a boat conformation

with the Cl and Pt atoms prow and stern out of the plane of the other four. This plane is at right angles to that of the cyclobutane ring. Thus, there is clearly an inequivalence of C2 and C4 shown by one of the carbon atoms approaching the position above the metal, while the other is on the outside of the molecule (see Figure 4.2). The distances from the platinum atom were calculated using the X-ray coordinates supplied by Neidle *et al.*[23]

The ^{13}C CP/MAS spectrum of the impurity $[Pt(NH_3)_2(CBDCA)]_n$, (Figure 4.3), shows a very similar pattern to that of the pure compound. In fact the spectrum is almost identical apart from the presence of a single resonance at 29.4 ppm. instead of two peaks. The slight, low frequency shift of 2-3 ppm. is present in all peaks compared to ^{13}C NMR data of the pure, solid compound and is thus attributable to chemical shift measurement inaccuracies. The ^{13}C spectral data obtained for this unknown product is consistent with the presence of 1,1 cyclobutanedicarboxylate with C2 and C4 carbons being equivalent as observed on the NMR timescale.

In solution, ring-flipping of the six-membered chelate ring takes place and causes the C2 and C4 atoms to be no longer 'seen' at a definite distance from the platinum atom. In the solid-state, such rapid conformational movement is very unlikely, and so the presence of a single resonance for C2 and C4 carbons can only mean a change in structure. The high insolubility and stability of the compound implies that the structure must be polymeric.[24]

FIGURE 4.3 ^{13}C CP/MAS spectrum of $[Pt(CBDCA)(NH_3)_2]_n$

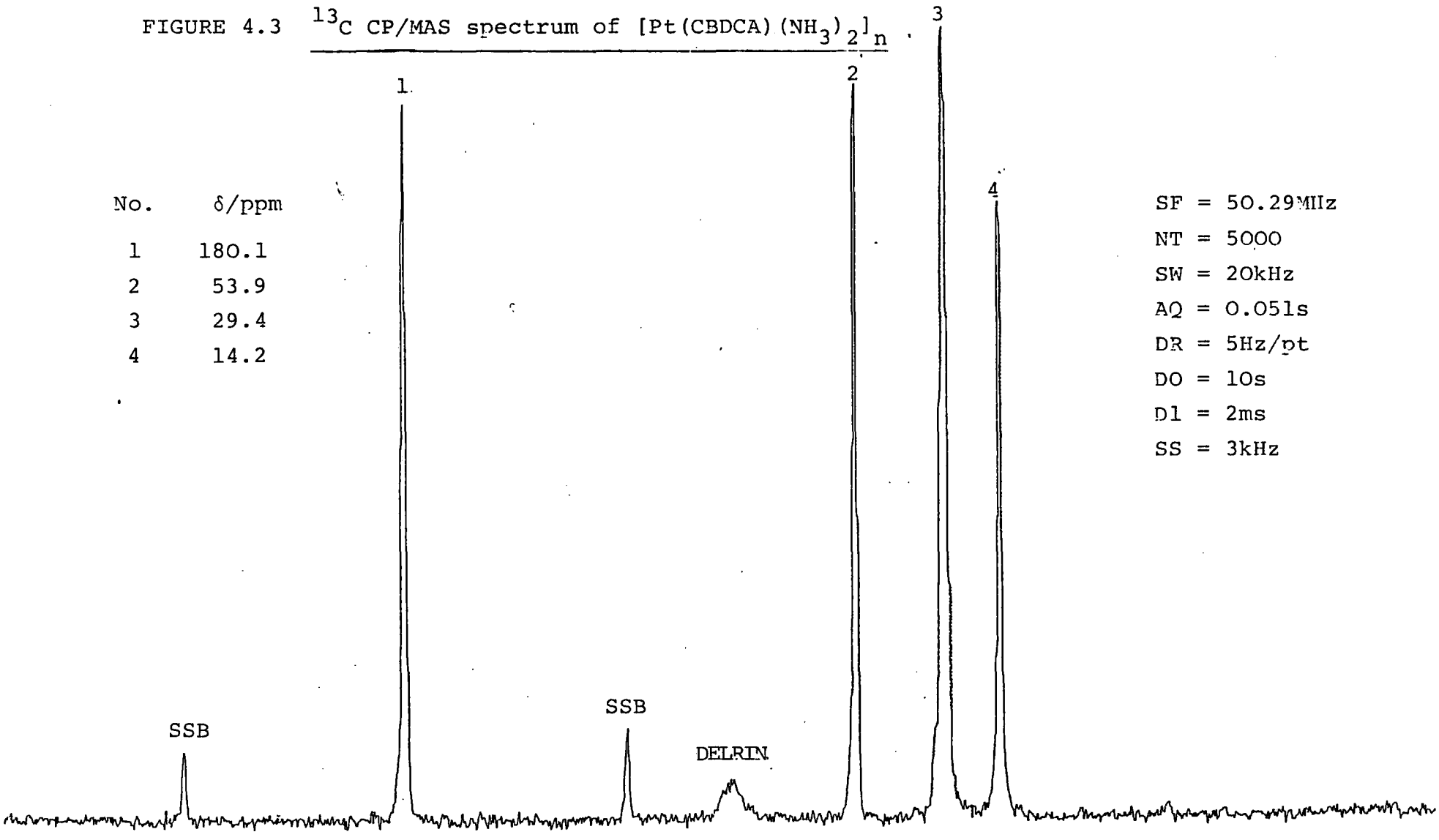

No.	δ/ppm
1	180.1
2	53.9
3	29.4
4	14.2

SF = 50.29MHz
NT = 5000
SW = 20kHz
AQ = 0.051s
DR = 5Hz/pt
DO = 10s
D1 = 2ms
SS = 3kHz

Figure 4.4 SUGGESTED STRUCTURE OF POLYMERIC FORM OF $[Pt(CBDCA)(NH_3)_2]$

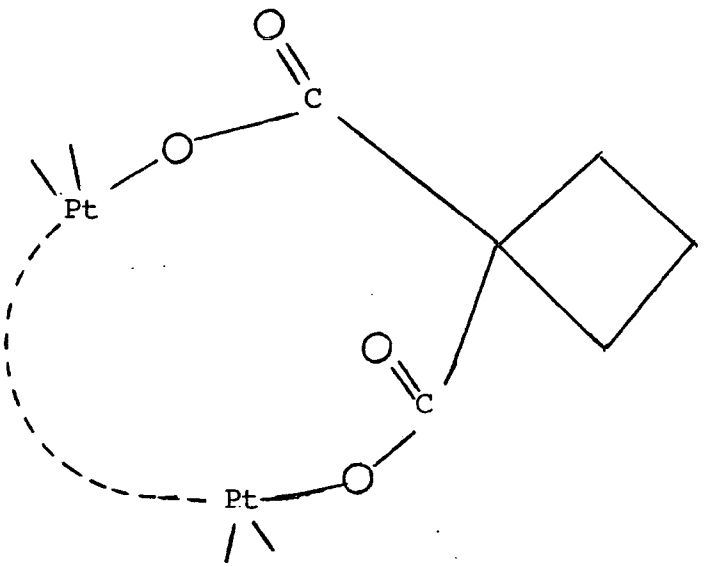

The structure of the polymer $[Pt(CBDCA)(NH_3)_2]_n$ is thought to be units of the monomer $[Pt(CBDCA)(NH_3)_2]_n$ with a platinum-oxygen bond 'broken' so that the platinum atom can attach itself to another $[Pt(NH_3)_2(CBDCA)]$ unit, (see Figure 4.4). The C2 and C4 carbons are thus rendered equivalent in the polymer lattice due to the relatively long distance away from the platinum atom, and also the lack of restraint on the cyclobutane ring caused by the amorphous nature of the compound. This amorphous property also makes any X-ray crystallographic studies impossible.

4.4 Dichloro(1,5-Cyclooctadiene)Platinum(II), $[PtCl_2(COD)]$

Dichloro(1,5-cyclooctadiene)platinum(II) has been used frequently for the synthesis of various platinum complexes by ligand substitution reactions. The central platinum atom is

bonded to two chlorine atoms and also the two olefin bonds of the cyclooctadiene ring (see Figure 4.5).

Figure 4.5 DICHLORO(1,5-CYCLOOCTADIENE)PLATINUM(II)

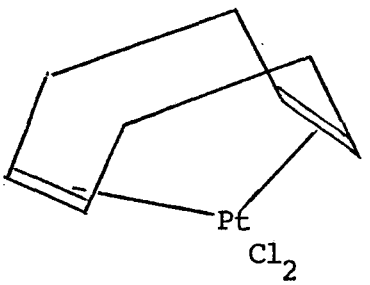

The ^{13}C CP/MAS spectrum, obtained at 22.633 MHz, shows two broad, featureless peaks due to the two different types of carbon present (see Figure 4.6); the most intense peak at 32.9 ppm. being due to the aliphatic carbons and the broad resonance at 103.8 ppm due to the four olefin carbons. The latter peak also gives rise to spinning side bands (with one side band concealed under the aliphatic peak) due to some anisotropy present. The ^{13}C solution-state spectrum (see Figure 4.7) gives the same information with, of course, much greater resolution. Taking into account solid-state line-widths, the chemical shifts are the same in both spectra showing there to be no major structural change on going from solution to solid-state. Platinum satellites are present in the solution-state spectrum, (peaks 2 & 4) due to coupling between the olefin carbons and the platinum nucleus ($J_{C,Pt}$=153Hz); this would be concealed in the solid-state spectrum due to the broad linewidth.

FIGURE 4.6 ^{13}C CP/MAS spectrum of $[PtCl_2)COD)]$

(low-field, solid-state)

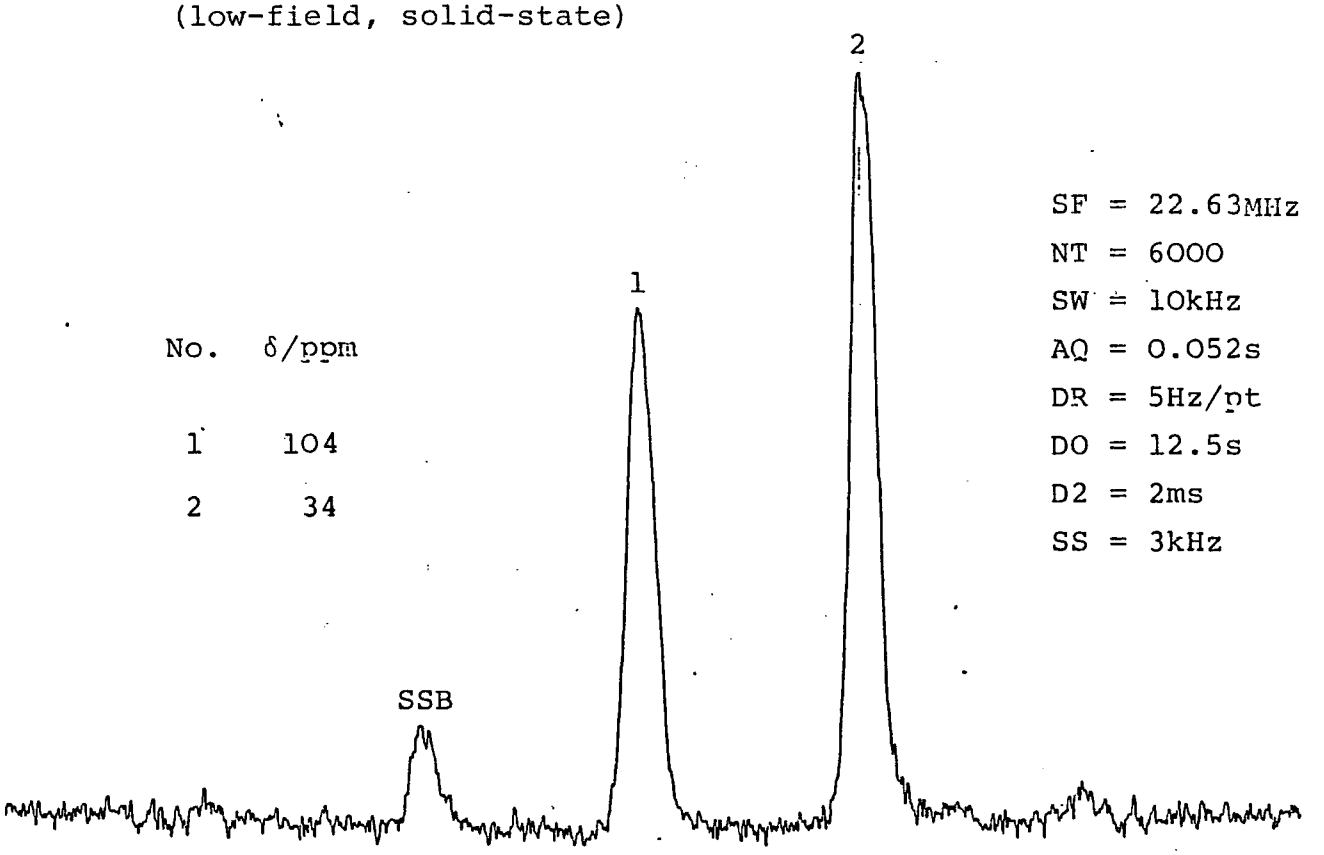

No.	δ/ppm
1	104
2	34

SF = 22.63MHz
NT = 6000
SW = 10kHz
AQ = 0.052s
DR = 5Hz/pt
DO = 12.5s
D2 = 2ms
SS = 3kHz

FIGURE 4.7 ^{13}C Solution-state Spectrum of $[PtCl_2(COD)]$

(SF = 25MHz)

No.	δ/ppm
1	101
2	31

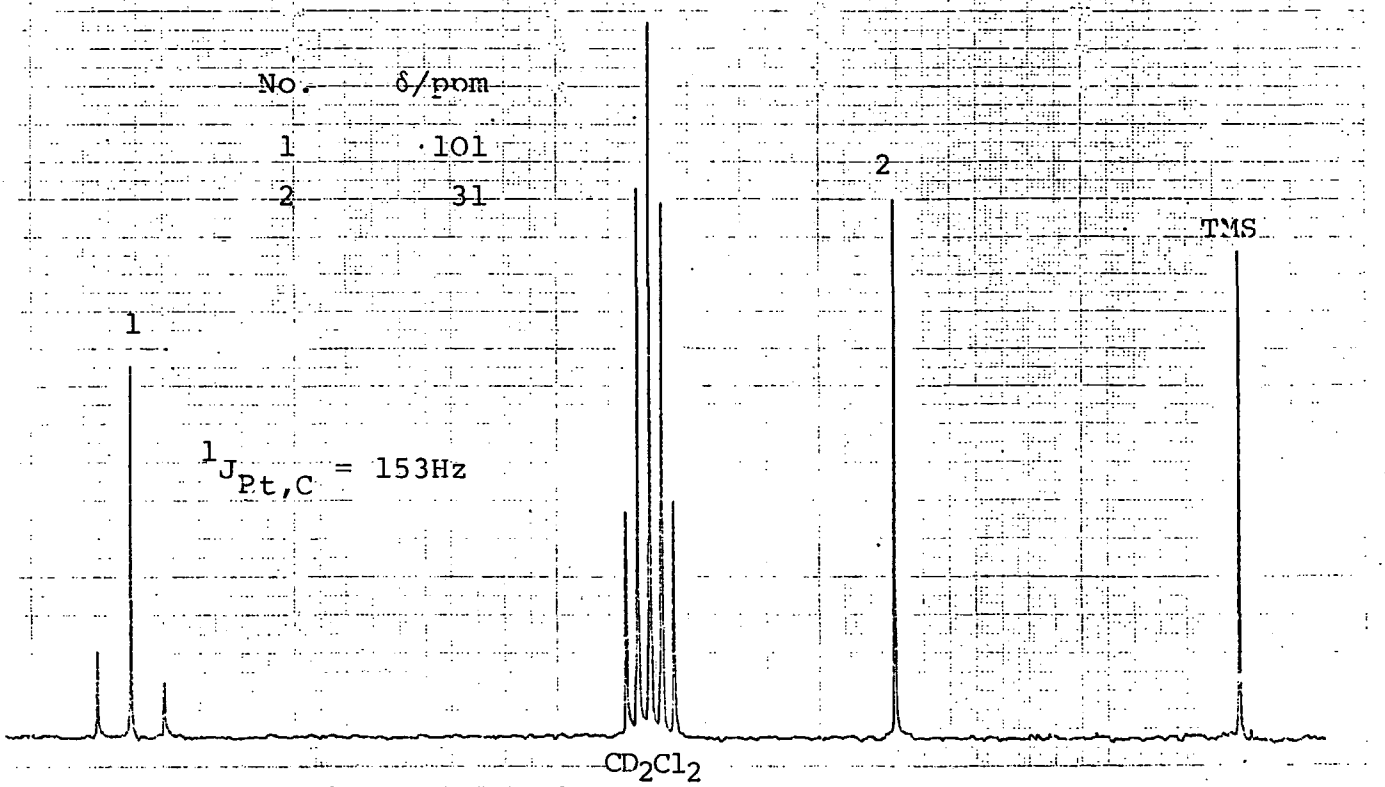

The ^{13}C solution-state NMR spectrum has also been obtained for the free ligand, 1,5-cyclooctadiene.[25] Two resonances were recorded for the aliphatic and olefin carbons appearing at 28.2 ppm. and 128.5 ppm. respectively. The low frequency shift of *c a*. 25 ppm. shows the shielding effect of the olefin carbon bonds complexing to the platinum. A report concerning this effect has also been made by Waddington and Jennings,[10] using ^{13}C CP/MAS NMR, in which the solid and solution-state ^{13}C NMR were obtained for dichloro(norbornadiene)-platinum(II). The olefinic resonance appears at 78 ppm. which is a low frequency shift of 63 ppm. on coordination to platinum, since the olefinic resonance for uncomplexed norbornadiene is at 141 ppm. The solid-state ^{13}C spectrum exhibits only broad bands for each type of carbon and no fine structure is seen.

The broadness of the peaks in the 22.63 MHz, ^{13}C CP/MAS spectrum of $[PtCl_2(COD)]$ does suggest some splittings due to crystallographic inequivalences could be concealed. Any dipolar interaction with the chlorine atoms present would be very small due to the interatomic distances involved. A high field ^{13}C spectrum obtained, operating at 50.29 MHz, reveals some interesting fine structure related to the crystal structure (see Figure 4.8). Each of the broad peaks has been split into four, with peak 7 having a relative intensity of two. There appear to be two explanations for these results. Firstly, there could be four crystallographically independent molecules per unit cell, or secondly, asymmetry induced in the solid-state, rendering each of the aliphatic and olefin carbons within each molecule inequivalent. The latter explanation is

FIGURE 4.8 ^{13}C CP/MAS spectrum of Solid $[PtCl_2(COD)]$

(High-field, SF = 50.29MHz)

Conditions as for Fig. 4.6

Peak No.	δ/ppm
1	102.8
2	102.0
3	99.1
4	95.3
5	32.2
6	29.8
7	26.4

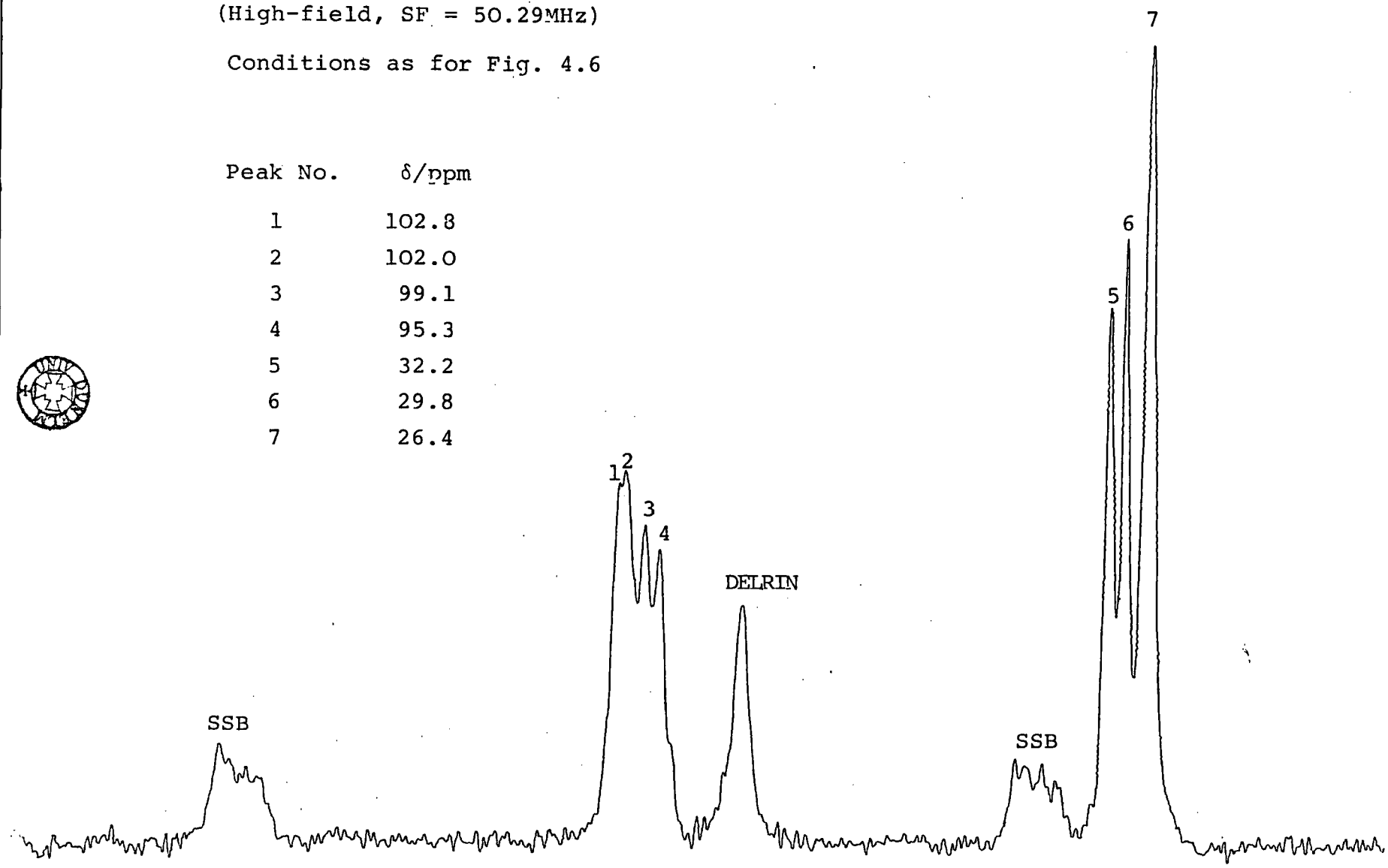

most likely as there would certainly be some distortion in the cyclooctadiene ring caused by the bonding to the platinum; this effect would be motionally averaged in the solution state.

The X-ray structure of this compound has been obtained, space group $P2_12_12_1$(orthorhombic),[26] (see Figure 4.9). The data shows that both the chlorine atoms are at normal distances from the central platinum (2.322 and 2.299 Å) suggesting equivalent double bonds to the platinum, close examination reveals several geometric deformations.

Figure 4.9 X-RAY CRYSTAL STRUCTURE OF DICHLORO-(1,5-CYCLOOCTADIENE)PLATINUM(II).[26]

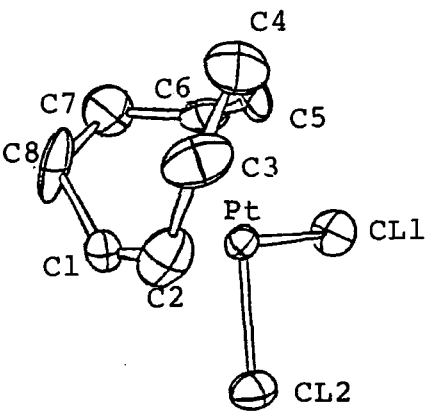

The most pronounced deformation has been observed in the bonding distances of C_5-Pt[2.209Å] *vs.* C_6-Pt[2.156Å], indicating a slipping of the C_5=C_6 bond axis with respect to $PtCl_2$. Compared to this, only a small variation in the bonding distances of C_1-Pt and C_2-Pt [2.215 *vs.* 2.203Å] has been observed. This geometric deformation of the cycloocta-

diene ring caused by the asymmetrical bonding of the olefin bonds to the platinum results in a lack of symmetry over the whole ligand , thus creating four crystallographically non-equivalent olefin and aliphatic carbons. It is impossible, therefore, to assign any of the carbon atoms belonging to the aliphatic or olefin groups to any peak in each of the "quartets".

4.5 Discussion of Solid- and Solution-State ^{31}P Chemical Shifts and ^{31}P-^{195}Pt Coupling Constants

Phosphorus-31 chemical shifts for square-planar platinum(II) phosphine complexes have been well documented in the solution-state.[21] An early solution-state NMR study of *cis* and *trans* tertiary phosphine complexes of platinum(II), by Grim, Keiter and McFarlane, produced some chemical shift data which agrees well with this work.[27] (A negative convention for chemical shift measurements was used however).

As can be seen from Table 4.2.1, the experimental solution and solid-state shifts compare very well indicating no change in structure and only slight effects from solvation and temperature differences. Due to motional averaging in solution the two phosphine ligands in the *cis* and *trans* isomers give rise to a single resonance as has been observed in all the ^{31}P solution-state spectra. In the solid-state, the ^{31}P spectra show a high sensitivity to crystallographic effects with most spectra exhibiting more than one non-equivalent site.

The solid and solution state, phosphorus-platinum coupling constants compare very well reflecting a consistent geometric arrangement of the two phosphine ligands in the square

TABLE 4.2.1 SOLID AND SOLUTION STATE ^{31}P NMR DATA FOR PLATINUM(II) PHOSPHINES

No.	Compound	SOLID		SOLUTION		
		$\delta_{^{31}P/ppm}$ [a,b]	$^{1}J_{P,Pt/Hz}$ [b]	$\delta_{^{31}P/ppm}$ [c,d]	$^{1}J_{P,Pt/Hz}$ [d]	Solvent
1.	*cis*-$[PtMe_2(PEt_3)_2]$	10.3	1905	9.7	1865	CD_3CN
		11.7	1827			
2.	*cis*-$[Pt(\underline{C}\text{-}C_3H_5)_2(PPh_3)_2]$	22.2	1796			
		26.6	2123	insufficiently soluble		
		29.0	2018			
3.	*cis*-$[PtMe_2(PPh_3)_2]$	26.1	1817	insufficiently soluble		
		29.3	1978			
4.	*cis*-$[PtPh_2(PPh_3)_2]$	15.4	1756	18.35	1763	CH_2Cl_2
		20.4	1805			
5.	*trans*-$[PtCl_2(PEt_3)_2]$	13.1	2393	12.2	2397	CH_2Cl_2
6.	*cis*-$[PtCl_2(nBu_3P)_2]$	4.1	3514	0.5	3508	CH_2Cl_2
		5.2	3496			
7.	*trans*-$[PtCl_2(nBu_3P)_2]$	5.8	2420	4.5	2385	CH_2Cl_2
8.	*cis* $[PtCl_2(PPh_3)_2]$	7.6	3587			
		11.0	3881	14.3[e]	3673[e]	$CDCl_3$
		12.4	3723			
9.	*trans* $[PtCl_2(PPh_3)_2]$	17.7	2555			
		19.6	2594	19.8[e]	2637[e]	$CDCl_3$
		21.6	2611			

a. Chemical shift, measured in ppm, relative to external reference, 85% H_3PO_4.

b. Digitization rate 17Hz/Pt.

c. Chemical shift, measured in ppm, relative to external reference, 85% phosphoric acid-d_3/D_2O.

d. Digitization rate, 10Hz/Pt.

e. L. Benni, H.C. Clark, J.A. Davies, C.A. Fyfe and R.E. Wasylishen, J.A.C.S. 1982, 104, 438.

planar complexes. In both of the isomeric pairs, $[PtCl_2(nBu_3P)_2]$ and $[PtCl_2(PPh_3)_2]$ the ^{195}Pt-^{31}P coupling constant in the *cis* isomer is significantly larger than the coupling constant in the *trans* isomer. It was Piddock, Richards and Venanzi who first reported this significant difference between *cis* and *trans* tertiary phosphine complexes of platinum(II).[28] This difference was regarded as being due to the increased π bonding between the phosphorus and platinum in the *cis* isomer, in which the platinum can use the dxy, dxz and dyz orbitals, while the *trans* isomer can use only the dxz and dzy orbitals (with the x axis defined as the P-Pt-P direction). Moreover, one would expect the phosphorus atoms to have a higher electron density than those in the *trans* isomer because of increased back donation by the electrons of platinum d orbitals (see Figure 4.10).

FIGURE 4.10 The two *trans* groups compete for dπ density on the metal

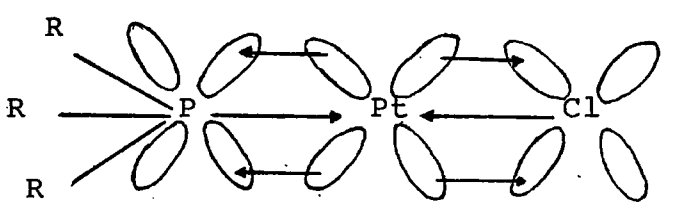

This difference between the coupling constants of the *cis* and *trans* isomers is noted to be largest when the anionic ligands have a low π bonding capacity, as is the case for the chloride.[28] Furthermore, the chemical shift of the isomer is always to lower frequency than the *trans* isomer due to an increased electron density surrounding the phosphorus atoms which is in accordance with simple shielding concepts. The importance of π-bonding

in these platinum(II) complexes can be further demonstrated by considering the Pt-P coupling constants of the alkyl phosphines (see Table 4.2.2). One would expect the Pt-P coupling constant of *cis*$[PtCl_2(PR_3)_2]$ (R=Et,Ph) to be less than the corresponding methyl derivative, because of σ inductive effects. That is, the electronegativity of Cl would strengthen the Pt-Cl bond and weaken the Pt-P bond. As both Cl and Me have very small π-acceptor capacities,[29] these results can only be explained in terms of π-bonding, where the chloride is a very strong π-donor.

TABLE 4.2.2 PLATINUM-PHOSPHORUS COUPLING CONSTANTS OF Pt(II) COMPLEXES OF THE TYPE *CIS*$[PtX_2(PR_3)_2]$

	X	R	$^1J_{P,Pt}$/Hz	
SOLUTION-	Me	Et	1865	
STATE	Cl	Et	3520	(Reference 27)
SOLID-	Me	Ph	1978, 1817	
STATE	Cl	Ph	3723, 3881, 3589	

4.6 Phosphorus-31 shielding tensor study

In the solid-state, the chemical shift is dependent on the orientation of the molecule in the magnetic field and the three dimensional shielding of the nucleus may be determined, which can give much more information regarding structure and bonding than can be obtained in solution. Clear trends in individual tensor components may be observed, from the studies of closely related compounds, which would normally be obscured by motional averaging in solution. Using spinning sideband

analysis,[30] the principal elements of the ^{31}P shielding tensor have been determined for a series of tertiary phosphine complexes of platinum(II), (see Table 4.3). The first point to note is that all of the shielding anisotropy values[1] are negative and are of similar magnitude, indicating no dramatic change in the expected coordination and molecular structure. Secondly, all the compounds exhibit non-axial symmetry ($\eta>0$), as would be predicted from the lack of symmetry present in these square planar complexes. A graphical portrayal of the ^{31}P shielding tensor components readily reveals a greater range of tensor shifts compared to the isotropic shifts (see Figure 4.11).

FIGURE 4.11 Graphical Representation of ^{31}P Shielding Tensor Components

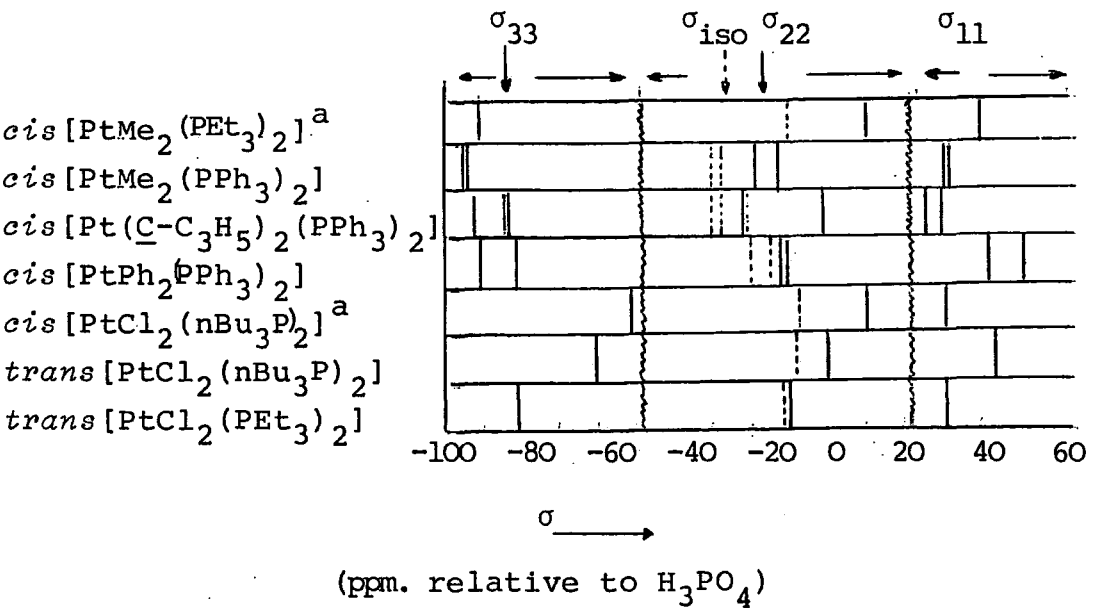

(a). Average isotropic chemical shift indicated.

A clear example of this range can be seen in comparing the *cis* and *trans* isomers of $[PtCl_2(nBu_3P)_2]$. The isotropic chemical shifts show a difference of only *c a.* 1 ppm. between the two isomers, which is rather misleading considering the

TABLE 4.3 PHOSPHORUS-31 SHIELDING TENSOR DATA

No.	COMPOUND	SPINNING[a] SPEED/Hz	/ppm. σ_{iso}[b]	σ_{33}[d]	σ_{22}[d]	σ_{11}[d]	δ	η
1.	*cis*-$[PtMe_2(PEt_3)_2]$[c]	2525	-10.3 -11.7	-89.0	13.2	42.8	-78.0	0.38
2.	*cis*-$[Pt(\underline{C}\text{-}C_3H_5)_2(PPh_3)]$	2487	-22.2 -26.6 -29.0	-91.5 -84.2 -85.9	0.3 -23.1 -26.1	24.6 27.6 25.0	-69.3 -57.6 -56.9	0.35 0.88 0.90
3.	*cis*-$[PtMe_2(PPh_3)_2]$	2530	-26.1 -29.3	-95.3 -96.1	-13.3 -20.3	30.3 28.5	-69.2 -66.8	0.63 0.73
4.	*cis*-$[PtPh_2(PPh_3)_2]$	2330	-15.4 -20.4	-82.6 -89.3	-12.0 -13.5	48.5 42.0	-67.2 -68.9	0.90 0.81
5.	*trans*-$[PtCl_2(PEt_3)_2]$	2670	-13.1	-80.7	-9.7	51.1	-67.6	0.90
6.	*cis* -$[PtCl_2(nBu_3P)_2]$[c]	2612	-4.1 -5.2	-52.4	9.4	28.9	-47.7	0.41
7.	*trans*-$[PtCl_2(nBu_3P)_2]$	1880	-5.8	-61.6	0.9	43.3	-55.8	0.76

a. Spinning speed chosen to maximize the number of sidebands without confusion taking place with satellites.

b. The shielding values are measured in ppm. relative to 85% H_3PO_4. For chemical shifts on the δ scale the signs should be reversed.

c. Due to incomplete resolution of lines, the average isotropic chemical shift and average height of each pair of sidebands is used in the analysis of the spectrum.

d. Haeberlen convention used, $|\sigma_{33}-\sigma_{iso}| > |\sigma_{11}-\sigma_{iso}| > |\sigma_{22}-\sigma_{iso}|$

different structures. The principal tensor components, however, are quite different indicating a marked variation in structure. It must be noted that it is generally not possible to relate the principal tensor values to the molecular axis system from the spectrum alone. A close examination of the alkyl platinum phosphines discloses only a slight variation in σ_{33} values. There is, however, a small increase in σ_{33} for the alkyl-triphenylphosphines on increasing the size of the alkyl group. This would be consistent with bulky groups causing more screening, and shows the sensitivity of the experiment. It is difficult to conclude more precise information regarding the ^{31}P shielding tensors without full single-crystal studies. Although, they do provide a much more complete basis on which to construct structure relationships than do the isotropically averaged solution data.

4.7 *Cis*-dimethyl bis(triethylphosphine)platinum(II), $[PtMe_2(PEt_3)_2]$

As with all the tertiary phosphine platinum(II) complexes, there are 3 spin-½ nuclei, excluding ^{1}H, which may be studied on the solid-state using CP/MAS NMR to obtain an overall picture of molecular and crystallographic structure (^{13}C, ^{31}P and ^{195}Pt). However, it is not always possible to obtain a solid-state ^{195}Pt spectrum due to shielding anisotropy problems (see Chapter Five). *Cis* dimethyl(bis-triethylphosphine)-platinum(II) (see Figure 4.12) is one of the compounds that such an overall NMR study has been achieved.

FIGURE 4.13. ^{13}C CP/MAS spectra of *cis*$[PtMe_2(PEt_3)_2]$

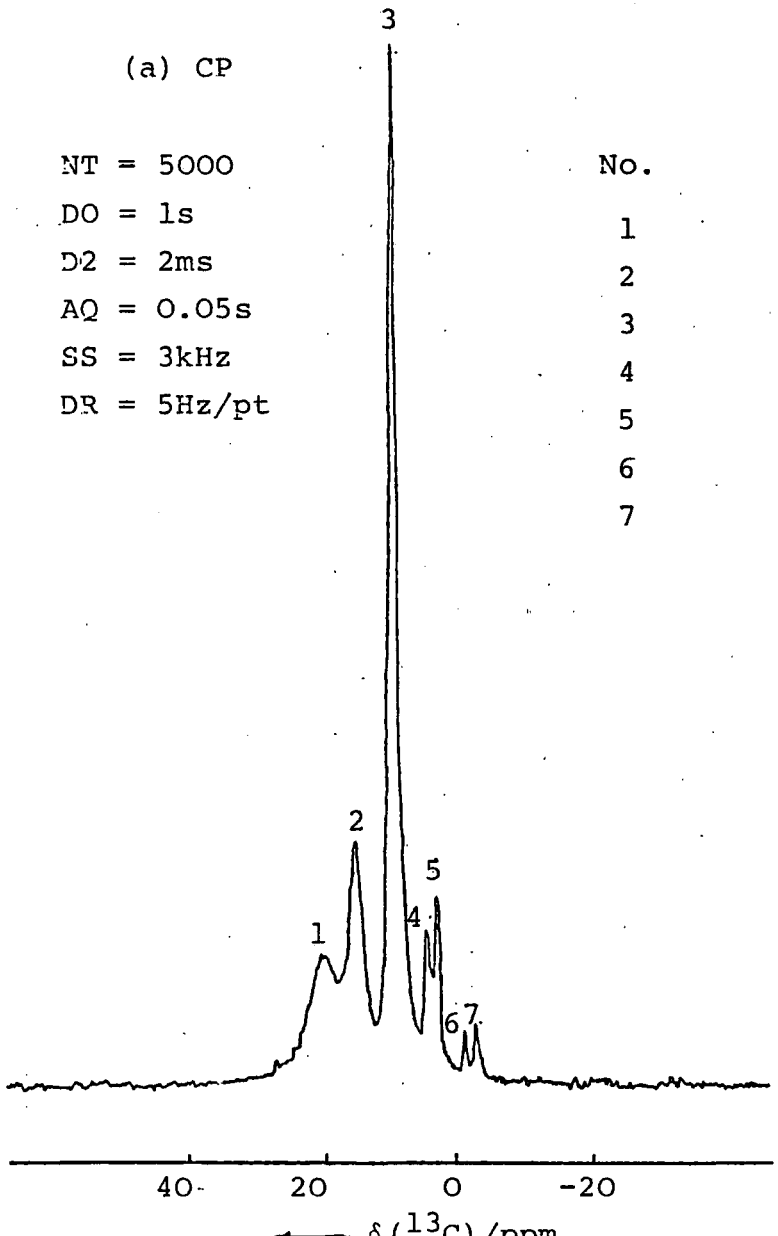

No.	δ/ppm
1	20.7
2	15.3
3	9.2
4	4.2
5	2.6
6	-1.5
7	-3.3

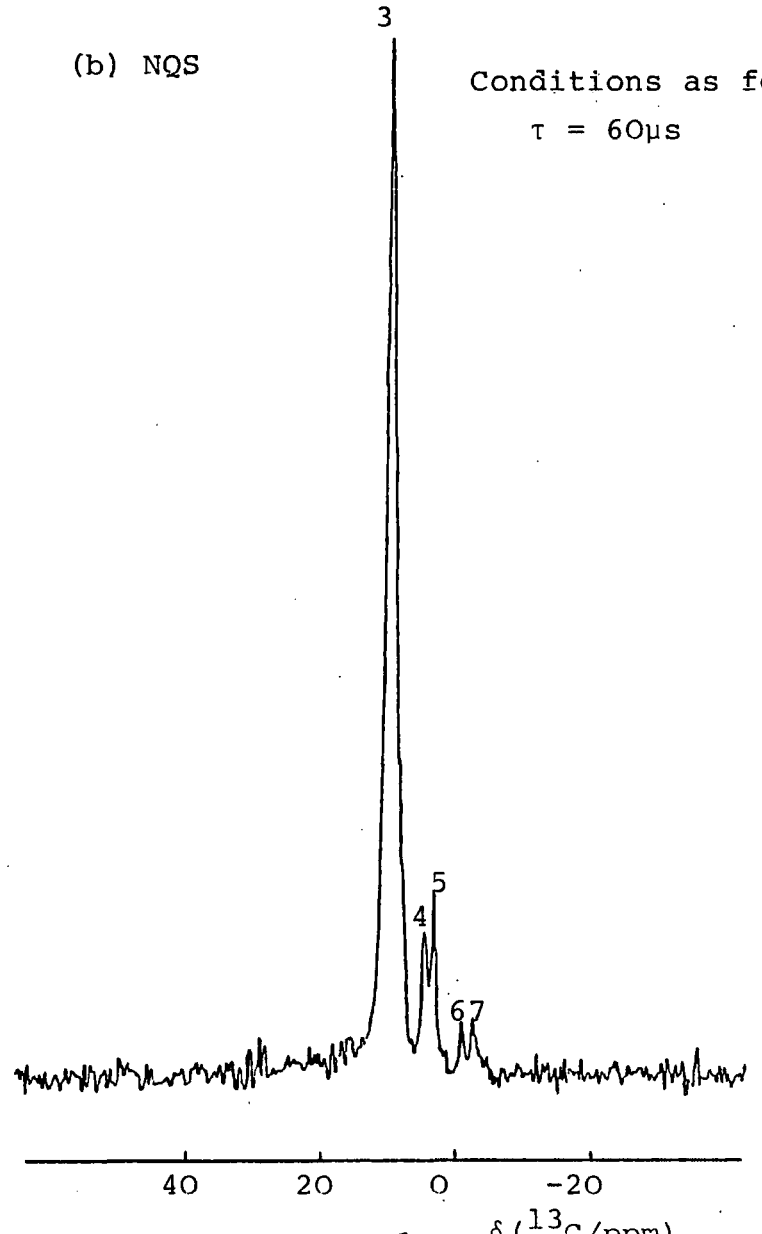

FIGURE 4.12 *Cis*-$[PtMe_2(PEt_3)_2]$

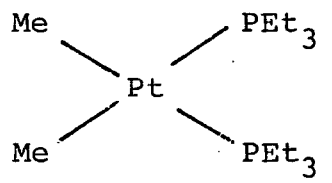

The proton relaxation parameters of *cis*$[PtMe_2(PEt_3)_2]$ were found to be T_1 = 0.8S and $T_{1\rho}$ = 15mS, which are very favourable for cross-polarization. High field (B_o = 4.7T) ^{13}C MAS solid-state spectra were obtained using cross-polarization and non-quaternary suppression techniques (Figures 4.13(a) and 4.13(b)). As the NQS spectrum only shows ^{13}C resonances due to methyl carbons, it can easily be deduced that the methyl carbons of the triethylphosphine groups give rise to the most intense peak at 9.2 ppm. Due to the shielding of the platinum, the directly bonded methyl groups appear at a lower frequency, 2.6 and 4.2 ppm. Any platinum satellites present would have an intensity of *c a.* 25% of the main carbon peak and the splitting, $J_{Pt,C,}$ would be in the region of 600 Hz for methyl carbons directly bonded to platinum.[22] If peaks 4-7 (Figs. 4.13(a) and (b)) are examined closely, then it appears that 6 and 7 are satellites of 4 and 5, with the other two satellites concealed under peak 3 (see Figure 4.14).

FIGURE 4.14 Methyl Region of Carbon Spectrum (Fig.4.13) showing concealing of Pt Satellites

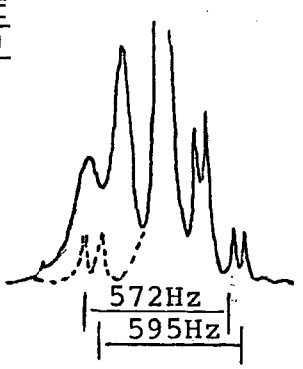

$^1J_{C,Pt}$ = 595, 572Hz (±20Hz)

FIGURE 4.15 ^{13}C CP/MAS spectrum of *cis* $[PtMe_2(PEt_3)_2]$

No.	δ/ppm
1	15.3
2	9.9
3	6.2
4	4.4
5	2.1
6	-7.0
7	-11.0

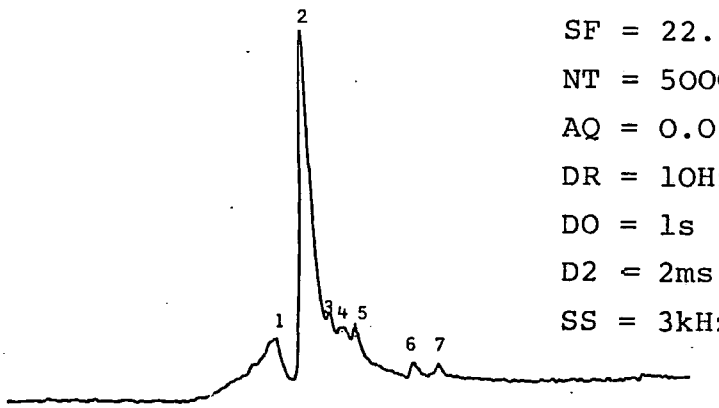

SF = 22.63MHz
NT = 5000
AQ = 0.052s
DR = 10Hz/pt
DO = 1s
D2 = 2ms
SS = 3kHz

The two peaks at -1.5 and -3.3 ppm. can be confirmed as satellites by comparison with a low-field spectrum (Figure 4.15). The resolution is not very good in the low-field case making assignments slightly more difficult. However, the two weakly intense peaks at -7.0 and -11.0 ppm. can be shown to be platinum satellites of the two peaks at 4.4 and 2.1 ppm. There is also the possibility that the splittings in both spectra are due to *trans* coupling between the methyl carbons and phosphorus nuclei across the platinum, which is known to be quite large.[22] In this case, the central resonances of the methyl carbons would be split by the same magnitude in both the high and low field

spectra (*i.e.* equal to $J_{C,P}$). However, inspection of both spectra reveals the splittings to be different (in Hz) but that the chemical shifts are the same within experimental error. Thus the two peaks at 2.6 and 4.2 ppm. (Figure 4.13) are due to two non-equivalent methyl group sites. Without X-ray crystallographic data it cannot be determined whether this inequivalence is due to asymmetry within the molecule or two crystallographically independent molecules per unit cell. As in the high field spectrum, only two platinum satellites are visible at low field (-7.0 and -11.0 ppm.), the other two satellites concealed under the broad peak at 15.3 ppm. The chemical shifts of these satellites may be predicted by knowing the ratio of the two magnetic fields used. That is, chemically shifted peaks will be split (relative to each other) more in the high field than the low field by the ratio of the two field strengths (in Hz); whereas peaks caused by coupling to another nucleus, will be split by the same amount in both cases.

Interestingly, there is only one peak for the methyl carbons of the triethylphosphine groups, which could show a spatial dependence of the crystallographic effects, rendering only the platinum bonded methyl carbons non-equivalent.

Alternatively there could be splittings from crystallographic non-equivalence which are concealed under the substantial linewidth. In the low field spectrum (Figure 4.15) the methylene carbons of the phosphine ligands give rise to a broad and featureless peak at *c a*. 15.3 ppm. Concealed under this broad linewidth could be carbon-phosphorus scalar couplings as well as non-equivalence due to different conformations of the triethylphosphine ligands. The broadness of the line does suggest some motion being present, as the ethyl groups would not be so hindered as the methyls directly bonded to platinum. (Possible broadening by carbon-phosphorus dipolar coupling, calculated to be ∿2kHz, would be eliminated by MAS at 3kHz). The high field spectrum (Figure 4.13) resolves this broad peak into two, with an intensity ratio of 2:1, which suggest non-equivalence present. More precise information concerning the conformation of the triethylphosphine ligands is available from ^{31}P CP/MAS NMR, where there are fewer environments giving rise to relatively straightforward spectra.

The ^{31}P CP/MAS of *cis*-$[PtMe_2(PEt_3)_2]$ shows two central peaks at 11.7 and 10.3 ppm., flanked by platinum satellites with $/^1J_{PtP}/$equal to 1827 and 1905 Hz (see Figure 4.16). The two phosphorus resonances could be due to two non-equivalent crystallographic sites for the molecule as a whole or to a molecular site symmetry which is lower than the molecular symmetry, *i.e*, the effect may be intermolecular or intramolecular in origin. In theory, it should be possible to differentiate between the two cases by the presence or absence of scalar coupling between the two inequivalent phosphorus

FIGURE 4.16 ^{31}P CP/MAS spectrum of *cis*[$PtMe_2(PEt_3)_2$]

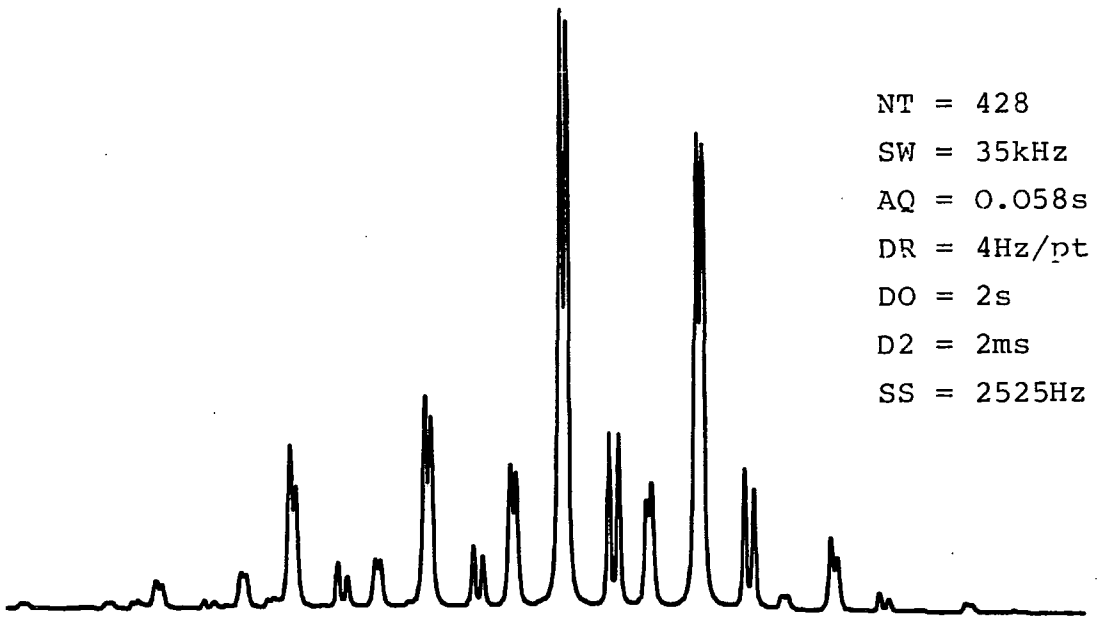

FIGURE 4.21 ^{31}P CP/MAS spectrum of *cis*[$Pt(\eta^1C_3H_5)_2(PPh_3)_2$]

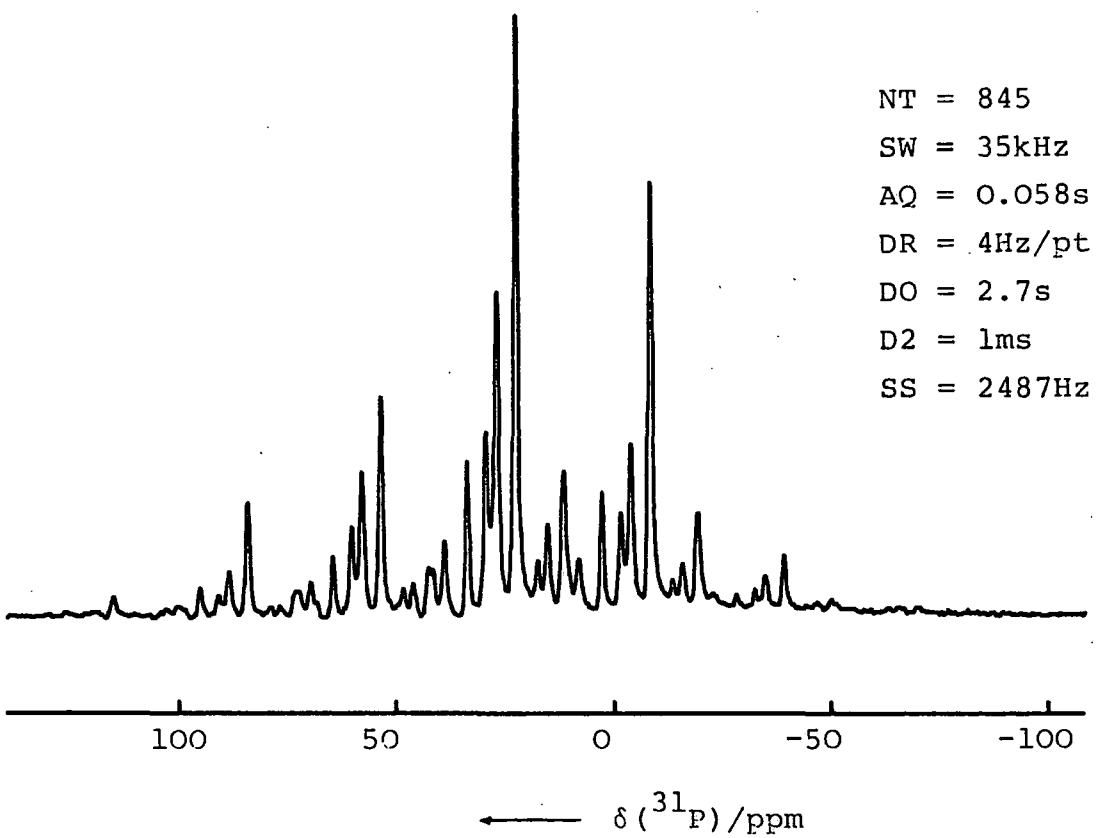

nuclei in the molecule. Unfortunately, this is likely to be too small to be seen in the solid-state (the value of $/^2J_{PPtP}/$ for *cis* phosphorus nuclei is expected to be $\sim$ 2 Hz[28]). The ^{31}P solution-state NMR spectrum obtained for this compound shows only a single resonance at 9.7 ppm due to motional averaging rendering the two *cis* phosphorus equivalent. There is also a single value of $/^1J_{P,Pt}/$ (=1865 Hz) which is in excellent agreement (to 1 Hz) to the average of the two solid-state values of 1827 and 1905 Hz. Further information regarding the molecular structure is available from shielding tensor parameters as previously discussed. However, due to the incomplete resolution of the two phosphorus resonances, individual shielding tensor component comparisons are difficult. The large negative anisotropy, as is present for all of the *cis* platinum(II) phosphines studied, is indicative of the lack of symmetry in the solid-state as well as a large deshielding present in one direction caused by the bonding to platinum.

The problem of whether the two phosphorus resonances arise because of inter- or intramolecular effects may be resolved by considering the ^{195}Pt CP/MAS spectrum. Clearly, the number of platinum resonances represents the number of crystallographically non-equivalent sites. That is, it gives information regarding intermolecular effects. Thus the presence of a single resonance at -4654 ppm. (relative to $PtCl_6^{2-}/D_2O$) shows that there is only one crystallographically independent molecule in the unit cell (see Chapter Five for complete discussion of ^{195}Pt spectrum). The appearance of two phosphorus resonances in the ^{31}P CP/MAS spectrum is due to non-equivalent triethyl-phosphine groups in the molecule.

FIGURE 4.17 X-ray crystal structure of *cis*[$PtMe_2(PEt_3)_2$]

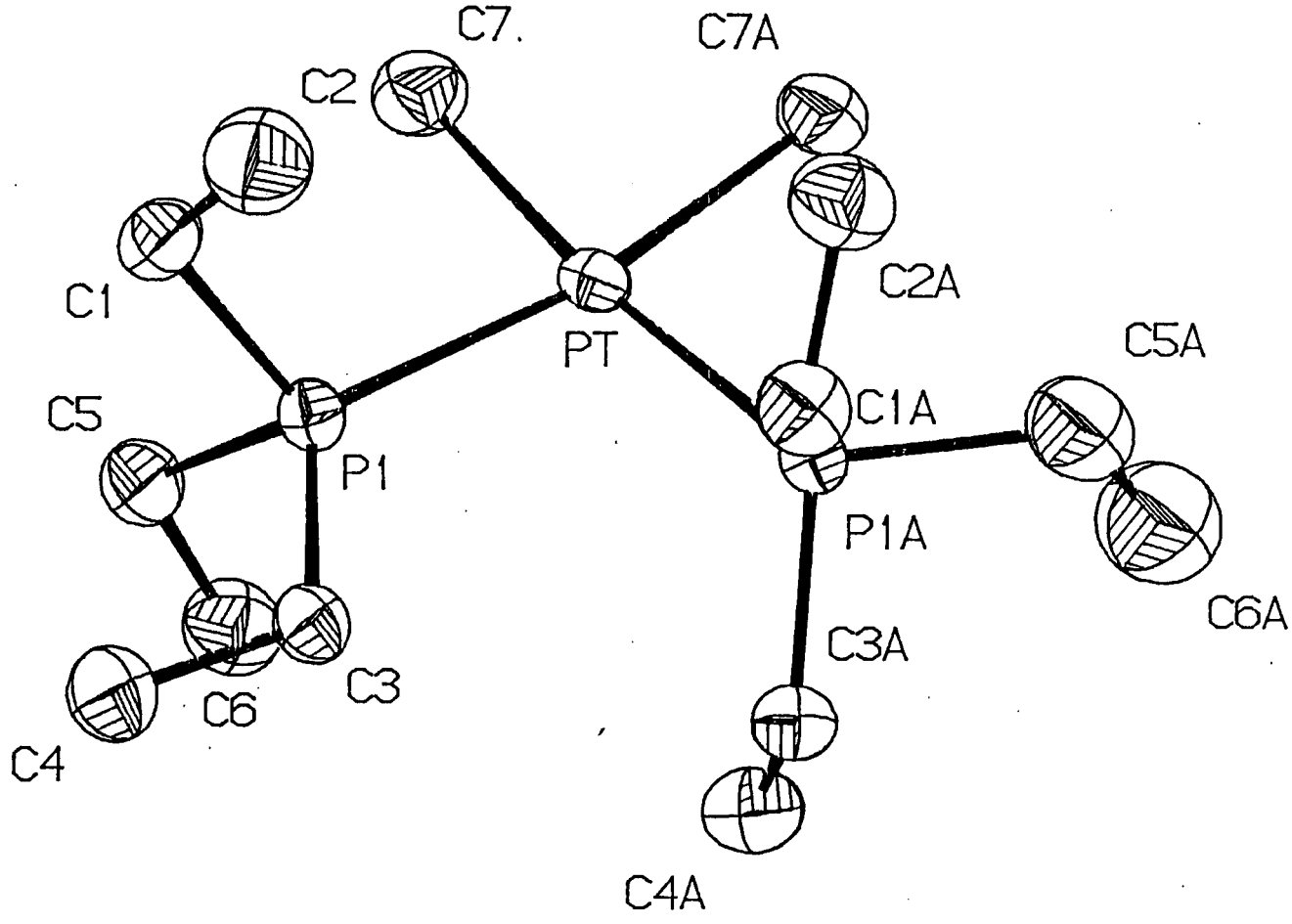

One crystallographically independent molecule in the unit cell, space group $P2_1/n$. Different conformations of the two PEt_3 groups shown.

Finally to conclude this solid-state NMR study of *cis* dimethyl (bis-triethyl phosphine) Platinum(II) an X-ray crystal structure was obtained (see Figure 4.17). The data agrees with the solid-state NMR study of one crystallographic site with different conformations for the two triethylphosphine groups. There is a total lack of symmetry within the molecule which agrees with the ^{13}C solid-state data of two methyl resonances and broad peaks for the ethyl carbons of the PEt_3 groups. The sensitivity of the NMR experiment can be clearly shown by examining the bond lengths and bond angles (see Table 4.4(a) and 4.4(b). The two platinum-phosphorus bond distances are 2.292Å and 2.295Å, that is, a difference of only 0.003Å. Yet, the difference in the ^{31}P-^{195}Pt coupling constants in the solid-state was found to be 78Hz. The difference in the bond angles is also shown to be similar showing the sensitivity degree of the definition of non-equivalence in solid-state NMR.

TABLE 4.4(a) BOND LENGTHS (A)

P(1)-Pt	2.292(4)	P(1A)-Pt	2.295(4)
C(7)-Pt	2.118(9)	C(7A)-Pt	2.095(9)
C(1)-P(1)	1.823(9)	C(3)-P(1)	1.840(8)
C(5)-P(1)	1.845(9)	C(2)-C(1)	1.498(11)
C(4)-C(3)	1.523(11)	C(6)-C(5)	1.485(12)
C(1A)-P(1A)	1.868(10)	C(3A)-P(1A)	1.836(9)
C(5A)-P(1A)	1.835(13)	C(2A)-C(1A)	1.490(14)
C(4A)-C(3A)	1.501(13)	C(6A)-C(5A)	1.477(17)

TABLE 4.4(b) BOND ANGLES (deg.)

P(1A)-Pt-P(1)	100.3(2)	C(7)-Pt-P(1)	86.1(3)
C(7A)-Pt-P(1)	169.3(a)	C(7)-Pt-P(1A)	173.5(a)
C(7A)-Pt-P(1A)	90.0(3)	C(7A)-Pt-C(7)	83.5(4)
C(1)-P(1)-Pt	111.9(3)	C(3)-P(1)-Pt	121.4(3)
C(5)-P(1)-Pt	114.2(3)	C(3)-P(1)-C(1)	102.5(4)
C(5)-P(1)-C(1)	100.8(4)	C(5)-P(1)-C(3)	103.4(4)
C(2)-C(1)-P(1)	114.5(7)	C(4)-C(3)-P(1)	117.3(6)
C(6)-C(5)-P(1)	119.7(3)	C(5A)-P(1A)-Pt	121.1(4)
C(3A)-P(1A)-C(1A)	99.6(4)	C(5A)-P(1A)-C(1A)	99.0(5)
C(5A)-P(1A)-C(3A)	100.8(5)	C(2A)-C(1A)-P(1A)	112.9(6)
C(4A)-C(3A)-P(1A)	114.7(6)	C(6A)-C(5A)-P(1A)	117.1(8)

4.8 *Cis*-[dicyclopropyl bis(triphenylphosphine)-Platinum(II)], $[Pt(C\text{-}C_3H_5)_2(PPh_3)_2]$

Carbon-13 solid-state spectra were obtained for this compound at 22.6 and 50.3MHz operating frequencies. The low-field spectrum using CP/MAS only (Figure 4.18) shows an interesting doublet in the aliphatic region with a splitting of 60Hz. This splitting is due to two crystallographically non-equivalent carbons from the cyclopropyl groups as confirmed from the high field spectrum (Figure 4.19), which contains two peaks with a splitting of 123Hz. Taken into account a resolution of 15Hz/Pt, the increase in splitting on going from low field to high field is due to chemical shift effects. Although the splitting is consistent, the actual chemical shifts are different and is no doubt due to a calibration error. The ^{13}C spectrum obtained at 50.3MHz, due to its greater sensitivity, contains platinum satellites with $J_{C,Pt} \simeq 462$Hz. This carbon-

FIGURE 4.18 Low-field ^{13}C CP/MAS spectrum of *cis*[Pt($\underline{c}C_3H_5$)$_2$(PPh$_3$)$_2$]

No.	δ/ppm
1	130.7
2	127.5
3	20.5
4	17.8
5	9.6

SF = 22.63MHz
NT = 10,000
SW = 10kHz
AQ = 0.051s
DR = 5Hz/pt
D0 = 2.7s
D2 = 1ms
SS = 3kHz

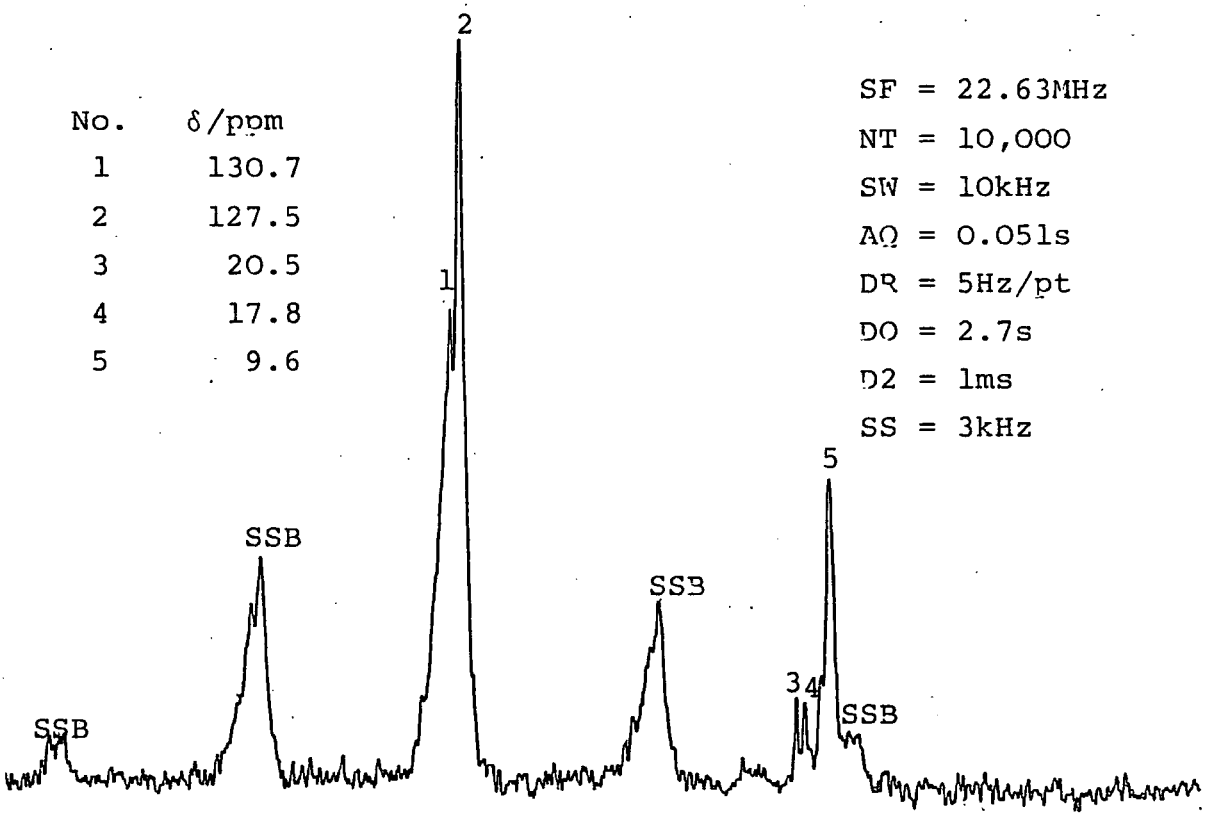

FIGURE 4.19 High-field ^{13}C CP/MAS spectrum of *cis*[Pt($\underline{c}C_3H_5$)$_2$(PPh$_3$)$_2$]

S.F. = 50.29MHz
S.W. = 15.6kHz
AQ = 0.066s
DR = 4Hz/pt
(other conditions as above)

* impurity

No.	δ/ppm		
1	140.6		
2	136.9		
3	131.5		
4	128.5		
5	124.7		
6	25.9		
7	23.5	9	14.2
8	16.6	10	10.0

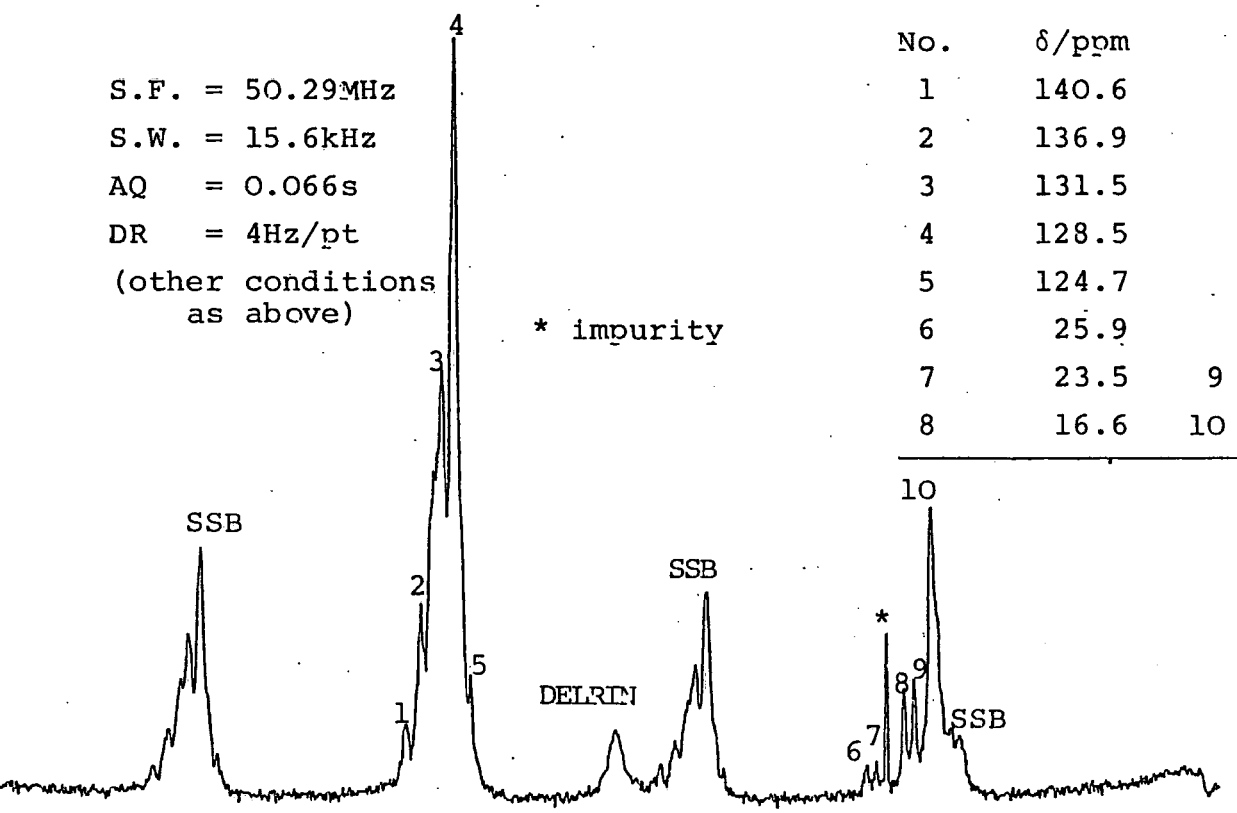

platinum coupling constant is of similar magnitude to the one bond ^{13}C-^{195}Pt coupling constants recorded in solution-state.[22] Thus, given the relative intensity and coupling values, the two peaks at 16.6 and 14.2 ppm. (high field) must be due to the methine carbons of the cyclopropyl groups. The broader peak at 10.0 ppm. accounts for the methylene carbons, while the extremely narrow peak at 21.0 ppm. must either be due to an impurity or some external RF source. The NQS spectra obtained at both fields did not reveal any information regarding the molecular structure of the compound (Figure 4.20).

FIGURE 4.20 *cis*[dicyclopropyl(bis-triphenylphosphine)Platinum(II)]

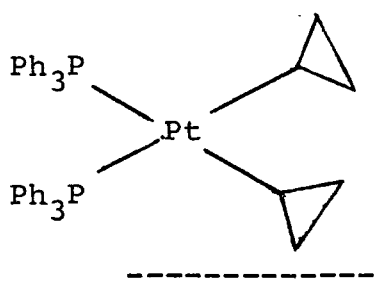

The ^{31}P CP/MAS spectrum of *cis*[Pt(C-C_3H_5)$_2$(PPh$_3$)$_2$] (Figure 4.21) reveals very strange splittings. There are three centrebands at 29.0, 26.6 and 22.2 ppm. flanked by platinum satellites ($^1J_{P,Pt}$ = 2018, 2123 and 1796 Hz respectively). A clearer view may be seen by an expansion of the spectrum (Figure 4.22) and it may be shown that the centrebands plus sidebands are approximately of an intensity ratio 1:2:4. One would normally expect two phosphorus peaks of similar intensity due to the non-equivalence of the PPh_3 ligands. Without any X-ray crystallographic data or ^{195}Pt solid-state NMR data the appearance of three different intensity peaks cannot be explained. However, it should be noted that different cross-polarization

FIGURE 4.22 ^{31}P CP/MAS spectrum of *cis*[Pt($\underline{c}C_3H_5$)$_2$(PPh$_3$)$_2$]

(Expanded)

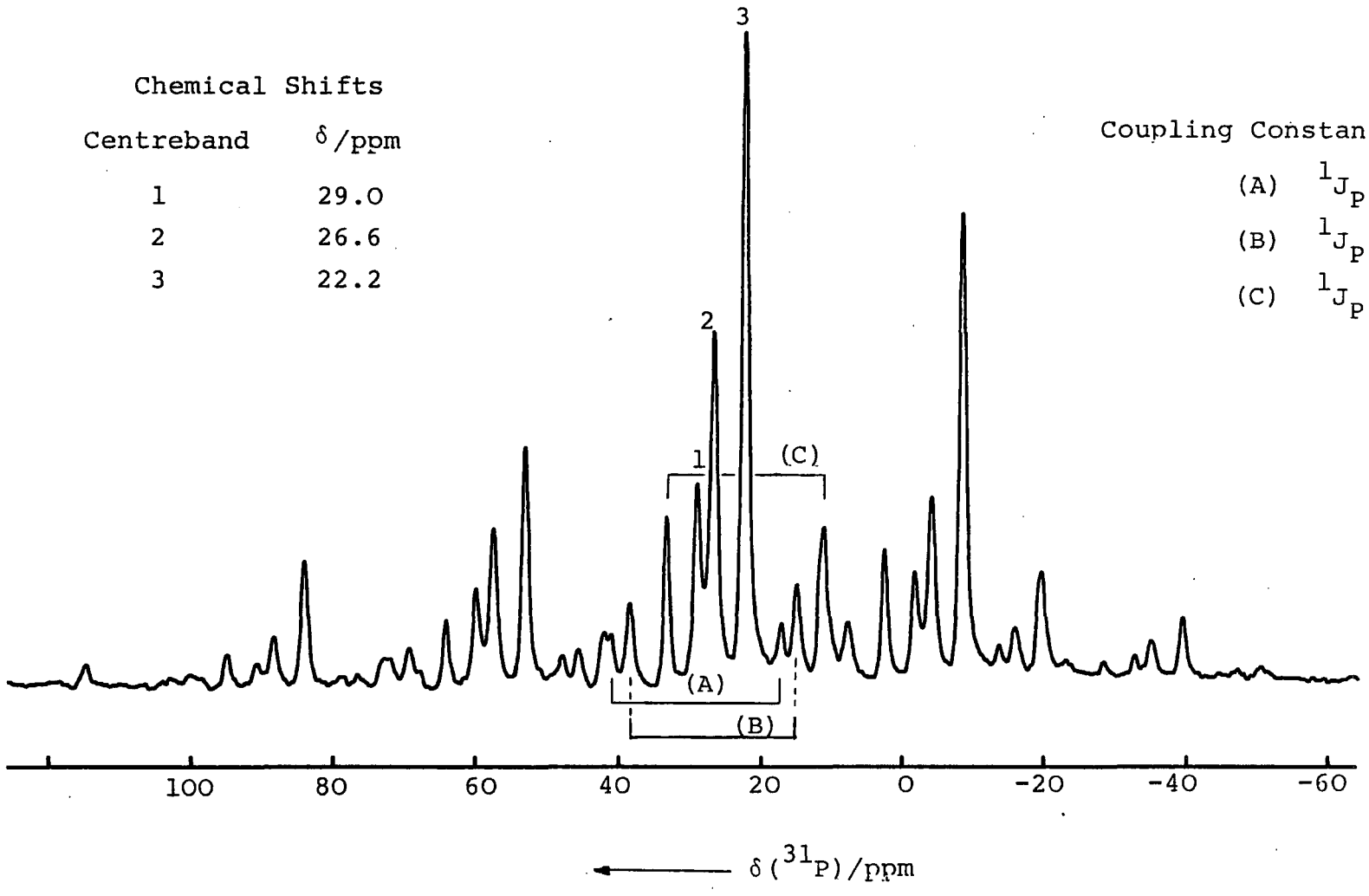

rates can account for spurious intensities and also the possibility of impurities present, although very unlikely, cannot be ignored.

A close examination of the phosphorus NMR data (see Tables 4.2.1 and 4.3) shows that the environment of one of the phosphorus atoms is very different to the other two. The most intense peak at -22.2 ppm. has a very low ^{195}Pt-^{31}P coupling constant (1796Hz) suggesting a relatively weak platinum-phosphorus bond. The chemical shifts of all three phosphorus sites are equally spaced implying similar environments. However, the values for σ_{22} show that there is a difference of *c a.* 23 ppm. of the low frequency peak compared to the very similar values of the less intense peaks.

A further point, which at present cannot be explained, is that the ^{13}C data reveals two non-equivalent cyclopropyl sites present, which does not agree with the ^{31}P NMR data of three different chemical sites. As mentioned before, X-ray crystallographic data is needed to attempt to resolve this problem.

4.9 *Cis*[Dimethyl(bis-triphenylphosphine)Platinum(II)]C[$PtMe_2(PPh_3)_2$]

The carbon-13 MAS spectra were obtained using cross-polarization with multiple contacts and non-quaternary suppression, at 50.3MHz (see Figures 4.23 and 4.24). The methyl region should be the same in both spectra although, the NQS spectrum should have eliminated all non-quaternary carbon resonances in the phenyl region. The two aromatic peaks

FIGURE 4.23 ^{13}C CP/MAS spectrum of *cis* $[PtMe_2(PPh_3)_2]$

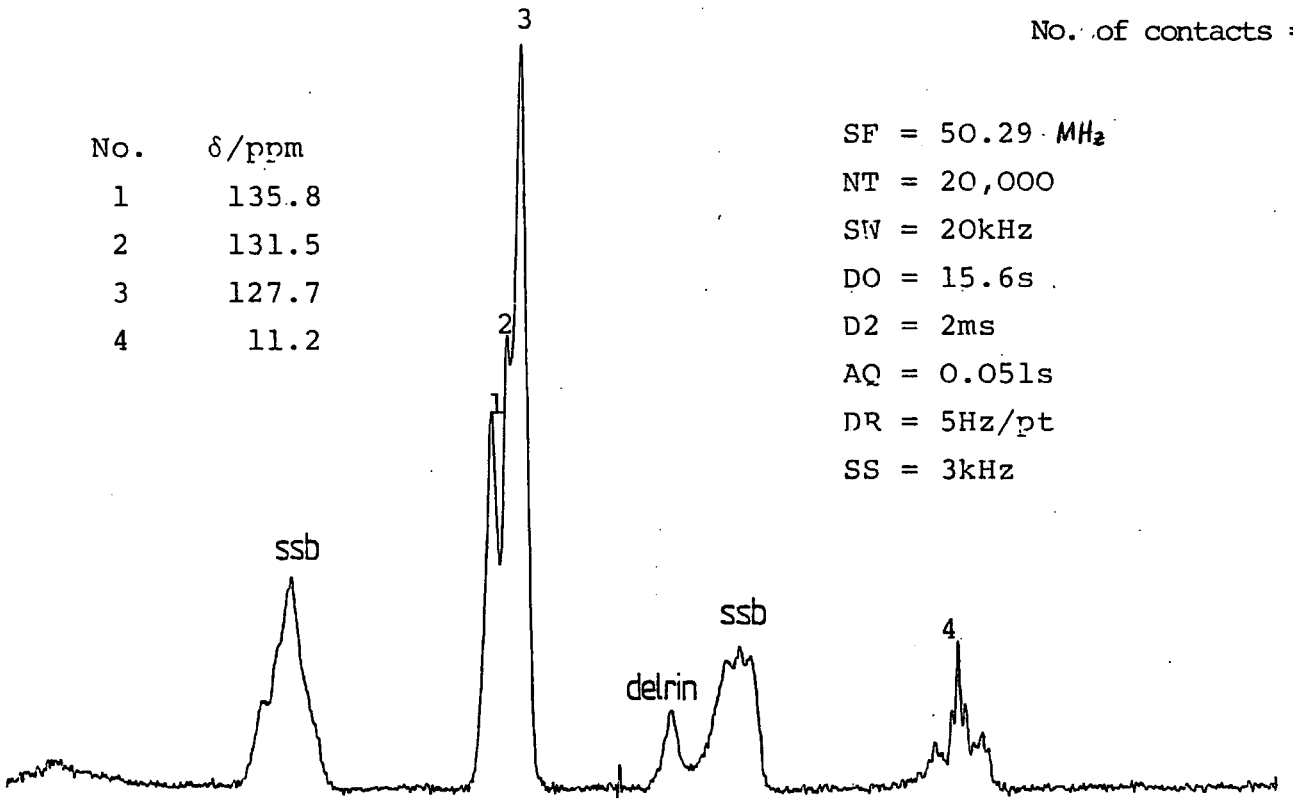

FIGURE 4.24 ^{13}C NQS/MAS spectrum of *cis* $[PtMe_2(PPh_3)_2]$

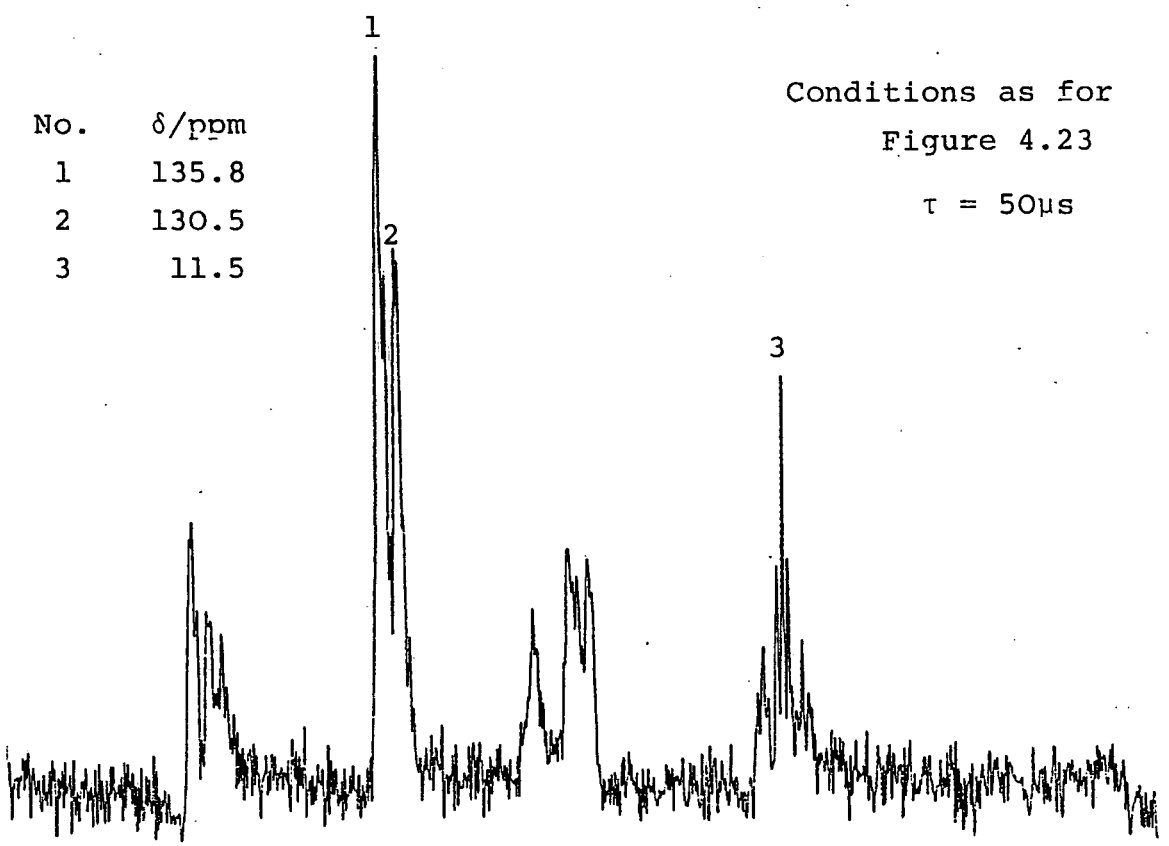

present in the NQS spectrum (Fig. 4.24) have an approximate intensity ratio of 2:1. Phosphorus-carbon scalar coupling could account for this if the total sum of intensities of the centrebands and their respective spinning sidebands were equal. This effect is not observed and furthermore, the ^{13}C-^{31}P dipolar coupling, which would account for such an effect,[31] would be eliminated by magic-angle spinning at *c a.* 3kHz. Such a splitting can be explained if the conformations of the triphenylphosphine groups are considered (see Figure 4.25).

FIGURE 4.25 *Cis*[$PtMe_2(PPh_3)_2$]

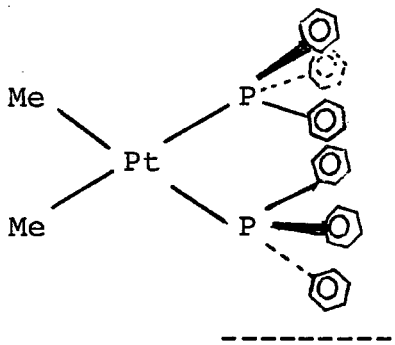

The two main peaks at *c a.* 136 and 130 ppm. are due to the six quaternary carbons of the triphenylphosphine ligands. It therefore follows that two types of phenyl rings are present caused by contortion of the PPh_3 groups in the solid-state, thus accounting for the 4:2 ratio observed in the NQS spectrum. The further splittings seen could be due to carbon-phosphorus scalar coupling, which should be around 70Hz for phenylphosphines.[32] However, given the level of noise present, one cannot be certain as to whether these splittings are real.

The methyl region shows some interesting splittings which can arise through non-equivalence and/or carbon-phosphorus and carbon-platinum scalar coupling. An expansion of this region

from the NQS spectrum (see Figure 4.26) appears to display a triplet of triplets. This splitting pattern can be caused by a methyl carbon coupling to two phosphorus atoms to produce a triplet and then also coupling to the directly bonded platinum producing satellites of the triplet. It may be that the triplet pattern is a deceptively simple ABX system, whereby the X part is the ^{13}C resonance and the A and B parts are the ^{31}P resonances. The condition for the X part to coalesce from four lines into a triplet is that the quantity $(\delta_{AB} + L)^2/2\ J_{AB}$ must be less than the resolution ($\Delta\nu$ = 20Hz/pt), where $\delta_{AB} = \nu_A - \nu_B$ = 260Hz (see Figure 4.28) and $L = \frac{1}{2}(J_{AX}-J_{BX})$.[44] If $J_{AB}(\equiv {}^2J_{P,P})$ is of a sufficiently large value and L makes a significant negative contribution then such a coalescence may take place.

FIGURE 4.26 Expansion of Methyl region from NQS Spectrum (see Figure 4.24)

No.	δ/ppm
1	19.3
2	17.7
3	15.8
4	13.1
5	11.5
6	9.7
7	7.2
8	5.6
9	3.6

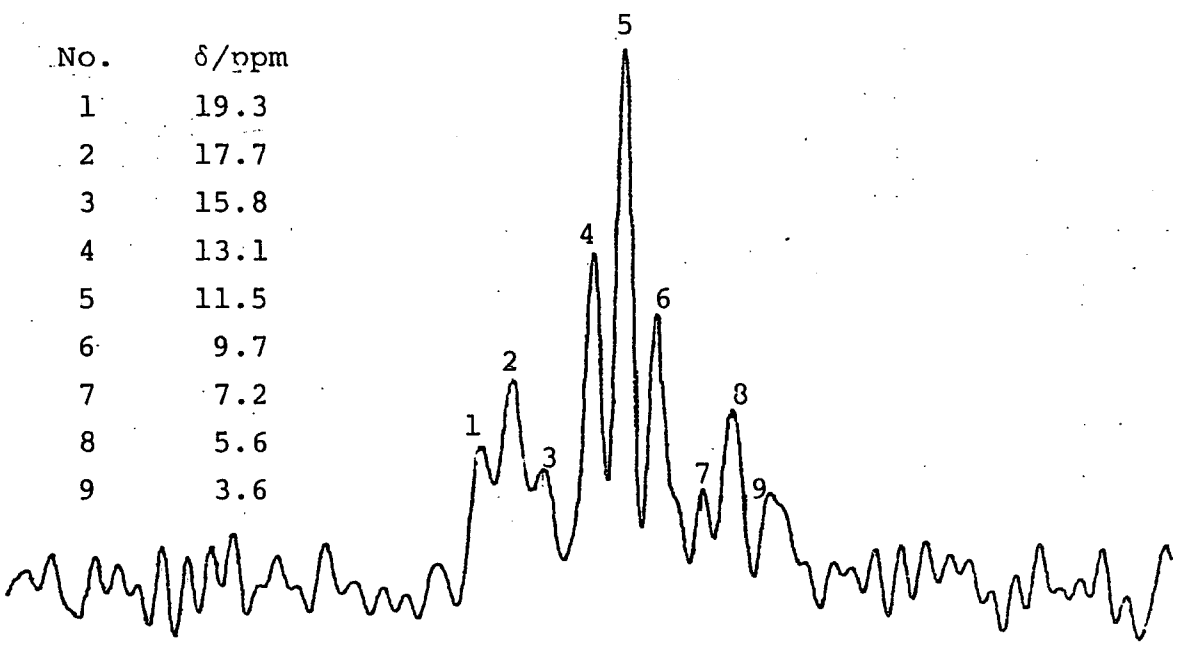

As seen from Figure 4.26 the outer triplets are approximately one quarter of the intensity of the main triplet showing the

presence of carbon-platinum coupling. The value of $^{1}J_{C,Pt}$ was found to be ∿610Hz which is consistent with solution-state NMR data.[22] The appearance of a single methyl resonance indicates the two methyl groups, within the molecule are equivalent.

The lines could, however, conceal splittings due to more crystallographically independent sites present, although this may be likely given the linewidth (∿40Hz), a separation of methyl resonances, caused by intramolecular effects, for a similar compound was found to be ∿90Hz (Section 4.7). In an attempt to confirm the explanation of the splittings seen in the methyl region, a low field (22.6MHz) spectrum was obtained, as the splittings should remain constant if they are due to scalar couplings. However, due to poor sensitivity and resolution and the appearance of a spinning side band, little information was retrieved. The observation, at high field, of one methyl resonance and a triplet, due to ^{13}C - ^{31}P coupling, indicates the presence of only one crystallographically independent molecule per unit cell which contains two non-equivalent triphenylphosphine groups. This can be verified by phosphorus-31 and platinum-195 solid-state spectra.

The ^{31}P CP/MAS spectrum (Figure 4.28) exhibits two phosphorus resonances at 26.1 and 29.3 ppm. with platinum satellites present due to phosphorus-platinum scalar coupling ($^{1}J_{P,Pt}$ = 1817 and 1978Hz). No solution-state NMR data was available for this compound due to insufficient solubility. The difference of 3.2 ppm. between the two isotropic chemical shifts of the two phosphorus atoms reflects the greater in-

FIGURE 4.28 ^{31}P CP/MAS spectrum of *cis*-$[PtMe_2(PPh_3)_2]$

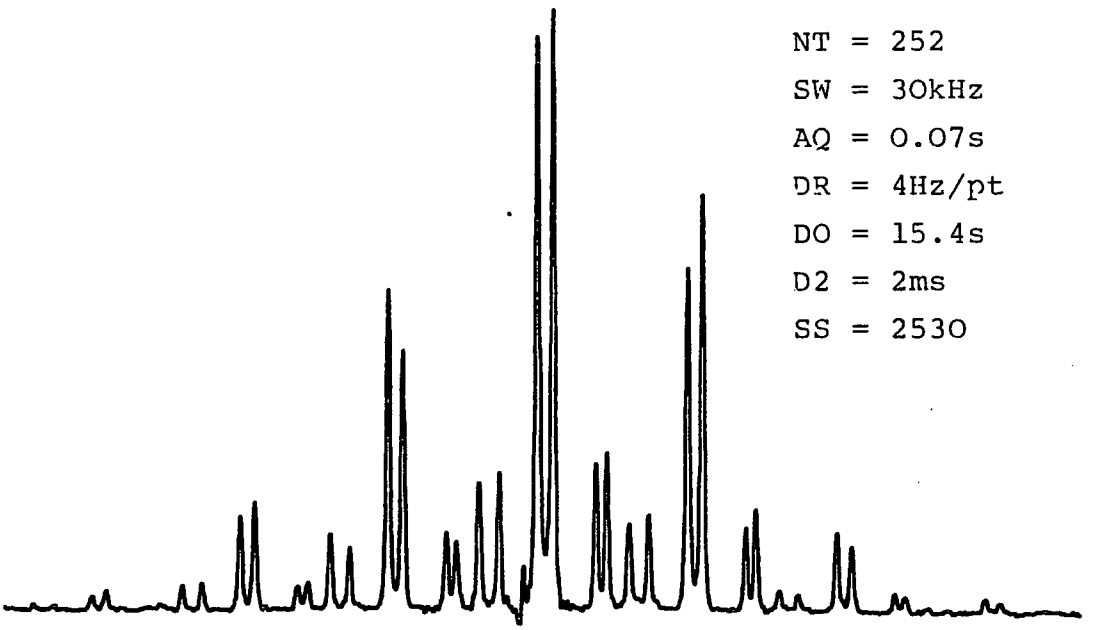

FIGURE 4.30 ^{31}P CP/MAS spectrum of *cis*-$[PtPh_2(PPh_3)_2]$

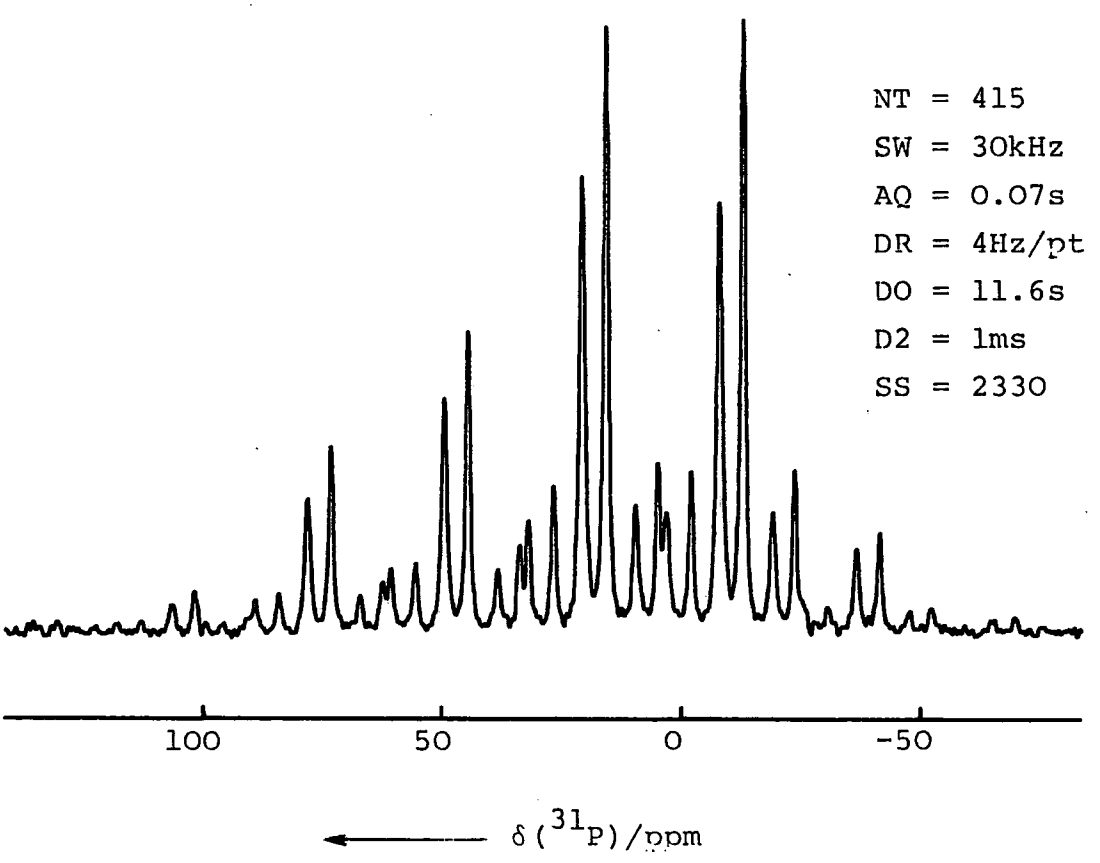

equivalence of the triphenyl phosphine groups than was observed for the triethylphosphine groups of *cis*$[PtMe_2(PEt_3)_2]$. This is no doubt caused by the greater steric strain imposed by the bulky phenyl groups attached to the phosphorus atoms of *cis*$[PtMe_2(PPh_3)_2]$. The difference in hindrance is also exemplified by comparing the proton relaxation parameters of *cis*$[PtMe_2(PEt_3)_2]$ (T_1=0.85 and $T_{1\rho}$=15ms) and for $[PtMe_2(PPh_3)_2]$ (T_1=12.45 and $T_{1\rho}$=70ms). The long T_1 and $T_{1\rho}$ measurement for the latter compound is indicative of very little motion in the lattice, whereas the short T_1 value of 0.8 seconds for *cis*$[PtMe_2(PEt_3)_2]$ reveals some motion present which is likely due mainly to the triethylphosphine groups, as spin diffusion averages the T_1s of all the protons present. It must be noted, however, that these relaxation measurements give only an indication as to whether motion may be present in the lattice and that for a full study, variable-temperature relaxation and CP/MAS experiments need to be carried out.

The difference in ^{31}P chemical shifts of the two phosphorus nuclei is shown to be mainly due to the variation in σ_{22} values (see Table 4.3), which accounts for the different intensities of the central peaks and spinning sidebands. As with $[PtMe_2(PEt_3)_2]$ solid-state ^{195}Pt CP/MAS NMR proved to be successful for this compound, (see Chapter Five for full details). Only one ^{195}Pt resonance was observed, at -4682 ppm. (relative to $PtCl_6^{2-}/D_2O$) which confirms the previous hypothesis of there being a single crystallographic site in the unit cell. The ^{195}Pt spectrum exhibits four central peaks due to the scalar coupling of platinum-195 to two different types of phosphorus nuclei present, the values obtained being

$/^{1}J_{Pt,P}/$ = 1825 and 1979Hz, which agree very nicely with the ^{31}P solid-state data.

4.10 *Cis* Diphenyl bis(triphenylphosphine)platinum(II)

As would be expected, the low and high field ^{13}C CP/MAS spectra reveal little information, due to the number of carbon resonances present in the aromatic region and the small chemical shift difference between the directly bonded phenyls and triphenyl phosphine groups. However, the NQS spectrum obtained at 50.3MHz, exhibits two peaks at 129.8 and 132.2 ppm. due to quaternary carbons of the triphenylphosphine groups (see Figure 4.29). The ^{13}C resonances due to the two phenyl groups bonded to platinum are likely to be concealed under this band, as the intensities will be relatively small. The ratio of peak height intensities for the two resonances seen is 2:1 and is very similar to the splitting seen for the ^{13}C NQS spectrum of *cis*$[PtMe_2(PPh_3)_2]$, (see Figure 4.24). A similar treatment to that afforded to the latter spectrum is therefore appropriate, given the similarities in molecular composition. The presence of two peaks for the phenyl carbons does not indicate that the phosphine ligands are non-equivalent, but merely suggests this as one of the possible explanations.

The ^{31}P CP/MAS spectrum (see Figure 4.30) does show the phosphorus atoms to be inequivalent as can be predicted considering the two previous cases of *cis*$[PtMe_2(PEt_3)_2]$ and $[PtMe_2(PPh_3)_2]$. The two chemical shifts of 15.4 ppm. and 20.4 ppm. are smaller than the shifts observed for the other two *cis* phenylphosphine compounds, discussed earlier, suggesting

FIGURE 4.29 ^{13}C NQS/MAS spectrum of $[PtPh_2(PPh_3)_2]$

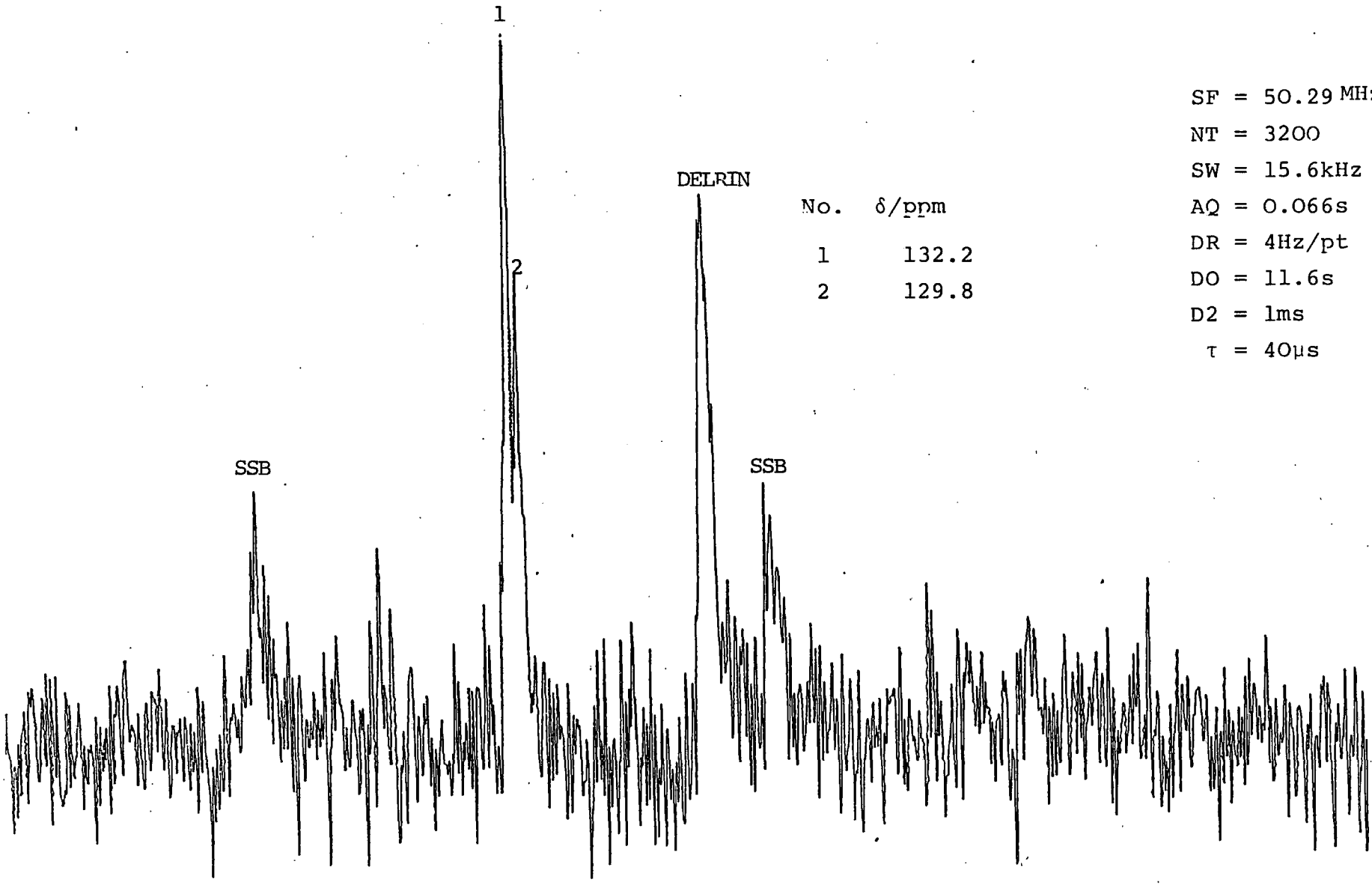

No.	δ/ppm
1	132.2
2	129.8

SF = 50.29 MHz
NT = 3200
SW = 15.6kHz
AQ = 0.066s
DR = 4Hz/pt
DO = 11.6s
D2 = 1ms
τ = 40μs

some extra shielding of the phosphorus nuclei caused by the presence of the phenyl ligands. However, there is no significant difference between the shielding tensor components for each ^{31}P resonance to suppose that this shielding is dominant in any one direction. The phosphorus-31 solution-state NMR spectrum obtained for this compound shows a single phosphorus resonance at 18.4 ppm with two platinum satellites present ($^{1}J_{P,Pt}$ = 1763Hz). The solid and solution-state ^{31}P NMR are compared in Figures 4.31(a) and (b), and illustrates the effects of motional averaging on shielding anisotropy and crystallographic inequivalences present in the solid-state.

The intensity differences observed in both the slow and fast spinning ^{31}P spectra are not attributable to shielding anisotropy effects. These effects would be due to two reasons: (i) different cross-polarization rates for the two phosphorus atoms, or (ii) linewidth variations. A variable contact experiment revealed no change in the peak heights but an accurate measurement of the linewidths showed a small difference between the two resonances. This variation could be due to several effects[7] and is likely to be caused by some difference in motion in the vicinity of the two phosphorus atoms.

A comparison of the ^{31}P solid-state data of *cis*-$[PtPh_2(PPh_3)_2]$ to that of the other *cis* alkylphosphines, previously discussed, suggests that the non-equivalence observed is almost certainly due to intramolecular effects. However, without ^{195}Pt solid-state NMR or X-ray crystallographic data, the possibility of intermolecular effects cannot be ruled out.

FIGURE 4.31 ^{31}P spectra of *cis*[$PtPh_2(PPh_3)_2$]

(a) Solid-state
(CP/MAS)

$\delta_{^{31}P}$ = 20.4,15.4 ppm

$^1J_{P,Pt}$ = 1756,1805Hz

NT = 64
SS = 3kHz
(Conditions as for Fig.4.30)

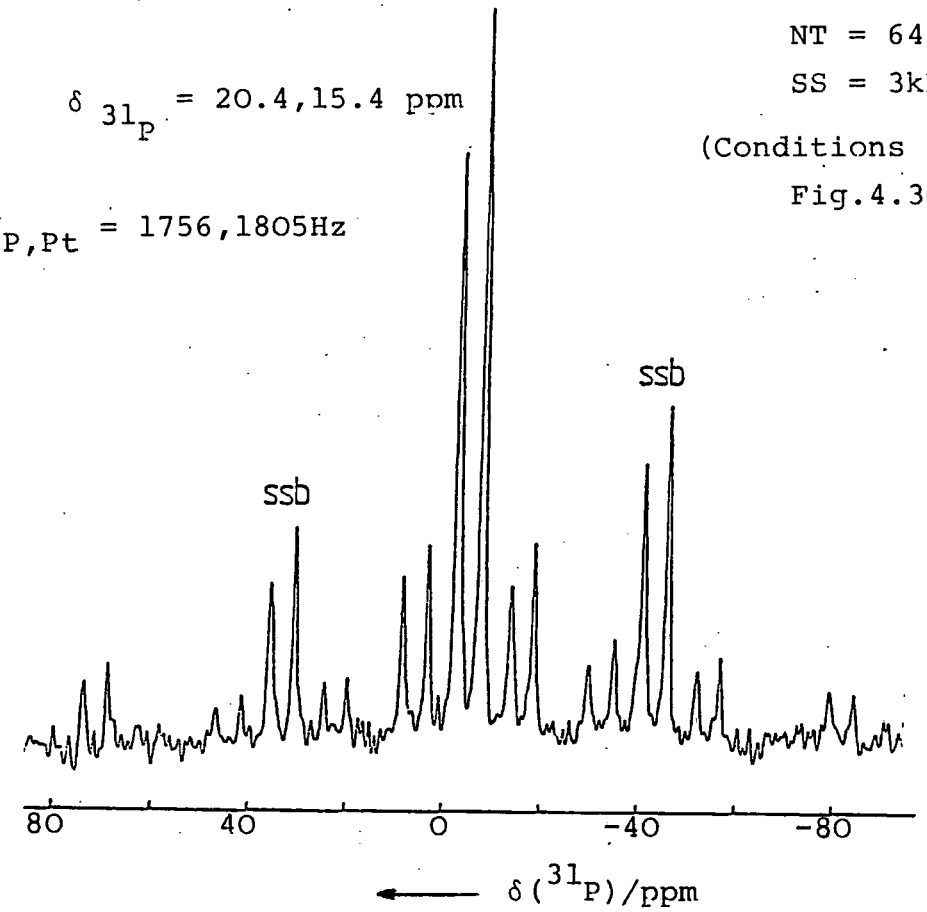

(b) Solution-state
(^1H decoupled)

$\delta_{^{31}P}$ = 18.35ppm

$^1J_{P,Pt}$ = 1763Hz

NT = 64
DO = 3s
SW = 20kHz
solvent = $CHCl_2$

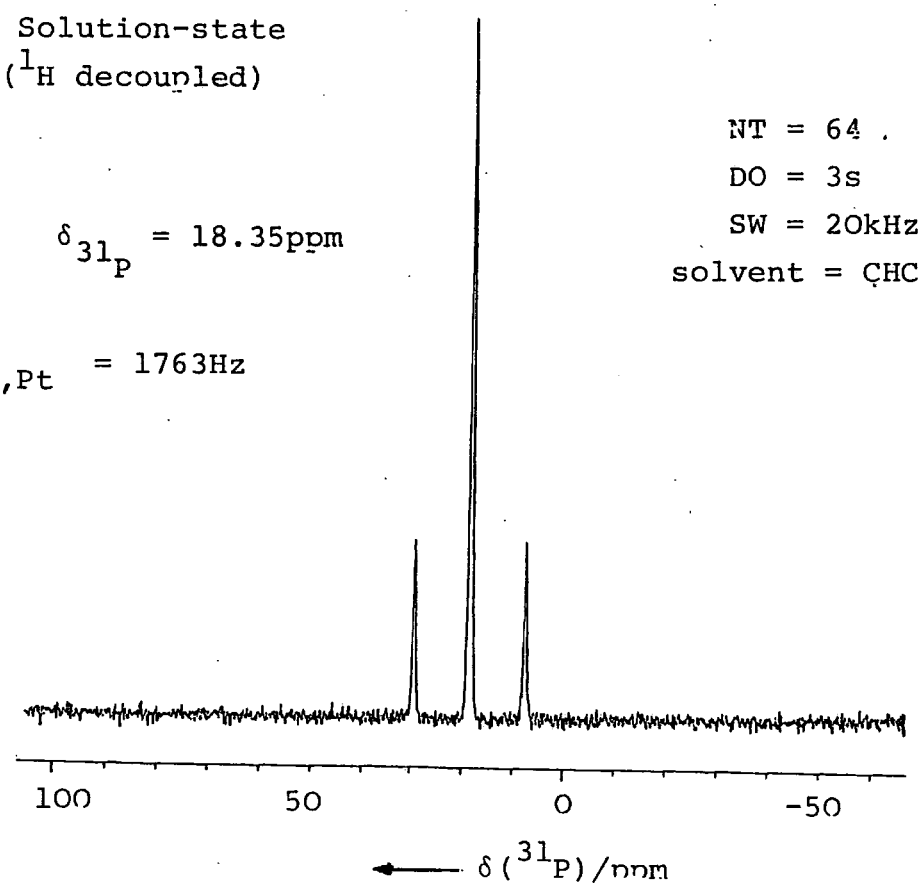

4.11 *Trans* [dichloro bis(triethylphosphine)Platinum(II)]
(Discussion of $^{2}J_{P,P}$ constants included)

The ^{31}P solution-state spectrum for this compound shows a single peak at 12.2 ppm. with a platinum-phosphorus coupling of 2397Hz. This agrees excellently with the ^{31}P solid-state data (see Figure 4.32) of a single ^{31}P resonance at 13.1 ppm. and a ^{31}P-^{195}Pt coupling of 2393Hz, which shows there to be no change in structure on going from the solid-state to solution-state. If the two phosphorus atoms were non-equivalent in the solid-state then there should be a phosphorus-phosphorus coupling of ∿400-600Hz, as has been observed for *trans* $^{2}J_{P,P}$ across a metal atom for several compounds.[21] The fact that this coupling is not observed in the solid-state spectrum does not rule out any intramolecular non-equivalence induced in the crystal lattice. If the ratio of ^{31}P-^{31}P coupling to the chemical shift difference ($^{J}/_{\delta}$) for the two *trans* ^{31}P nuclei is small (*c.a.* ≤0.1), the system approximates to a first order AX spectrum and consists of four equally intense lines, one pair due to the A and one to the X nucleus. As the ratio increases the inner line in each doublet grows at the expense of the outer line. At very high ratios the two outer lines become of negligible intensity and the two inner lines coalesce to give the single line A_2. A solution-study investigation carried out on this compound by Goodfellow and Taylor[33] using $^{1}H\{^{31}P\}$ INDOR spectroscopy found $^{2}J_{P,P}$ to be +436Hz. The maximum chemical shift difference between the two *trans* phosphorus atoms will be of the order of the observed linewidth (*c a.* 100Hz). Therefore the $^{J}/_{\delta}$ ratio will be at least 4.0, giving rise to an A_2 spectrum, *i.e.* a single line will be observed.

FIGURE 4.32 ^{31}P CP/MAS of *trans*[$PtCl_2(PEt_3)_2$]

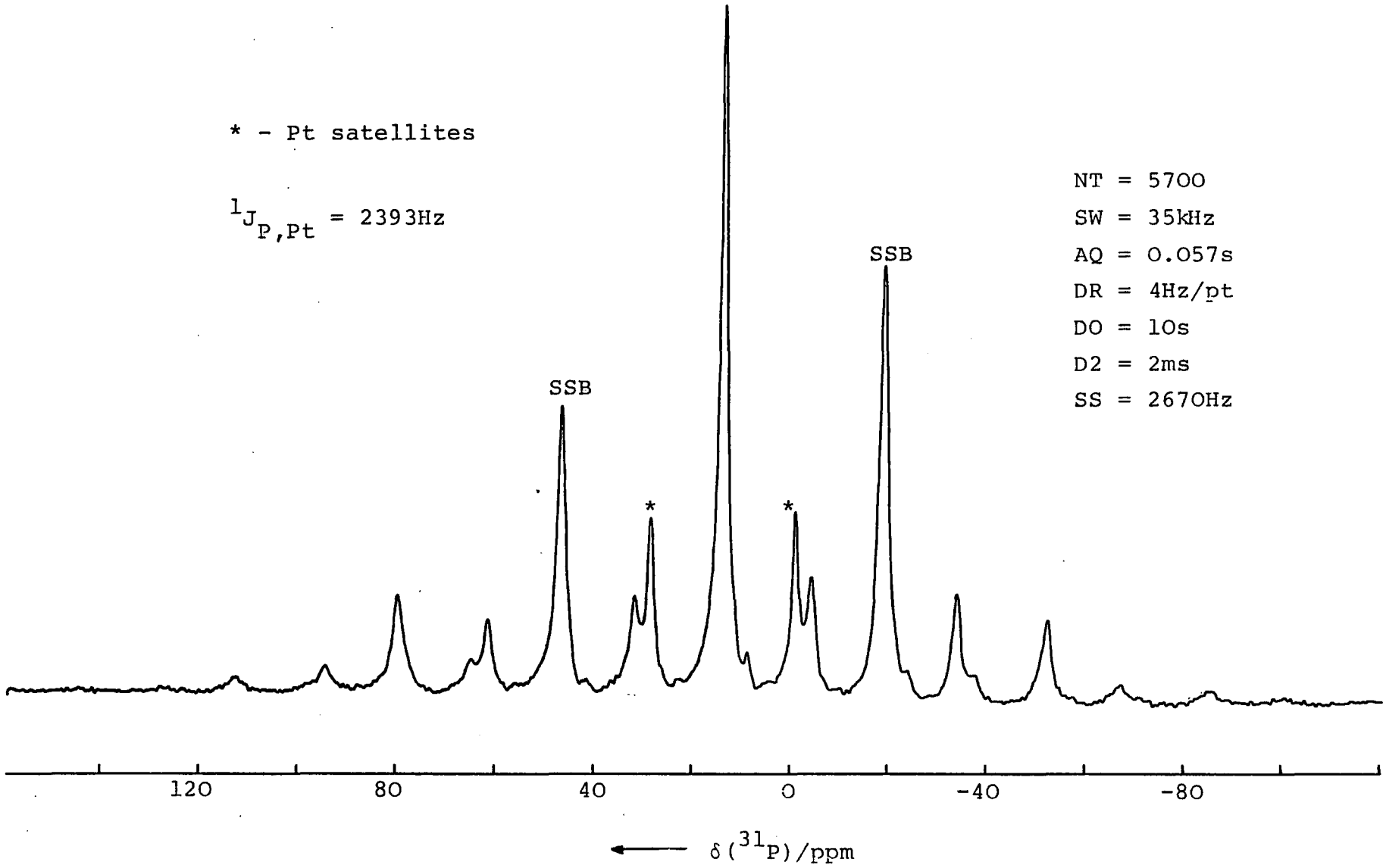

An extra point to note is that Allen and Piddock[29] have found the value of $/^2J_{P,P}/$ for *cis* $[PtMe_2(PEt_3)_2]$ to be *c a.* 2Hz. The chemical shift difference due to the intramolecular non-equivalence in the solid-state was found to be *c a.* 112Hz, therefore as $^J/\delta$ <0.1, an AX spectrum should be observed (four equally intense lines) however the substantial line-widths (≥100Hz) conceal this.

4.12 *Cis* and *Trans* [dichloro bis(tri-n-butylphosphine)Platinum(II)]

The ^{13}C solid-state spectra obtained for these two isomers were found to reveal some interesting structural differences between the *trans* and *cis* isomers.

FIGURE 4.33 *Cis* and *trans* isomers of [dichloro bis(tri-n-butylphosphine)Platinum(II)]

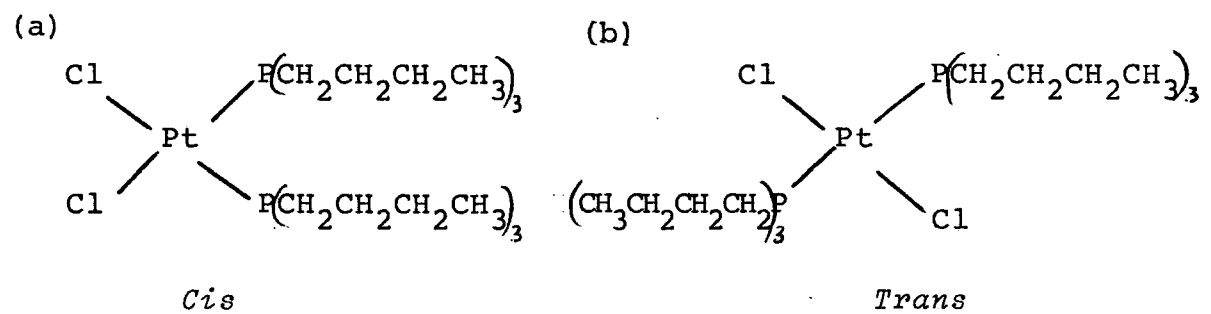

Cis *Trans*

The ^{13}C CP/MAS spectrum for the *cis* isomer (Figure 4.34(a) exhibits a broad band at ∿27 ppm. and also two "doublets" at 15.1, 15.8 ppm. and 17.1, 18.3 ppm; the latter pair of lines having twice the intensity of the high frequency lines. The NQS spectrum (Figure 4.34(b)) shows the doublets to be due to the methyl groups of the nBu_3P ligands. There is also a small amount of methylene carbon resonance remaining due to an

FIGURE 4.34 ^{13}C CP/MAS spectra of *cis*$[PtCl_2(nBu_3P)_2]$

(a) CP/MAS
SF = 50.29MHz
NT = 5000
AQ = 0.010s
DR = 3Hz/pt
DO = 5s
D2 = 2ms
SS = 3kHz

No.	δ/ppm
1	28.4
2	26.8
3	21.9
4	18.3
5	17.1
6	15.8
7	15.1

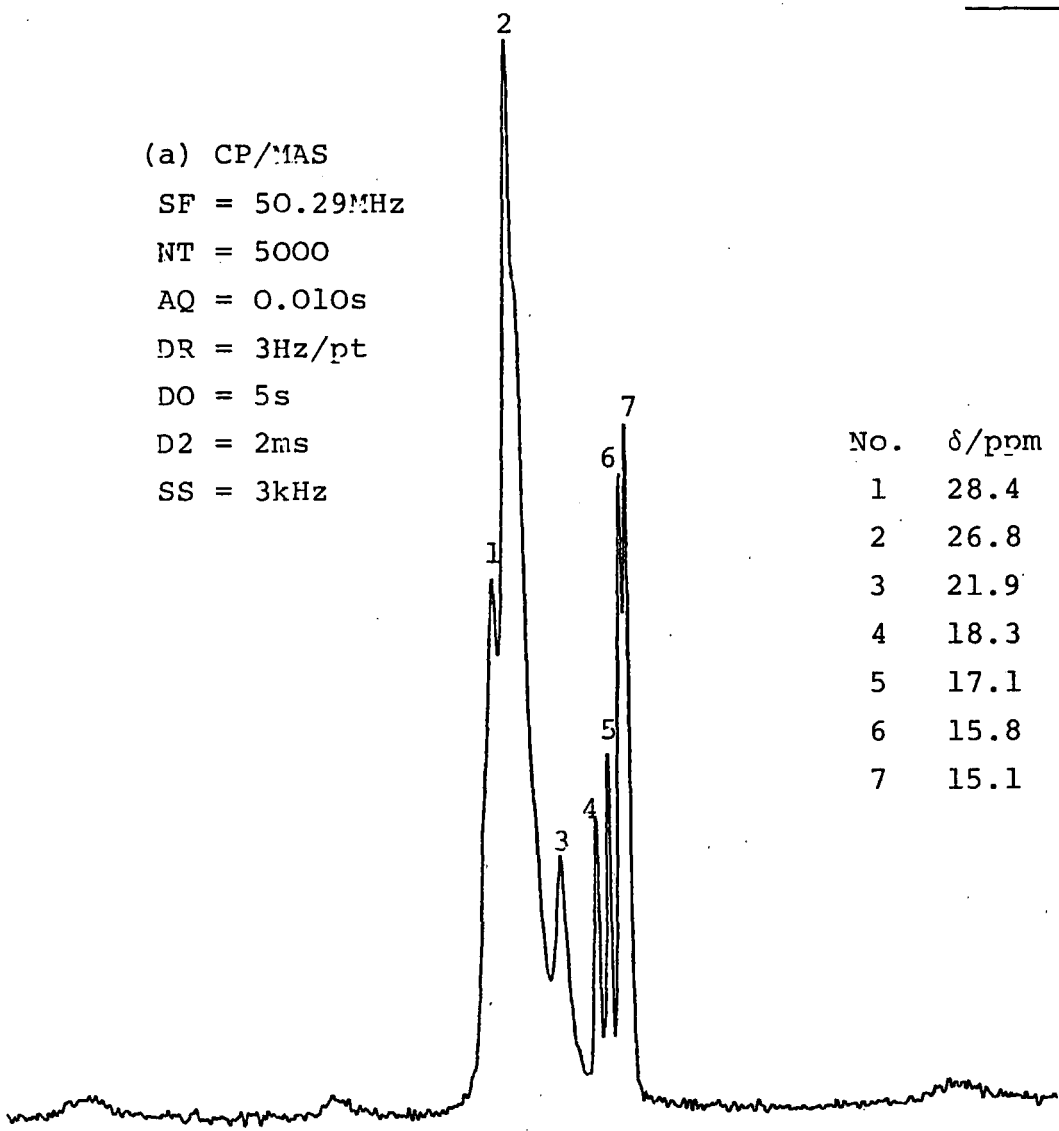

(b) NQS

τ = 60μs

(conditions as for (a))

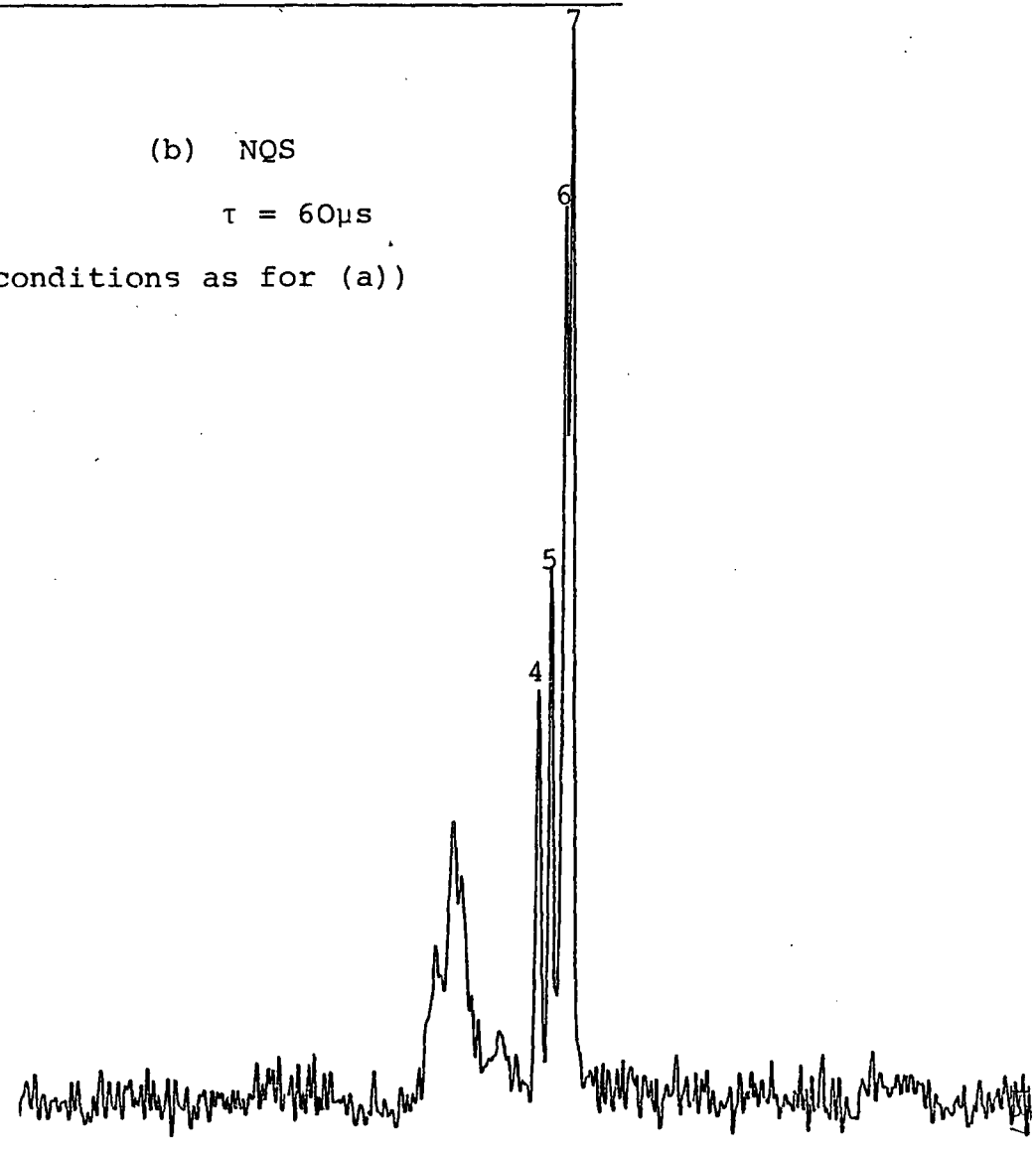

insufficient length of τ (delay window in FID) used. Any ^{13}C-^{13}P scalar coupling present between the methyl carbons and the phosphorus atoms would not be observed due to its expected low magnitude ($^{4}J_{C,P}$ ~10Hz[32]).

The splittings of the methyl resonances can be explained by considering conformational effects of the nBu_3P ligands, (see Figure 4.35), which is similar to that seen for the phenyl resonances of *cis* $[PtR_2(PPh_3)_2]$ (R = Me, Ph).

FIGURE 4.35 Non-equivalence of nBu_3P ligands attached to platinum.

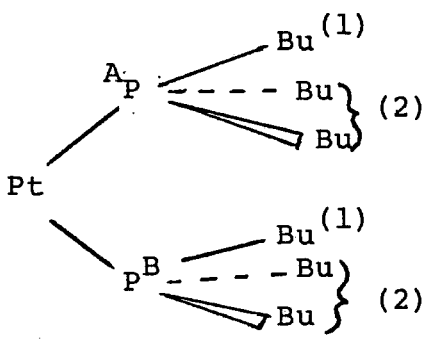

(Number of equivalent Butyl groups from each ligand indicated, ambiguously assigned).

The most intense doublet at 15.8 and 15.1 ppm. arises due to two equivalent butyl groups from each non-equivalent nBu_3P ligand, the second doublet at 18.3 and 17.1 ppm due to the remaining non-equivalent butyl groups.

The carbon-13 solid-state NMR data agrees well with the ^{31}P CP/MAS spectrum (Figure 4.36). This shows two central peaks at 5.2 and 4.1 ppm. with two ^{195}Pt-^{31}P coupling constants of 3514 and 3496 Hz which can be considered equivalent given the digitization rate of 17Hz/Pt. The two phosphorus resonances are almost certainly due to two non-equivalent phosphorus atoms

FIGURE 4.36 ^{31}P CP/MAS spectrum of *cis* $[PtCl_2(nBu_3P)_2]$ (expansion)

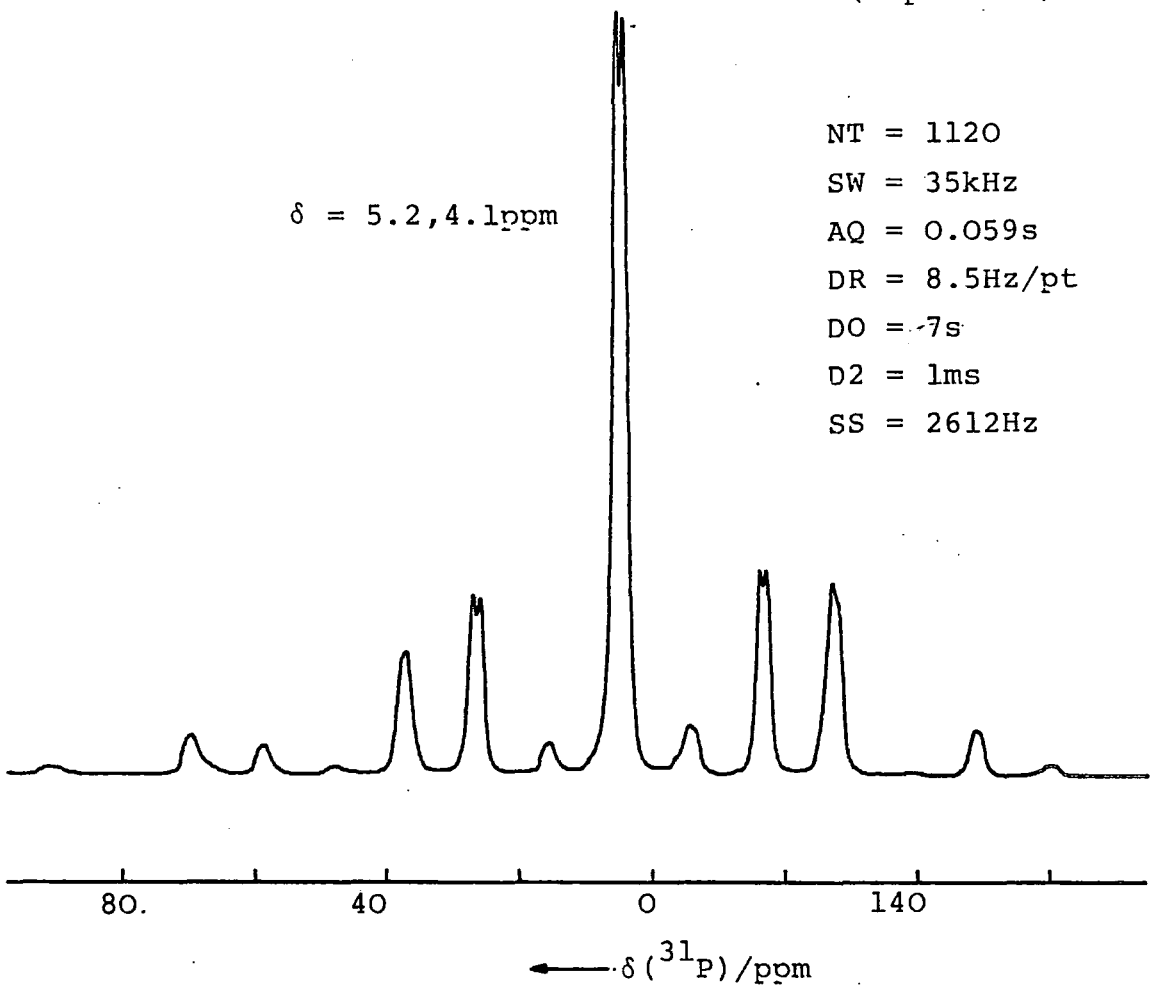

FIGURE 4.39 ^{31}P CP/MAS spectrum of *trans* $[PtCl_2(nBu_3P)_2]$ (expansion)

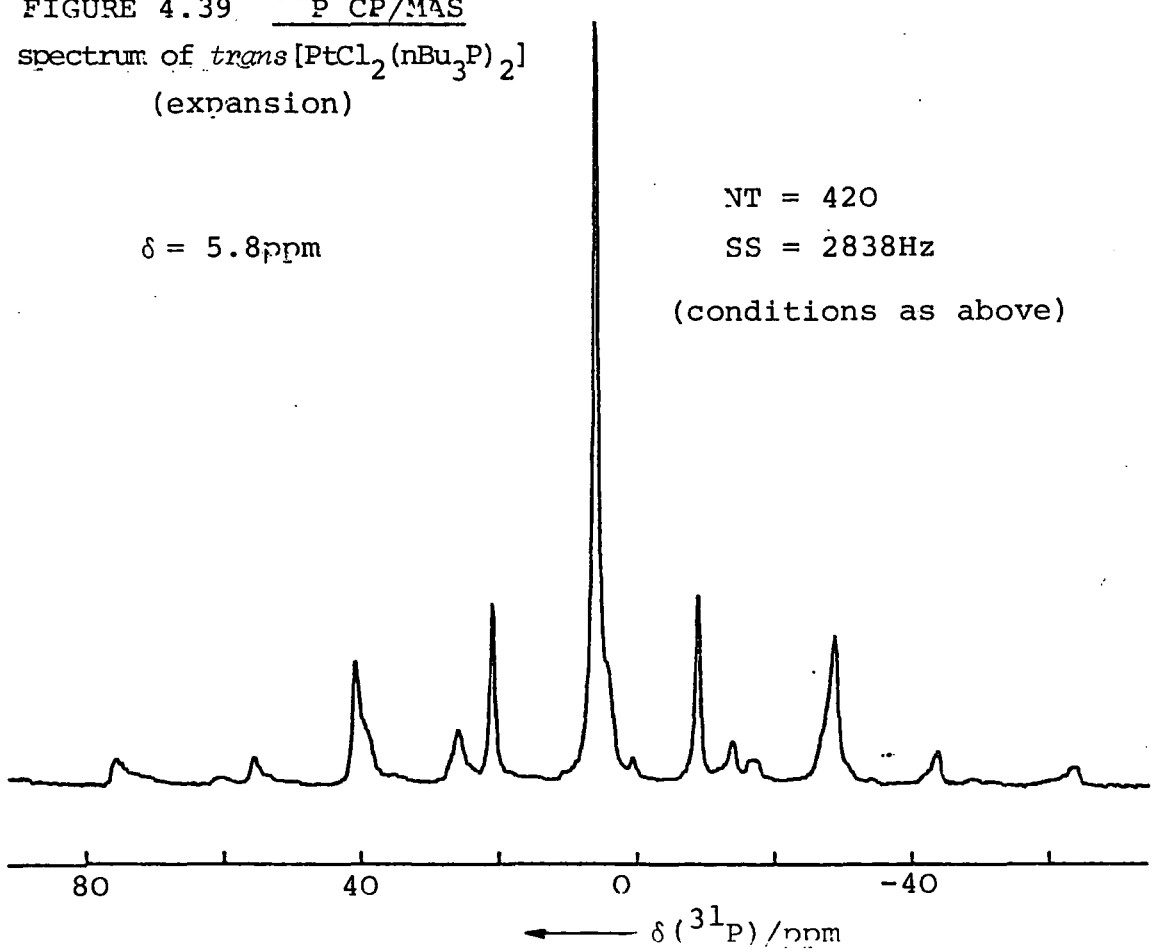

present within the molecule given the ^{13}C NMR data. The very small crystallographic splitting of 1.1 ppm, and the presence of a single ^{31}P-^{195}Pt coupling constant, shows the non-equivalence of the two nBu_3P ligands compared to that seen from other *cis* tertiary phosphines of platinum(II) and illustrates the sensitivity of ^{13}C NMR spectra of *cis* $[PtCl_2(nBu_3P)_2]$.

The methylene region of the ^{13}C NMR spectrum of *trans* $[PtCl_2(nBu_3P)_2]$, (Figure 4.37), shows similar features to that of the *cis* isomer. It is very difficult, however, to assign anything due to the expected difference in chemical shifts for each carbon of the n-butyl groups, also, ^{13}C-^{31}P coupling constants are likely to be present (10-80Hz). The NQS spectrum (Figure 4.38) confirms the presence of a single peak for the methyl carbons at 14.1 ppm. Unlike the cis isomer, the ^{13}C spectra of *trans* $[PtCl_2(nBu_3P)_2]$ show no confirmation inequivalences present. In addition to this, the phosphorus-31 spectrum (Figure 4.39) also shows a single resonance at 5.8 ppm. with a platinum-phosphorus coupling constant of 2420Hz, which agrees well with the solution-state data (see Table 4.2.1). The ^{31}P solid-state NMR data thus conclusively show that the crystal structure of *trans* $[PtCl_2(nBu_3P)_2]$ contains only one independent molecule per unit cell with the two nBu_3P ligands equivalent.

4.13 *Cis* and *trans* [Dichloro bis(triphenylphosphine)Platinum(II)]

The ^{31}P solution-state NMR data obtained for the *cis* and *trans* isomers of $[PtCl_2(PPh_3)_2]$ show, as expected, single ^{31}P

FIGURE 4.37

^{13}C CP/MAS spectrum of *trans*$[PtCl_2(nBu_3P)]$

SF = 50.29MHz
NR = 4000
SW = 10kHz
AQ = 0.102s
DR = 3Hz/pt
DO = 5s
D2 = 1ms
SS = 3kHz

No.	δ/ppm
1	26.8
2	24.4
3	20.7
4	17.1
5	14.1

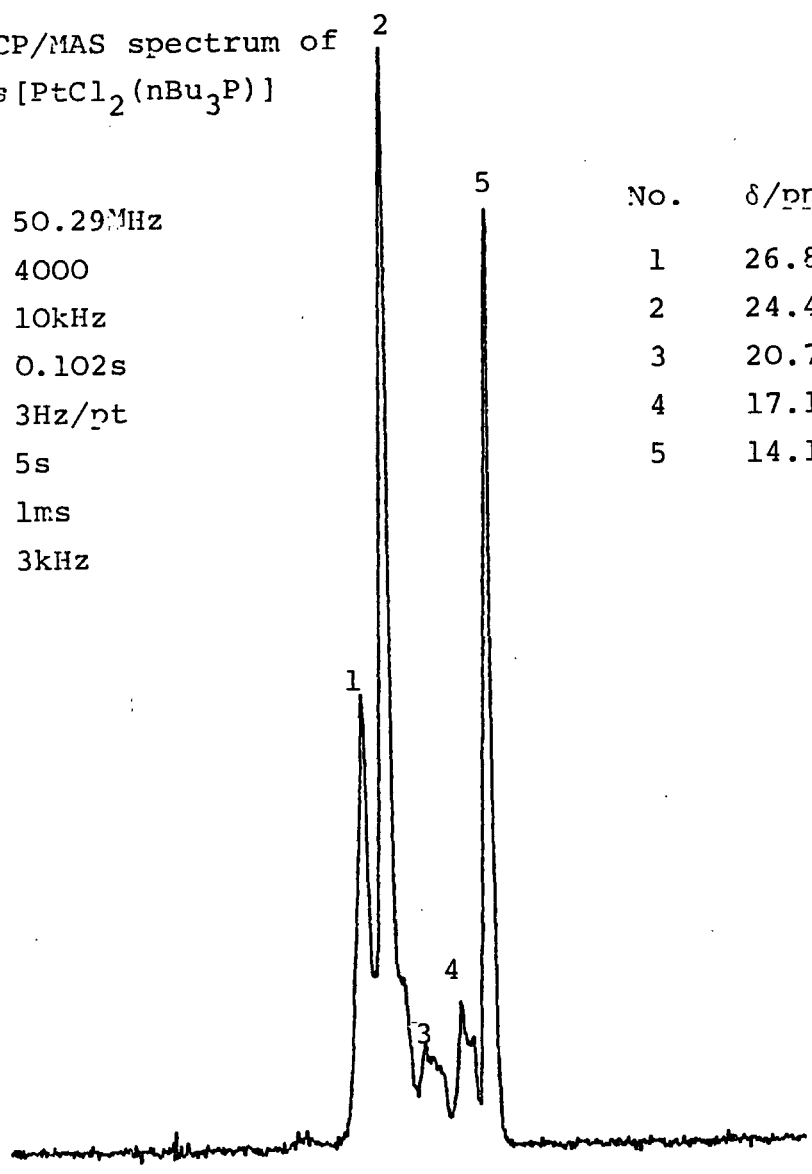

FIGURE 4.38

^{13}C NQS/MAS spectrum of *trans*$[PtCl_2(nBu_3P)_2]$

τ=100μs

(conditions as for Fig.4.37)

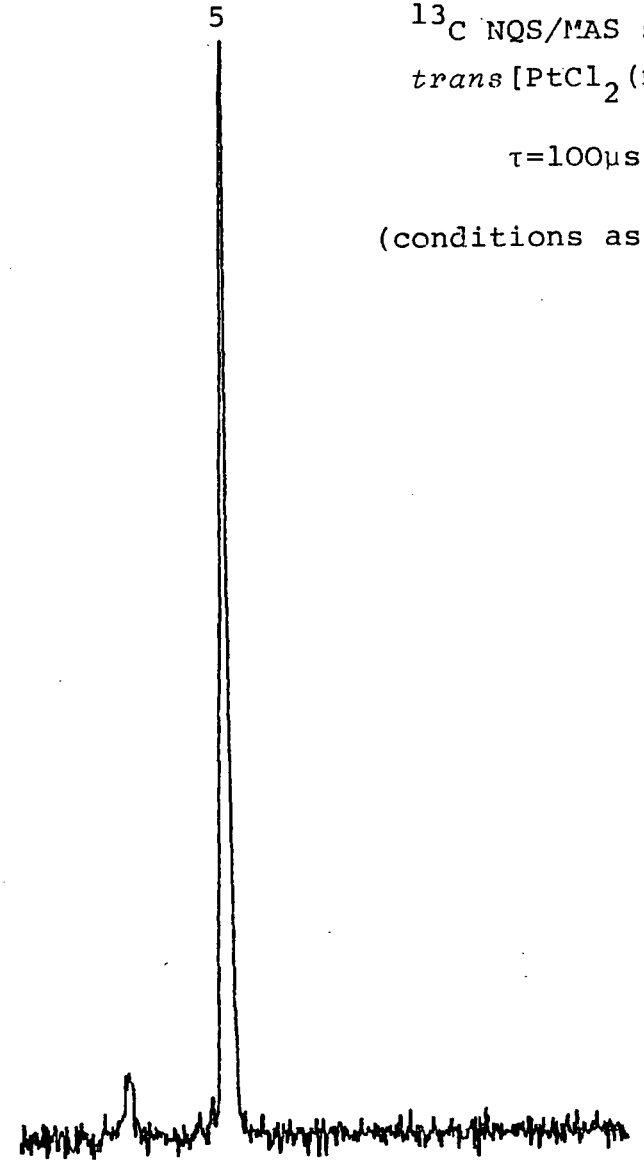

resonances at 14.3 and 19.8 ppm. respectively due to motional averaging of any inter- and intramolecular inequivalences present in the solid-state. The ^{31}P solid-state spectrum for the *cis* isomer (Figure 4.40) exhibits a very different splitting to that predicted considering the other *cis*-phosphines studied. Instead of the expected pair of equally intense peaks caused by intramolecular non-equivalence, there are three lines of ratio 1:1:2 at a slightly lower frequency shift to that obtained in solution ($\delta_{^{31}P}$ = 12.4, 11.0 and 7.6 ppm. respectively). In addition to this, three phosphorus-platinum coupling constants were observed ($^{1}J_{P,Pt}$ = 3723, 3881 and 3589Hz). Intramolecular non-equivalence can only account for two ^{31}P resonances, therefore there must be at least two non-equivalent crystallographic sites in the unit cell. Such a splitting, for example, could arise if one site has a mirror plane passing through the centre of the molecule rendering the two *cis* phosphorus atoms equivalent, while the other site could have a lower symmetry causing intramolecular inequivalence.

The ^{13}C NQS spectrum of the *cis* isomer (Figure 4.41) agrees with the ^{31}P solid-state NMR results in that at least three types of quaternary carbon are present giving rise to three lines of ratio 1:2:1 (see Figure 4.41). It cannot be determined whether the extra splittings in the phenyl region are real or due to superimposed noise. The ^{13}C NQS spectrum of *trans* $[(PtCl_2(PPh_3)_2]$ gives rise to only one peak at 127.9 ppm. which indicates only one type of quaternary carbon present and therefore both PPh_3 ligands are equivalent in the molecule. The last statement is not unreasonable considering the results

FIGURE 4.40 ^{31}P CP/MAS spectrum of *cis* $[PtCl_2(PPh_3)_2]$

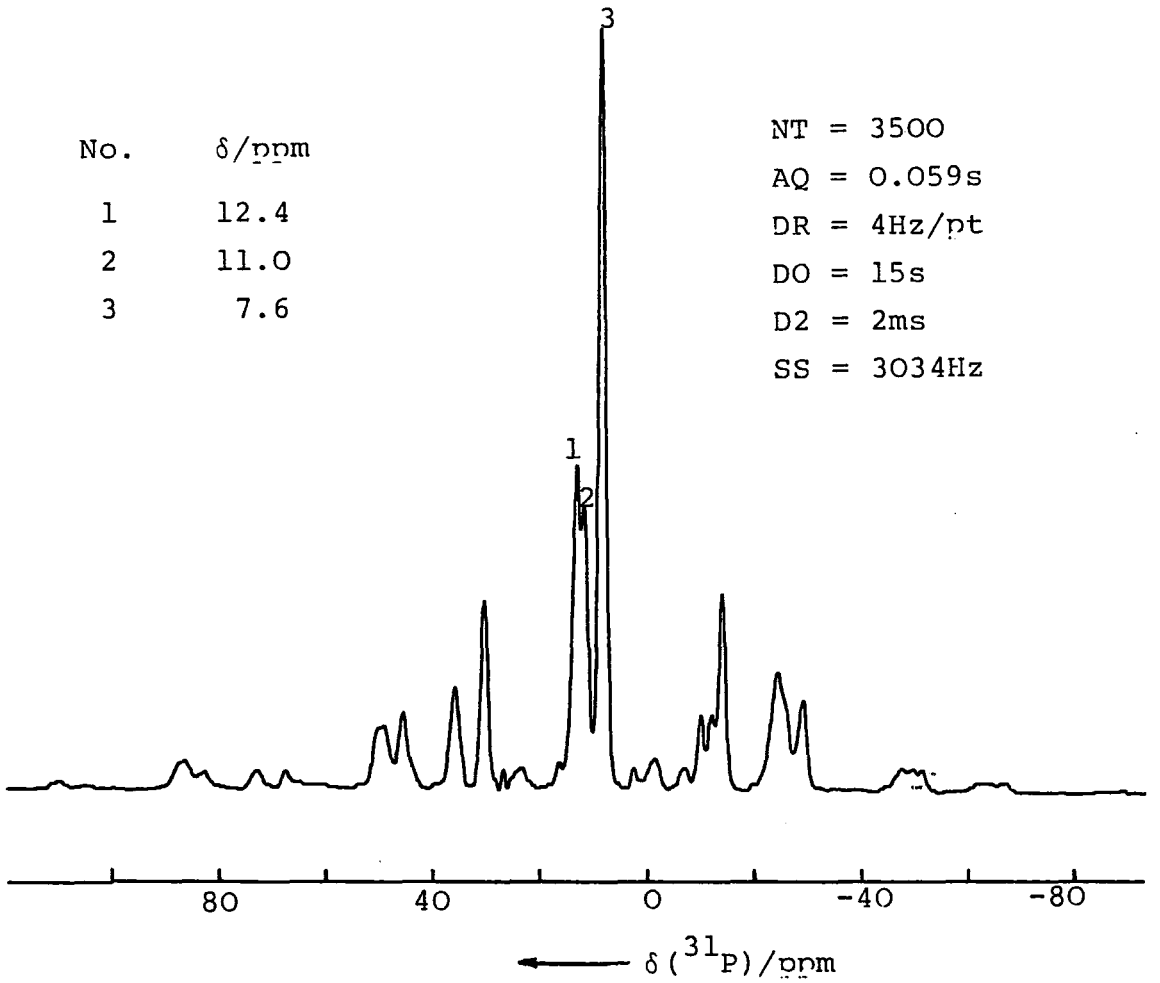

FIGURE 4.42 ^{31}P CP/MAS spectrum of *trans* $[PtCl_2(PPh_3)_2]$

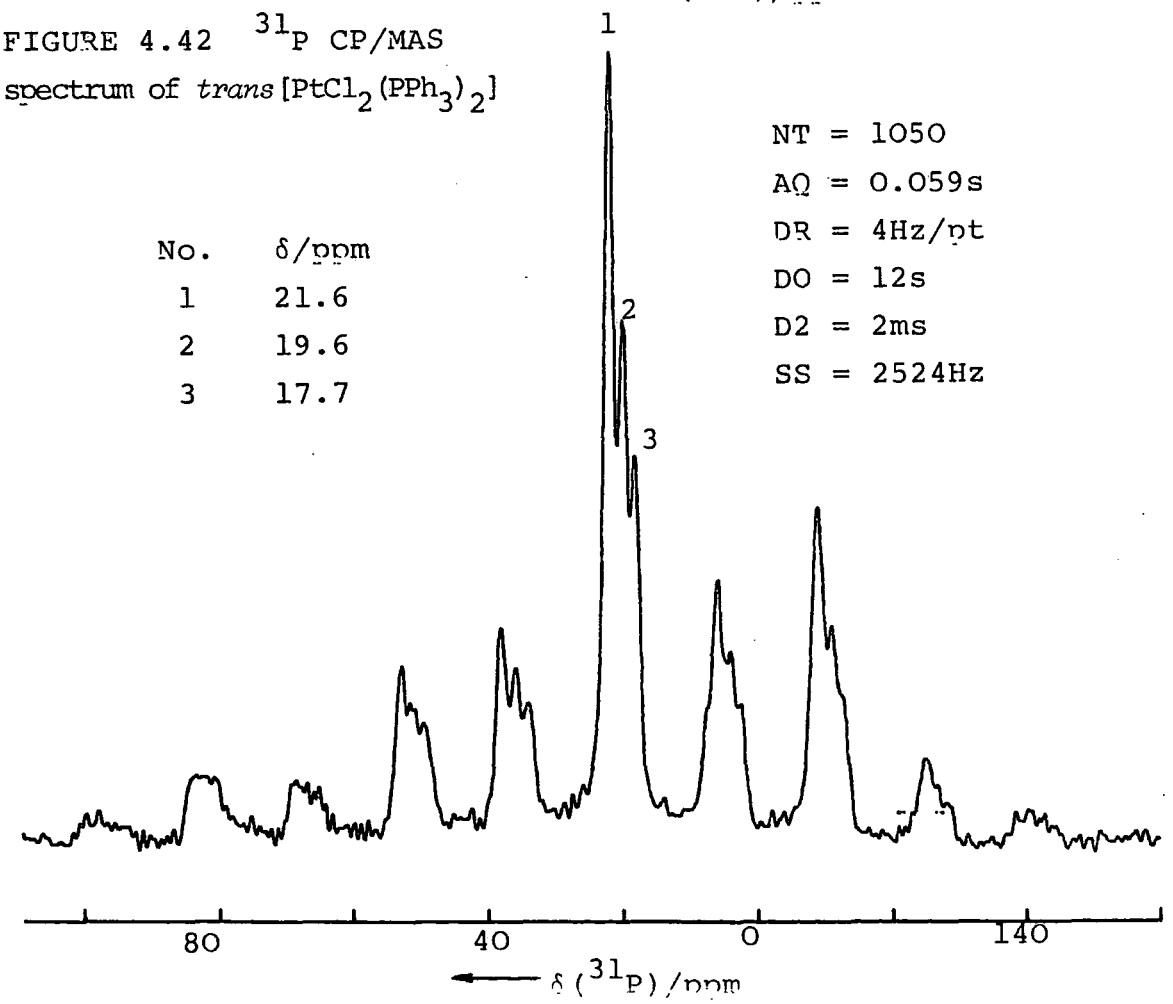

FIGURE 4.41 ^{13}C NQS/MAS spectrum of *cis*$[PtCl_2(PPh_3)_2]$

No.	δ/ppm
1	132.6
2	131.2
3	128.6
4	123.7

SF = 50.29MHz
NT = 5500
SW = 20kHz
AQ = 0.051s
DR = 5Hz/pt
DO = 15s
D2 = 2ms
SS = 3kHz

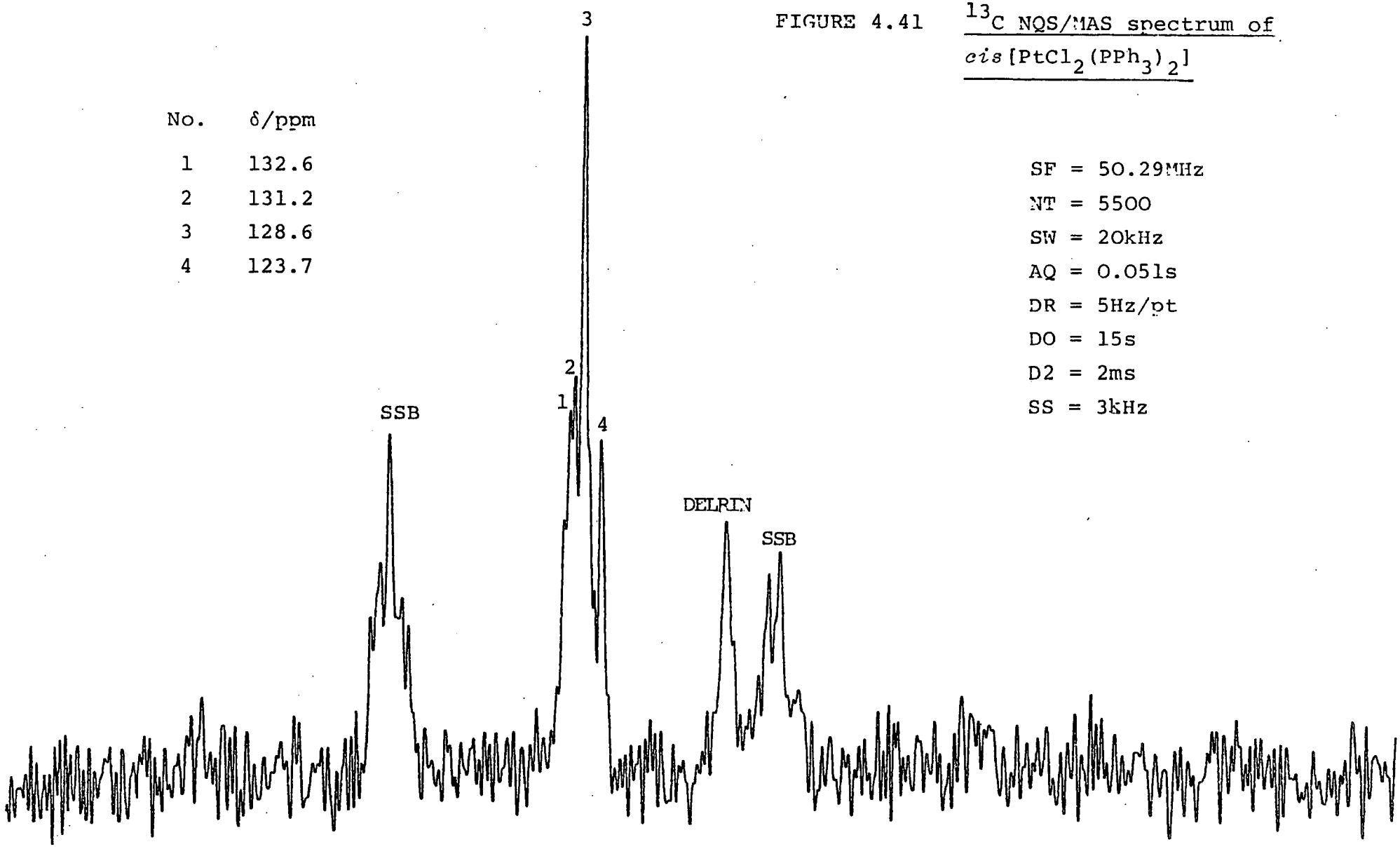

of *trans* $[PtCl_2(PEt_3)_2]$ and $[PtCl_2(nBu_3P)_2]$. However, the ^{31}P CP/MAS spectrum of the *trans* isomer does not give rise to the expected single resonance but three lines at 21.6, 19.6 and 17.7 ppm in the approximate ratio of 5:3:2 respectively (see Figure 4.42). The two most intense ^{31}P resonances have the same ^{31}P-^{195}Pt coupling constants associated with them ($/^1J_{P,Pt}/$ = 2604Hz) and a value of 2555Hz is observed for the third phosphorus chemical site.

An independent ^{31}P NMR study has been carried out on the *cis* and *trans* isomers of $[PtCl_2(PPh_3)_2]$ by Fyfe and co-workers,[18] and reveals results which vary considerably with those obtained above (see Table 4.5).

TABLE 4.5 COMPARISON OF ^{31}P SOLID-STATE NMR RESULTS OBTAINED FOR *CIS* AND *TRANS* $[PtCl_2(PPh_3)_2]$

ISOMER	δ/ppm[a]	$^1J_{P,Pt}$[a]/Hz	δ/ppm[b]	$^1J_{P,Pt}$[b]/Hz
Cis	12.4, 11.0, 7.6	3723, 3881, 3589	12.9 8.6	3877, 3623
Trans	21.6, 19.6, 17.7	2604, 2555	20.9, 19.0	2695, 2559

(a) Results obtained in this work.
(b) Reference 18.

The results obtained by Fyfe *et al*[18] are those that would be expected considering the likelihood of intramolecular in-equivalences. The bulkiness of the phenyl groups is likely to impose steric strain in the *trans* molecule rendering the two PPh_3 ligands non-equivalent, unlike *trans* $[PtCl_2(PEt_3)_2]$ and $[PtCl_2(nBu_3P)_2]$ in which the phosphine ligands remain equivalent as in solution.

As can be seen from Table 4.5, the chemical shifts and coupling constants are of similar magnitude in both sets of data. The only discrepancy concerns the number of ^{31}P resonances from different chemical sites present. An explanation for the different results may be sought from the methods of preparation and X-ray crystallography data.

The crystal structure of the *cis* $[PtCl_2(PPh_3)_2]$ has been obtained,[34] and shows there to be one independent molecule in the asymmetric unit. However, it must be noted that the full formula of structure was *cis* $[PtCl_2(PPh_3)_2] \cdot C_3H_6O$, *i.e.*, there was acetone of solvation present. This structure is said to contain discrete well resolved *cis* $PtCl_2(PPh_3)_2$ molecules with the acetone of solvation filling in the cavities. There are no intermolecular contacts of the Van der Waals type with the main molecule, and the acetone of solvation fills what would have otherwise been gaps in the crystal lattice. The two PPh_3 ligands within the molecule are shown to be inequivalent agreeing with the ^{31}P solid-state NMR data obtained by Fyfe *et al.*[18] Of course, this is assuming that this NMR data is of the same compound *cis* $[PtCl_2(PPh_3)_2] \cdot C_3H_6O$ as no mention is given to any crystal of solvation present.

The compound studied in this work was *cis* $[PtCl_2(PPh_3)_2] \cdot CH_2Cl_2$. Therefore the difference in the two sets of ^{31}P NMR data (Table 4.5) can be attributed to the different crystals of solvation present. A further independent ^{31}P NMR study, carried out by Knight *et al*,[42] of the *cis* isomer reveals a spectrum with exactly the same appearance as in Figure 4.40. Although no chemical shifts are reported the ^{31}P-^{195}Pt coupling constants are given as 3725, 3715 and 3546Hz. The solvent of

crystallization for this compound being methylene chloride.

It is most probable that the *trans* isomer studied by Fyfe *et al* also contains acetone of solvation. The ^{31}P spectrum shown in Figure 4.42 is of *trans*$[PtCl_2(PPh_3)_2]$ with methylene chloride of solvation, thus causing its similarity with the *cis* isomer. Little information was obtained from the ^{13}C NQS spectrum exhibiting only a single peak at 128 ppm. The explanation of the discrepancies may be proved by re-synthesizing from CH_2Cl_2 and acetone solutions separately and then obtaining both the ^{31}P CP/MAS spectra and X-ray crystal structures.

4.14 Platinum-Tin Bonded Systems: ^{31}P CP/MAS Study of [Chloro(trichlorostannyl)*bis*(triphenylphosphine)Platinum(II)]

Metal-metal bonds in transition metal complexes are becoming of increasing interest in academic circles. In the case of platinum coordinated to tin there is also an industrial interest as platinum complexes of tertiary phosphines combine with tin(II)dichloride to provide active hydrogenation and hydroformylation catalysts. Full characterization of catalysts is often necessary; however, in some cases it is not possible to dissolve a solid sample, such that the structural integrity of the sample is retained, for solution-state analysis. Such samples are often amorphous or otherwise unsuitable for X-ray work and so solid-state NMR is the obvious choice of analysis given the presence of spin-½ nuclei.

The syntheses of the *cis* and *trans* isomers of $PtCl(SnCl_3)(PPh_3)_2$ were attempted using known methods.[43] An orange and off-white compound resulted from the *cis* and

trans syntheses respectively, which agreed with that noted in the literature. Atomic absorption showed the orange product to contain 16% Cl and 14% Pt which differs considerably with the calculated values of $PtCl_2(SnCl_3)(PPh_3)_2$, 14.5% Cl and 19.9% Pt. The ^{31}P CP/MAS obtained for this compound revealed little information, containing two very broad peaks at 9.5 and 21.1 ppm. No difference could be seen between the IR spectra of both compounds and solution-state analysis was ruled out by the fact that dissociation was said to take place in solution. Elemental analysis of the off-white product gave the proportions 14.3% Cl and 19.8% Pt, which were much more consistent with the theoretical, calculated values. The isomeric properties of this compound were determined using phosphorus-31 solid-state NMR.

Two different ^{31}P CP/MAS were obtained at variable spinning speeds (2606 and 3174Hz). In both spectra, (Figures 4.43 and 4.44) two phosphorus resonances are observed at 29.7 and 14.4 ppm. with associated ^{195}Pt satellites ($/^{1}JP,Pt/$ = 3209 and 3636Hz). The ratios of the ^{31}P centre-bands are different and can be accounted for by the additional linewidth of the low frequency peak. This is most likely due to a difference in motion between the two PPh_3 ligands. The magnitude of the platinum-phosphorus couplings is very similar to that observed in *cis* dichloro-tertiary phosphines of platinum(II) (see Table 4.2). Extra splittings are seen by observing the ^{31}P spectrum at a higher spinning speed (Figure 4.44). Tin-satellites are observed from the high frequency phosphorus resonance, showing coupling of phosphorus to the isotopes Tin-119 and Tin-117, which have not been

^{31}P CP/MAS spectra of *cis*[PtCl($SnCl_3$)(PPh_3)$_2$]

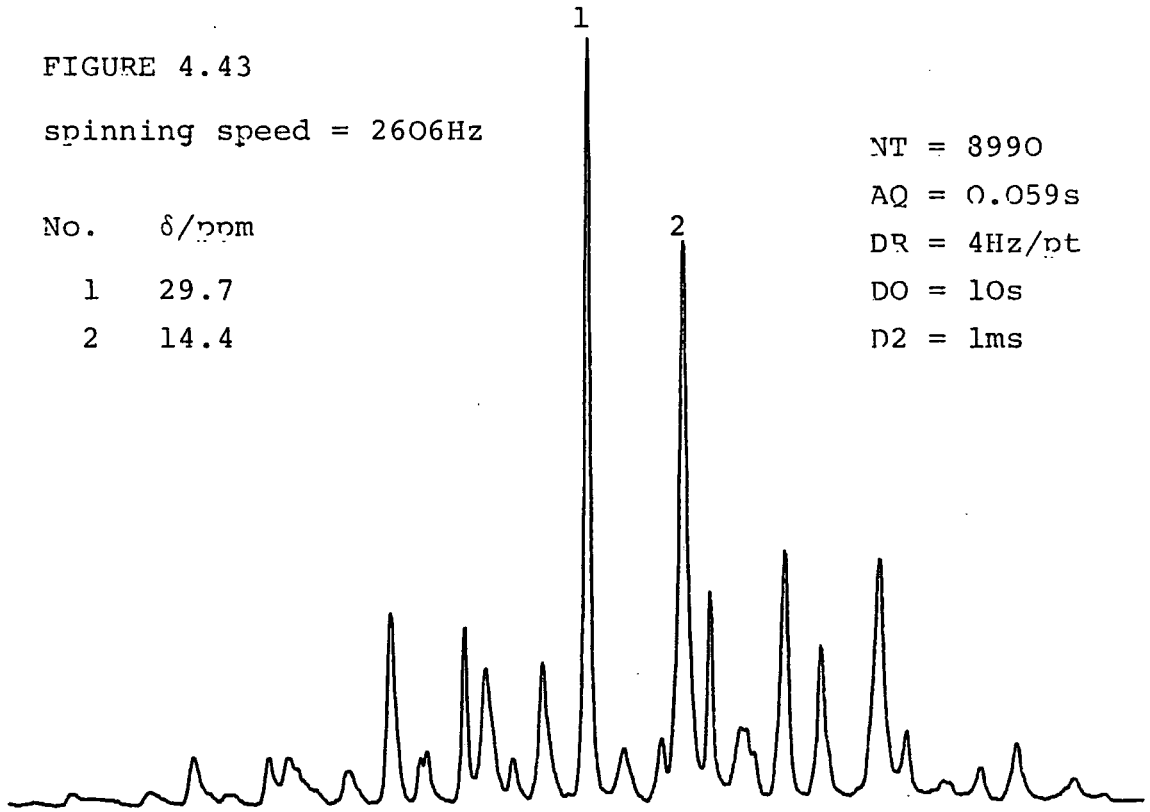

FIGURE 4.43

spinning speed = 2606Hz

No.	δ/ppm
1	29.7
2	14.4

NT = 8990
AQ = 0.059s
DR = 4Hz/pt
DO = 10s
D2 = 1ms

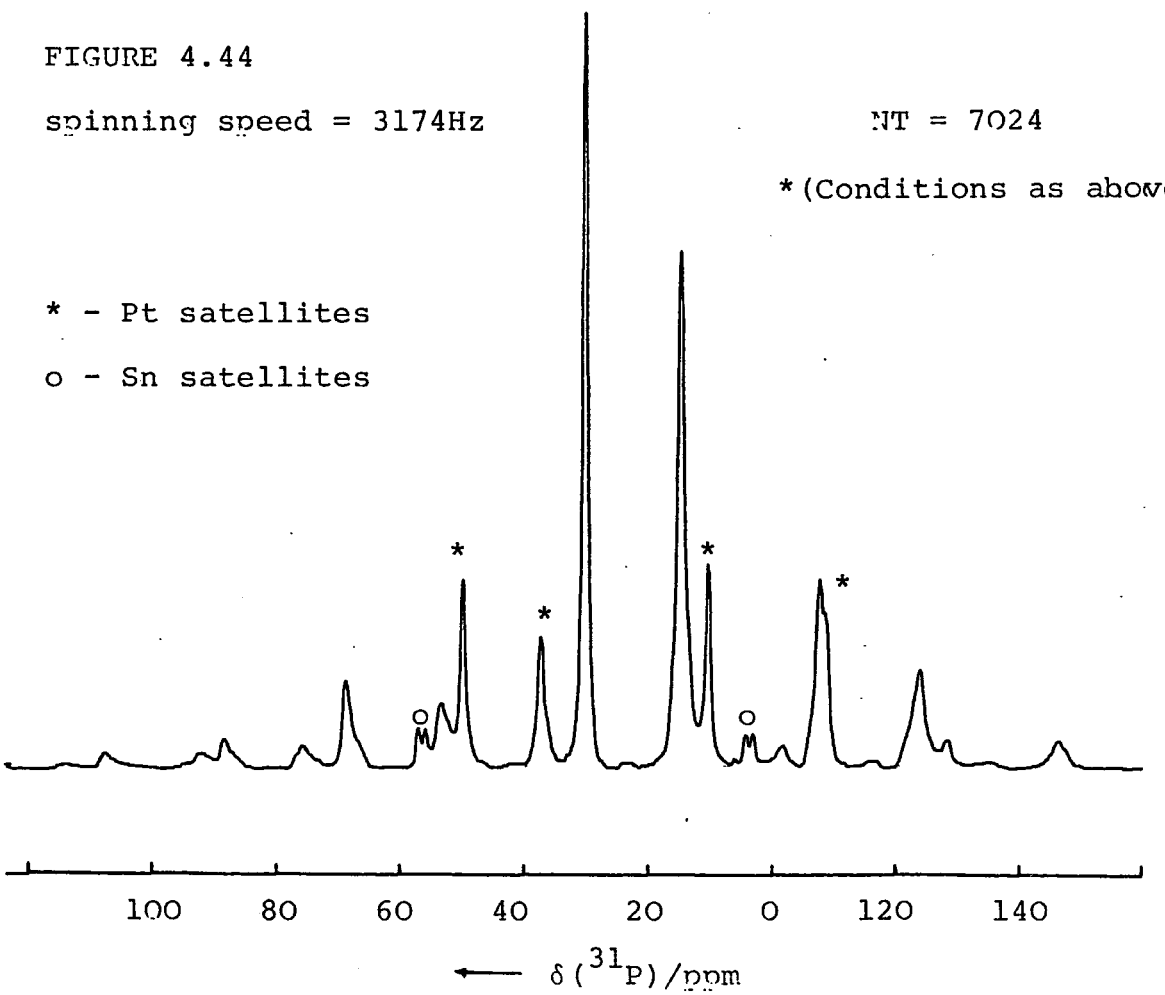

FIGURE 4.44

spinning speed = 3174Hz

NT = 7024

*(Conditions as above)

* - Pt satellites

o - Sn satellites

observed in the solid-state before ($^{2}J_{P}$, $^{119}_{Sn}$ = 4373Hz, $^{2}J_{P},^{117}_{Sn}$ = 4186Hz). The presence of tin satellites was checked by showing the ratio of $\gamma^{119}_{Sn}/\gamma^{117}_{Sn}$ to be equal to the ratio J_{P}, $^{119}_{Sn}/J_{P}$, $^{117}_{Sn}$, and that the heights of the satellites are ∿5% of the central peak (taking into account the natural abundances of 8.58% and 7.61% for the 119 and 117 tin isotopes respectively).

FIGURE 4.45 *Cis* and *trans* isomers of $[PtCl(SnCl_3)(PPh_3)_2]$

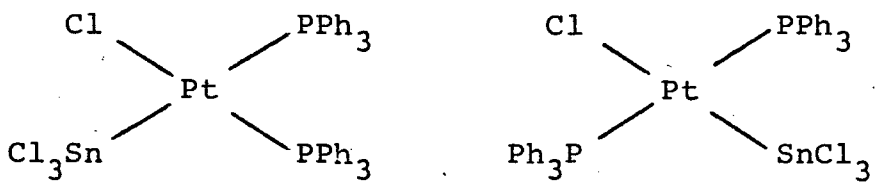

cis *trans*

The reason why ^{195}Pt - ^{31}P coupling is seen for both resonances and ^{31}P - $^{119/117}Sn$ coupling only seen for one can be explained by considering the molecular structure of the two isomers (Figure 4.45). As mentioned earlier, the magnitude of the ^{195}Pt - ^{31}P coupling constants suggests the presence of the *cis* isomer. If the *trans* isomer was present, the ^{195}Pt - ^{31}P coupling constant would be of the order of 1800Hz, furthermore, there would be two small values of *cis* $^{2}J_{P,Sn}$. That is, if any phosphorus-tin coupling was observed it would be present for both phosphorus resonances. A final point to note is that the phosphorus resonances in the *trans* isomer would be very similar. The separation between the two ^{31}P peaks of over 15 ppm. and the magnitude of the P-Pt and P-Sn coupling constants shows that the off-white product is in fact the *cis* isomer, contrary to that noted in the literature.[43]

TABLE 4.6 ^{31}P Solution-state NMR Data for $[PtCl(SnCl_3)(PPh_3)_2]$[a]

Isomer	$\delta^{b}_{31P/ppm}$	$^{1}J^{c}_{(Pt,P\ trans)}$	$^{1}J^{c}_{(Pt,P\ cis)}$	$^{2}J^{c}_{(Sn,P\ trans)}$	$^{2}J^{c}_{(Sn,P\ cis)}$
cis[d]	26.2, 7.9	3107	3634	4298	216
trans[e]	17.5	-	2327	-	226

a. In CH_2Cl_2 at 25°C.

b. Chemical shifts relative to external 85% H_3PO_4.

c. In Hz; the *cis* and *trans* labelling for the coupling constants are with respect to the trichloride ligand.

d. Actual phosphine ligand is $(p\text{-tolyl})_3P$.

e. Actual phosphine ligand is $(p\text{-ClPh})_3P$.

The solution-state ^{31}P NMR studies of almost identical compounds have been obtained,[35] (see Table 4.6), and agree very well with the solid-state ^{31}P NMR data showing conclusively that the spectrum (Figure 4.44) is of the *cis* isomer. In solution-state, a small value of ^{2}J(Sn-P *cis*) was obtained (216Hz), this is concealed in the solid-state due to substantial linewidths of ≥100Hz.

A difference in $J_{Pt,Sn}$ of ≃ 12kHz between the cis and trans isomers of $Pt(SnCl_3)(PPh_3)_2$ would have been expected, had the attempts to obtain ^{195}Pt and ^{119}Sn solid-state spectra proved successful.

4.15 Phosphorus-31 NMR Study of the η^1 and η^2-coordination in (mesityl(diphenylmethylene)phosphine)*bis*(triphenyl phosphine)platinum(0)

Phosphaalkenes, $R_2C{=}PR'$, and phosphaalkynes, $RC{\equiv}P$, can act as either $\eta^1(\sigma)$-phosphorus donors (Figures 4.46(a) and (c)) or $\eta^2(\pi)$ donors (Figures 4.46(b) and (d)) towards transition metals.

FIGURE 4.46

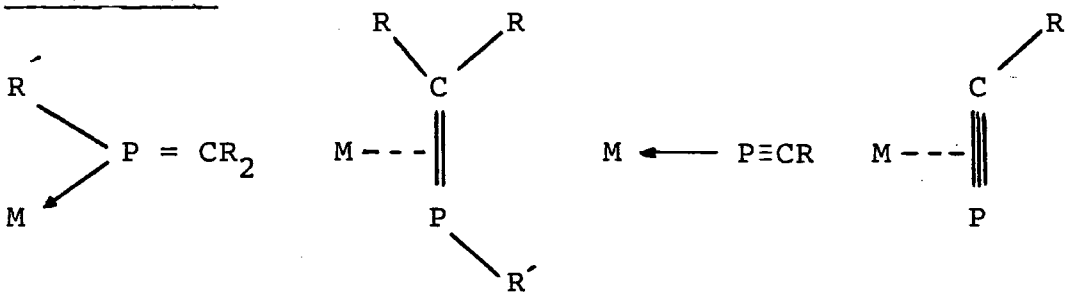

(a) (b) (c) (d)

The delicate balance of factors determining η^1 or η^2-phosphaalkene bonding is illustrated by a report on several Pt(σ) complexes in which the bonding mode differed, *e.g.* η^1 in PtL_3 and $PtL_2(^tBuCP)$ but η^2 in $PtL[(PPh\,CH_2)_3CMe]$, (L = P(mesityl)=CPh_2).[36] The different types of coordination were studied in solution using ^{195}Pt and ^{31}P NMR.

It is possible that the solid-state may contain a different type of coordinated ligand to that present in the solution-state. Bickelhaupt *et al* have studied the phosphaalkene $(Ph_3P)_2Pt(mesP{=}CPh_2)$ in solution, using ^{31}P NMR, and in the solid-state, using X-ray crystallography.[37] This compound may exist in two possible forms, (1) with the P=C function pi-bonded to the platinum atom (Figure 4.47(a)) and (2) the function sigma-bonded (Figure 4.47(b)).

FIGURE 4.47 The two types of coordination for the mesityl(diphenylmethylene)phosphine ligand

(a)

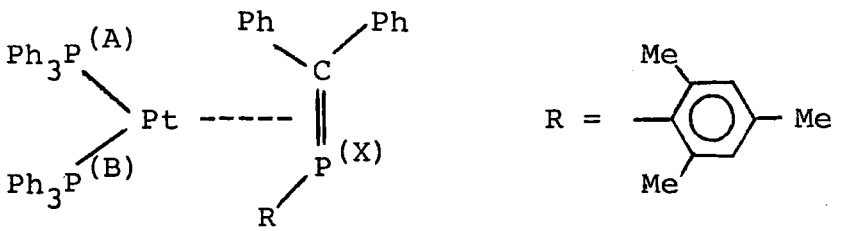

π-bonded (η^2)

(b)

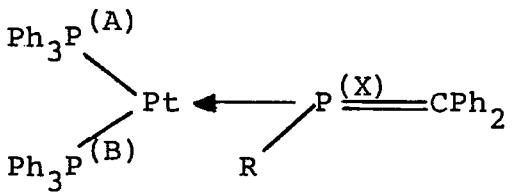

σ-bonded (η^1)

The ^{31}P NMR solution-state spectrum of this compound obtained at room temperature was found to be broad, however at -55°C (±1) the ^{31}P NMR spectrum (at 101.26MHz) was sharp and showed some interesting features (see Table 4.7).

TABLE 4.7 SOLUTION-STATE ^{31}P NMR DATA FOR $(Ph_3P)_2Pt(MesP{=}CPh_2)$[a]

	b	$^1J_{Pt,P}$ c	$^2J_{P,P}$ c
P(A)[d,e]	21.9 (22.8)	3359 (3368)	P_AP_B 29.6 (29.3)
P(B)[d,e]	22.2 (24.2)	3392 (3398)	P_BP_X 11.1 (9.8)
P(X)[d]	-33.5 (-30.9)	505 (498)	P_XP_A 56.4 (53.7)

(a) Values in parenthesis from J.Nixon *et al*[38] (in toluene solution at -50°C).

(b) In ppm relative to external 85% H_3PO_4; toluene-d_8 , -56.5°C .

(c) In Hertz.

(d) Letters relate to those in Figure 4.50

(e) Ambiguously assigned.

The ^{31}P NMR solution data reveals three phosphorus resonances due to the three different types of phosphorus environments in the molecule. While the ^{31}P NMR parameters of the two non-equivalent triphenylphosphine phosphorus atoms are normal, those of the P(X) atom are quite unusual. The very low value of $^{1}J_{Pt,P}$ (505Hz) for the third phosphorus atom coupling to platinum, suggests that P(X) is not directly bonded to the platinum, for which one would expect a value of 3-4kHz, indicating the presence of the η^2 coordination in solution. Furthermore, the large value of $^{2}JP_XP_A$ (56.4Hz) can be interpreted as *pseudo trans* coupling, whereas the small value of $^{2}J\ P_BP_X$ resembles a *cis* coupling, which would be consistent with the $\eta^2(\pi)$ bonded structure (Figure 4.47(a)). An extra point to note is that if the σ-bonded structure was present in solution $^{1}J\ P_AP_X$ and $^{2}J\ P_BP_X$ would be almost equivalent and significantly larger in magnitude.

The X-ray crystal structure determined for the compound shows discrete monomeric units in which the Pt atom has a distorted trigonal coordination.[37] All three phosphorus atoms are in one plane with the platinum and sigma coordinated. The bond angle at P_X (R-$\hat{P}$=C) is 108.5° which is smaller than that expected for sp^2 hybridization (120°) but similar to that of sp^3 hybridization, indicating a sigma-bonded system present. Since the solution NMR data and the solid-state X-ray structural information were at variance, a high resolution solid-state ^{13}C and ^{31}P NMR study was undertaken.

The ^{13}C CP/MAS spectrum of $(Ph_3P)_2Pt(mesP{=}CPh_2)$ (Figure 4.48) shows a very complex aromatic region (123.7-154.0 ppm) and two peaks at 23.7 and 21.7 ppm, (peak height

FIGURE 4.48 ^{13}C CP/MAS spectrum of $Pt(PPh_3)_2(P(mesityl)=CPh_2)$

No.	δ/ppm
1	153.5
2	143.9
3	140.9
4	138.2
5	133.4
6	128.4
7	127.4
8	23.7
9	21.7

SF = 50.29MHz
NT = 7500
SW = 20kHz
AQ = 0.051s
DR = 5Hz/pt
D0 = 10s
D2 = 5ms
SS = 3kHz

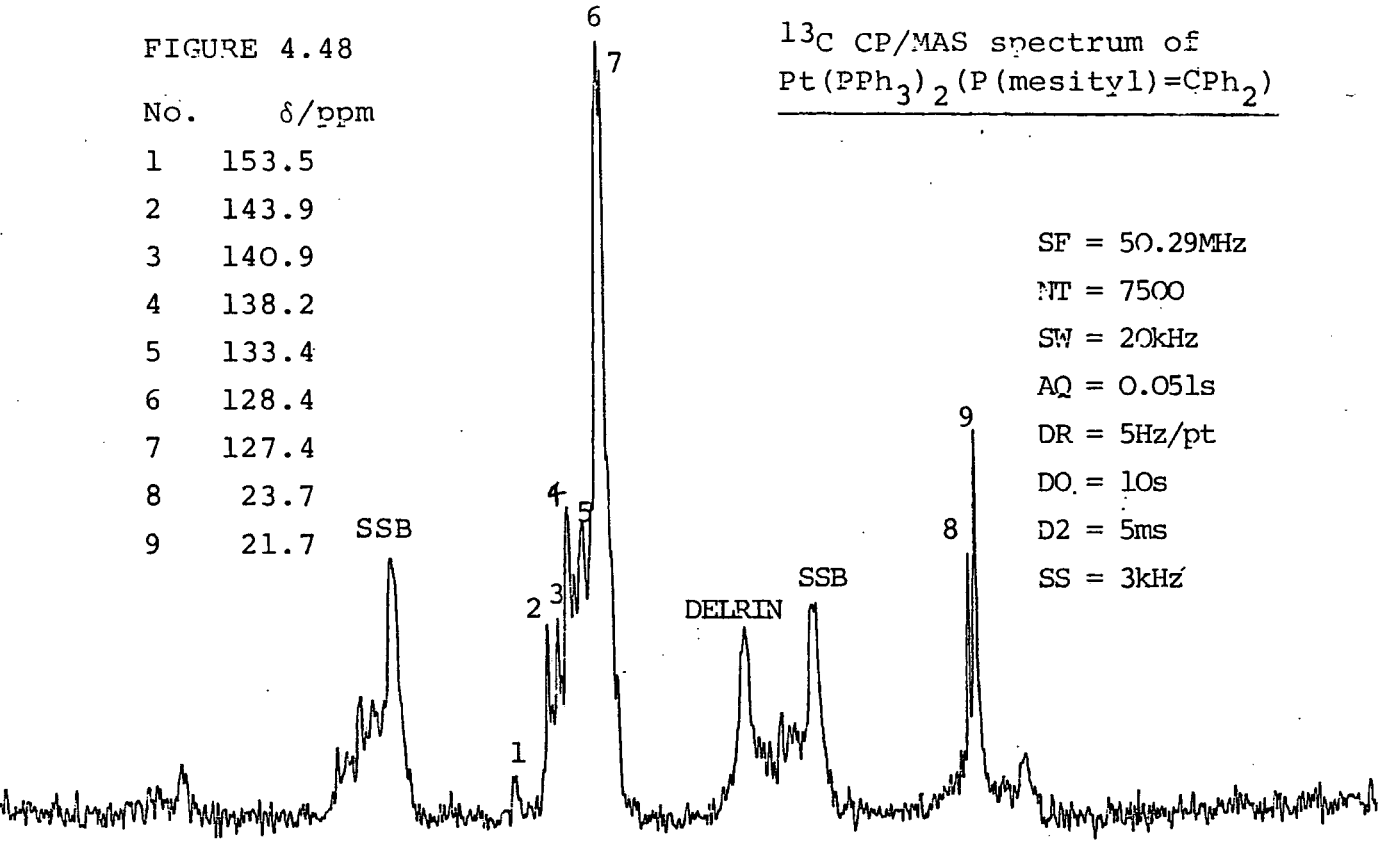

FIGURE 4.49 ^{13}C NQS/MAS spectrum of $Pt(PPh_3)_2(P(mesityl)=CPh_2)$

No.	δ/ppm
1	153.3
2	144.0
3	140.8
4	137.4
5	135.7
6	130.2
7	23.4
8	21.7

Conditions as above
τ=50μs

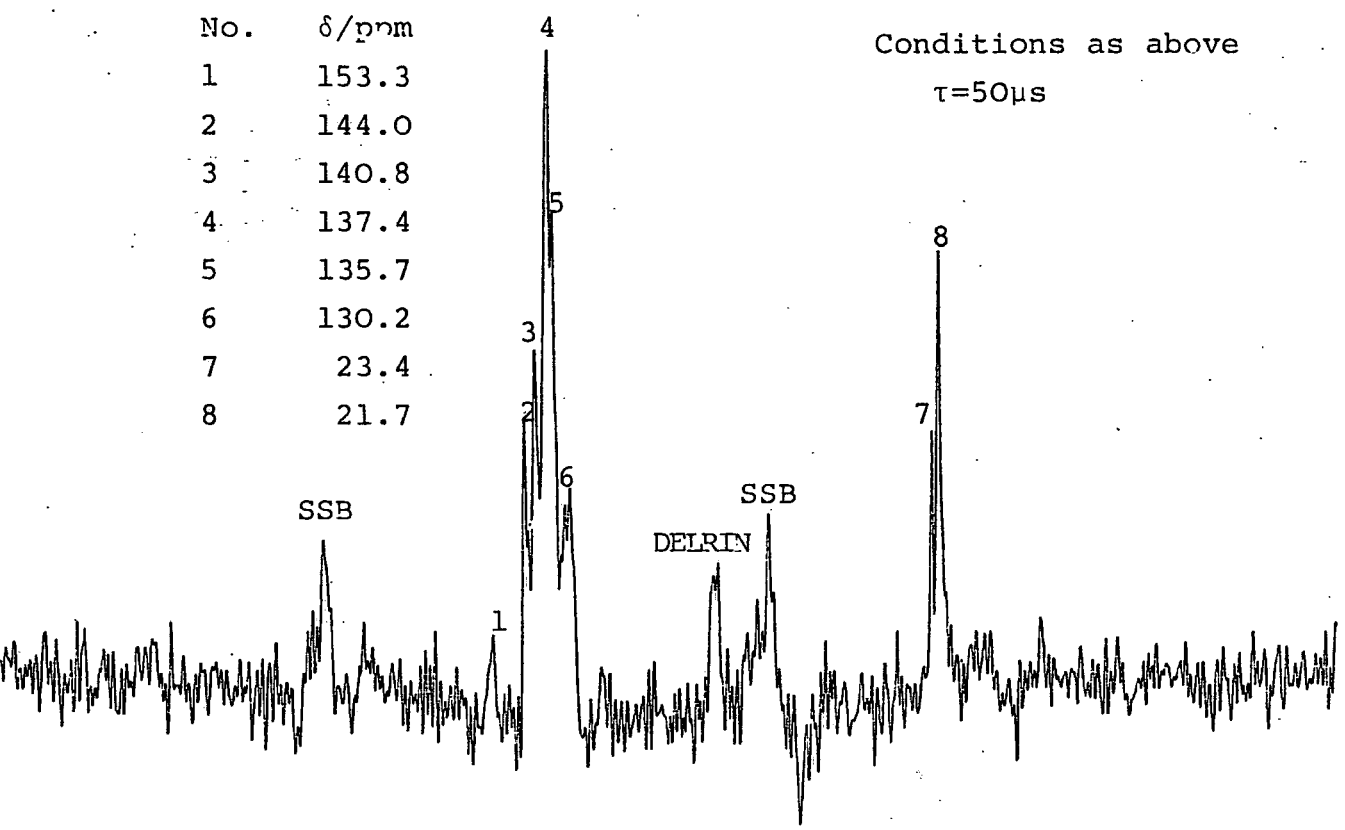

ratio, 2:1) which can be readily assigned to the two types of methyl group of the mesityl group. The ^{13}C NQS spectrum (Figure 4.49) does not improve the assignment difficulties of the aromatic region. However, there is a peak, of low intensity, at 153 ppm. which appears in both the ^{13}C spectra. This resonance is *ca.* 10 ppm. to high frequency from the main aromatic region and also has a relative intensity which can be seen to increase on going from the CP only to the NQS spectrum, suggesting the resonance of a single carbon site present. The splitting of the peak shown in the CP spectrum (Figure 4.48), due to better sensitivity and resolution than from NQS, is equal to 43Hz. The solution-state ^{13}C NMR data for the C=P carbon appears at 193.4 ppm with $^{1}J_{PC}$ = 43.5Hz. It is therefore possible that the peak at 153 ppm in the solid-state is due to the C=P carbon, with the shielding difference (∿40 ppm.) caused by the coordination of the ligand to the platinum.

The solid-state ^{31}P NMR spectrum of $Pt(PPh_3)_2$(P-(mesityl) = CPh_2) is completely in agreement with that expected from X-ray crystallographic studies and confirms the presence of the σ-bonded (η^1) structure. The two centre bands (Figure 4.50) labelled A and B are due to the two phosphorus atoms P_A and P_B of the PPh_3 ligands. The band marked B is split into four lines whereas A is apparently split into three lines, (Figure 4.51). However, with resolution enhancement (Figure 4.52) 'B' can be seen clearly to consist of four lines. This part of the spectrum is the AB part of an ABX system, with the A and B resonances each giving rise to four lines due to phosphorus-phosphorus coupling (see Figure 4.53).

FIGURE 4.50 ^{31}P CP/MAS spectrum of $Pt(PPh_3)_2(P(mesityl)=CPh_2)$

NT = 4000
SW = 85kHz
AQ = 0.048s
DR = 5Hz/pt
DO = 10s
D2 = 1ms
SS = 2940Hz

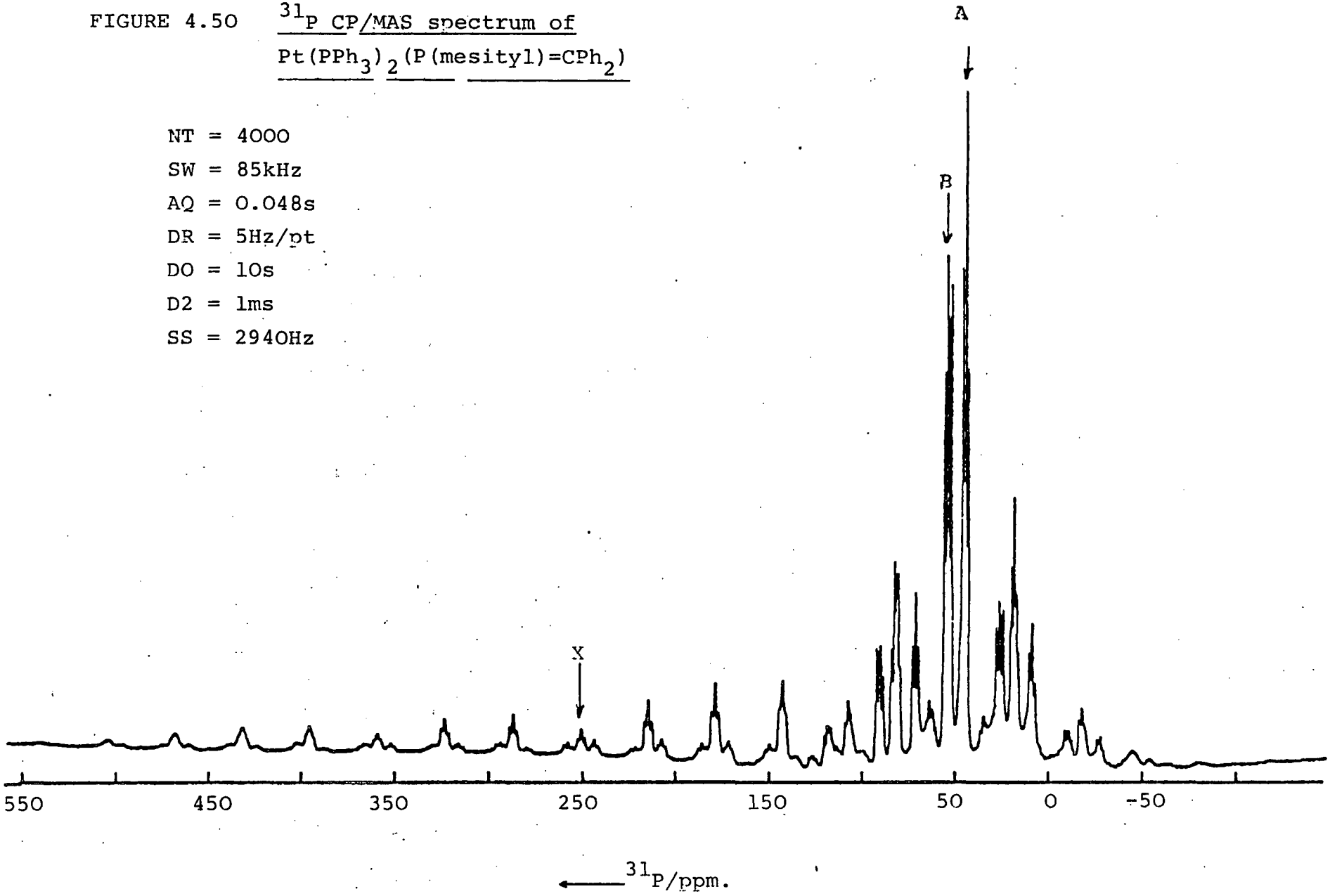

FIGURE 4.51 ^{31}P CP/MAS spectrum of $Pt(PPh_3)_2(P(mesityl)=CPh_2)$

Expansion of Figure 4.50 in P_A and P_B region

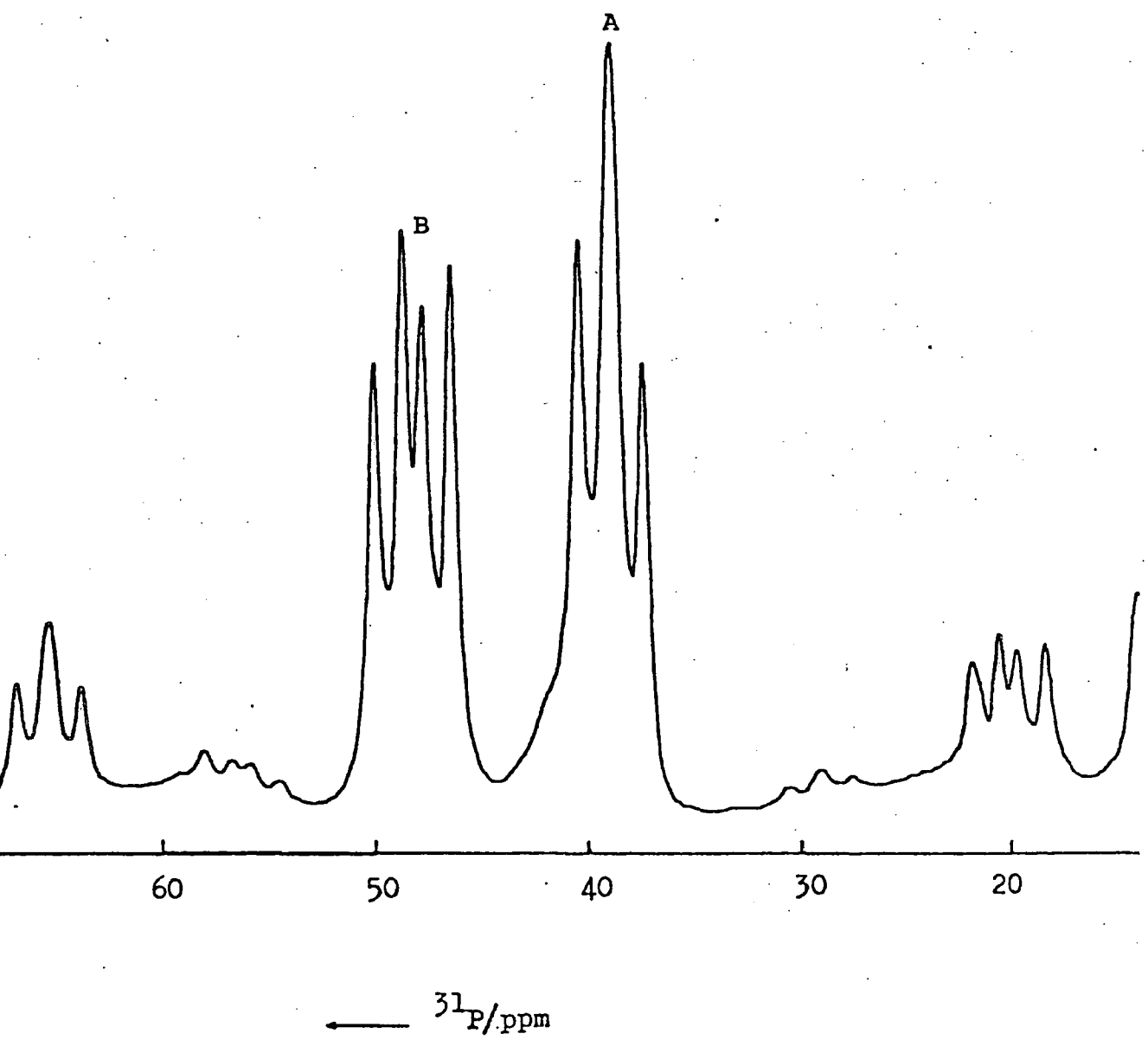

FIGURE 4.52 Expanded and Resolution enhanced spectrum of P_A and P_B from Figure 4.50

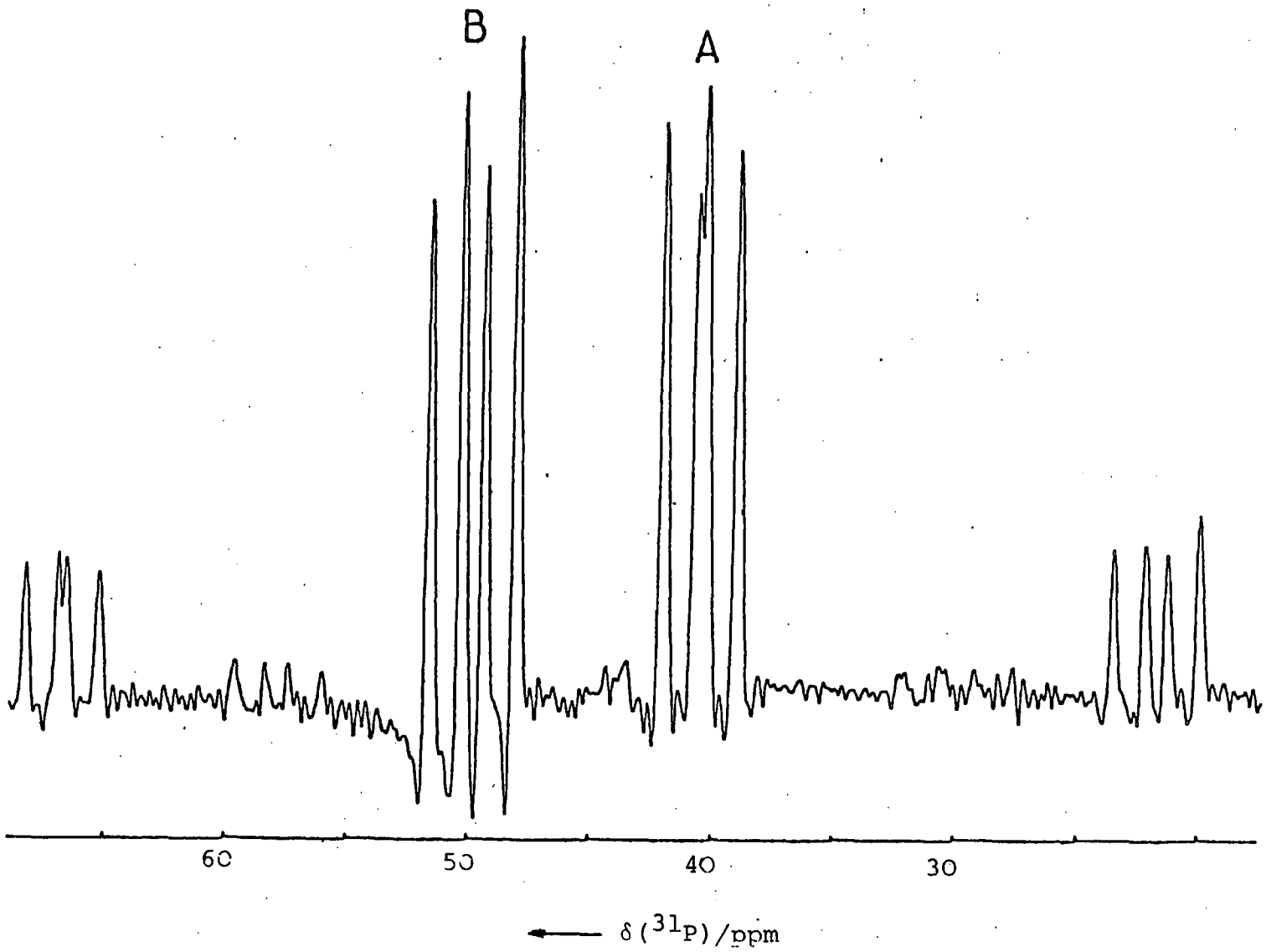

FIGURE 4.53 Schematic representation of ^{31}P - ^{31}P coupling in $(Ph_3P)_2Pt(mesityl\ P=C\ Ph_2)$

$(J_{AB}) = 109Hz$
$(J_{AX}) = 135Hz$
$(J_{BX}) = 183Hz$

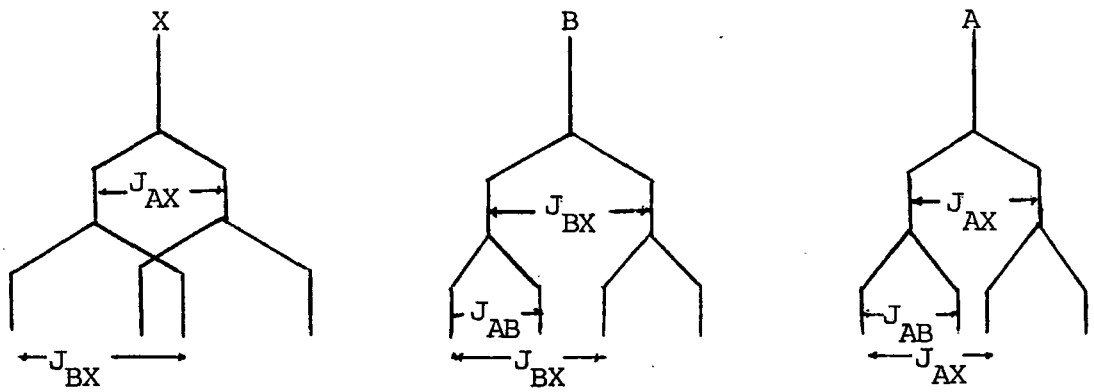

The outer four peaks on each side of the AB spectrum (Figure 4.52) are platinum satellites of A and B with $^1J_{P,Pt}$ = 4254 and 4550Hz respectively.

The resonance of the P_X phosphorus of the phosphaalkene was more difficult to locate because of its lower intensity (Figure 4.50) arising from a much larger shielding anisotropy as shown by the number of spinning sidebands present. In theory, sideband analysis can be used to obtain the magnitude and sign of the shielding anisotropy as well as the principal tensor components.[30,40] However, all the sidebands need to be observed for the Maricq and Waugh method;[30] this is not the case for the spectrum of the phosphaalkene, where sidebands are concealed under the A and B bands. The Herzfield and Berger method[40] only requires a few sidebands, but relies heavily on a good signal to noise. Such an analysis was performed for the slow-spinning spectrum (Figure 4.54) but did not yield any sensible results. An estimation of the

FIGURE 4.54 ^{31}P CP/MAS spectrum of $Pt(PPh_3)_2(P(mesityl)=CPh_2)$

Conditions as for Figure 4.50
except spinning speed = 2345Hz

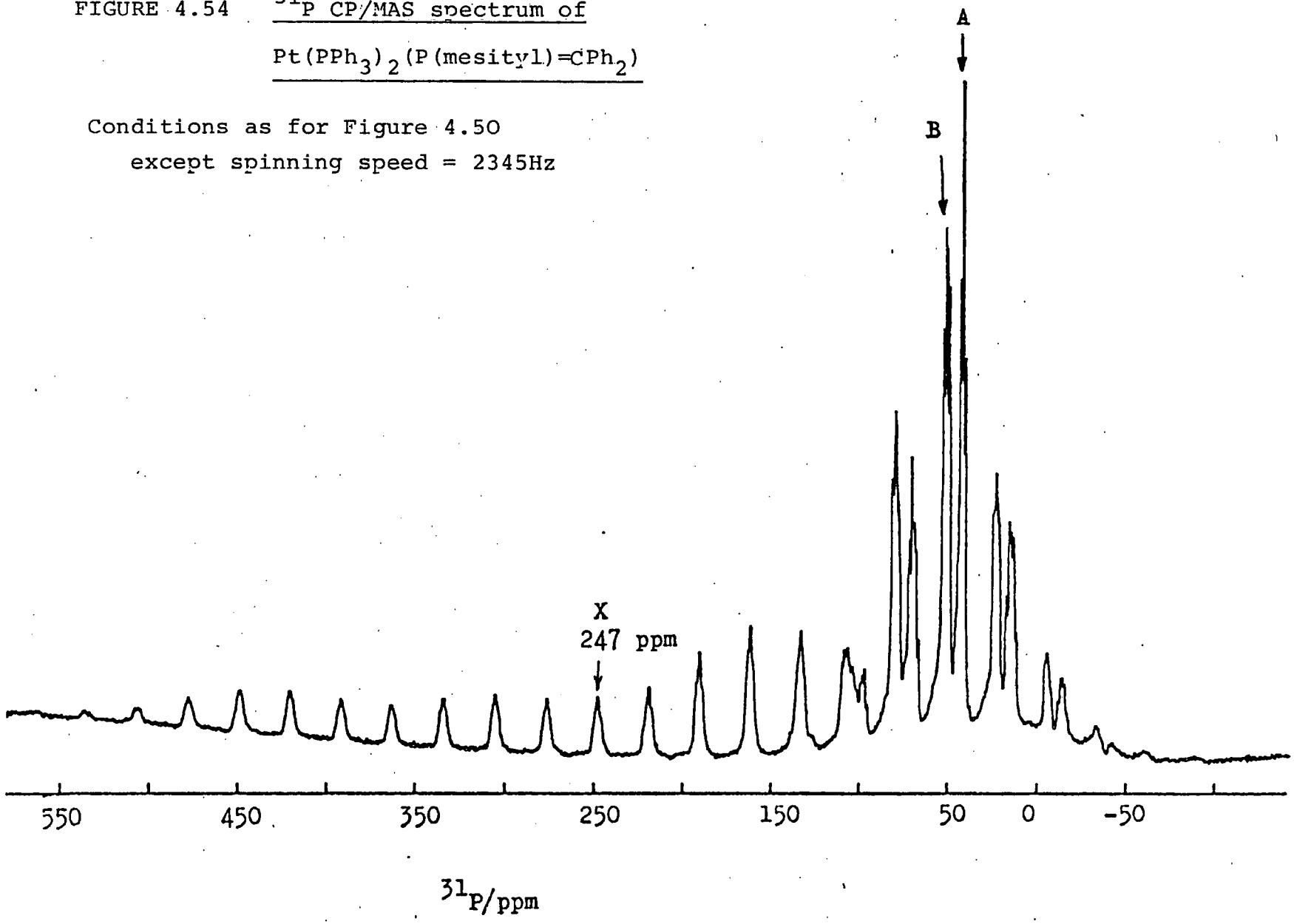

shielding anisotropy is *ca.* 300 ppm. which is very large for phosphorus.

TABLE 4.8 ^{31}P NMR DATA FOR $Pt(Ph_3P)_2(P(mesityl)=CPh_2)$ IN THE SOLID-STATE

	δ^a	$^1J_{P,Pt}$ [b]	$^2J_{P,P}$ [b]
P_A	40.5	4250	109 (P_AP_B)
P_B	49.8	4550	183 (P_BP_X)
P_X	247	4720	137 (P_XP_A)

(a) In ppm. rel. H_3PO_4.

(b) In Hz.

Confirmation of the position of the P_X centre band, which is determined by the isotropic chemical shift, was established by varying the spinning speed. The chemical shift of P_X was found to be 247 ppm, which is close to that observed for the free ligand (δ=233 ppm.[41]) and very different from that of the side-bonded η^2-ligand observed in solution. The observation of platinum satellites for P_X (Figure 4.55) reveals a large ^{31}P - ^{195}Pt coupling constant of 4720Hz which is consistent with the phosphorus lone pair interacting directly with the metal, and therefore showing the η^1-bonded phospha-alkene to be present. Interestingly, $|^1J_{Pt,P_X}|$ for the phosphaalkene is larger than $|^1J_{Pt,P_A}|$ or $|^1J_{Pt,P_B}|$ for the PPh_3 ligands which no doubt reflects the greater s-character of the former in which the phosphorus is formally sp^2 hybrid-ised. The solid-state ^{31}P chemical shift and scalar coupling data are listed in Table 4.8.

The ^{31}P solid-state NMR results establishes the dual η^1 and η^2 coordination behaviour of the ligand P(mesityl) = CPh_2

FIGURE 4.55 Expansion of the P_X part of spectrum in Fig. 4.50 showing ^{195}Pt satellites

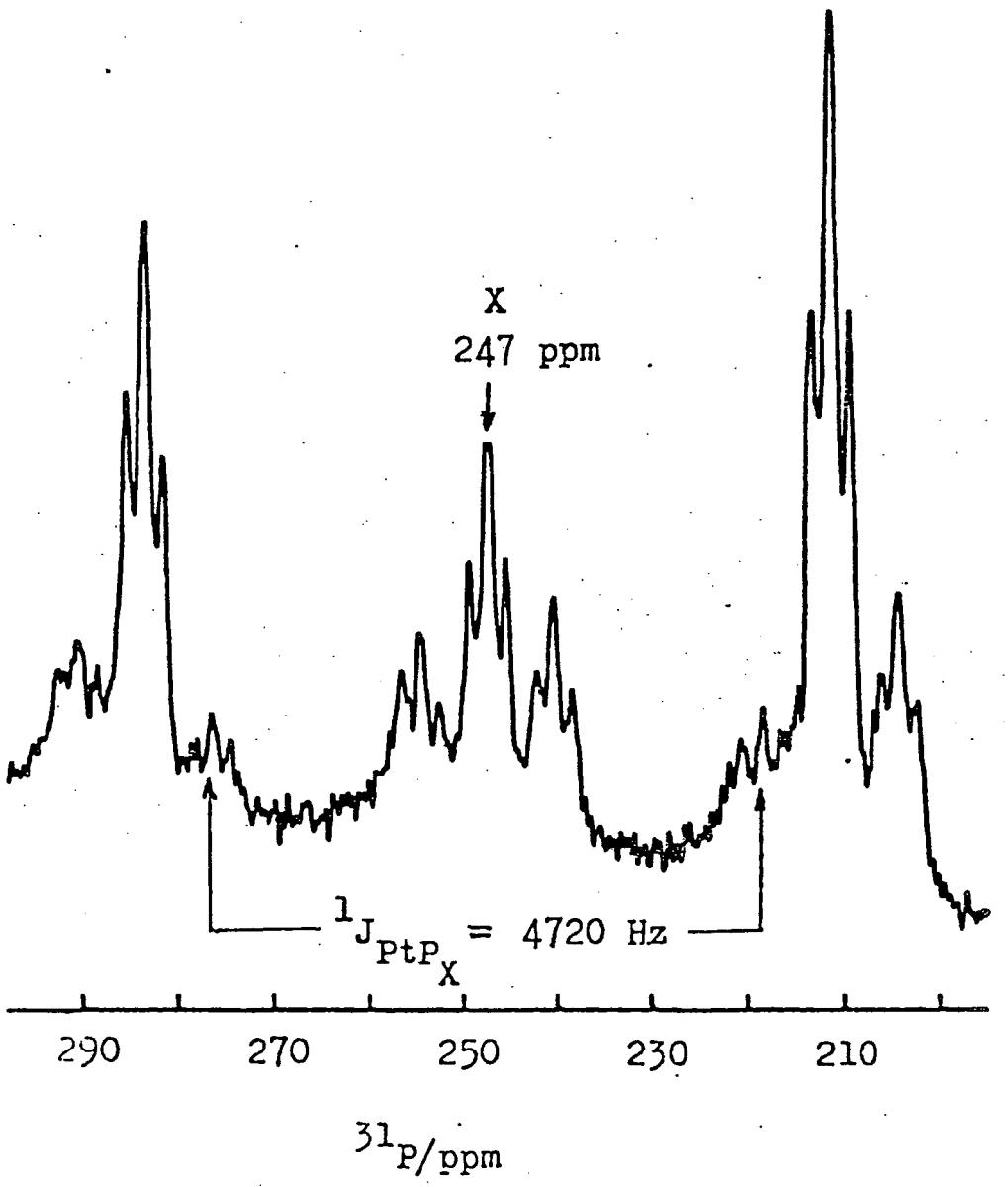

in $Pt(PPh_3)_2(P(mesityl)=CPh_2)$ and are in good agreement with a study by Bickelhaupt *et al*[39] carried out independently. These authors have also investigated solution dynamic behaviour and undertaken a theoretical analysis of the electronic and steric factors governing the coordination behaviour of phosphaalkenes.

4.16 Conclusion and Further Studies

The carbon-13 and phosphorus-31 solid-state NMR work has demonstrated the usefulness of the two techniques as probes for molecular and electronic structures of transition metal complexes. The sensitivity of the ^{31}P nucleus to electronic, steric and geometric arrangements has been shown *via* shielding parameters and scalar couplings. The ability of ^{13}C solid-state NMR to give detailed information regarding the structural arrangements of organic ligands has been exemplified by the study of the tertiary phosphines of platinum(II) and of the polymer $[Pt(CBDCA)(NH_3)_2]_n$, where other forms of solid and solution-state analysis were impossible. Both techniques have been used to give crystallographic information concerning inter and intramolecular effects, *e.g.*, the study of *cis*-$[PtMe_2(PEt_3)_2]$. Finally, the solid-state ^{31}P NMR analysis of $(Ph_3P)_2(mesitylP=CPh_2)Pt(0)$ has illustrated how the technique can be used as a bridge between solution-state and X-ray crystallographic studies.

Due to the large and ever increasing variety of phosphorus containing platinum complexes there will always be further studies possible using ^{13}C and ^{31}P NMR. More specifically, by studying other types of tertiary phosphines of

platinum(II), greater correlations can be drawn by the examination of coupling constants (P,Pt) and shielding tensor components. However, in order to clarify existing analyses, ^{195}Pt solid-state NMR spectra need to be obtained, although this may be very difficult taking into account the shielding anisotropy problems. Also, X-ray crystallography would provide useful information concerning the cause of crystallographic non-equivalences present. If it is possible to obtain crystals for a given compound then it should be possible, in addition to X-ray crystallography, to obtain NMR single-crystal data. The orientation of the principal shielding anisotropy tensor components would then be assigned to the molecular coordinate system and so trends can be seen for a group of similar compounds concerning the different shieldings on any particular molecular axis.

REFERENCES (CHAPTER FOUR)

1. J. Schaefer and E.O. Stekskal, J.Am.Chem.Soc., 1976, (98), 1031.

2. C.S. Vannoni, Acc.Chem.Res., 1982, (15), 201.

3. R.E. Wasylishen and C.A. Fyfe, Ann.Rep.Spec. 1982 (12) 287.

4. G.R. Hays, The Analyst, 1982 (107), 241.

5. B.C. Gernstein, Analyt,Chem. 1983 (55), 899A.

6. G.E. Balimann, C.J. Groombridge, R.K. Harris, K.J. Packer and S.F. Tanner, Phil.Trans.Roy.Soc. 1981 (A299), 643.

7. W.L. Earl, A.N. Garroway and D.L. van der Hart, J.Mag.Res. 1981 (44), 361.

8. J. Schaefer and E.O. Stejskal, Topics in C-13 NMR, Vol.3, Chapt.4, Ed. G. Levey, J. Wiley & Sons, N.Y.284, 1979.

9. M.M. Maricq, J.S. Waugh, J.C. Fletcher, M.J. McGlinchey, J.Am.Chem.Soc. 1978, (100), 6902..

10. M.D. Waddington and P.W. Jennings, Organometallics, 1 (1370), 1982.

11. C. Groombridge, Ph.D. Thesis, University of East Anglia, 1983.

12. 'Phosphorus-31 NMR-Principles and Applications', Ed. D. Gorenstein, Academic Press, Florida, 1984.

13. W.P. Rothwell, J.S. Waugh and J.P. Yesinowski, J.Am.Chem. Soc. 1980, 102, 2637.

14. J. Herzfield, A. Roufosse, R. Haberkorn, R.G. Griffin and M.J. Glimcher, Phil.Trans.Roy.Soc., London 1980, (B289), 459.

15. I.J. Cox, Ph.D. Thesis, University of East Anglia, 1984.

16. J.W. Diesveld, E.M. Menger, H.T. Edzes and W.S. Veeman, J.Am.Chem.Soc. 1980, 102, 7935.

17. E.M. Menger and W.S. Veeman, J.Mag.Res. 1982, (46), 257.

18. C.A. Fyfe in "Solid-State NMR for Chemist", Chapter 7, p.376, CFC Press, 1984;
L. Bemi, H.C. Clark, J.A. Davies, C.A. Fyfe and R.E. Wasylishen, J.Am.Chem.Soc. 1982, (104), 438.

19. C.A. Fyfe, H.C. Clark, J.A. Davies, P.J. Hayes and R.E. Wasylishen, J.Am.Chem,Soc.1983, (105), 6577.

20. H.C. Clark, J.A. Davies, C.A. Fyfe, P.J. Hayes and R.E. Wasylishen, Organometallics, 1983 (2), 177.

21. P.S. Pregosin and R.W. Kunz, "^{31}P and ^{13}C NMR of Transition Metal Phosphine Complexes", Springer-Verlag, Berlin, 1979.

22. B.E. Mann and B.E. Taylor, "^{13}C NMR Data for Organometallic Compounds", Academic Press, 1981.

23. S. Neidle, I.M. Ismail and P.J. Sadler, J.Inorg.Bio. 1980, 13, 205.

24. C.J. Barnard, Private Communication.

25. N. Bloembergen, J.Chem.Phys. 1957, 27, 595.

26. A.B. Goel, J. Goel and D. van der Veer, Inorg.Chim.Acta, 1982 (65), 1205.

27. S.O. Grim, R.L. Keiter and W. McFarlane, Inorg.Chem. 1967, (6), 1133.

28. A. Pidcock, R.W. Richards and L.M. Venanzi, Proc.Chem. Soc. 1962, 184.

29. F.H. Allen and A. Piddock, J.Chem.Soc.(A), 1968, 2700.

30. M.M. Maricq and J.S. Waugh, J.Chem.Phys. 1979, (70), 3300.

31. K.W. Zilm and D.M. Grant, J.Am.Chem.Soc. 1981 (103), 2913.

32. T.A. Albright, W.J. Freeman and E.E. Schweitzer, J.Org.Chem.1975,(40),3437.

33. R.J. Goodfellow and B.F. Taylor, J.C.S. Dalton, 1974, 1676.

34. G.K. Anderson, H.C. Clark, J.A. Davies, G. Ferguson and M. Parvez, J.Cryst.Spect.Res., 1982 (12), 449.

35. S. Carr, R. Colton, D. Dakternieks, J.Organomet.Chem., 1983, (249), 327.

36. S.I. Al-Resayes, S.I. Klein, H.W. Kroto, M.F. Meidine and J.F. Nixon, J.Chem.Soc.Chem.Comm., 1983, 930.

37. Th.A. Van der Knaap, F. Bickelhaupt, H. Van der Poel, G. Van Kozen, and C.H. Szam, J.Am.Chem.Soc.104 (1982),1756.

38. H.W. Kroto, S.I. Klein, M.F. Meidine, J.F. Nixon and R.K. Harris, K.J. Packer and P. Reams, J.Organomet. Chem., 1985 (280), 281.

39. Th.Van der Knaap, F. Bickelhaupt, J.G. Kraykamp, G. Van Koten, J.P.C. Bernards, H.T. Edzes, W.S. Veeman, E. de Boer and E.J. Baerands, Organometallics (in Press).

40. J. Herzfield and A.E. Berger, J.Chem.Phys. 1980, (73), 6021.

41. Th.C. Klebach, R. Loliens, R. Bickelhaupt, J.Am.Chem. Soc.1978 (100), 4886.

42. S. Knight, I.J.F. Poplett, Tamu Newsletter, 301-14.

43. M.C. Baird, J.Inorg.Nucl.Chem. 1967 (29), 367.

44. R.J. Abraham and H.J. Bernstein, Can.J.Chem. 39(1961),216.

CHAPTER FIVE

HIGH-RESOLUTION SOLID-STATE ^{195}Pt NMR

5.1 Introduction and Literature Survey

The only naturally occurring isotope of platinum with non-zero spin, ^{195}Pt has $I=\frac{1}{2}$. The natural abundance of 33.8% and a receptivity D^C (relative to carbon) of 19.1 makes it a favourable nucleus for NMR studies, (see Table 2.2). However, the high cost of platinum compounds has meant that ^{195}Pt solution-state NMR has only in the last few years become a popular analytical tool with the advent of superconducting magnets.

The primary advantages of studying a metal nucleus is the relative spectral simplicity and also chemical shift sensitivity. Chemical shift effects have been well illustrated in two ^{195}Pt NMR reviews by Kidd and Goodfellow[1] and also Pregosin.[2] An illustration of these effects is the substitution of one halogen for another, which changes $\delta_{^{195}Pt}$ by hundreds and sometimes thousands of ppm. In general, the ^{195}Pt NMR signal due to molecules with the heavier, "softer", ligands appears at a lower frequency relative to those with the "harder" ligands which appear higher in the periodic table, though there is no satisfactory theoretical support for this.[2,3]

There has been considerable interest in platinum complexes ever since the discovery that cis-$[Pt(NH_3)_2Cl_2]$ (cisplatin) and a number of analogues possess antitumour activity.[4] Cisplatin, the first of metal anti-tumour drugs, is already in use as an approved form of therapy for bladder, testicular and ovarian cancers in humans, with a high proportion of cures.[5] Second generation drugs have now emerged on the

basis of comparable therapeutic activity to cisplatin associated with considerably reduced toxicity.[6] In the pharmaceutical area, full characterization is vital, and information from many sources must be collated. Solution-state ^{195}Pt NMR has already been applied in this area with significant results.[7-9]

Another broad area of use for platinum compounds is in catalysis. In particular, platinum compounds are commonly used as catalysts for hydrogenation, oxidation, dehydrogenation and hydrogenolysis reactions.[10] Solution-state ^{195}Pt NMR has also been successfully used in this area.[3] In addition, there have been recent studies of alumina-supported platinum catalyst using broad-line, solid-state ^{195}Pt NMR by spin-echo sequences.[11]

Despite the favourable properties of the platinum nucleus, a ^{195}Pt NMR signal can be rather elusive. The chemical shift range for Pt(IV) complexes is *c.a.* 13000 ppm[1] which can pose a problem in locating a signal. The situation is relatively improved for the other oxidation states of platinum, with Pt(II) compounds spanning *c.a.* 3000 ppm around δ = -4000 ppm[2] and Pt(0) compounds covering 2000 ppm around δ = -5500 ppm.[12]

Although the use of high magnetic fields is advantageous for sensitivity purposes, high resolution solution-state NMR studies of platinum complexes are often hampered by linewidth problems on increasing the B_o field. The characteristic 1:4:1 triplet in ^{1}H and ^{13}C NMR spectra of Pt complexes produced by scalar coupling, has been found to 'disappear' at high magnetic fields due to linebroadening (and also for

Pt(II) complexes at low field).[13] Lallemand *et al* explained this trend in terms of strong field dependence of ^{195}Pt relaxation because of the dominance of the shielding anisotropy mechanism. Measurement of the ^{195}Pt spin-lattice relaxation time at two field strengths supported this explanation.[13] Subsequent studies by Sadler *et al*[14] have shown that the corrected linewidths of the ^{195}Pt satellites in the ^{1}H spectrum follow a dependence on the square of the field. The contribution of the shielding anisotropy to relaxation in the case of extreme narrowing is given by

$$\frac{1}{T_{1\sigma}} = \frac{2}{15} \gamma^2 B_o^2 \Delta\sigma^2 \tau_c \qquad (5.1)$$

$$\frac{1}{T_{2\sigma}} = \frac{7}{45} \gamma^2 B_o^2 \Delta\sigma^2 \tau_c \qquad (5.2)$$

for cylindrically symmetric molecules ($\Delta\sigma = \sigma_{//} - \delta_{\perp}$). Hence a plot of proton linewidth *versus* B_o^2 should be linear if shielding anisotropy provides the dominant relaxation mechanism. Another feature of the two above equations is that observable coupling may be restored at higher temperatures, owing to a shorter correlation time τ_c.[13]

The magnitude of the shielding anisotropy $\Delta\sigma$ for ^{195}Pt in a Pt(II) complex was calculated by Lallemand *et al* to be *c a* . 900 ppm. However, this was correctly recalculated by Doddrell *et al* [15] and found to be *c.a* . 7500 ppm. The latter authors have determined the shielding anisotropy, by multifield ^{195}Pt relaxation measurements, of two octahedral Pt(IV) complexes to be in the range of 1000 ppm. Further, Dechter *et al*[16] have shown the shielding anisotropy for the Pt(II) complex $[Pt(acac)_2]$ to be in the order of 10,000 ppm, demonstrating the pronounced effect of the square-planar geometry on the

shielding anisotropy and subsequent relaxation behaviour of ^{195}Pt.

The relative sensitivity of ^{195}Pt ($\mathcal{D}^C$=19.1) and the low magnetogyric ratio (γ=5.77 x 10^7 rad $T^{-1}s^{-1}$) makes it very suitable for cross-polarisation studies in the solid-state. However, despite this potential, there has only been one report of solid-state ^{195}Pt NMR exhibiting static and MAS spectra.[15] The spectra of the two studied Pt(IV) complexes, $[Me_3Pt\text{-}(acac)]_2$ and $[Me_3Pt]_2SO_4.4H_2O$, revealed a large shielding anisotropy (*c.a.* 1000 ppm). The large values of $\Delta\sigma$ that are expected for most Pt complexes[13-16] can create severe problems in direct NMR observation of the solid-state by either spectral width limitations or sensitivity problems. In principle, this problem can be solved for ^{195}Pt MAS NMR spectra by the use of the TOSS sequence,[17] which suppresses sidebands leaving the isotropic resonances. However, this method is known to partially fail when $\Delta\sigma/\nu_R$ is large.[18] Moreover, the spinning sidebands, produced if the spinning speed ν_R is less than the breadth of the static chemical shift pattern (σ_{11}-σ_{33}), can reveal important information regarding the shielding tensor components. Such parameters can be used to show structural trends unobtainable from other well-known analytical methods.

The purpose of the work covered in this chapter is to systematically evaluate the potential of solid-state ^{195}Pt NMR, as little is known about the technique. Thus, the spectra presented are from a wide variety of compounds which show the possible chemical applications of solid-state ^{195}Pt NMR. Each case is discussed individually, incorporating factors influencing linewidths as well as the effects of scalar and dipolar coupling of the ^{195}Pt nucleus to spin-½ and quadrupolar nuclei.

5.2 ^{195}Pt Shielding Tensor Evaluation

In principle the static spectra, and hence the spinning sideband manifolds may be influenced by a number of anisotropic interactions. For the platinum compounds studied in this work, the major effect is likely to arise from the shielding tensor. High power proton decoupling was used to remove the influence of (Pt,H) dipolar (and indirect) coupling interactions. The atoms directly bonded to platinum are C, O, N, P and Cl. The major isotopes of carbon and oxygen have zero spin and can therefore be discounted. Calculations based on typical Pt-X distances give values for the relevant dipolar interaction constants, $(\mu_o/4\pi)\gamma_{Pt}\gamma_X(^h/_{2\pi})r_{PtX}^{-3}$ of 144, 868 and 203Hz respectively for X = ^{14}N, ^{31}P and ^{35}Cl. These values are substantially less than the observed static bandwidths. Therefore, for simplicity, it has been assumed that the effective tensor components determined are those for the platinum shielding only. It is probable that the effect of dipolar interactions is to cause the shielding anisotropy to be slightly overestimated when N or Cl are directly bonded to Pt.

The principal shielding tensor components (Table 5.1) were calculated using the Maricq and Waugh method.[39] In three cases the consistency of the results was checked by experiments at different spinning speeds. For two of the compounds the consistency was impressive (agreement to within 14 ppm, when $/\sigma_{33}-\sigma_{11}/$ is *c a.* 400 ppm in one case and *c a.* 800 ppm in the other). In the other case, agreement is not so good (37, 48 and 12 ppm for the three components). Of course, the accuracy of the Maricq and Waugh method[39] is heavily dependent on the sidebands towards the extreme of the envelope,

TABLE 5.1 ^{195}Pt SHIELDING TENSOR PARAMETERS[a]

COMPOUND	Spinning Speed/ Hz	σ_{iso}	σ_{33}[b]	σ_{22}[b]	σ_{11}[b]	δ[b]	η[b]	solution σ_{iso}/ ppm.	solvent
		ppm.							
$K_2[Pt(OH)_6]$	3200	-3476[c]	-3218	-3567	-3643	258	0.29	-3290[d]	1M KOH
	1907		-3222	-3574	-3632	254	0.23		
cis-$[PtMe_2(PEt_3)_2]$	3000	4654[c]	5058	4649	4256	404	0.97	4653[e]	CD_3CN
	2500		5054	4639	4267	400	0.93		
cis-$[PtMe_2(PPh_3)_2]$[h]	2630	4682[f]	5099[g]	4624[g]	4323[g]	417[g]	0.72[g]	Insoluble	
$[Pt(en)_3]Cl_4.2H_2O$	3000	943[i]	585	1070	1174	-358	0.29	Insoluble	
	2600		622	1022	1186	-322	0.51		
cis-$[PtCl_4(NH_3)_2]$	2620	237[i]	367	209	134	130	0.58	145[j]	H_2O
trans-$[PtCl_4(NH_3)_2]$	3130	404[i]				k		-	
$K_2[PtCl_6]$	3000	-172[i]				*l*			
$Na_2[PtCl_6].6H_2O$	3000	-85[i]				k		0[m]	D_2O

(a) The shielding values are in ppm relative to $[PtCl_6]^{2-}/D_2O$. For chemical shifts on the δ scale the sign should be reversed.[2]

(b) As discussed in the text the data, strictly speaking, refer to average tensors which may be affected, *inter alia* by heteronuclear dipolar interactions as well as shielding anisotropy.

(c) Measurement accuracy ±1 ppm.

(d) Reference No.9.

(e) This work, Digitization rate 5 Hz/Pt.

(f) Digitization rate 7 Hz/pt.

(g) Average value taken from each doublet sideband.

(h) Additional spectrum obtained at 2274Hz spinning speed; the isotropic values agree with those previously obtained (S/N too poor for any tensor calculations).

(i) Measurement accuracy ± 2 ppm.

(j) Reference No. 7.

(k) Smaller anisotropy (see text).

(*l*) No effective anisotropy observed (see text).

(m) By definition.

where the signal to noise ratio is at its poorest. Spectra at slower spinning rates are likely to yield the more accurate results, since they are closer to reconstructing the envelope of the powder pattern, though in compensation the signal to noise ratio decreases as the number of sidebands increases.

Shielding anisotropies, $\sigma_{33}-\sigma_{iso}$ (written as δ, and not to be confused with the chemical shift) and asymmetries, $\eta=(\sigma_{22}-\sigma_{11})/\delta$, have also been calculated and are reported in the Table. As for the individual shielding tensor components, results at two different spinning speeds are consistent for $K_2[Pt(OH)_6]$ and *cis*-$[PtMe_2(PEt_3)_2]$, but the variations for $[Pt(en)_3]Cl_4.2H_2O$ are considerable, particularly for η.

5.3 Isotropic Shifts

All the compounds studied showed a single isotropic chemical shift for the solid state. This could indicate that the crystal structures have only equivalent sites for Pt in their respective unit cells. This is indeed known to be true for $K_2[Pt(OH)_6]$,[38] and our X-ray results indicate this is the case for *cis*-$[PtMe_2(PEt_3)_2]$ also. However, it is possible that in the other cases the substantial linewidths could conceal small splittings from crystallographic non-equivalence, though the sensitivity of Pt chemical shifts to chemical effects suggests non-equivalence should give rise to significant shift differences.

The solution-to-solid chemical shift change is variable for the Pt compounds studied (Table 5.1). For example, the

shift change is negligible for *cis*$[PtMe_2(PEt_3)_2]$. However, for $Na_2(PtCl_6).6H_2O$ the magnitude of the difference is 85 ppm, while for *cis*$[PtCl_4(NH_3)_2]$ is 92 ppm. In view of the large chemical shift range[1] for ^{195}Pt and the established effects of solvent, these effects of the phase change must be regarded as only modest. For $K_2[Pt(OH)_6]$, the shift difference on changing phase is somewhat larger (186 ppm) but it should be noted that the medium used for the solution-state measurement (namely, 1 mol dm^{-3} KOH) is an aggressive one.

The variation in isotropic chemical shifts is, as expected, quite large. The factors affecting the chemical shifts of heavy metal nuclei are many and varied. The electronegativity of the substituents attached directly to the platinum atom is known to be of importance in this respect.[2] For the small number of Pt^{IV} complexes studied here, the chemical shift increases with increasing electronegativity (O>Cl>N), as expected from solution-state data, *i.e.* δ/ppm for $K_2[Pt(OH)_6]$ > $Na_2[PtCl_6].6H_2O$ > *cis*$[PtCl_4(NH_3)_2]$ > $[Pt(en)_3Cl_4.2H_2O]$.

5.4 Potassium Hexachloroplatinate, K_2PtCl_6

Single pulse ^{195}Pt NMR can be used to successfully study solid platinum complexes provided the shielding anisotropy is small. An ideal system is K_2PtCl_6 which requires few transients to obtain a reasonable signal to noise (see Figure 5.1). The MAS and static spectra show a single peak with no apparent shielding anisotropy present, with a chemical shift of $\delta_{^{195}Pt}$ = 172 ppm. The spectrum is to be expected, considering the crystal structure of the compound. X-ray crystallography

FIGURE 5.1

^{195}Pt spectra of solid K_2PtCl_6

NT = 300
SW = 20kHz
DO = 5s
90° pulse length = 5μs

(a) STATIC

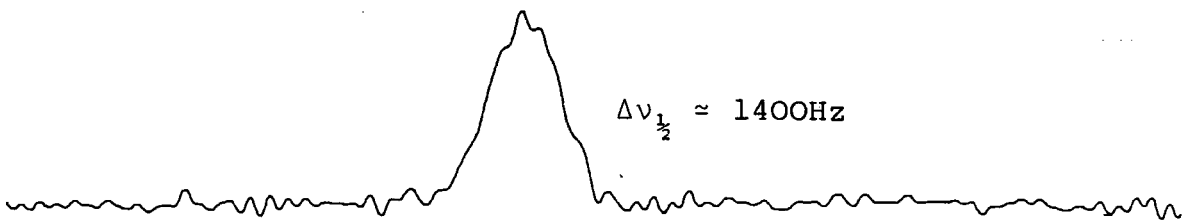

(b) MAS, 3kHz

δ_{iso} = 172 ppm

{conditions as for (a)}

$\Delta\nu \simeq$ 1100Hz

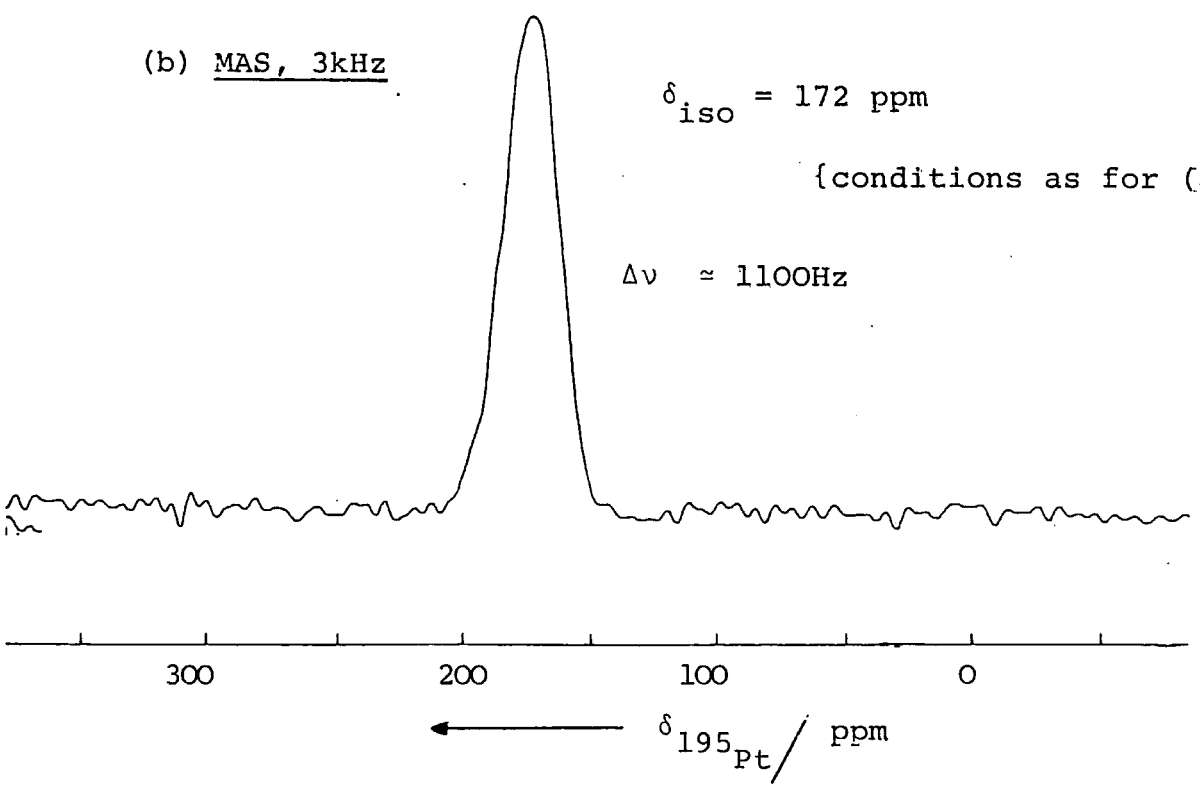

studies show that K_2PtCl_6 has a cubic structure with a space group Fm3m.[19] The shielding of the platinum nucleus is therefore independent of its orientation with respect to B_o.

In theory, a nucleus with a cubic environment should exhibit an equal intensity peak in both MAS and static spectra, (assuming the same experimental conditions). However, as shown in Figure 5.1, the static spectrum has a considerably reduced intensity relative to the MAS case. In order to test the effect of magic-angle spinning on the ^{195}Pt spin-lattice time, a series of experiments was performed varying the recycle delay time with all the other experimental conditions kept constant (see Figure 5.2). As can be seen from the spectra (Figure 5.2), a shorter recycle delay produces a greater difference in intensities between the static and MAS peaks. The peaks in the MAS spectra appear to relax much faster than those in the static spectra.

The effect of sample rotation at the magic-angle on the spin-lattice relaxation time T_1 has been addressed by Kessemeier and Norberg.[20] Their ^{31}P NMR results on metal phosphides show that the ^{31}P T_1 increases upon magic-angle spinning ($\nu_R >> \Delta\nu_{\frac{1}{2}}$). The explanation for this phenomenon is said to be due to the elimination of ^{31}P-^{31}P dipole coupling which renders spin diffusion to be ineffective in producing equilibrium among nuclei and in transporting spin energy toward impurity centres.[20] However, this mechanism is unlikely to be relevant to the above case as homonuclear interactions are not involved, and particularly because of the opposite effect occurring.

FIGURE 5.2

MAS RELAXATION EFFECTS OF K_2PtCl_6

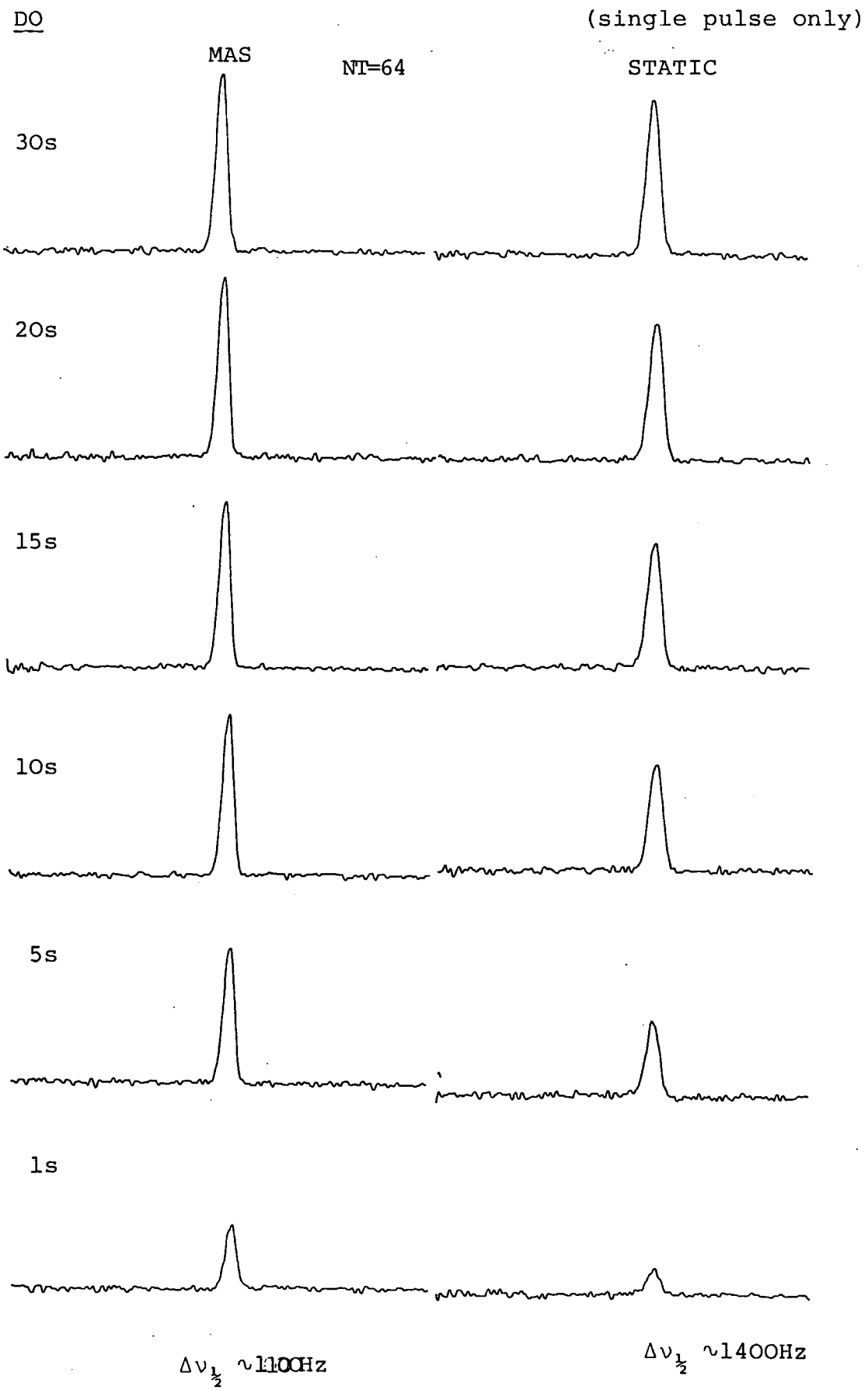

A more pertinent case has been studied by Andrew *et al*, which involves the ^{31}P solid-state MAS/NMR study of phosphorus pentachloride.[21] The ^{31}P spectrum was found to contain two chemically shifted peaks due to the equally populated ionic species PCl_4^+ and PCl_6^-. These two different phosphorus nuclei were observed to have different spin lattice relaxation times T_1 (PCl_4^+, T_1 = 6s; PCl_6^-, T_1 = 0.6s). The dominant relaxation mechanism of the phosphorus nuclei is thought to be dipolar coupling with the quadrupolar nuclei present. A greater degree of rotational motion of the PCl_6^- ions could then account for the different relaxation times.[21]

Evidence of a quadrupolar interaction between the platinum and chlorine nuclei is shown by the large linewidths of 1100Hz MAS and 1400Hz for the static case. The only reported case of an interaction between a spin-½ nucleus to a quadrupolar chlorine nucleus was from the ^{13}C NMR spectrum of the polymer PCTFE.[22] The observed broadening is attributed to a residual ^{13}C-^{35}Cl dipolar coupling. Depending on the ratio of the Zeeman and quadrupole interaction energies, the chlorine spins may be orientated along the Zeeman field or fixed at some definite orientation in the principal axis system of the molecular electric field gradient tensor. If the Cl moments are coupled more strongly to the electric field gradient than to the Zeeman field, the dipolar interaction is not removed by MAS.[23-25] In the PCTFE case, no splittings were observed, presumably because motion caused rapid relaxation of the chlorine nuclei.[23] In the limit, if the Cl spin-lattice relaxation rate is fast enough "self-decoupling" will be induced.[26]

The lack of shielding anisotropy present for the ^{195}Pt nucleus in K_2PtCl_6 and the absence of any splittings is indicative of motion present producing similar effects to that seen in the ^{13}C spectrum of PCTFE.[22] The effects of relaxation and motion have been studied for a similar anion, $SnCl_6^{2-}$, by Brown *et al.*[27] The authors believe that sudden reorientation of the anion causes changes in the orientation of the electric field gradient tensor axes, and so provides an efficient relaxation path for the chlorine nuclei. This mechanism is borne out by the observation that $T_1(^{35}Cl)$ decreases with increasing temperature. By analogy, any such motional effects in the anion, $PtCl_6^{2-}$, are likely to cause the spin-½ platinum nucleus to relax *via* rapidly fluctuating dipolar interactions with the chlorine nuclei (not averaged by MAS). If there is fast restricted motion present in the solid, such that molecules reorient rapidly about one defined axis, the magic-angle spinning effectively 'adds' to the motion,[28] thus increasing the ^{195}Pt relaxation rate. Furthermore, the decrease in linewidth observed by MAS is likely to be due to terms in the Hamiltonian expressions containing $(3\cos^2\theta-1)$. A complete reduction would not be possible due to other angular terms present.[29]

5.5 Sodium Hexachloroplatinate(IV)-Hexahydrate $Na_2[PtCl_6].6H_2O$

Two common techniques used for obtaining high resolution NMR spectra, cross-polarisation (CP) and single-pulse only (SP), are exemplified in the ^{195}Pt spectra of $Na_2[PtCl_6).6H_2O$,

FIGURE 5.3

^{195}Pt NMR studies of solid $Na_2PtCl_6.6H_2O$

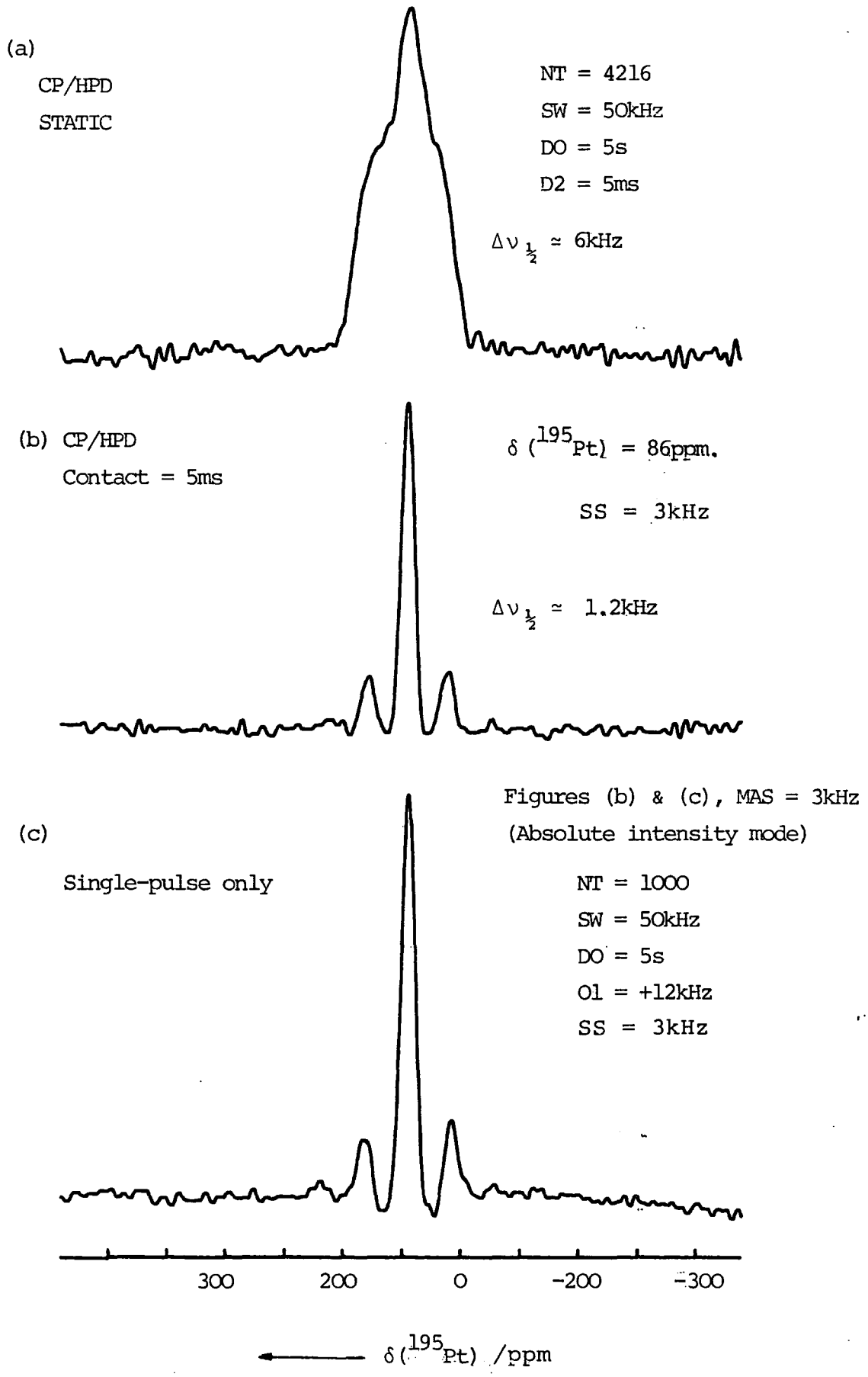

(Figure 5.3b/c). The intensities differ considerably, with the SP spectrum having the greater intensity. The compound under study is particularly interesting because of the presence of indirectly bonded protons in the form of interstitial water molecules.

In theory, cross-polarisation would be expected to have a significant advantage over the alternative single-pulse technique. The recycle delay may be dramatically reduced by waiting only the order of $T_1(^1H)$ instead of $T_1(^{195}Pt)$. Furthermore, there is a possible enhancement of $\gamma_{^1H}/\gamma_{^{195}Pt} \sim 4.6$ due to the transfer of magnetization from ^1H spins to the ^{195}Pt magnetization. However, Figure 5.3b does not exhibit such an enhancement. This is likely to be due to either: (i) an experimental factor whereby the Hartmann-Hahn condition is not met, or (ii) if the $T_{1\rho}(^1H)$ is very short, coupled with a slow cross-polarization rate, then there will not be a maximum transfer of magnetization from the protons to the ^{195}Pt spins (see Figure 5.4). The efficiency of mutual energy exchange between the two types of spins (*c f.* spin diffusion) is inversely proportional to the platinum-proton bond distance[30] ($r_{Pt,H}$). Thus, the relatively long distance of the H_2O protons from the central ^{195}Pt nucleus considerably increases the cross-relaxation time[30] between the ^{195}Pt and ^1H spins, thereby decreasing the rate of rise of the ^{195}Pt magnetization (Figure 5.4b).

FIGURE 5.4

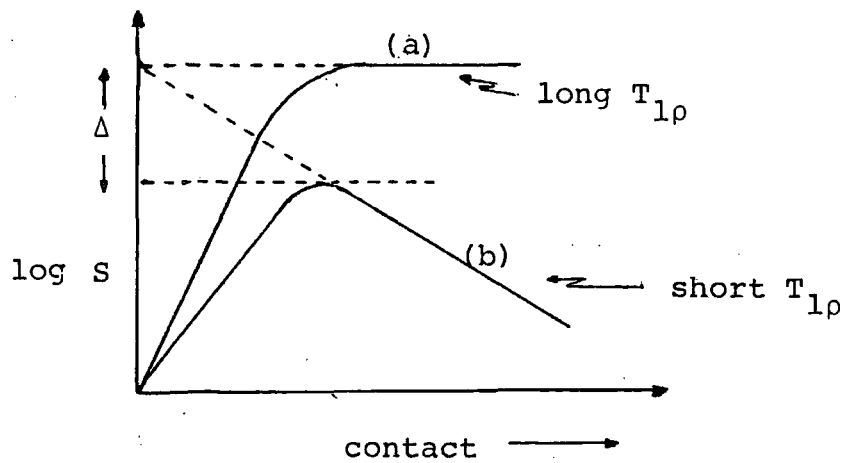

A schematic plot to show two types of cross-polarisation rate:

(a) a fast cross-polarisation rate with a long $T_{1\rho}$.

(b) slow CP rate and short $T_{1\rho}$.

If the difference Δ in signal intensity (S) is considerably greater than the enhancement factor $\gamma_{1_H}/\gamma_{195_{Pt}}$, then the signal intensity from a single pulse spectrum will be, in principle, greater than that for a CP spectrum.

Although a slow CP rate is likely to be a significant contributory factor to the difference in intensities between the CP and SP spectra (Figure 5.3), relaxation effects have not been taken into account. It is probable that the ^{195}Pt nucleus will relax rapidly *via* a fluctuating dipolar interaction with the surrounding chlorine nuclei.[21] This effect is likely to be more pronounced for the Pt nucleus than for the protons present.[27] Therefore, assuming rapid spin-lattice times (for ^{195}Pt and ^{1}H), the experimental recycle delay for

the two spectra (DO = 5 secs) has been assumed to be sufficient for a full relaxation of the magnetization involved in each case. (This was tested by a short series of variable recycle delay experiments).

The linewidths of the central peak in the single-pulse only and CP (with high-power decoupling spectra) are very similar (∿1.2kHz) implying no significant broadening present from ^{195}Pt-^{1}H dipolar coupling. This contribution is unlikely to be fully eliminated by MAS, as spin diffusion (^{1}H-^{1}H) limits the lifetime of the ^{195}Pt nucleus coupled to the protons and thereby affects the coherent averaging of the dipolar coupling[30] (*i.e.* for the condition $\nu_R \ll \Delta\nu_{HH}$). Therefore, only the CP spectrum (with high-power decoupling) will eliminate proton dipolar effects.

A further point to be borne in mind when considering the advantages of each technique is baseline effects. The cross polarisation pulse sequence incorporates spin temperature inversion,[31] which removes artifacts in the FID causing baseline roll. This facility is not present in the single-pulse programme, hence the distortion present (Figure 5.3c).

The substantial linewidth observed (∿1.2kHz) is most likely due to dipolar coupling effects between the platinum and chlorine nuclei, not fully eliminated by MAS, as postulated for K_2PtCl_6. The presence of further quadrupolar nuclei (^{23}Na) is unlikely to have much influence on the ^{195}Pt linewidth. The crystal structure has not been reported for this compound and so the Na-Pt distance is unknown. However, an approximate calculation (using the K-Pt distance from K_2PtCl_6[19]) gives a dipolar coupling constant of $D_{Na,Pt} \simeq 100Hz$.

The single ^{195}Pt resonance flanked by two weak spinning sidebands (Figure 5.3b/c) is indicative of a small anisotropy. The static spectrum (Figure 5.3a) ratifies this, displaying a non-axially symmetric powder pattern with an effective shielding anisotropy (may be affected *inter alia* by heteronuclear dipolar interactions) of *c a.* 110 ppm. (The absence of a substantial sideband pattern in the MAS spectrum prevents any accurate shielding tensor analysis). The lack of symmetry within the lattice (relative to K_2PtCl_6) is likely to be due to the location of the interstitial water molecules.

In the quest for further structural information, the ^{23}Na MAS spectrum was obtained. The characteristics of the ^{23}Na nucleus make it a favourable one to study, (see Table 2.1) requiring very few transients for a high signal-to-noise spectrum. The solid-state ^{23}Na MAS spectrum, as shown in Figure 5.5, exhibits a very narrow peak ($\Delta\nu_{\frac{1}{2}} \sim 100Hz$) at $\delta_{^{23}Na} = 7.2$ ppm. This result shows the presence of only one type of sodium environment present in $Na_2[PtCl_6].6H_2O$.

In order to determine the effect of the interstitial H_2O molecules in the crystalline structure of the compound, a dehydrated sample was studied by ^{23}Na and ^{195}Pt MAS NMR, (Figure 5.5). The ^{23}Na MAS spectrum interestingly displays a narrow peak at 7 ppm ($\Delta\nu_{\frac{1}{2}} \sim 100Hz$) and a somewhat broader peak at -11.5 ppm ($\Delta\nu_{\frac{1}{2}} \sim 250Hz$). The explanation of the two ^{23}Na spectra (Figures 5.5a and 5.5b) may be expedited by briefly considering the quadrupolar effects present (for $I=\frac{3}{2}$).

Magic-angle spinning averages the 1st order quadrupolar interaction for the $m_I = -\frac{3}{2} \leftrightarrow -\frac{1}{2}$ and $m_I = \frac{1}{2} \leftrightarrow \frac{3}{2}$ transitions, (*c.f.* heterogeneous dipolar interactions), the $m_I = -\frac{1}{2} \leftrightarrow \frac{1}{2}$ trans-

FIGURE 5.5

^{23}Na MAS studies of $Na_2PtCl_6.6H_2O$

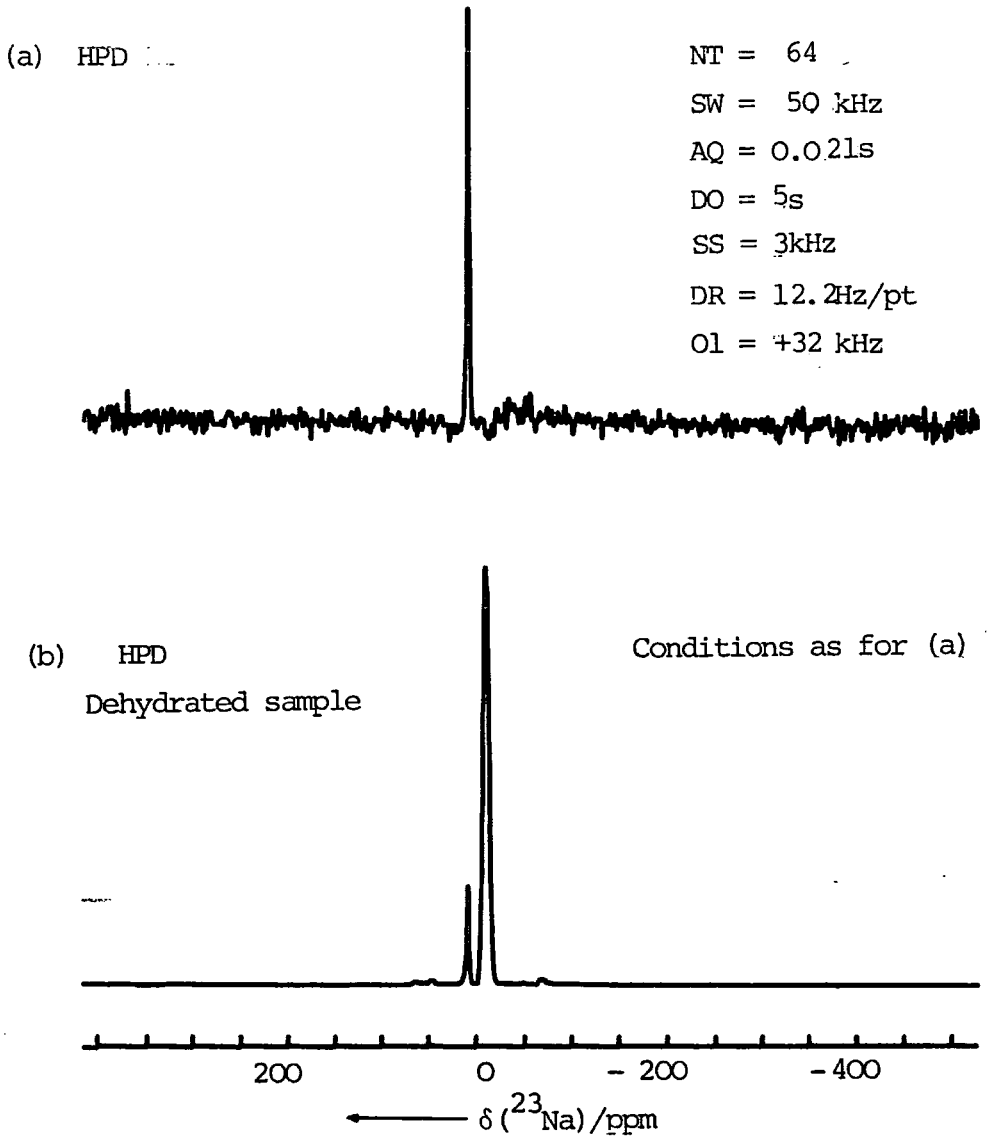

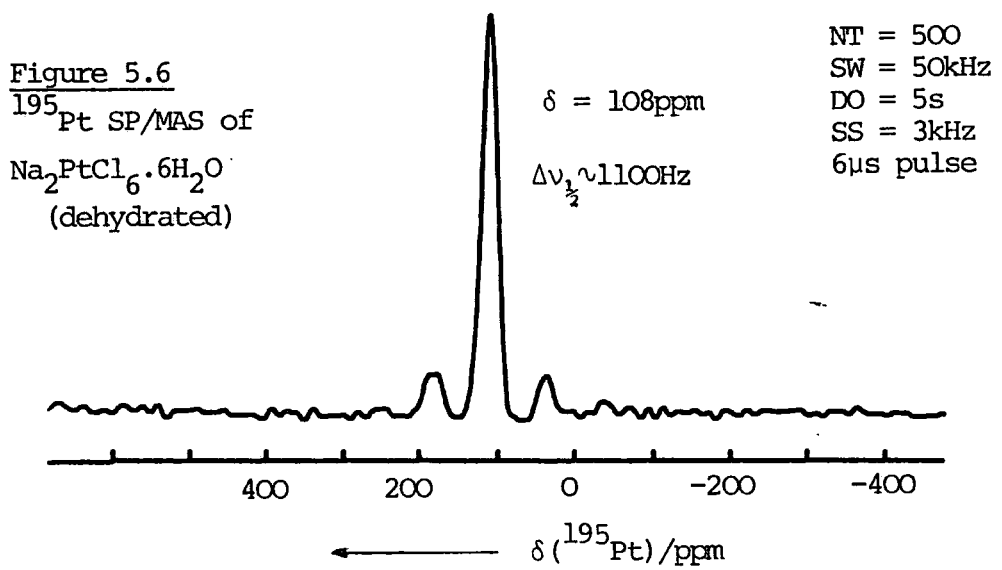

Figure 5.6
^{195}Pt SP/MAS of
$Na_2PtCl_6.6H_2O$
(dehydrated)

ition has no first-order contribution. Therefore, the NMR spectrum of a powder containing a single environment of nucleus $I=\frac{3}{2}$ (or in general any spin) will consist of a single, sharp resonance at the Zeeman transition frequency ν_o, if only 1st order quadrupolar effects are considered (ignoring all other NMR interactions). However, broadening usually occurs due to second order quadrupolar interactions which are not averaged by MAS.[32] This 2nd order term contains a factor ν_Q^2/ν_L, (where ν_Q and ν_L are the quadrupolar and Larmor frequencies respectively). Hence, the broadening effect is dependent on the electric field gradient, and therefore ultimately on the symmetry of the molecule (*i.e.* any sites of tetrahedral, octahedral, cubic or spherical symmetry will have, in principle, zero field gradient).[34] Other possible broadening effects not removed by MAS can be due to motions present causing rapid relaxation of the quadrupolar nucleus.[27] It is therefore likely that the two types of ^{23}Na peak exhibited in Figure 5.5b arise from either two different structural (*i.e.* involving symmetry) or motional environments.

The influence of crystalline water in $Na_2[PtCl_6].6H_2O$ has also been studied by Hales *et al* using ^{35}Cl NQR spectroscopy.[35] The results of dehydration show that the loss of water results in an increase in the ^{35}Cl NQR linewidth, implying successive degradation of the octahedral structure of $Na_2[PtCl_6].6H_2O$.

In addition, the effects of H_2O on the ^{23}Na NMR resonance have been investigated by Veeman *et al*.[36] The ^{23}Na MAS/NMR studies of the zeolite Na-ZSM-5 show that the ^{23}Na resonance broadens on dehydration, and shifts to low frequency by *c a.* 25 ppm. As with the earlier case[35] discussed, the increase

in linewidth on dehydration suggests that the bare Na^+ ions are situated in less symmetric environments than the hydrated sodium ions. This hypothesis is confirmed by a low-field ^{23}Na NMR study, which produced an increase in linewidth implicating the presence of second order quadrupolar interactions.[33]

It can be concluded from these results that the ^{23}Na resonance at 7 ppm arises from the relatively symmetrical environment of the hydrate, $Na_2[PtCl_6].6H_2O$. The presence of a weak resonance at 7 ppm in the ^{23}Na spectrum of the dehydrated sample (Figure 5.5b) implies either some absorption of water on packing or retention of H_2O during dehydration. The broader peak at -11.5 ppm is undoubtedly due to the dehydrated species which contains a distorted and unsymmetric structure giving rise to second order quadrupolar effects. This is in agreement with the findings of Hales *et al*,[35] showing that the loss of interstitial water molecules produces a degradation in the symmetrical structure (as shown by a narrow ^{23}Na resonance) leading to a broadened peak. The ^{195}Pt spectrum of the dehydrated sample (Figure 5.6) is not so informative. The high frequency shift of *c a.* 23 ppm implies some sensitivity of the ^{195}Pt nucleus to a change in crystalline environment, although the observed linewidth of *c a.* 25 ppm introduces considerable uncertainty.

5.6 Potassium Hexahydroxyplatinate, $K_2[Pt(OH)_6]$

The spectrum (Figure 5.7) of $K_2[Pt(OH)_6]$ might be expected to be similar to that of $K_2[PtCl_6]$, except with a sub-

FIGURE 5.7

^{195}Pt CP/NMR SPECTRA OF SOLID $[K_2Pt(OH)_6]$

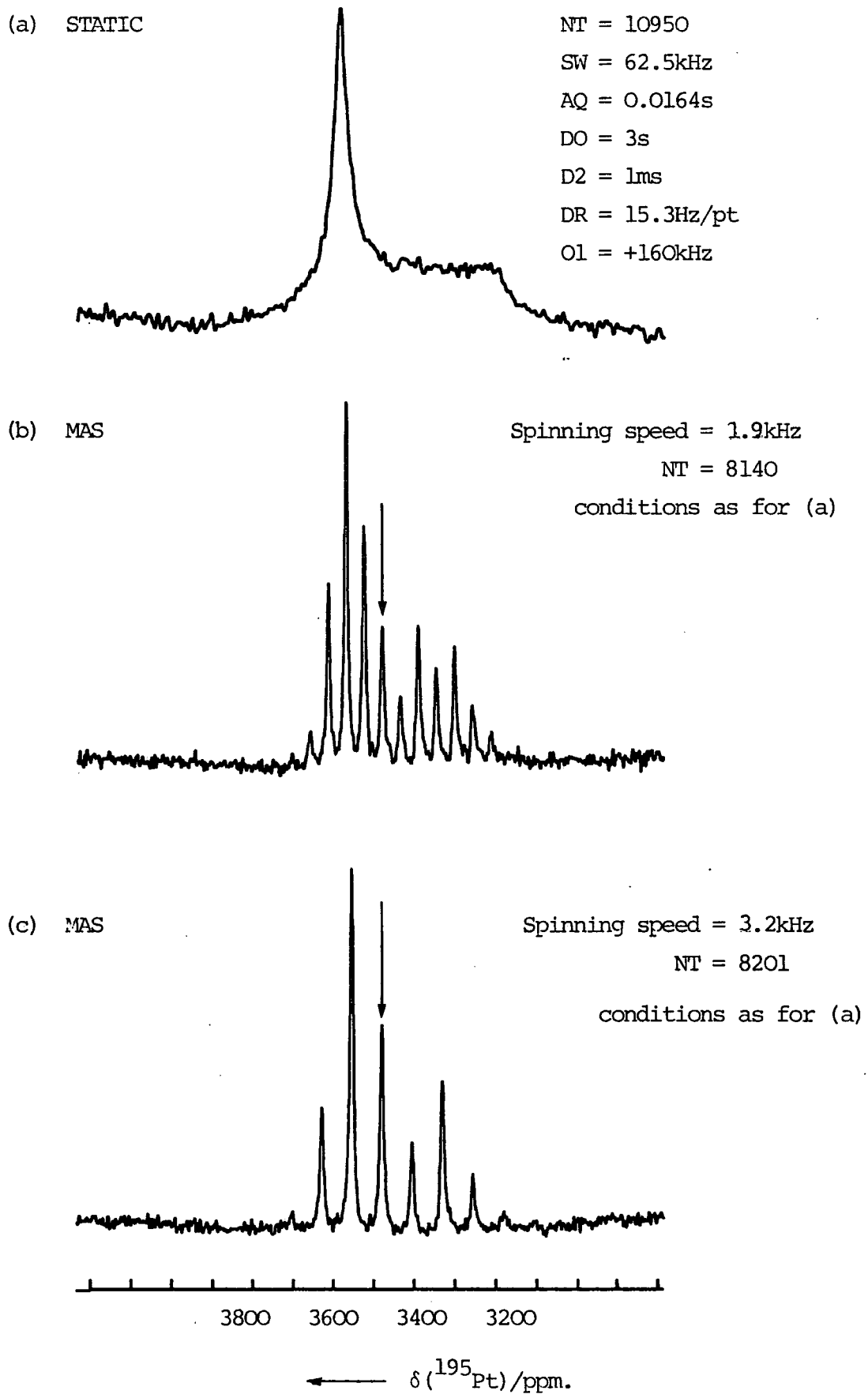

stantially narrower linewidth because of the absence of quadrupolar nuclei directly bonded to the platinum. However, in this case the observed shielding anisotropy is, at first sight, surprisingly substantial, especially as there can be little contribution to the proton-decoupled static bandshape from dipolar interactions, since the dominant isotope of oxygen is non-magnetic and the potassium ions are relatively distant from platinum. The crystal structure obtained for this compound[37] shows it belongs to the rhombohedral system (space group $R\bar{3}$) and that there is only one crystallographically independent molecule per unit cell (which is consistent with the presence of a single ^{195}Pt resonance). The platinum atom is surrounded by six equidistant oxygen atoms (2.016Å) in an octahedron (Figure 5.8). One would therefore expect to see a very small anisotropy for the platinum, giving rise to few (if any) sidebands in the ^{195}Pt spectrum. The observed shielding anisotropy therefore suggests a lowering of symmetry in the crystal structure further away from Pt than the oxygen atoms, as is, indeed, implied by the $R\bar{3}$ space group.

The lack of cubic site symmetry (*c f.* K_2PtCl_6) for the Pt atoms may be seen clearly if the X-ray results are considered in more detail. Potassium ions are positioned around the platinum atoms in the form of a bicapped trigonal antiprism (Figure 5.8), which is consistent with the existence of a $\bar{3}$ symmetry axis at the platinum atom. This has two implications. Firstly, there is an anisotropy in the environment at platinum, thus accounting for the existence of spinning sidebands. Secondly, axial symmetry in the platinum environment is indicated, which should lead to a zero asymmetry factor

FIGURE 5.8 Crystal structure of $K_2[Pt(OH)_6]$

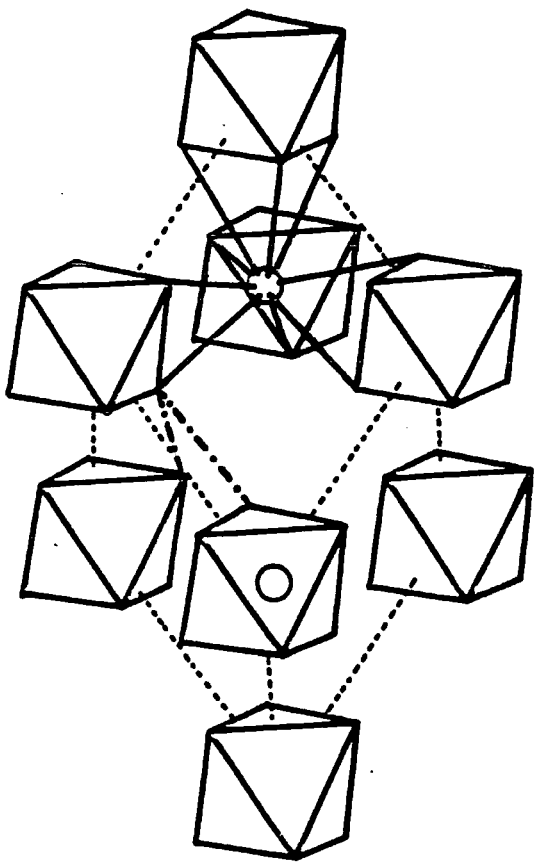

The coordination polyhedron about platinum in the crystal structure of $K_2[Pt(OH)_6]$, shown schematically. The directions of two of the hydrogen bridges are shown by the dashed lines. The potassium ions are indicated by the two small circles, with the nine K-O directions shown by strong lines.

in the ^{195}Pt shielding, contrary to the results given in Table 5.1. The calculations have been checked using both methods[38,39] of deriving shielding tensor components from spinning sidebands, and $\eta \sim 0.25$ is consistently obtained, though it is difficult to estimate the experimental errors involved and there was considerable divergence between the two values obtained by the Herzfeld and Berger method[39] (η=0.43 and 0.17 for the two spinning speeds of 3200 and 1907 Hz). Moreover, the difficulty of measuring second and third moments accurately, necessary for the Maricq and Waugh method,[38] is well known (see Chapter Two). Furthermore, the spinning sideband calculations are not very sensitive to the asymmetry parameter in conditions of nearly axial symmetry.

The static spectrum ^{195}Pt spectrum for $K_2[Pt(OH)_6]$ has been obtained, and is illustrated in Figure 5.7(a). This appears to indicate axial symmetry, though the bandshape is somewhat distorted by dead-time problems. It is possible the appearance may be consistent with a small non-zero asymmetry in $\underline{\sigma}$ if there is substantial linebroadening. The value of σ_{33}, given by the turning point of the static bandshape, is in good agreement with that obtained from the spinning sideband calculations. The results for σ_{22} and σ_{11} derived, bracket the marked maximum in the static bandshape. There would appear to be three possible explanations for these results. Firstly, the NMR results (including sideband analysis) may be consistent with axial symmetry within experimental error. Secondly, the X-ray results may be misleading in that the platinum environment may not be axially symmetric. The latter possibility arises either because the protons (not accurately

located by the X-ray study) may not provide complete axial symmetry around the platinum because of some disorder in the structure undetected by X-ray analysis. It should be recalled that NMR shifts reflect the local environment with great sensitivity, whereas X-rays respond to relatively long-range order. The authors of the X-ray study believe there are hydrogen bridges between neighbouring Pt octahedra, and this may be a source of structural disorder. The third possibility, though regarded as unlikely, is that the shielding tensor values are actually different for the MAS and static cases. If the second argument is true, then it is possible that the observed values of σ_{11} and σ_{22} are averaged by some motional process. As σ_{33} is unaffected by the "motion", (*i.e.* the value is approximately the same for sideband analysis and from the static bandshape) it must lie on a rotation axis, which would be the C_3 unique axis passing through the platinum atoms. The averaging of σ_{11} and σ_{22} would give rise to an axial static bandshape. Such motional averaging of the principal shielding tensor elements has been observed for hexamethylbenzene, changing from a non-axial bandshape at low temperatures to an axial bandshape at high temperature.[40] The difference between the MAS and the static ^{195}Pt spectrum of $K_2[Pt(OH)_6]$ may be accounted for by magic-angle rotation modulating the motion so as to give an effectively static situation. It may be noted that the rotation rate is of the same order of magnitude as $\sigma_{22}-\sigma_{11}$, expressed in Hz. Experimental evidence of any MAS modulation of motion could only be verified by a variable temperature MAS study. In addition, some effects might be observed by spinning at

speeds less than 1 kHz. However, this was not feasible within the available MAS system. The accuracy of the shielding tensor analysis or the authenticity of axial symmetry present could be investigated further by a computer simulation of the sideband intensities.[38]

5.7 Tris(ethylene diamine) platinum(IV) Tetrachloride-Dihydrate

A solid-state spectrum of $[Pt(en)_3]Cl_4.2H_2O$ was obtained at two spinning speeds, (see Table 5.1 and text) as shown in Figure 5.9. By analogy with the octahedral complexes $K_2[Pt(OH)_6]$ and $K_2[PtCl_6]$, the atoms directly bonded are all the same and thus given such molecular symmetry one would expect a modest shielding anisotropy. However, the observed anisotropy is substantial (*c a.* 350 ppm), and this must arise from a lack of symmetry in the environment more than one bond removed from platinum. For octahedral tris(ethylenediamine) metal complexes,[41] there are two enantiomorphous ways of orientating the chelate rings about the metal atom (see Figure 5.10(a)). Moreover, since the ethylenediamine chelate rings are themselves puckered, and therefore chiral (Figure 5.10(b)), there are, in principle, four enantiomorphous pairs of diastereomers. The NMR spectrum suggests that only one crystallographic site is present. However, this does not necessarily mean there is a single enantiomer. It is possible that the observed linewidth contains unresolved splittings. Moreover, if the space group of the unit cell contains a mirror plane, two enantiomers could be present in the unit cell, related by symmetry and therefore crystallographically equivalent, giving rise to a single ^{195}Pt resonance. The ring

FIGURE 5.9

^{195}Pt CP/MAS spectra of $[Pt(en)_3]Cl_4.2H_2O$

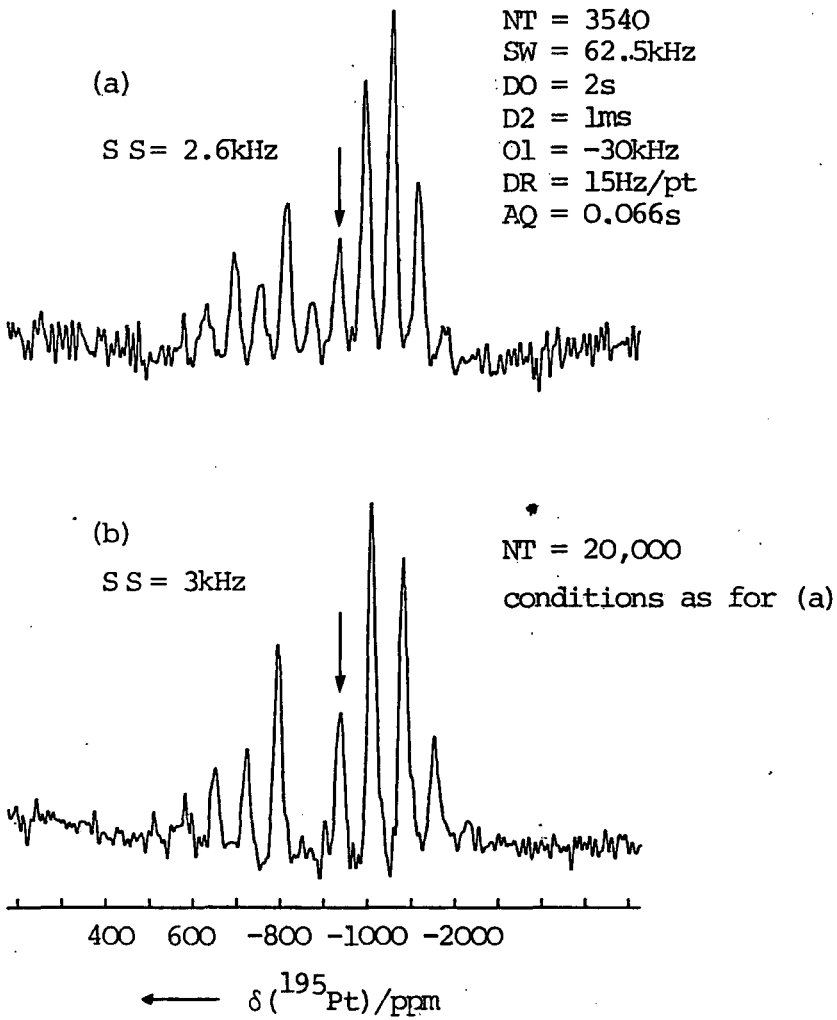

FIGURE 5.10

Stereochemistry of ethylenediamine complexes[41]

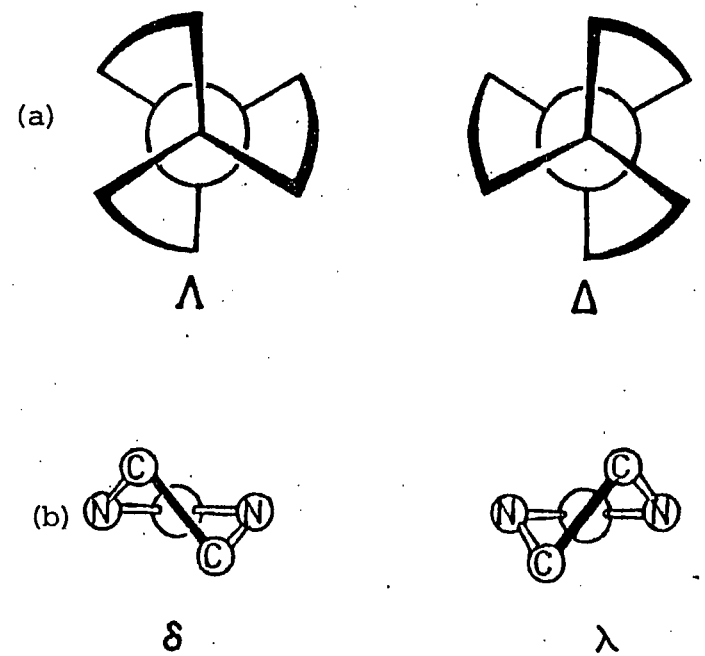

(a) Orientation of chelate rings in octahedral systems.

(b) Ring-puckering for individual chelate rings.

puckering effect, as well as hydrogen bonding and other intermolecular interactions could account for the large anisotropy seen.

5.8 Diamminetetrachloroplatinum(IV)

The spectrum of *cis*-$[Pt(NH_3)_2Cl_4]$ is displayed in Figure 5.11 showing a non-axial symmetry and relatively small anisotropy (see Table 5.1). This implies that, even with the presence of two types of directly-bonded ligands to platinum, the surrounding electronic environment is unexpectedly relatively symmetrical with respect to the octahedral complexes of $K_2[Pt(OH)_6]$ and $[Pt(en)_3]Cl_4.2H_2O$. This point again stresses the importance of intermolecular symmetry on the magnitude of the shielding anisotropy. No single-crystal X-ray diffraction study of *cis*-$[Pt(NH_3)_2Cl_4]$ is known, which is surprising in view of its close relation to *cis*-$[PtCl_2(NH_3)_2]$, the anti-cancer drug. The solid-state spectrum indicates the presence of a single crystallographic site.

The NMR study of *trans*-$[Pt(NH_3)_2Cl_4]$ gives rise to a spectrum (Figure 5.11b) exhibiting a considerably smaller anisotropy, as indicated by the intensity of the sidebands, than was obtained for the *cis* isomer. This is partly to be expected considering the higher molecular symmetry for the *trans* isomer. The only X-ray study of *trans*-$[Pt(NH_3)_2Cl_4]$ is reference 42, which merely confirms the octahedral symmetry of the molecule and gives values for the Pt-N and Pt-Cl bond lengths (2.35Å and 2.31Å respectively). The chemical shift difference between the two isomers is modest ($\Delta\delta$=167 ppm) for solid-state ^{195}Pt NMR spectroscopy. However, without shield-

FIGURE 5.11

^{195}Pt MAS spectra of $[NH_3)_2PtCl_4]$

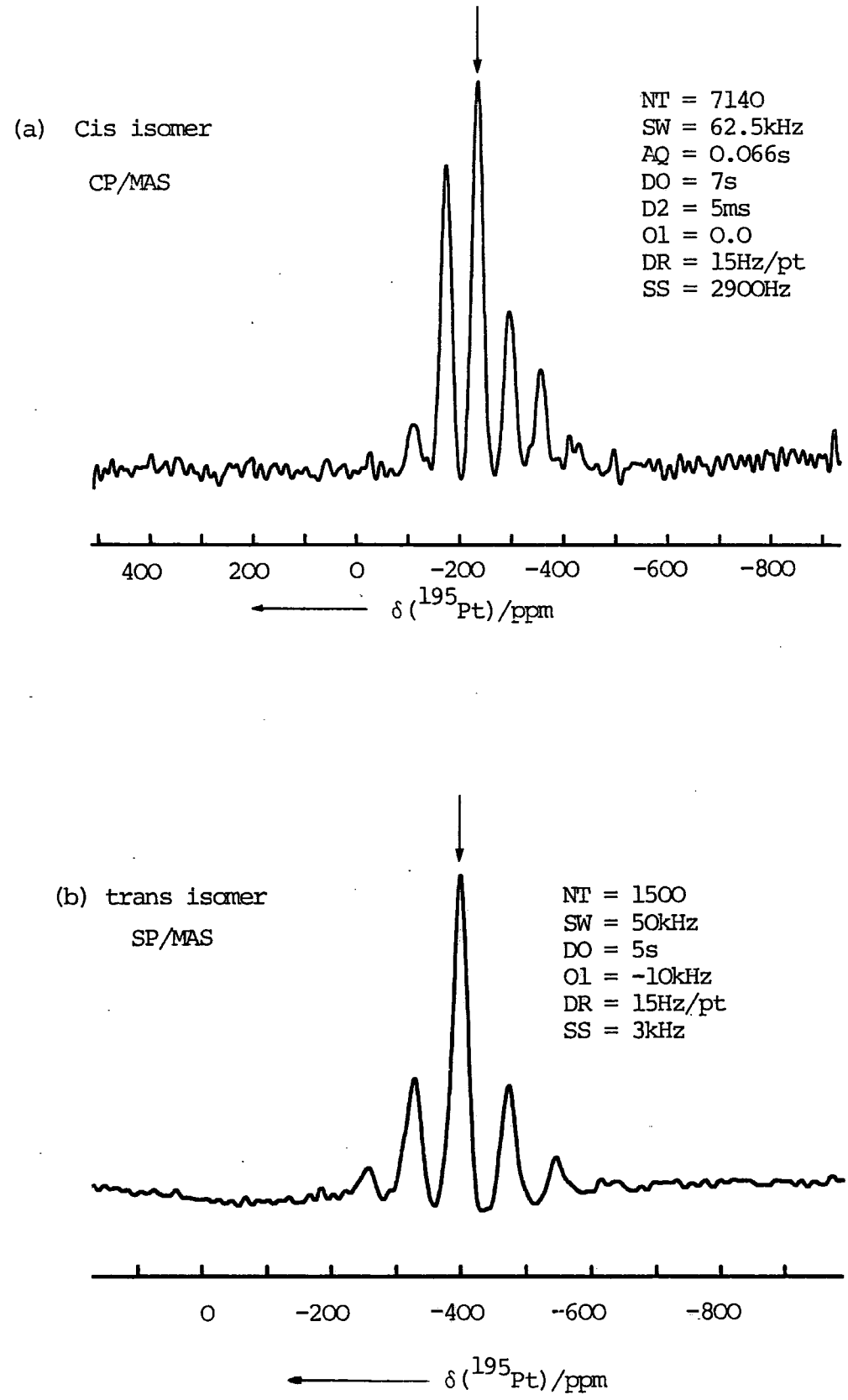

ing tensor data for the *trans* isomer, (the small number and relatively low intensities make spinning sideband analysis difficult) the difference is inconsequential. Isomer effects of Pt(IV) complexes have been studied in the solution state[1] and show little difference in chemical shifts. Coupling constants form a more sensitive indicator to the change in electronic environment (see Chapter Four). However, it is rare for scalar coupling to be observed between a spin-½ nucleus and a quadrupolar nucleus (*e.g.* ^{14}N, ^{35}Cl), because of rapid quadrupolar relaxation leading to broadening of the resonance. However, ^{195}Pt-^{14}N scalar coupling has been observed in the solution-state, at high temperatures,[14] where the increase in motional activity leads to self-decoupling.[34] Thus, unresolved splittings due to isotropic indirect (^{195}Pt, ^{14}N), (^{195}Pt, ^{35}Cl) and (^{195}Pt, ^{37}Cl) coupling will probably contribute to the linewidths in the solid-state spectra.

It is perhaps not surprising that these compounds studied, which contain directly-bonded quadrupolar nuclei,exhibit the broadest linewidths (*c a.* 1kHz) as it has been found that magic-angle spinning fails to remove completely the dipolar coupling between a quadrupolar nucleus and a spin-½ nucleus.[22-25] If the quadrupole moments are coupled more strongly to the efg than to the Zeeman field, the ^{195}Pt-Cl/N dipolar interaction will not be removed by MAS. For a platinum nucleus coupled to Cl, the presence of two abundant quadrupolar chlorine isotopes complicates the situation. The observed linewidths may be influenced further by the relaxation behaviour of the quadrupolar nuclei. This effect may range from linebroadening

in the region of slow and intermediate relaxation to line-narrowing due to self-decoupling for rapidly relaxing nuclei.[2

5.9 Phosphorus-containing Platinum(II) complexes

(i) *cis*-Dimethyl bis(triethylphosphine)platinum(II)

The ^{195}Pt spectrum of *cis*-$[PtMe_2(PEt_3)_2]$ gives rise to a multitude of sidebands and illustrates several features of chemical interest. The variable spinning speed experiments (Figures 5.12a/b) show there are three centrebands present with the middle band situated at δ = -4654 ppm. The intensity ratio of the three sideband manifolds is found to be 1:2:1. The centrebands are equally separated with a spacing of 1893Hz, which undoubtedly represents $|^1J_{Pt,P}|$, though the width of central component suggests there may be two different values for this parameter. Indeed some of the spinning sidebands of the central resonance show an incipient splitting. The solution-state spectrum of *cis*-$[PtMe_2(PEt_3)_2]$ exhibits a triplet pattern because of coupling to two equivalent phosphorus nuclei, the magnitude of the coupling constant being 1860Hz (measured with a digitization rate of 19Hz/pt).

The single ^{195}Pt chemical shift in the solid-state spectrum, which compares very closely with the solution-state result, indicates the presence of only one crystallographically independent site for the molecule in the unit cell. The ^{31}P NMR results give additional information concerning the molecular structure of this compound. The two phosphorus resonances, indicating two crystallographically non-equivalent sites are due to a molecular site symmetry which is lower than the

FIGURE 5.12

^{195}Pt CP/MAS spectrum of *Cis* $[PtMe_2(PEt_3)_2]$

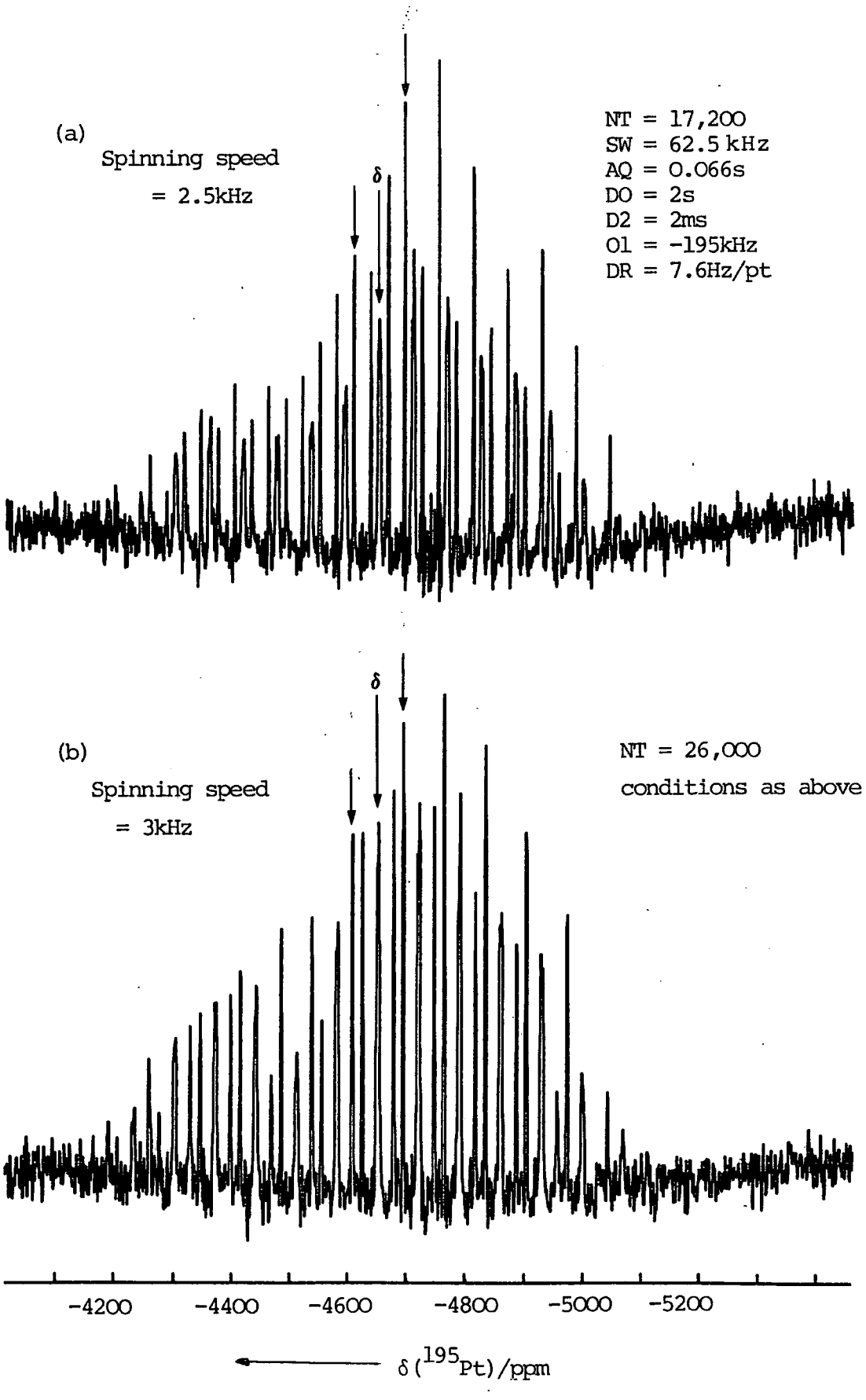

molecular symmetry, *i.e.* intramolecular non-equivalence. X-ray crystallographic data has been obtained for the compound, confirming these solid-state NMR results (Chapter Four).

Since the middle centreband of the ^{195}Pt spectrum is unresolved the system may be treated approximately as a three spin AX_2 case. Three tensor properties need to be taken into account when analysing the sideband manifolds, namely (a) indirect (^{195}Pt,^{31}P) coupling ($\underline{J}$), (b) dipolar (Pt,P) coupling (D); and (c) ^{195}Pt shielding ($\underline{g}$). The AX_2 case has the advantage that the middle manifold of sidebands corresponds to zero total spin component of the phosphorus nuclei. Its effective anisotropy is uninfluenced by (Pt,P) coupling of either type, and therefore an analysis of this manifold gives the principal components of the ^{195}Pt shielding tensor unambiguously, thus reducing the number of unknowns. A detailed analysis of the outer sidebands for this AX_2 case is not possible using the theory determined in Chapter Two, (and applied in Chapter Six). The non-linearity of the molecule and the presence of two dipolar axes means that the various assumptions made no longer apply. However, examination of the spectra reveals a similar spread of frequencies for the two outer sideband manifolds, which indicates that there is only a small coupling contribution to the effective anisotropy. The poor signal to noise in the extremities of the spectrum is an important factor in considering accurate analysis of the subspectra. The ^{31}P spectrum displays Pt-P coupling in the form of platinum satellites, with two sideband manifolds resulting from the Pt-P doublet. However, a close inspection of the subspectra reveals no significant difference between the two spreads of frequency.

(ii) *cis*-[Dimethyl bis(triphenylphosphine)platinum(II)]; c-$[PtMe_2(PPh_3)_2]$

As may be predicted, the ^{195}Pt spectrum (Figure 5.13) of *cis* $[PtMe_2(PPh_3)_2]$ is very similar to that of its triethylphosphine analogue. The 'pull' of electrons from the phenyl groups of the PPh_3 ligands is likely to cause some deshielding as noted previously with respect to the ^{31}P chemical shifts (see Table 5.2).

TABLE 5.2

	$\delta(^{195}Pt)$/ppm	$\delta(^{31}P)$/ppm
$PtMe_2(PEt_3)_2$	-4654	10.3, 11.7
$PtMe_2(PPh_3)_2$	-4682	26.1, 29.3

The phenyl groups are two bonds away from the platinum atom and the shift data therefore illustrate the sensitivity of the ^{195}Pt nucleus. The directly attached phosphorus nucleus produces a shielding effect on the platinum nucleus[3] and thus the low frequency shift can be considered to be entirely due to the electron rich phenyl substituents in the phosphine ligands.

The ^{195}Pt spectrum clearly shows four centrebands arising from the X part of a pseudo ABX system. The coupling of a ^{195}Pt nucleus with two non-equivalent phosphorus nuclei produces a doublet of doublets with $/^1J_{Pt,P}/$=1824, 1979Hz. (Digitization resolution = 7Hz/pt). This is in excellent agreement with the ^{31}P results of 1817 and 1978 Hz. One would expect *a priori* to see an AB pattern in the ^{31}P spectrum due to the J coupling of the intramolecular non-equivalent phosphorus nuclei. Such a coupling is thought to be very

FIGURE 5.13 ^{195}Pt CP/MAS spectrum of *Cis* $[PtMe_2(PPh_3)_2]$

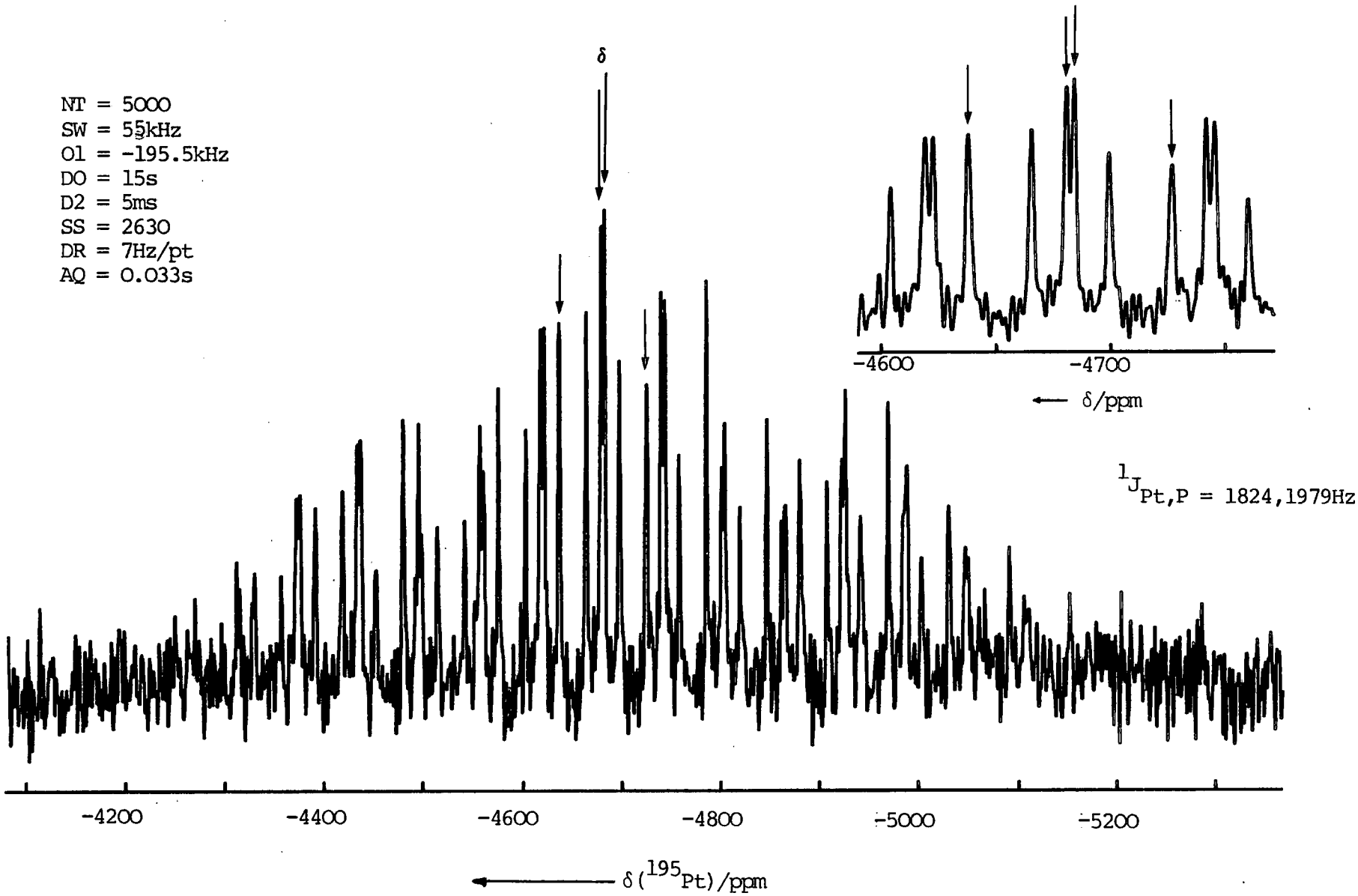

small, thus producing an AX spectrum; (by virtue of the fact that $\delta_{AB}(^{31}P)$ = 3.2 ppm (256Hz) and so $J/\delta < 0.1$).[44] Unfortunately, the resolution does not permit the observation of such a splitting pattern.

A comparison of the principal shielding tensor components for $[PtMe_2(PEt_3)_2]$ and $[PtMe_2(PPh_3)_2]$ (Table 5.1) shows that the difference in isotropic chemical shifts is mainly attributable to the elements σ_{11} and σ_{33}. This is to be expected considering the molecular symmetry and fundamental difference between the two compounds containing perpendicular phosphine ligands. The large values of η calculated for both compounds indicates a substantial deviation from axial symmetry; this was also found to be the case from the ^{31}P NMR study (Chapter Four).

The relatively high resolution of both ^{195}Pt spectra ($\sim$100Hz linewidths) is comparable with that obtained for the solid-state ^{31}P spectra. The favourable linewidth is observed due to a lack of quadrupolar nuclei or any other substantial broadening mechanism (*e.g.* bulk susceptibility or motional effects). However, it is unlikely that any significant improvement can be made on such resolution using the same rotor system. If a large anisotropy is present, as for this case, a slightly off-set angle (or any rotor instability) can cause considerable linebroadening.

REFERENCES - Chapter Five

1. R.G. Kidd and J. Goodfellow, "NMR and the Periodic Table", Eds. R.K. Harris and B.E. Mann, Academic Press, New York, 1978, p.249-257.

2. P.S. Pregosin, Coord., Chem., Rev., 1982, (44), 247.

3. P.S. Pregosin, Chimia, 1981 (35), 43.

4. B. Rosenberg, L. van Camp, J.E. Trosko, V.H. Mansour, Nature (London), 1969, (222), 385.

5. C. Hunt, Education in Chemistry, 1984, (July), 111.

6. M.J. Cleare, Plat.Met.Rev., 1982, (29), No.2, 72.

7. I.M Ismail and P.G. Sadler, Acs.Symp.Str., 1983, (209), 171.

8. M. Chikuma and R.J. Pollock, J.Mag.Res., 1982, (47), 324.

9. T.G. Appleton, R.D. Berry, C.A. Davis, J.R. Hall and H.A. Kimlin, Inorg.Chem., 1984, (23), 35.

10. G.J.K. Acres, Plat.Met.Rev., 1984, (28), No.4, 150.

11. H.T. Stokes, C.D. Makowka, P. Wang, S.L. Rudaz, C.P. Slichter, J.Mol.Cat., 1983, (20), 321.

12. R. Benn, H.M. Buch, R.D. Reinhardt, Mag.Res.Chem., 1985, (23), 559.

13. J. Lallemand, J. Soulié, J. Chottard, J.C.S.Chem.Comm., 1980, 436.

14. I.M. Ismail, S.J.S. Kerrison and P.J. Sadler, Polyhedron, 1982, (1), 57.

15. D.M. Doddrell, P.F. Barron, D.E. Clegg and C. Bowie, J.C.S. Chem.Comm., 1982, 575.

16. J.J. Dechter and J.K. Walewski, J.Mag.Res., 1984, (59), 146.

17. W.T. Dixon, J.Chem.Phys., 1982, (77), 1800.

18. D.P. Raleigh, E.T. Olejniezak, S. Vega and R.G. Griffin, J.Am.Chem.Soc., 1984, (106), 8302.

19. R.J. Williams, D.R. Dillin and W.O. Milligan, Acta Cryst., 1973, (B29), 1369.

20. H. Kessemeier and R.E. Norberg, Phys.Rev., 1967 (155), 321.

21. E.R. Andrew, A. Bradbury, R.G. Eades and V.T. Wynn, Phys.Letts., 1973, (4), 99.

22. W.W.Fleming, C.A. Fyfe, J.R. Lyerla, M. Vanni and C.S.Yannoni, Macromolecules, 1980, (13), 460.

23. E. Kundla and M. Alla, Proc XX Cong.Ampere, Talinn 1978, p.92, Published 1979 (Springer-Verlag, Berlin), Eds. E.I. Kundla, E.T. Lippmaa and T. Saluvere.

24. E.M. Menger and W.S. Veeman, J.Mag.Res., 1982, (46), 257.

25. G.E. Balimann, C.J. Groombridge, R.K. Harris, K.J.Packer, B.J. Say and S.F. Tanner, Phil.Trans.Roy.Soc., 1981, (A299), 647.

26. H.W. Spiess, U. Haeberlen and H. Zimmermann, J.Mag.Res., 1977, (25), 55.

27. R.J.C. Brown, B.K. Hunter, M. Mackowiak and S. Segel, J.Mag.Res., 1982, (80), 218.

28. E.R. Andrew, Int.Rev.Phys.Chem., 1980, (1), 195.

29. N. Zumbulyadis, P.M. Henrichs, R.H. Young, J.Chem.Phys., 1981, (75), 1603.

30. C.S. Yannoni, Acc.Chem.Res., 1982, (15), 201.

31. E.O. Stejskal and J. Schaefer, J.Mag.Res., 1975,(18), 560.

32. E. Oldfield, R.A. Kinsey, B. Montez, T. Ray and K.A.Smith, J.Chem.Soc., Chem.Comm., 1982, 254.

33. G.E. Maciel, "Magnetic Resonance, Introduction, Advanced Topics and Applications to Fossil Energy, 71-110, Eds. L. Petrakis and J.P. Fraissard, D. Reidel, 1984.

34. R.K. Harris, "NMR Spectroscopy, A Physicochemical View", Pitman, 1983.

35. J. Hales, M. Rakos, J. Lasanda, J. Jankura, C. Belica, V. Fischer, J.Mol.Struct., 1983, (83), 69.

36. K.F.M.J. Scholle, H.A.J.M. Bakkum and W.S. Veeman, Chapt.11, Ph.D. Thesis, Univ. of Nijmegen, 1984.

37. V.G. Bandel, C. Platte and N. Trömel, Acta Cryst., 1982, (B38), 1544.

38. M.M. Maricq and J.S. Waugh, J.Chem.Phys., 1979, (70), 3300.

39. J. Herzfeld, and A.E. Berger, J.Chem.Phys., 1980, (73), 1021.

40. A.Pines, M.G. Gibby and J.S. Waugh, Chem.Phys.Lett., 1972(15), 373.

41. F.A.Cotton and G. Wilkinson, "Advanced Inorganic Chemistry", Third Edition, J.Wiley and Sons.

42. N.V. Belov, G. Bokii, L.A. Popova, Izvest.Akad.Navk.SSSR, 1947, (8), 249, (cited, "The Chemistry of Platinum and Palladium", F.R. Hartley, Applied Science, London 1973).

43. F.H.Allen and A.Piddock, J.Chem.Soc.(A), 1968, 2700.

44. R.J. Abraham, 'The Analysis of High Resolution NMR Spectra', Elsevier, 1971.

CHAPTER SIX

HIGH-RESOLUTION TIN-119 SOLID-STATE NMR

6.1 Introduction

Solution-state ^{119}Sn NMR has now been in use for over 25 years, and is now regarded as a routine analytical technique. There are three non-zero naturally occurring isotopes of elemental tin, ^{115}Sn, ^{117}Sn and ^{119}Sn, all having a spin-½ nucleus. ^{119}Sn is chosen as the most suitable nucleus to study mainly due to its higher natural abundance (see Table 6.1).

TABLE 6.1 NUCLEAR MAGNETIC MOMENTS AND NATURAL ABUNDANCE OF TIN ISOTOPES[1]

Isotope	Nat. Abundance %	Mag[c] moment[b] μ	Relative Sensitivity[a]
^{115}Sn	0.35	- 0.913	3.50×10^{-2}
^{117}Sn	7.61	- 0.995	4.52×10^{-2}
^{119}Sn	8.58	- 1.041	5.19×10^{-2}

a. At constant field, $^{1}H = 1.00$
b. Nuclear magnetons.

The large chemical shift range of over 2200 ppm[2] makes the tin nucleus very sensitive to small modifications in structure. A considerable amount of solution-state data has been tabulated in reviews which gives valuable structural information concerning bonding and coordination.[2,3] However, very little work has been published regarding solid-state ^{119}Sn NMR. The only report cited concerns the solution and solid-state chemical shifts of nBu_2SnCl_2.[4] However, the solid-state spectrum is hardly high-resolution giving rise to a broad line with a total width of *ca.* 200 ppm. The lack of work in this area is surprising considering the several inconclusive studies in the solid-state by X-ray crystallography.[5] In addition, the

receptivity of ^{119}Sn is twenty-five times greater than that of carbon, and a fairly low magnetogyric ratio (γ = 10 x 10^7 rad T^{-1} s^{-1}) which makes it very suitable for cross-polarisation in the solid-state.

In order to assess the potential of ^{119}Sn solid-state NMR using the CXP200 spectrometer, a range of tin compounds was studied. The ^{119}Sn spectra obtained, using HPD, CP and MAS are discussed in detail and correlations with available X-ray data and solution-state ^{119}Sn NMR have been made. The tin systems under study have included the type R_3SnX (where R = Alkyl, Ph and X = F, OH, Cl); these tend to have different coordinations in the solution and solid-state. Where necessary, side band analyses have been used to reveal extra structural information regarding the geometry and symmetry in the crystal lattice. In addition, two of the compounds studied (Me_3SnF and nBu_3SnF) contain information regarding the interaction of tensor properties, namely, (i) dipolar coupling, (ii) indirect scalar coupling and (iii) shielding anisotropy.

6.2 Sensitivity of Tin-119 CP/MAS: Study of Ph_3SnR (R = Me, Et, Bu, and Ph)

Although the first high resolution CP/MAS ^{119}Sn signal in the present work was observed using trimethyl tin hydroxide, this was not a suitable candidate for tuning purposes as the large spread of spinning sidebands meant that a reasonable signal was visible only after *ca.* fifty scans (Recycle delay = 12s). An ideal sample for setting the Hartmann-Hahn

matching condition would be one that contained undistorted tetrahedral molecules of the type R_4Sn, which would give rise to a narrow single peak. The only compound of this type known to exist in the solid-state is $SnPh_4$. However, although this sample gives rise to a single peak with a reasonable linewidth (Figure 6.1) the recycle time needed between each scan is *ca.* 5 minutes. Other compounds were studied due to their relatively undistorted tetrahedral geometry, abundance of protons and lack of any other abundant spin>½ nuclei.

TABLE 6.2 CHEMICAL SHIFT DATA FOR Ph_3SnR

	Solid-State			Solution-State		
Compound	δ/ppm[a,b]	$\Delta\nu_{\frac{1}{2}}$/Hz	Recycle Delay	δ/ppm[a]	Solvent	Ref.
Ph_3SnMe	-78	80	30s	-93	20% CH_2Cl_2	6
Ph_3SnEt	-81	83	30s	-98	30% CCl_4	7
Ph_3SnBu^n	-97[c]	750	30s	-111	C_6H_{12}	8
Ph_4Sn	-121	70	300s	-137	$CHCl_2.CH_2Cl$	9

a. Chemical shifts relative to external reference, neat $SnMe_4$.

b. Digitization rate = 5Hz/pt

c. Error ±1ppm.

The ^{119}Sn solid-state spectra of all the above organotin compounds (Table 6.2) exhibited a single tin resonance indicating the presence of a single crystallographic site. The correlation with solution-state ^{119}Sn NMR chemical shifts is reasonable considering temperature and solvent effects. The general trend of decreasing chemical shift with an increasing

FIGURE 6.1 - $SnPh_4$

NT = 1

D2 = 10ms

AQ = 0.1s

^{119}Sn CP/MAS Spectra of Ph_3SnR

(ss = 3kHz)

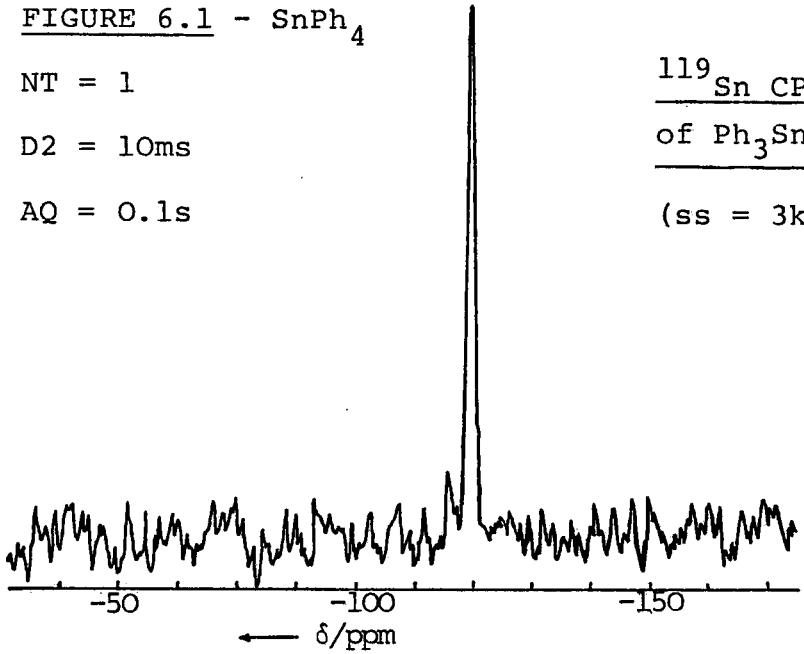

FIGURE 6.2 - Ph_3SnMe

NT = 1

D2 = 1ms

AQ = 0.051s

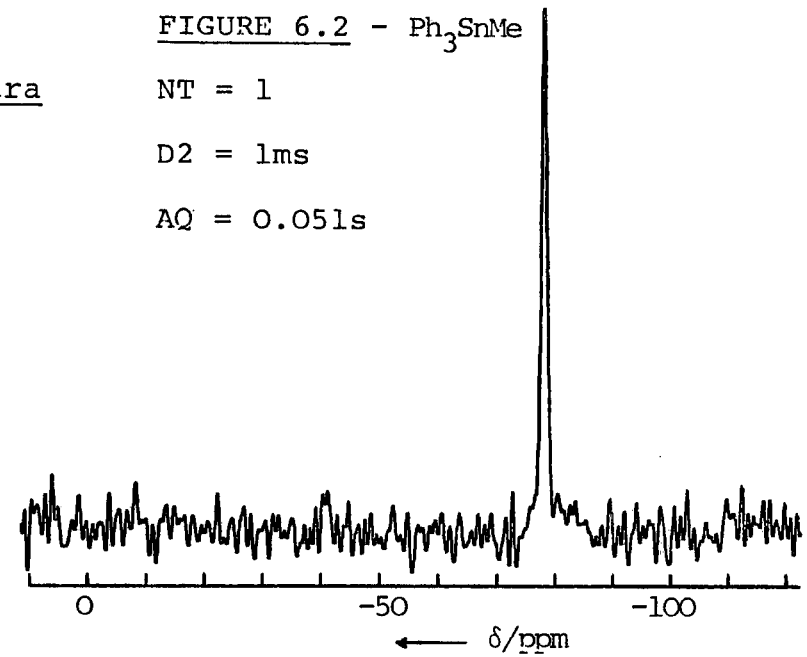

FIGURE 6.3 - Ph_3SnEt

NT = 90

D2 = 1ms

AQ = 0.026s

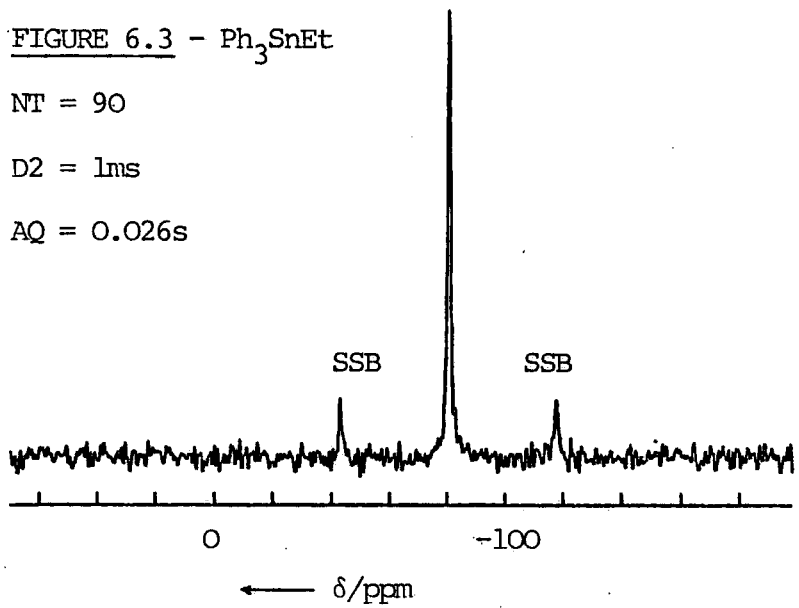

FIGURE 6.4 - Ph_3SnBu^n

NT = 132

D2 = 1ms

AQ = 0.026s

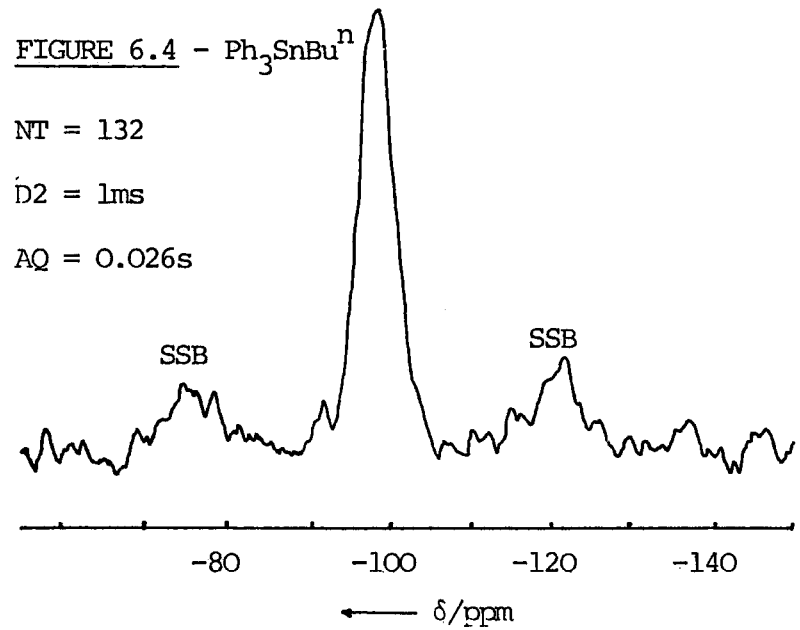

size of R is apparent for both solution and solid-state data. The explanation for this is mainly due to the increase in shielding of the tin nucleus caused by the larger organic groups.

The only X-ray crystallographic data available on these set of compounds is for Ph_4Sn,[10] (space group $P\bar{4}2_1C$, one independent molecule per unit cell) the tetraphenyl tin has a $\bar{4}$ symmetry, each phenyl group is planar, the tin atom is lying on the phenyl plane and each ring is orientated so that it approximately eclipses one of the Sn-C bonds related by operation of the $\bar{4}$ axis. The tin coordination is exactly tetrahedral ($C\text{-}\hat{S}n\text{-}C = 109.8^{o}$), therefore giving rise to a single ^{119}Sn peak with a minimum linewidth of $\sim$70Hz (see Figure 6.1).

Ph_3SnMe gives rise to a single line ($\Delta\nu_{\frac{1}{2}} \sim 80Hz$); the small increase in linewidth observed could be due to a slight distortion in the tetragonal shape of the molecule (Figure 6.2). The spectrum of Ph_3SnEt (Figure 6.3) exhibits spinning side bands indicating some increased shielding anisotropy present, no doubt because of a larger distortion in the tetragonal lattice framework. The spectrum of Ph_3SnBu^n (Figure 6.4) is somewhat of an anomaly with a linewidth of $\sim$750Hz. The reason for this unexpected phenomenon is not clear. It could be that paramagnetic impurities are present or some motional property in which the molecular motion corresponds to the decoupling field strength.

6.3 Trimethyltinhydroxide, Me_3SnOH

This compound was found to be very sensitive to cross-polarisation due to the large number of protons at only two bonds away from the tin atom. The ^{119}Sn solid-state spectrum obtained by CP/MAS reveals a multitude of spinning sidebands due to a large shielding anisotropy present (see Figure 6.5). As indicated on the spectrum, there are two ^{119}Sn resonances present and their associated sideband manifolds emanating from two distinct crystallographic sites. Using 1st moment analysis and spinning speed variation the two ^{119}Sn NMR centrebands were found to be at δ_{Sn} = -99 and -152 ppm with respect to the signal for neat liquid tetramethyltin. These shifts should be compared with those recorded for the solution-state Me_3SnOH with values ranging from +118ppm to +128ppm.[11,12] The very substantial low-frequency shift for the solid-state is indicative of *penta* or *hexa*-coordination, as is well known for a variety of tin compounds.[2]

Trimethyltinhydroxide has been studied by solution and solid-state infrared spectroscopy[13] and also X-ray crystallography.[14] The former results show that there is no hydrogen bonding in either the solid or solution states, although marked differences are observed between the spectra in the two states. The authors believe that the principal species in solution appears to be a dimer (see Figure 6.6a), whereas in the solid it takes the form of a linear polymer (Figure 6.6b).

FIGURE 6.5 ^{119}Sn CP/MAS spectrum of Me_3SnOH

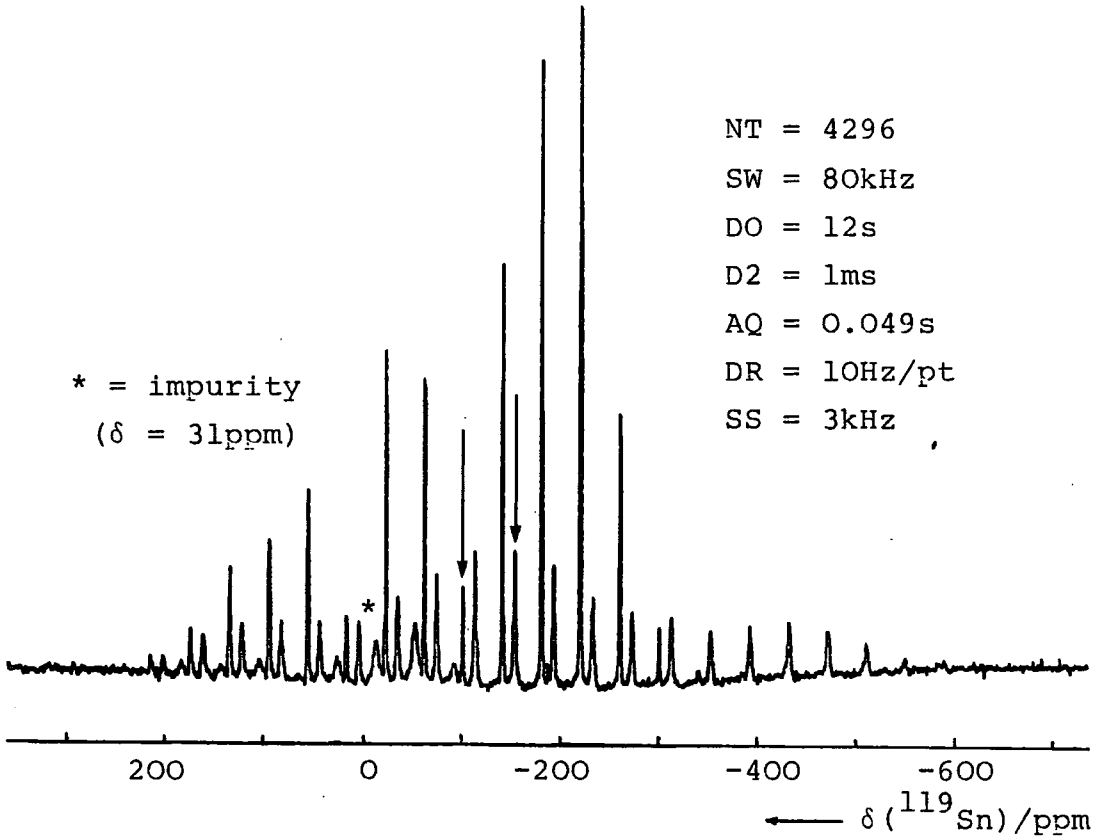

FIGURE 6.8 ^{119}Sn CP/MAS spectrum of Ph_3SnOH

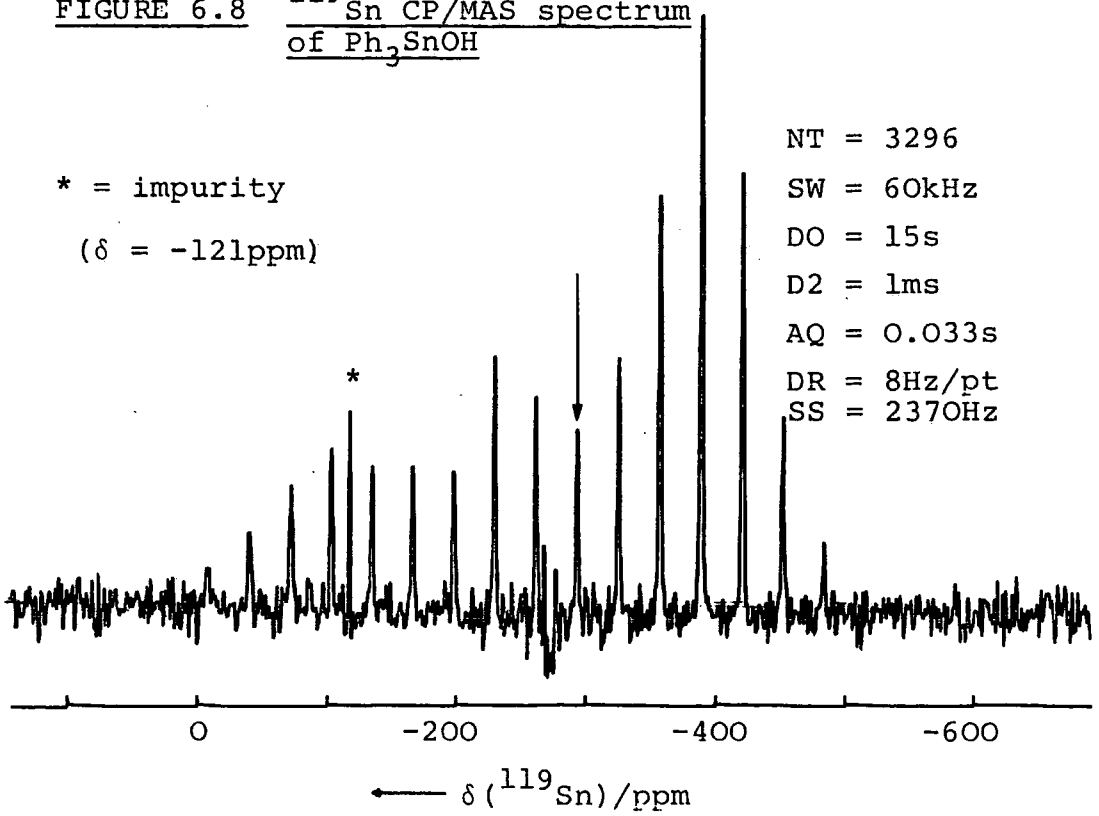

FIGURE 6.6 The two different structural forms of Me_3SnOH

(a) (b)

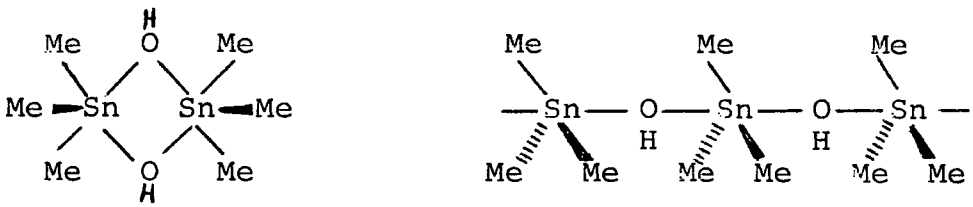

Dimer Linear polymer

The only report of X-ray crystallographic data for Me_3SnOH cited gives a rather vague discussion that fails to make it clear what constitutes the asymmetric unit of the crystal structure.[14] The paper talks of there being chains of trimethyltin groups and hydroxyl groups arranged alternately to form an 8_3 helix. The trimethyltin group is planar but inclined at about 15^{o} with respect to the plane perpendicular to the chain axis. However, the study is inconclusive and there is no mention of two distinct sites as observed from the solid-state NMR spectrum.

It is unlikely that the dimer (Figure 6.6(a)) is present in solution as the tin is *penta*coordinated in this structure, therefore there would only be a relatively small difference between the solid and solution-state chemical shifts.

In addition to the two main sideband manifolds, there is an additional resonance at δ_{Sn}=31.3ppm. Due to the lack of intensity this is thought to be an impurity. Trimethyltin hydroxide is prepared by the hydrolysis of trimethyltin chloride;[15] thus it is possible that some of this starting material has remained behind. The solution chemical shift

of Me_3SnCl is δ_{Sn} = 140-160ppm,[3] but it is known to polymerize in the solid-state which would give rise to a substantial low frequency shift as previously noted for *penta*-coordinated tin formation. The broad linewidth of the sidebands is most likely due to dipolar interactions with the quadrupolar chlorine nucleus present.

As well as containing information regarding the co-ordination of the tin atom and the crystallographic nature of the compound, the solid-state ^{119}Sn spectrum contains valuable shielding tensor information. The tensor components can be obtained by spinning sideband analysis as has been widely used in previous chapters. A glance at Figure 6.5 shows the low-frequency site has a considerably broader linewidth and a much larger shielding anisotropy than the other site. The results from a detailed analysis are given in Table 6.3.

TABLE 6.3 SHIELDING TENSOR PARAMETERS OF Me_3SnOH and Ph_3SnCH[a]

COMPOUND	SPINNING SPEED/Hz	σ_{iso}[b]	σ_{33}[d]	σ_{22}[d]	σ_{11}[d]	δ	η	solution δ/ppm[c]	solvent
Me_3SnOH	3010	99	-165	156	306	-264	0.57	118[e]	SATD CH_2Cl_2
		152	535	103	-182	383	0.75	128.1[f]	2% $CHCl_3$
								122.2[f]	8% $CHCl_3$
Ph_3SnOH	2370	298	26	388	480	-272	0.34	-82.5[g]	$CDCl_3$
								-86[h]	CH_2Cl_2

a. Solution chemical shifts and shielding tensor components are measured in ppm, relative to neat $SnMe_4$. For chemical shifts on the δ scale the signs should be reversed.

b. Measurement accuracy, digitization rate = 39Hz/pt.

c. Single ^{119}Sn resonance in solution only.

d. Assuming Haeberlen convention of $|\sigma_{33}-\sigma_{iso}| \geq |\sigma_{11}-\sigma_{iso}| \geq |\sigma_{22}-\sigma_{iso}|$

e. Reference 11; f. Reference 12; g. Reference 17, h. Reference 18.

As can be seen from the values of the principal shielding tensor components for the two sites, there are two very different environments present. The cause of broadening for the low frequency resonance is probably due to the increased shielding anisotropy making the linewidth very sensitive to magic-angle modifications. Without a repeated X-ray crystallography study it is not clear as to the absolute structure of the two chemical sites. However it can be concluded that there are two different types of polymeric chains present with tin *penta*coordinated as suggested by X-ray and IR studies.

A carbon-13 CP/MAS spectrum has been obtained for this compound (see Figure 6.7) and exhibits four peaks. At present, it is impossible to assign any of the peaks to a particular methyl group. An ^{13}C CP/MAS independent study has also been carried out on this compound by Lockhart and Manders[19] at a lower field of 15.08MHz. Two peaks are seen (ratio 2:1) flanked by tin satellites. Taking into account the difference in field strengths used it is unknown why there should be a difference between the two carbon-13 studies. However both studies show that the methyl groups are non-equivalent, indicating a removal of the C_{3v} axis caused by the asymmetry in the polymer chain. This is also exhibited by the ^{119}Sn solid-state spectrum where a non-axial powder pattern is present ($\eta>0$).

FIGURE 6.7 ^{13}C CP/MAS spectrum of Me_3SnOH

SF = 50.29MHz
NT = 5000
SW = 10kHz
AQ = 0.01s
DO = 7s
D2 = 1ms
DR = 10Hz/pt
SS = 3kHz

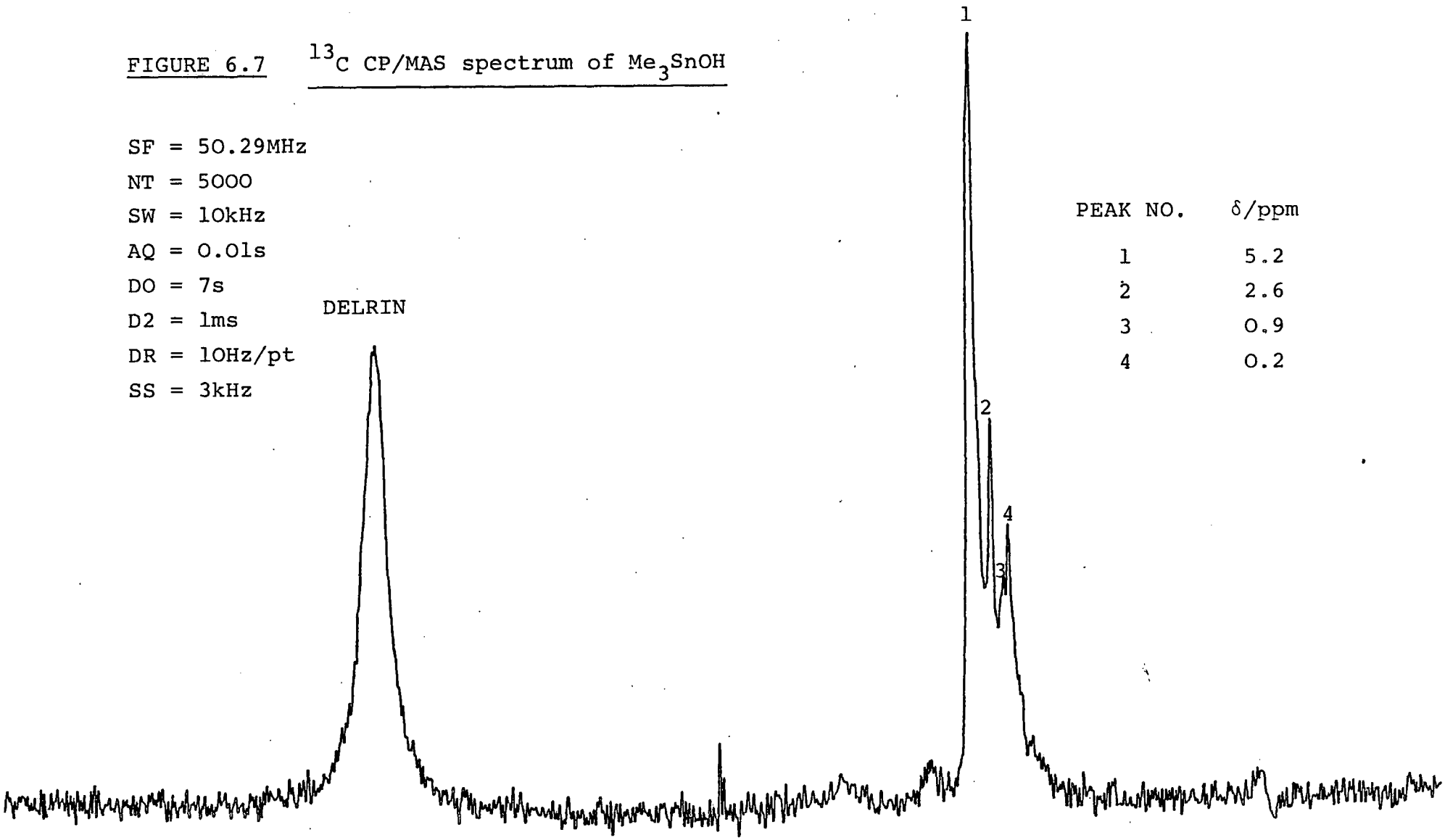

PEAK NO.	δ/ppm
1	5.2
2	2.6
3	0.9
4	0.2

6.4 Triphenyl tin hydroxide, Ph_3SnOH

The ^{119}Sn spectrum of triphenyl tin hydroxide (Figure 6.8) shows that there is only one crystallographic site present as indicated by a single resonance at -298ppm. As was noted for Me_3SnOH there is a considerable low frequency shift from the value observed in the solution-state, δ_{Sn}= -86ppm.[18] which is indicative of a *penta*coordinated tin. The large shielding anisotropy of the ^{119}Sn nucleus, giving rise to a multitude of sidebands, is no doubt caused by the asymmetrical environment in a polymer chain. This polymer chain is unlikely to be linear as there would then be a C_{3v} axis passing through the tin atom producing an axially symmetric bandshape although interchain effects could destroy axial symmetry. The tensor components were calculated using the method of Maricq and Waugh,[21] and are shown in Table 6.3. The substantial value of η=0.34 shows the divergence of C_{3v} symmetry through the tin.

An examination of the two sets of shielding tensor data for Me_3SnOH and Ph_3SnOH (Table 6.3) shows that the anisotropy values are very similar, -264 and -272ppm respectively. Furthermore, the sideband pattern of Ph_3SnOH (Figure 6.8) is very close in appearance to that of the high frequency resonance, sideband envelope of Me_3SnOH (Figure 6.5). This indicates that one of the tin environments in trimethyl tin hydroxide resembles that of the triphenyl analogue. This information cannot be obtained from the isotropic chemical shifts alone. The difference in chemical shifts in the solid-state is ∿200ppm between the high frequency site of Me_3SnOH

and Ph_3SnOH, which is virtually the same in the solution-state. This difference can thus be assigned to the shielding effect of the organic groups directly attached to the tin which is the same in both states.

The X-ray crystal structure obtained for Ph_3SnOH[20] shows there is only one crystallographically independent molecule in the unit cell agreeing with the solid-state NMR data. The structure of Ph_3SnOH consists of zig-zag chains in which the Ph_3Sn groups are planar at Sn and joined by OH groups, giving a trigonal bipyramidal geometry at Sn (Figure 6.9).

FIGURE 6.9 Schematic representation of Ph_3SnOH polymeric chain

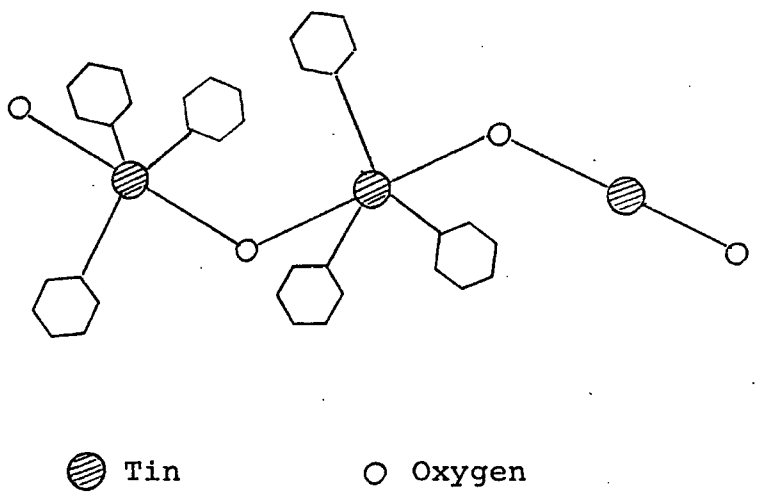

The two Sn-O distances are different (2.197 and 2.255 Å), despite the planarity of the C_3Sn fragment. The authors believe that this residual non-equivalence may be due to the presence of the hydroxyl proton whose position could not be identified. The Sn-O-Sn angle was found to be 137.8° and the Sn....Sn distance along the chain is 4.15Å. The three

independent Sn-C distances were found to be almost identical (2.131, 2.128 and 2.153Å) with a mean of 2.137Å, which is very close to that reported in Ph_4Sn (2.144Å)[10] and Ph_3SnCl (2.12Å).[22]

It is likely that the structure of one part of Me_3SnOH (that which gives rise to the high frequency resonance) is very similar to that found by X-ray studies of Ph_3SnOH, given the sensitivity of the NMR experiment. The other type of structure of Me_3SnOH is likely to be less symmetrical for the increase in anisotropy and greater asymmetry, there could also be motion present or rather an amorphous region which has produced the broader linewidth seen; this would account for the inconclusive report for the crystal structure of Me_3SnOH.[14]

An examination of Ph_3SnOH as a monomeric unit bridged by two hydroxyl groups would result in an axially symmetric band shape. However, the presence of a 'zig-zag' chain,along with asymmetric Sn-O distances render the structure non-axially symmetric and also with a large shielding anisotropy. Further evidence of a polymeric form of Ph_3SnOH could come from the observation of $^{119}Sn/^{117}Sn$ satellites. If tin-tin coupling was present a pair of doublets would be either side of the central resonance and sidebands with a relative intensity of ∿4%. However, due to possible overlap caused by the presence of sidebands ($\Delta\nu_{\frac{1}{2}}$>100Hz) and a limiting signal to noise such sightings of tin-tin satellites are improbable.

6.5 Triphenyltin Chloride. Ph_3SnCl

It would be expected that the ^{119}Sn CP/MAS spectrum of Triphenyltin chloride would exhibit a similar sideband pattern to that of Ph_3SnOH. Surprisingly, the spectrum contains narrow linewidths, a strange splitting pattern and shows a very small shielding anisotropy present (see Figure 6.10). There appear to be 3 sets of doublets; each doublet having a splitting of *ca.* 2ppm. (The line at -36.3ppm contains two peaks hence the "shoulder").

The solution-state ^{119}Sn spectrum has been obtained revealing a single peak observed at -48ppm (solvent CH_2Cl_2);[6] -44.7ppm (solvent $CDCl_3$),[17] and also checked in this work, using a vial of solution in the solid-state probe, $\delta_{^{119}Sn}$ = -46.5ppm, $\Delta\nu_{\frac{1}{2}} \sim 130$Hz (static, with decoupling). Thus taking into account solvent and temperature effects, the solid and solution-state chemical shifts are very comparable. This similarity is indicative of no intermolecular association, that is, no change in coordination of the tin atom. Therefore, it would appear by comparing solid and solution-state NMR results that triphenyltin chloride is tetrahedral in the solid-state.

The X-ray crystal structure has been carried out by a group of Russian workers who conclude from their studies that the unit cell (space group $P2_1/a$) consists of two independent molecules.[22] The geometrical parameters of the two molecules are shown to be very close in value. The coordination of the tin atom is observed to be slightly distorted tetra-

FIGURE 6.11 ^{119}Sn CP/MAS spectrum of nBu_2SnCl_2

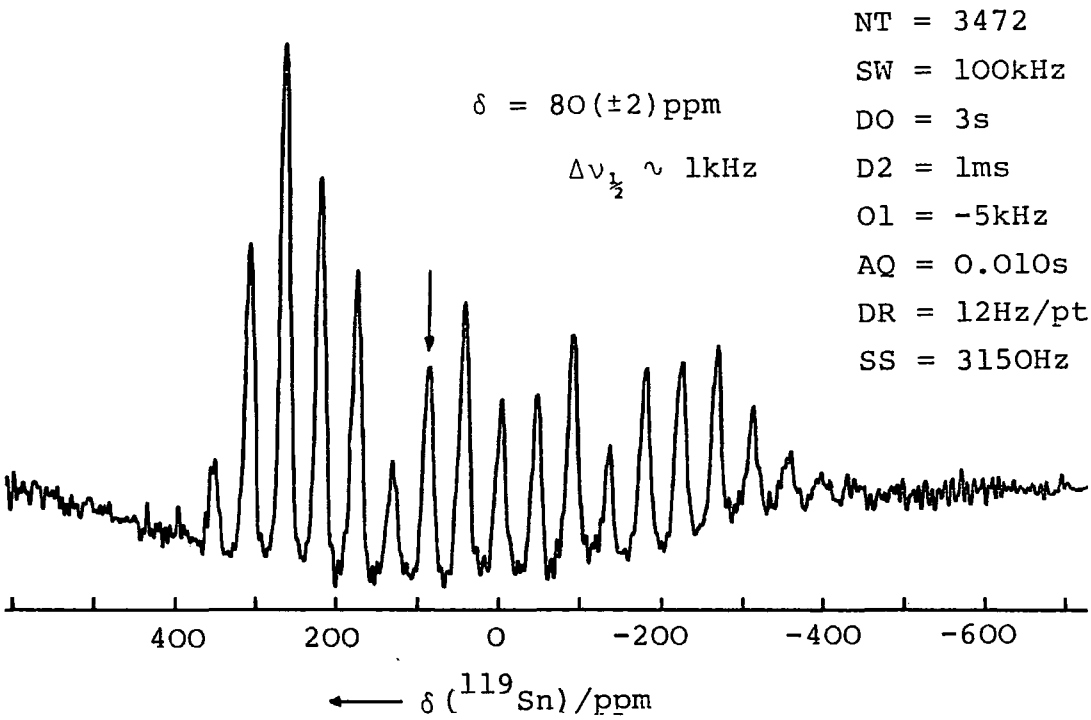

FIGURE 6.10 ^{119}Sn CP/MAS spectrum of Ph_3SnCl

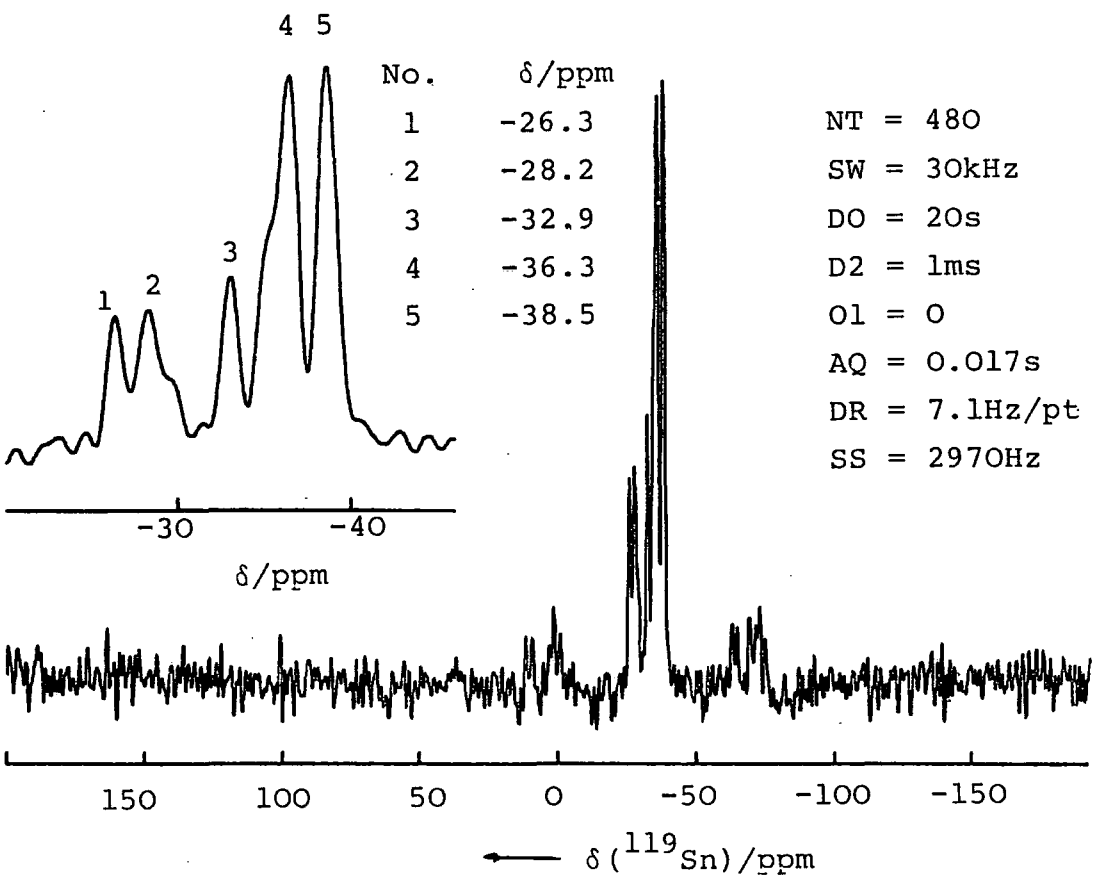

hedral; the C-Sn-C angles of 112.3° are slightly greater than the Cl-Sn-Cl angle of 106.4°. The deviations from the ideal value of 109.5° are not large and are believed to not arise from intermolecular coordination but from substituent effects on the tin atom. The shortest intermolecular Sn....Cl distance is ∿6Å which also provides evidence of no intermolecular association.

The strange splitting pattern observed in the spectrum of Ph_3SnCl is not readily reconcilable with that obtained previously. One possibility is that the two intense peaks at -36 and -38ppm might well be due to the expected non-equivalent Ph_3SnCl molecules as revealed by Bokii *et al.*[22] The observation of six peaks suggests six non-equivalent molecules present in the crystal lattice. This does not necessarily contradict the X-ray crystallographic findings,[22] as it must be noted that the averaging technique of X-ray crystallography may have only resolved two independent molecules. However this is thought to be unlikely. Another possibility is of course the presence of impurities; the compound was found to be pure as checked by chloride analysis and ^{119}Sn solution-state NMR.

The presence of quadrupolar nucleus (^{35}Cl) directly attached to the tin atom implies some sort of coupling present. The presence of scalar coupling (only) can be discounted as ^{119}Sn-^{35}Cl J coupling would give rise to a symmetrical quartet (or eight equally intense lines from two non-equivalent molecules). The most plausible reason for the spectral pattern is Sn-Cl dipolar coupling not removed by MAS (or a combination of J and dipolar coupling) due to the chlorine spins being

fixed at some orientation in the principal axis system of the molecular electric field gradient tensor. (This is discussed in detail in Section 6.7).

6.6 Di-n-butyl tin dichloride, nBu_2SnCl_2

The solid-state ^{119}Sn spectrum of nBu_2SnCl_2 shows a large spread of spinning side bands together with a single tin resonance at +80(±2)ppm (see Figure 6.11). The lines are broad (*ca.* 1 kHz) which is most likely caused by dipolar interactions with the chlorine nuclei.[23] This compound has also been studied by Lippmaa *et al*[4] in the solid-state where a chemical shift of δ_{Sn}=280ppm was recorded. However, no spinning sidebands were observed, only a single broad band with a linewidth of 200(±20)ppm. The isotropic chemical shift measured is somewhat doubtful; it is likely that this value was taken from the peak of the broad line, which in comparison with the results presented here suggests a powder pattern. If the ^{119}Sn spectrum obtained using the CXP200 spectrometer (see Figure 6.11) is examined then one can see that the most intense peak occurs at ∿250ppm. This region would also be the most intense from a powder (static) lineshape with a poor signal to noise (accounting for a width of only 200ppm observed). However, the most intense point in a powder pattern, or the most intense sideband, cannot be assumed to be the isotropic chemical shift. The value of +80ppm (as indicated by the arrow in Figure 6.11) was determined by 1st moment analysis and also checked by spinning speed variation.

The ^{119}Sn solution-state chemical shift of nBu_2SnCl_2 has been found to be 121.8ppm[4] (in 68% $CHCl_3$) and 123.4ppm[5] (in $CHCl_2$). The low frequency shift of *ca.* +42ppm does indicate a difference in molecular structure and furthermore a change in coordination. Although the difference between solution and solid-state ^{119}Sn chemical shifts is not as great as that found for Me_3SnOH and Ph_3SnOH, it is still considerable suggesting a similar intermolecular association producing polymeric chains. However, the secondary bonds to oxygen and other smaller electronegative substituents (*e.g.* N, S & F) are known to be stronger than those to chlorine.[24]

Although no X-ray crystallographic data have been obtained for nBu_2SnCl_2, there are structures available for similar compounds, Et_2SnCl_2, Me_2SnCl_2, Ph_2SnCl_2 and Me_2SnF_2. Dimethyl tin fluoride has been shown to consist of an infinite network of tin and fluorine atoms, with each tin linearly bridged to each of its four fluorine neighbours with methyl groups above and below this plane completing an octahedral coordination.[25] All Sn-F distances were found to be equivalent (2.12Å). The X-ray structure obtained for dimethyltin-chloride[26] shows that the inter and intramolecular Sn-Cl distances are not equivalent (3.54 and 2.40Å respectively). The bond angles found were Cl-$\hat{S}$n-Cl=93°, C-$\hat{S}$n-C=123° and C-$\hat{S}$n-Cl=109°. The authors have interpreted these results to suggest that the structure of Me_2SnCl_2 consists of chains of molecules with each tin atom substantially distorted from tetrahedral to octahedral. The tin and chlorine atoms are coplanar and the methyl groups are situated above and below the plane. The tin atoms are not colinear, but slightly

offset in a zig-zag fashion with each tin atom joined to its neighbours by two 'bridging' chlorine atoms (see Figure 6.12).

FIGURE 6.12 The structure of dimethyl tin dichloride

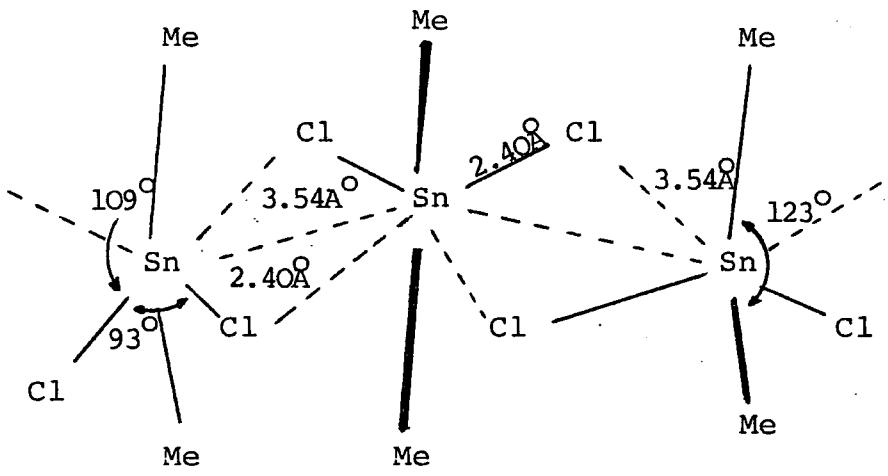

The tin-chlorine 'bridging' distance of 3.54Å is only 0.33Å less than the sum of the appropriate Van der Waals radii. However, the authors state categorically that association exists because of distortion of the tin atom from the approximate tetrahedral arrangement. This has also been found to be true for diethyltindichloride, where a similar polymeric structure is proposed.[24]

Given the solid-state NMR evidence as shown in Figure 6.11, it can be concluded that the structure of nBu_2SnCl_2 consists of chains of molecules, due to the presence of some bridging between the tin and intermolecular chlorines. The structure is likely to be similar to that proposed by Davies *et al*[26] (Figure 6.12) and thus accounts for the large shielding anisotropy and low frequency chemical shift observed. The shielding tensor parameters were calculated to be the following:

σ_{33} = 400ppm, σ_{22} = -280ppm, σ_{11} = -360ppm

η = 0.17, δ = 480ppm

The ambiguity of the presence of halogen bridges in the R_2SnX_2 type compound is increased by the crystallographic data for Ph_2SnCl_2.[27] In this case, two crystallographically independent, discrete molecules of Ph_2SnCl_2 are present in the asymmetric unit of the crystal. The shortest Sn....Cl contact in the crystal structure is 3.77Å and the authors have discounted any possibilities of intermolecular association. The deviation from regular tetrahedral geometry observed for both molecules is said to be an intrinsic property of the isolated molecules. Although, it is noted that it is not clear what a minimal non-bonding Sn....Cl contact distance might be since there is no very good measure of the Van der Walls radius for tin.

The uncertainty from X-ray crystallographic studies as to the presence of tin-halogen bridges shows the need for further solid-state ^{119}Sn NMR studies. It appears that any intermolecular association is evident by a substantial shielding anisotropy and a considerable low frequency chemical shift, (*vide infra*, discussion of quadrupolar effects).

6.7 Quadrupole Effects in ^{119}Sn Solid-State NMR Spectra of Tin-Chlorine Compounds: Study of Diammonium Hexachlorostannate (IV)

The ^{119}Sn solid-state spectrum of $(NH_4)_2SnCl_6$ shows an unfamiliar splitting pattern (see Figure 6.13). There is a single broad band present ($\Delta\nu_{\frac{1}{2}} \sim 1700$Hz) with eleven observable

FIGURE 6.13 ^{119}Sn CP/MAS spectrum of $(NH_4)_2SnCl_6$

No.	δ/ppm(±0.5)
1	-686
2	-690
3	-694
4	-698
5	-701
6	-706
7	-710
8	-713
9	-718
10	-721
11	-726

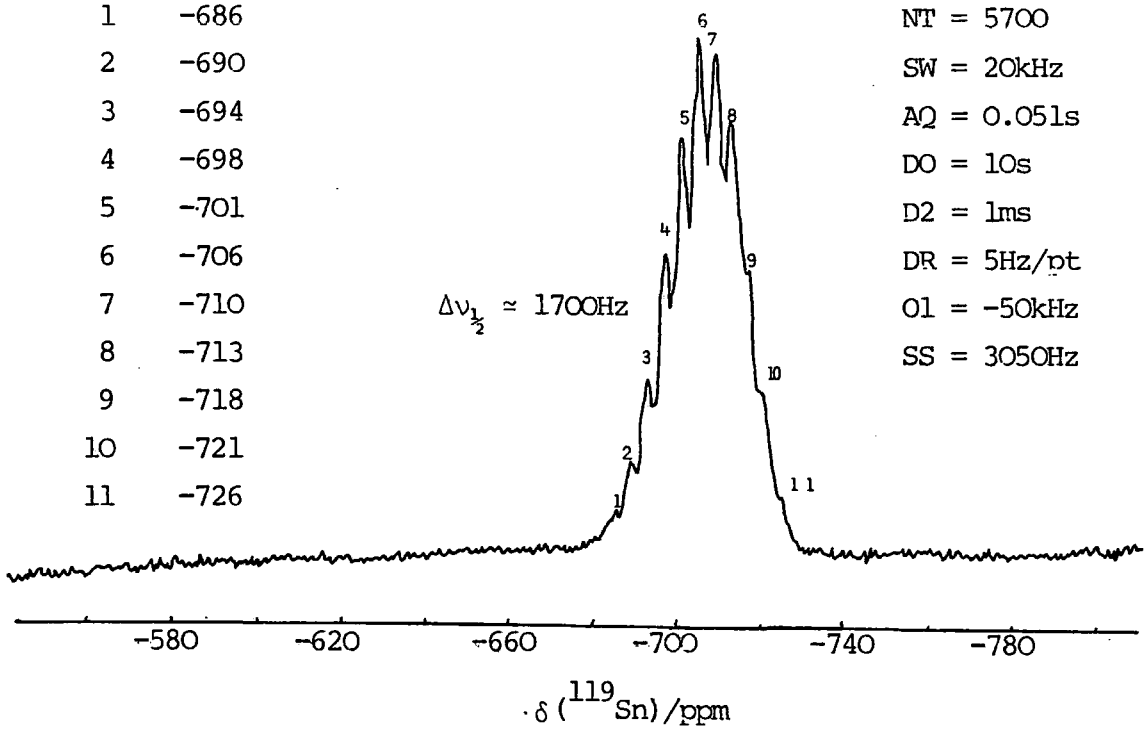

FIGURE 6.14 ^{119}Sn CP/MAS spectrum of $(NH_4)_2SnF_6$

No.	δ/ppm(±1)
1	-764
2	-786
3	-796
4	-806
5	-817
6	-828
7	-838

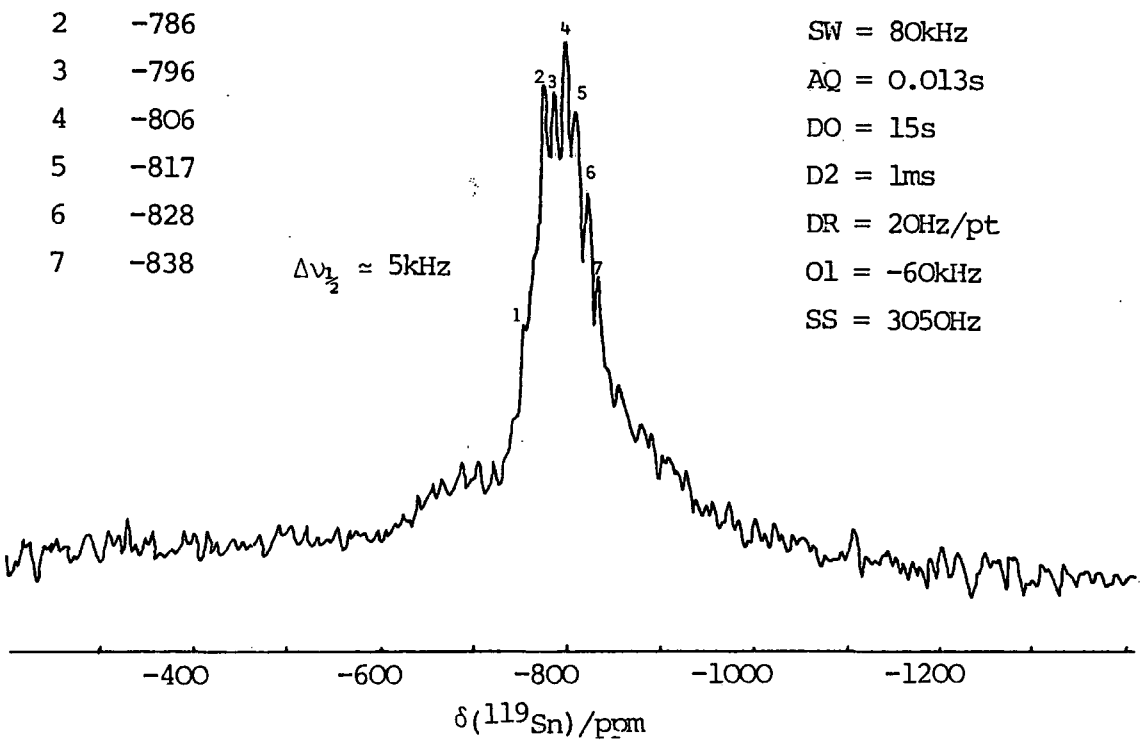

peaks superimposed. The splitting between each peak appears to be constant at *ca.* 4ppm (~300Hz); however some broadening present on one side of the lineshape makes chemical shift determination slightly ambiguous. The lack of spinning sidebands shows there to be a small (if any) shielding anisotropy present.

Diammonium hexachlorostannate (IV) has been studied using X-ray crystallography[28,29] and shows the unit cell to contain discrete octahedral $SnCl_6^{2-}$ ions, with 8 cations (NH_4^+) situated on the threefold axes. Each cation sits in a tetrahedral site formed by four Sn atoms and has a symmetric chlorine ligancy of 12. Each Sn-Cl bond has fourfold symmetry and is equivalent to all others. The lattice is cubic and the space group is Fm3m, thus showing the presence of a single tin site with no asymmetry present. Hence, the appearance of no spinning sidebands in the solid-state ^{119}Sn spectrum. Solid-state ^{35}Cl NQR data has also been obtained for $(NH_4)_2SnCl_6$[29] and in agreement with the X-ray crystallographic data, only a single ^{35}Cl NQR frequency is observed, and the electric field gradient at each chlorine atom has an asymmetry of zero.

The presence of a single crystallographic site for both the tin and chlorine nuclei indicates that the observed splittings in the solid-state spectrum are due to interactions between the spin-½ tin nucleus and six equivalent, spin-3/2, chlorine nuclei, namely dipolar and scalar coupling. Recently, several authors have reported high resolution ^{13}C solid-state NMR spectra in which the resonances of carbon-13 nuclei directly bonded to nitrogen were split into asymmetric doublets.[31-34]

These splittings were shown to arise from dipolar coupling between the ^{13}C and ^{14}N nucleus, not averaged by magic-angle spinning because of the large magnitude of the quadrupole interaction of the nitrogen-14 nucleus.

Magic-angle spinning eliminates broadening arising from dipolar interactions between two spins, if both spins are quantized along the magnetic field. Magic-angle spinning does not remove dipolar broadening completely if one of the spins is not quantized along the magnetic field. Such a situation can arise if one spin belongs to a quadrupolar nucleus subjected to both quadrupole and Zeeman interactions whereby $\nu_Q \sim \nu_L$.

Other quadrupolar effects have been observed in the solid-state ^{29}Si NMR spectrum of Albite.[35] An asymmetric doublet was observed at three different field strengths and was found to have a constant splitting. Since direct dipolar coupling to quadrupolar nuclei is inversely proportional to the applied field (*vide infra*), this factor is easily dismissed. The splitting was shown to be due to Si-Al J coupling by the simulation of six (2I+1) lorenztians of varying linewidths. The cause of this variation results from the different relaxation times of various aluminium spin states.

A combination of scalar and dipolar coupling has been observed in the ^{31}P solid-state CP/MAS spectra of a triphenyl phosphine copper (I) complex.[36] Phosphorus-31 spectra were observed at three fields revealing ^{31}P-^{65}Cu scalar coupling to be mainly present at high field (121 and 72MHz) giving rise to four equally spaced lines. Whereas, at the low

field (24MHz) dipolar coupling is dominant producing three broad asymmetric lines. A theoretical analysis has been obtained which shows that the spectra may be simulated by considering the combined effects of dipolar and scalar coupling.

Similar effects for chlorine containing compounds are rarely seen,[37] although broadening has been observed due to the interaction between carbon and chlorine.[23] The quadrupole interaction is affected by the direction of the electric field gradient. Any motion present can change the orientation of the electric field gradient tensor axes providing an effective relaxation mechanism. Motion which is very slow on a molecular time scale can lead to very rapid spin-lattice relaxation of the quadrupolar nuclei.[38] In favourable cases the transitions between the different spin-states of the quadrupolar nuclei are so rapid that the dipolar coupling with the spin-½ nuclei is averaged out, an effect known as self-decoupling.[39] Nuclei for which self-decoupling might be operational for the dipolar coupling with other spin-½ nuclei, are those with large quadrupole coupling constants ($e^2q\,Q/\hbar$). Such a nucleus is ^{35}Cl, which accounts for the lack of broadening observed in most cases. The reason why no splittings were observed in the only reported case of ^{13}C-^{35}Cl dipolar coupling, is that motion was always present even at the lowest temperature at which spectra were recorded.[23] At this low temperature, it is likely that motion, still present, would cause the system to lie somewhere between the completely hindered case (*i.e.* no relaxation) and the self-decoupling case. It is only in the hindered case that splittings would be observed.

The NQR study of $(NH_4)_2SnCl_6$ found the quadrupole resonance frequency, $\nu_Q(^{35}Cl)$, to be 15.453MHz.[29] The quadrupolar energy is given by the following equation:[40]

$$h^{-1}U_Q = \chi[3m_I^2 - I(I+1)]/[4I(2I-1)] \text{ (in Hz)} \qquad \text{(eqn. 6.1)}$$

where χ is known as the nuclear quadrupole constant $(=e^2Qq_{zz}/h)$. For $I = {}^3/_2$ (^{35}Cl), there is only one transition, $m_I=\pm{}^3/_2 \longleftrightarrow m_I=\pm\frac{1}{2}$. Therefore the quadrupole resonance frequency ν_Q is simply

$$\nu_Q = \frac{\chi}{2} \qquad \text{(eqn. 6.2)}$$

And so for $(NH_4)_2SnCl_6$, χ = 30.906MHz.

This value for the quadrupole coupling constant may be used to obtain a simulated splitting pattern for a spin-$\frac{1}{2}$ nucleus (^{119}Sn) coupled to a single spin-$^3/_2$ nucleus (^{35}Cl) as calculated by Menger and Veeman.[36] The paper[36] shows line positions that have been calculated arising from dipolar coupling with $S={}^3/_2$ (spin of quadrupolar nucleus) as a function of the parameter $K = -[(3e^2q_{zz}Q/4S(2S-1))/\gamma_S\hbar B_o]$. In addition, the line positions have been calculated for scalar coupling between the same nuclei and also the combined effects of scalar and dipolar coupling. From the graphical analysis, it can be seen that low values of K(<0.1) give rise to the expected quartet arising from scalar coupling only. This situation could occur at either high field (large values of B_o) or small values of the efg and quadrupole moment. At high values of K, however, (*e.g.* 0.5 ⟶ 1.0) there is considerable broadening and asymmetry, with only three lines present.

From a known value of the quadrupole coupling constant χ, and assuming the efg tensor is axially symmetric (known to be the case for $(NH_4)_2SnCl_6$, from NQR studies[29]), the parameter K may be calculated.

$$K = -\left[\frac{3e^2q_{zz}Q}{4S(2S-1)} \Big/ \gamma_S\hbar B_O\right] \qquad \text{(eqn. 6.3)}$$

Substituting $\chi = e^2Qq_{zz}/\hbar$ and $\nu_L = \frac{\gamma_S}{2\pi} B_O$

for ^{35}Cl, $S = {}^3/_2$, $\chi = 30.906$ MHz and $\nu_L = 19.618$MHz

($\nu_{^1H} = 200$MHz)

$$K = -\frac{\chi}{4\nu_L} = -0.394.$$

From the graphical analysis of dipolar coupling only between $I=\frac{1}{2}$ and $S={}^3/_2$ the K value of 0.394 gives rise to a doublet, a narrow "line" at high frequency and an approximately twice as broad "line" at high frequency; the splitting of the doublet is *ca.* one dipolar coupling constant unit.

The ^{119}Sn-^{35}Cl dipolar coupling constant is 311Hz, as calculated from the known tin-chlorine interatomic distance of 2.421Å. The graphical analysis for the combined dipolar and scalar coupling effects show that for K=0.394, there should be three lines present, two narrow and one very broad. The splittings are unknown as it has been assumed by the authors that $\gamma_I\gamma_S h^2/r^3 = {}^J/_2$ which is a completely ambiguous assumption if the scalar coupling (J) is unknown.

The ^{119}Sn spectrum of $SnCl_6^{2-}$ has been obtained in the solution-state and shows a single peak present at -733.0 ppm.[30] However, no splittings were observed due to ^{119}Sn-^{35}Cl

scalar coupling, presumably because molecular tumbling causes self-decoupling analogous to the case discussed earlier. Scalar coupling could be observed in the solid state if there was a slow rate of spin-lattice relaxation for the chlorine nucleus. By using a similar theorem to that of Pascal's triangle the number of splittings due to a single ^{119}Sn nucleus ($I=\frac{1}{2}$) coupled to six equivalent ^{35}Cl ($S=^{3}/_{2}$) nuclei may be calculated. The intensity ratios of lines calculated are 1:6:21:50:90:126:141:126:90:50:21:6:1.

Discounting the two peaks at the end, due to limiting signal to noise, leaves eleven lines with normalized ratios of:

8.3:28.9:68.8:123.8:173.3:193.9:173.3:,*etc.*

However, this does not take into account any line broadening effects and consequent overlapping of lines, thereby changing theoretical intensities. Experimentally, eleven lines are observed (Figure 6.13) with similar ratios. The normalized intensities of the resolved part of the spectrum (high frequency side) are as follows:

15:34:64:117:164:204:

Given the almost equivalent splittings and similar linewidths, it can be concluded that the spectral pattern is predominantly due to ^{119}Sn-^{35}Cl scalar coupling. It must be noted that this phenomenon is rare, with no reported cases of scalar coupling with chlorine observed in the solid-state. The asymmetry of the splitting pattern seen on the low frequency side is due to residual dipolar coupling, which is consistent with the calculated spectrum of spin-$\frac{1}{2}$ nucleus coupled to a single chlorine spin, from known NQR parameters, using the Menger and Veeman analysis.

Nuclear quadrupole resonance data has also been obtained for Ph_3SnCl and nBu_2SnCl_2.[41] Triphenyl tin chloride is a much easier system to handle as it consists of a single spin-½ and spin-$^3/2$ nucleus. Following the Menger and Veeman analysis the ^{119}Sn solid-state spectrum of Ph_3SnCl should give rise to a broad line with two narrow lines and a splitting equal in magnitude to $J_{Sn,Cl}$, given that for ν_Q=16.985 MHz K=0.43. It is possible that since the "broad line" encompasses two lines, the intensity may be twice that of the "narrow lines" given similar linewidths. In addition, the NQR study reveals two quadrupole resonances (16.750 and 16.985MHz)[41] showing that two types of chlorine sites are present, agreeing with the X-ray crystallographic data of two independent molecules in the unit cell.[22] Therefore, there will be two types of Sn-Cl quadrupolar interactions which would give rise to six lines, two very broad or double intensity and four narrow-width peaks (see Figure 6.10).

Two NQR frequencies were also observed for di-n-butyltin dichloride (ν_Q=15.982, 15.992MHz)[41] which would be due to inter or intra-molecular effects. The calculated value of K=0.41 implies that a similar spectrum to that of Ph_3SnCl would be expected. However, the presence of a single broad line reflects the rate of relaxation (caused by motion present) producing averaging between the two extremes: (i) fine structure due to dipolar and J coupling and (ii) self-decoupling.

In all three examples of quadrupole effects in ^{119}Sn solid-state NMR, the theoretical explanations can only be

proved by multi-field studies. For $(NH_4)_2SnCl_6$, a high field spectrum should show a much more symmetrical splitting pattern due to the lack of dipolar coupling effects, giving a reasonably accurate value for $/J_{Sn,Cl}/$. On the other hand, a low-field spectrum would, in theory, exhibit a very broad band with little, if any, fine structure due to the dominant dipolar interactions. An extra cause of splitting, which could appear in the high field case, is the quadrupolar interactions with the other chlorine isotope, ^{37}Cl, which has similar magnetic properties to that of chlorine-35 and a natural abundance of 24.5%.

A high-field study of Ph_3SnCl should simply show 4 equally spaced doublets due to scalar coupling and the presence of two non-equivalent crystallographic sites. The nBu_2SnCl_2 compound would be a more difficult system to study due to the presence of motion and a very large anistropy. However, a ^{119}Sn NMR study at a very low temperature would effectively 'freeze' any motions present, leading to narrower lines. In such a case, a multi-field study would distinguish between the scalar and dipolar contributions.

6.8 Diammonium Hexafluorostannate (IV), $(NH_4)_2SnF_6$

The ^{119}Sn solid-state spectrum of $(NH_4)_2SnF_6$ (Figure 6.14) exhibits a splitting which is apparently similar to that seen for $(NH_4)_2SnCl_6$. The average chemical shift is ∿100ppm to low frequency of the average shift of $(NH_4)_2SnCl_6$ ($\delta^{AV}_{^{119}Sn}$ =-810 and -710 ppm. respectively). This mean value for $(NH_4)_2SnF_6$ compares well with that obtained in solution for the hexafluoro-

stannate anion[30] ($\delta_{^{119}Sn}$ = -810.8ppm), and thus shows no evidence of intermolecular association in the solid-state. There has not been a crystal structure reported for $(NH_4)_2SnF_6$; however, X-ray structures are known for similar compounds of the type, M_2SnF_6 (where M=Li, Na, K and Cs).[42] In all these cases there is a single crystallographic site whereby the tin atom is observed to have an axially distorted octahedral environment of six fluorine atoms.

The observed fine structure is likely to arise from tin-fluorine scalar coupling. In addition to this there will be effects from the Sn,F dipolar coupling. For the structure of $Li_2SnF_6.2H_2O$,[43] there are two non-equivalent sites for the fluorines, with reported bond distances of Sn-F (equatorial)=1.962Å and Sn-F (Axial)=1.983Å. The mean value of these interatomic distances gives a tin-fluorine dipolar coupling constant of 5520Hz. If the system is approximated as being AX_6, then ignoring shielding and indirect coupling terms the rigid lattice linewidth should be of the order of *ca.* 6D($\sim 3 \times 10^4$Hz). The relevant dipolar term is a heterogeneous interaction which is modulated in the same way as the shielding anisotropy. Therefore, spinning about the magic-angle at *ca.* 3kHz should, in theory, give rise to a spectrum containing a complex spinning sideband pattern spanning the rigid lattice linewidth. The absence of sidebands implies the presence of random molecular motions leading to motional narrowing.

Examples of the combined effects of random molecular motion and mechanical motion have been given by Waugh[50] and

Andrew.[51] The observed linewidth for a powder, with isotropic molecular motion, rotating at the magic-angle can be expressed as[50]

$$\frac{1}{T_2} = \Delta^2 \tau_c \left[\frac{2}{1+\nu_r^2 \tau_c^2} + \frac{1}{1+4\nu_r^2 \tau_c^2}\right]$$

(*N.B.* The above equation does not hold for long correlation times).

where τ_c is the correlation time, Δ is the rigid lattice linewidth and ν_r is the rotation rate (Hz).
The residual bandwidth in the ^{119}Sn NMR spectrum of $(NH_4)_2SnF_6$ is found to be *ca.* 3kHz (see Figure 6.14). At the experimental spinning speed (ν_r=3kHz), a correlation frequency of 10^6Hz is required to narrow the rigid lattice linewidth to the observed value. The MAS rate needs to be greater than the internal molecular motion (10^6Hz) to produce further narrowing of the line, and such a fast rotation rate is impossible to achieve. Of course, the above assumes isotropic motion which is an oversimplification, but the qualitative conclusion is likely to be correct.

Taking into account the X-ray studies of related compounds,[42,43] both types of fluorine atom (equatorial and axial) will be averaged if the molecular motion involves a "jump" mechanism. In such a case, the fluorines would be rapidly exchanging between equatorial and axial positions. (At any one instant, the molecule would still appear to have two different sorts of fluorines present, consistent with the X-ray studies).

The solution-state ^{119}Sn NMR spectrum of the SnF_6^{2-} anion displays a septet due to the scalar coupling of the tin

nucleus to six equivalent fluorine nuclei, with $|^{1}J_{Sn,F}|$ = 1579Hz.[30] However, in the solid-state there would be likely to be coupling to two different sets of fluorine nuclei (equatorial and axial), in addition to this there would be significant ^{19}F-^{19}F dipolar coupling and to a lesser extent, scalar coupling. The average splitting observed in the fine structure is *ca.* 800Hz.

It is unclear as to why there is further broadening producing the underlying 'hump' in the spectrum. Indeed, without further information a more detailed assignment for the spectrum is impossible. A simpler system of the type M_2SnF_6, where each Sn-F bond was equivalent, would be very useful to study by ^{119}Sn solid-state NMR, and would produce a more readily interpretable spectrum. However, such an ideal compound may not be accessible. It is possible the antisymmetric J coupling (not averaged by MAS) may complicate matters further,[52] although no cases have been reported. A variable-temperature study, whereby the motions are effectively frozen out, would make a very interesting study. If there was no (or little) motion present then rapid magic-angle spinning could reduce the observed linewidth further [50] in the hope of revealing further fine structure. In addition to this a high field study would be very useful in assigning chemically shifted peaks.

6.9 A Study of AX_2 Spin Systems in the Solid-State: High-Resolution Tin-119 CP/MAS NMR of Tri-(n-Butyl)Tin Fluoride and Trimethyl Tin Fluoride

The solid-state ^{119}Sn spectrum of tri(n-butyl)tin fluoride is shown in Figure 6.15. As can be seen, the total spread of the spectrum is 500ppm. There are three sideband manifolds present; first moment calculations and experiments with variable rotation rates show that the centrebands are as indicated in Figure 6.15. A summing of intensities indicates that the intensity ratio of three spinning sideband manifolds is 1:2:1. The three centrebands are equally separated, with a spacing of 1291Hz.

These facts can be interpreted as indicating that the ^{119}Sn nuclei are effectively equally coupled to two fluorine nuclei, the coupling constant $|^1J_{Sn,F}|$ being 1291Hz, which is of the expected order of magnitude.[44] This interpretation implies that the tin is *penta*coordinated in the solid-state with tin-fluorine bridges present. Only one X-ray diffraction study has been cited which gives an incomplete structure determination.[42] X-ray diffraction patterns show that the compound is disordered in a lattice of trigonally symmetric tin atoms.

The chemical shift of the middle centreband is δ_{Sn} =-9.3ppm. In the solution-state, related compounds give chemical shifts in the region of $\delta_{Sn} \sim 70$ ppm.[2] The substantial shift to low frequency in the solid is another indication of the formation of *penta*coordinate tin. An additional peak is detected, at δ_{Sn}= 120.3ppm, and is assigned to an impurity due to the relative intensity and lack of side bands.

FIGURE 6.15 ^{119}Sn CP/MAS spectrum of nBu_3SnF

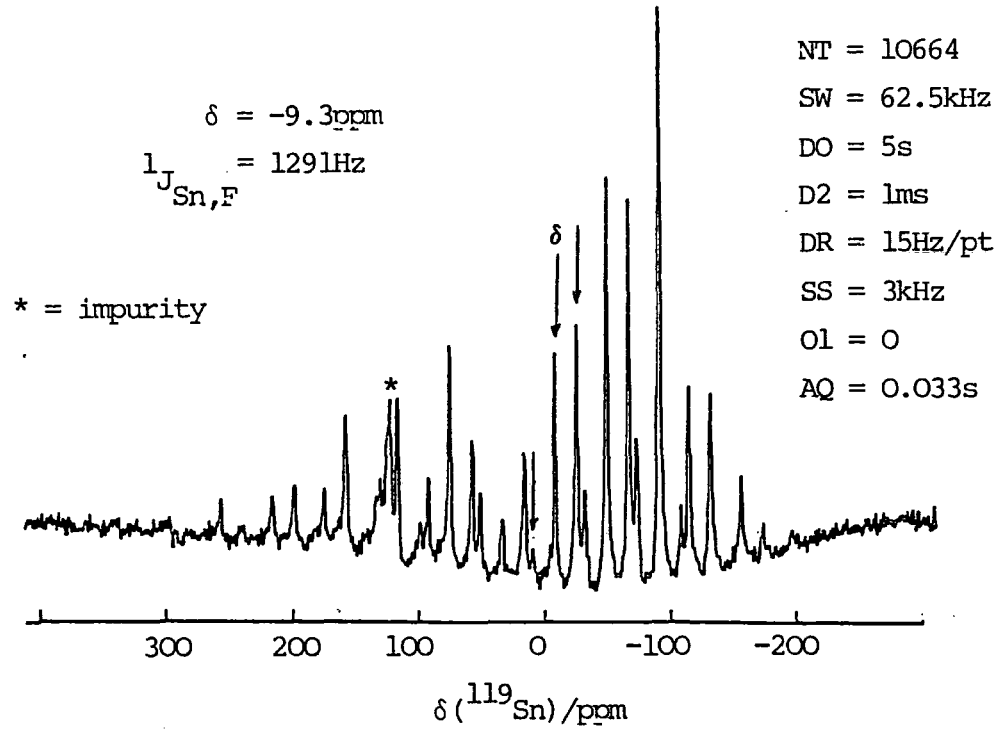

FIGURE 6.16 ^{119}Sn CP/MAS spectrum of Me_3SnF

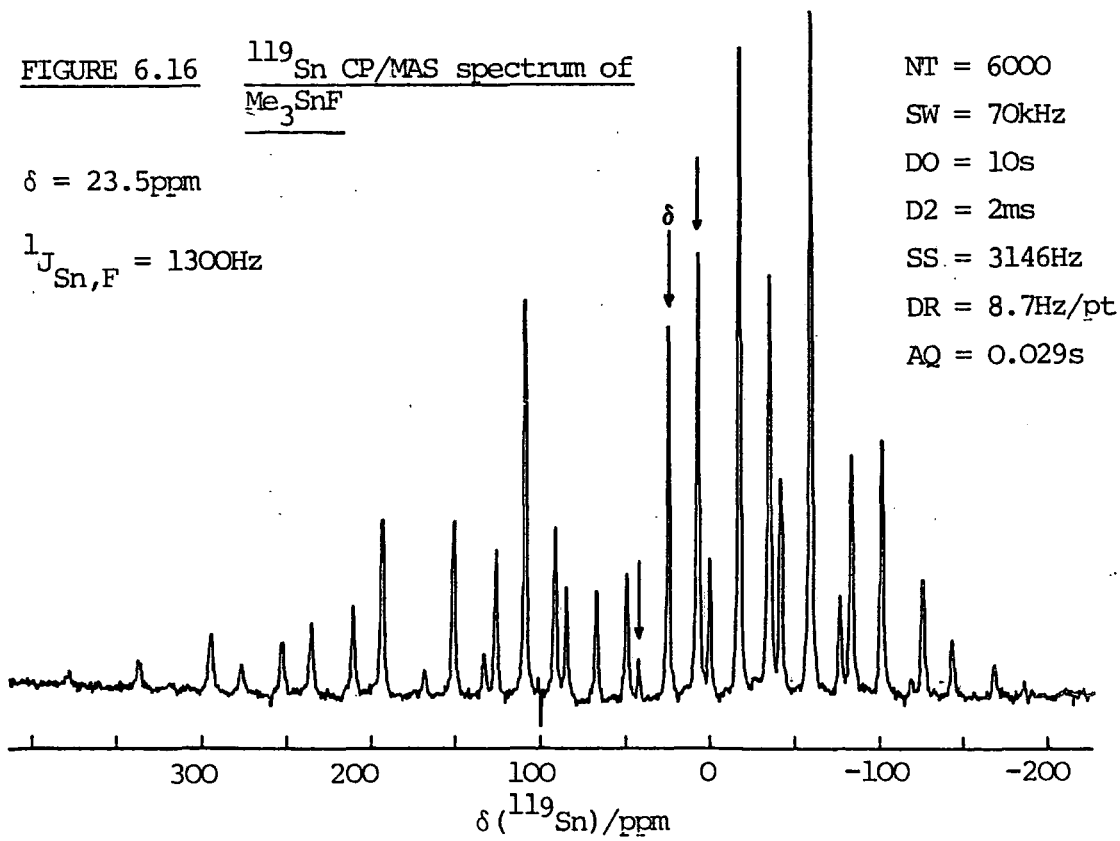

An improved spectrum was obtained for a very similar compound, Me_3SnF (see Figure 6.16). As with the ^{119}Sn spectrum of nBu_3SnF (Figure 6.15) there are 3 centrebands due to a single tin site coupling to two equivalent fluorines, $|{}^1J_{Sn,F}|$=1300Hz. One X-ray crystal structure that has been obtained for trimethyltin fluoride[45] is inconclusive due to anomalies in the electron density projections resulting from disorder of fluorine atoms within each chain and disorder of the chains with respect to one another. The two proposed structures are shown in Figures 6.17 and 6.18.

Figure 6.17 Figure 6.18

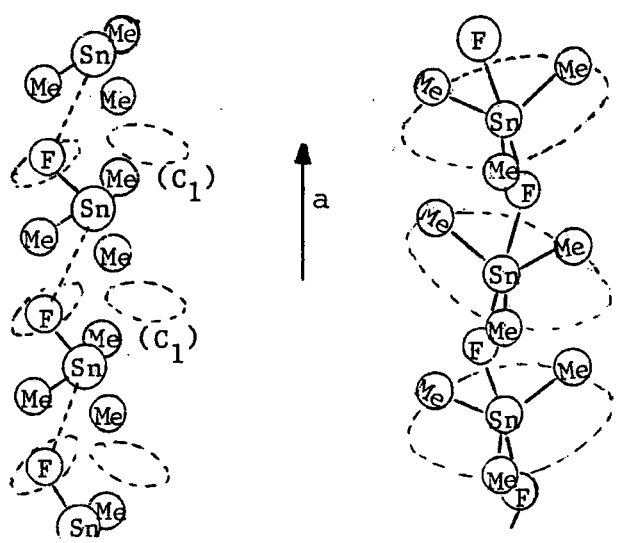

Possible structures for trimethyltin fluoride.[45]

Both structures consist of Me_3Sn groups and F atoms arranged alternately in a chain-like manner along the a-axis. The two interpretations are given by the observed electron-density distribution, both contain essentially five coordinate, and non-linear unsymmetrical Sn-F...Sn bridges, consistent with a non-ionic type of compound. One structure proposed is that within any one chain the atoms C_2 and C_3 are ordered and both displaced from the plane in the opposite direction to the Sn-F bond (Figure 6.17). The fluorine atoms are disordered, occupying any position on parts of a spherical surface centred about 2.15Å from one tin atom, so that Sn-F...Sn is not linear.

In the second structure (Figure 6.18) the Me_3Sn groups are planar and tilted alternatively with respect to the a-axis. As a consequence of this alternative tilting, the fluorine atoms must be ordered with respect to their alternate placing on either side of the Sn-Sn axis.

The authors believe that trimethyltin fluorine is not a purely ionic solid. If ionic species were present it would be expected that (a) the fluorine atom would lie on the axis of, and equidistant from, two tin atoms, and (b) the trimethyltin group would be a planar cation lying perpendicular to the tin-tin axis. Furthermore, the non-linear asymmetrical Sn-F...Sn arrangement is an indication of a covalent interaction present. The values obtained for the tin-fluorine bond distances are approximate with an intramolecular Sn-F value of $\sim$2.1Å and an intermolecular Sn-F distance of $\sim$2.2→2.6Å.

In an independent study, using IR and X-ray diffraction techniques, Yasuda *et al*[46] suggest an alternative structure whereby the trimethyltin group forms a planar equilateral triangular structure and is inclined to the plane perpendicular to the a axis (see Figure 6.19). One of the Sn-C bonds ($Sn-C_1$) lies along the c axis and furthermore, the trimethyltin groups and fluorine atoms are arranged alternately along the a axis.

FIGURE 6.19 Projection of the probable crystal structure of Me_3SnF[46]

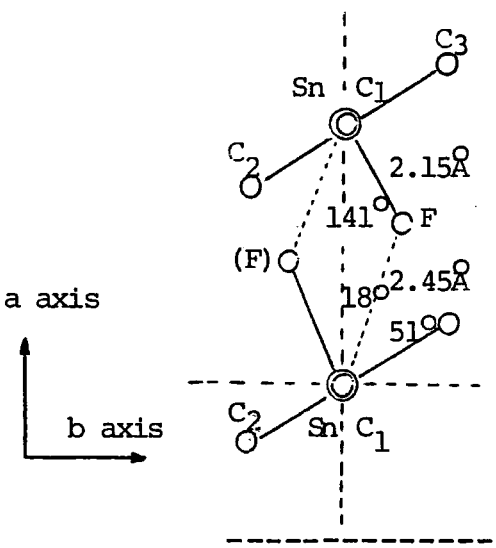

F and (F) indicates the two possible positions of the same potential energy.

The appearance of a triplet pattern in the ^{119}Sn solid-state spectrum of Me_3SnF can be explained by considering motion present in which the fluorines are rapidly (on the NMR timescale) exchanging between asymmetrical positions. The ^{119}Sn nucleus would therefore 'see' two equivalent fluorine nuclei at an equidistance. Alternatively, the triplet pattern may be deceptively simple, since the full spin system of an unsymmetrical chain of Sn and F atoms could be quite

complex. However, the simplest explanation, whereby the fluorines are lying midway between the atoms is at least as likely as the other two.

In both ^{119}Sn NMR spectra of Me_3SnF and nBu_3SnF, the three sideband manifolds show considerable differences in spread of intensity. This is clearly seen in the expansion of the spectrum of Me_3SnF (see Figure 6.20). The high frequency sideband manifold covers the largest range and the low frequency manifold the smallest range. It is clear that the ^{119}Sn anisotropy is influenced by the spin state of the attached fluorines. Three tensor properties need to be considered, namely: (i) dipolar (Sn,F) coupling, (ii) indirect ("scalar") (Sn,F) coupling, and (iii) ^{119}Sn shielding anisotropy. This tensorial interplay has been recently illustrated for a two spin (AX) case by Zilm and Grant,[47] in which ^{13}C-^{19}F coupling is studied from a powder pattern of CH_3F and also by Harris *et al*, who have used sideband analysis to extract tensor information for a $^{13}C/^{31}P$ case. The three spin AX_2, as exemplified by nBu_3SnF and Me_3SnF, should, in theory, be an easier system to handle, particularly if X-A-X linearity is assumed. The middle manifold of sidebands corresponds to the zero total spin component of the fluorine nuclei. Its effective anisotropy is therefore uninfluenced by (Sn,F) coupling of either type, and a sideband analysis of this manifold will give the three principal components of the ^{119}Sn shielding anisotropy. The method of Maricq and Waugh[21] has been used to obtain the shielding values as shown in Table 6.4.

FIGURE 6.20 ^{119}Sn CP/MAS spectrum of Me_3SnF (Expanded)

The three spinning sideband manifolds are shown, with arrows indicating the corresponding centrebands (with assigned spin states of F nuclei)

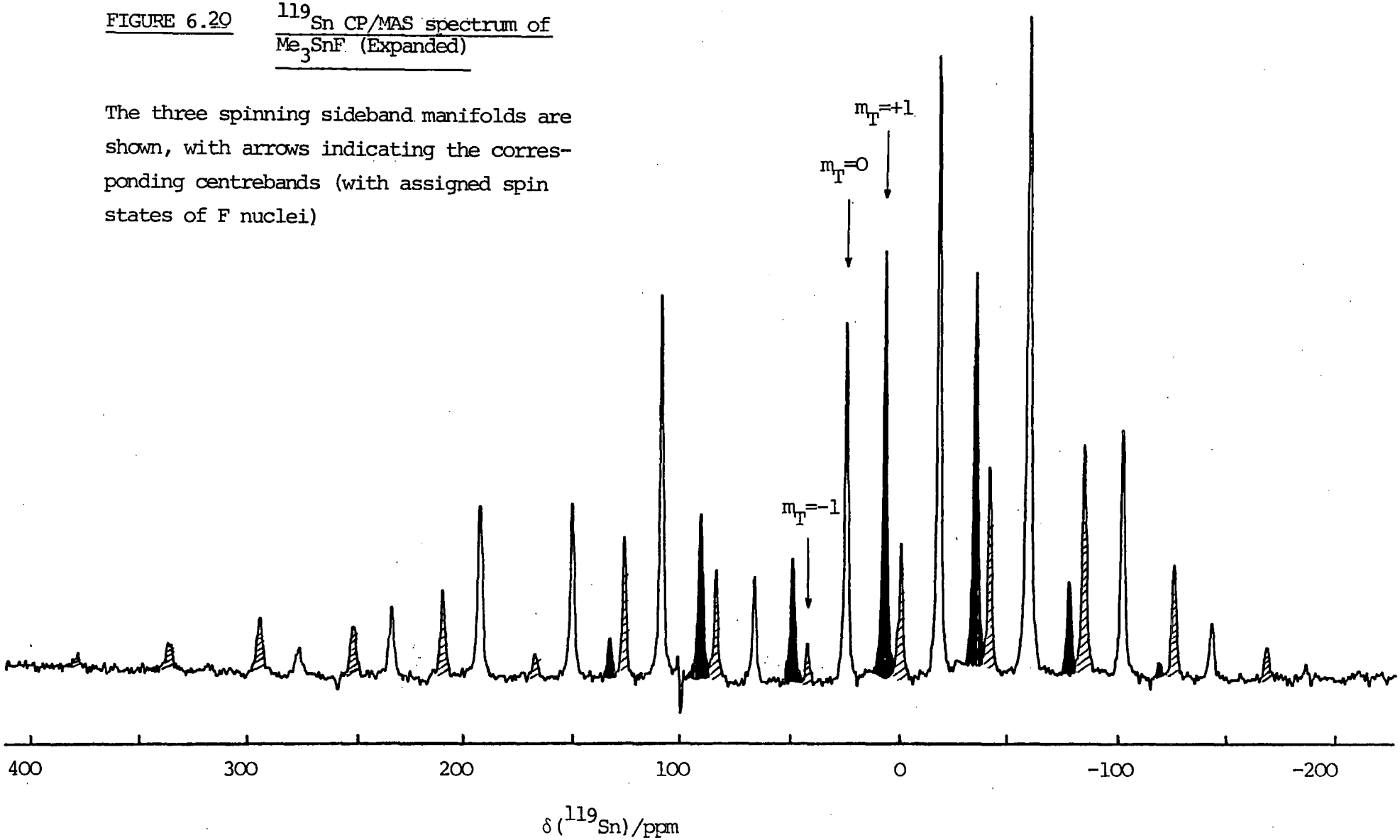

TABLE 6.4 ^{119}Sn SOLID-STATE NMR DATA FOR TRI(N-BUTYL)TIN FLUORIDE AND TRIMETHYLTIN FLUORIDE

	σ_{iso}[b]	σ_{33}	σ_{22}	σ_{11}	δ	η	$\lvert^1J_{Sn,F}\rvert$[b,c]
	←——————————ppm——————————→						
nBu_3SnF	9.3	-198	69	157	-207	0.42	1291
Me_3SnF	-23.5	-236	31	134	-212	0.48	1300

a. The shielding values are measured in ppm relative to $SnMe_4$.

b. Digitization rate 9 Hz/pt.

c. Measured in Hz.

The similarity in the solid-state structures of nBu_3SnF and Me_3SnF is shown by the almost identical values of $|^1J_{Sn,F}|$ and also the very similar values of shielding anisotropy (δ) and asymmetry (η), (Table 6.4). This indicates that the geometry and electronic environment of the two compounds are very much the same. The difference in isotropic shielding is caused by the influence of the alkyl groups attached to the tin atom, causing a uniform shielding through the molecule as can be seen by examination of the individual tensor components.

The ^{119}Sn NMR spectrum can be analysed further to supply information regarding the molecular geometry and also the direct and indirect spin-spin coupling between the ^{119}Sn and ^{19}F nuclei. The ^{119}Sn shielding tensor components (Table 6.4) clearly show that there is non-axial symmetry present which may arise either from intra-chain conformation or inter-chain interactions. As mentioned previously, given the presence of a triplet pattern the spectrum may be analysed as an AX_2 spectrum. The fluorines (as far as the ^{119}Sn

nuclei are concerned) must then be equivalent, therefore it is reasonable to assume that the Sn-F chain could be linear (as 'seen' on the N.M.R. timescale) with only one Sn-F dipolar axis present.

The relevant NMR parameters may be obtained from the following equations for an AX_2 system with a non-axial shielding tensor (see Chapter Two for details).

$$2\nu_{33} = T_3^+ + T_3^- \qquad \text{(eqn. 6.4)}$$

$$2\nu_B = (T_1^- + T_2^-) + (T_1^+ + T_2^+) \qquad \text{(eqn. 6.5)}$$

$$2D' = T_3^+ - T_3^- - 2J = (T_1^- + T_2^-) - (T_1^+ + T_2^+) + 4J \qquad \text{(eqn. 6.6)}$$

$$\alpha^+ = T_1^+ - T_2^+ \qquad \text{(eqn. 6.7)}$$

$$\alpha^- = T_1^- - T_2^- \qquad \text{(eqn. 6.8)}$$

$$(\alpha^+)^2 + (\alpha^-)^2 = 2\nu_A^2 + 18(D')^2 \qquad \text{(eqn. 6.9)}$$

$$(\alpha^+)^2 - (\alpha^-)^2 = 12\nu_A D \quad (2\cos^2\phi - 1) \qquad \text{(eqn. 6.10)}$$

where

$$\nu_B = \nu_{22} + \nu_{11} \qquad \text{(eqn. 6.11)}$$

$$\nu_A = \nu_{22} - \nu_{11} \qquad \text{(eqn. 6.12)}$$

$$D' = D - (J_{/\!/} - J_\perp)/3 \qquad \text{(eqn. 6.13)}$$

As there is no knowledge concerning the direction of the shielding tensors with respect to the molecule, assignments of T_{ii} can only be made arbitrarily. Therefore, all different assignments of T_{ii}, from the values obtained by sideband analysis, were tried. The values shown below (Table 6.5) were the only set found to give a reasonable result. Most combinations produced a negative value of ν_A^2 (equation 6.9), and the remainder gave unlikely results for ν_A.

TABLE 6.5 EXTREMA CALCULATED FROM MARICQ AND WAUGH SIDEBAND ANALYSIS[21]

"Stretched" subspectrum	"Squeezed" subspectrum
$T_3^+ = -176$ppm	$T_3^- = -83$ ppm.
$T_2^+ = -45$ppm	$T_2^- = -22$ ppm.
$T_1^+ = 344$ppm	$T_1^- = 122$ ppm.

Substituting the above values into equations (6.5)-(6.10) gives the following:

$\nu_{33} = -129$ppm,	$\nu_B = +200$ppm
$J = 17.5$ppm (1306Hz)	$D' = -64.25$ppm (-4795Hz)
$\alpha^+ = 399$ppm	$\alpha^- = 144$ppm
$\nu_A = \pm 230$ppm	$\nu_A = +230$ppm, $\phi = 70.67^\circ$
	$\nu_A = -230$ppm, $\phi = 19.34^\circ$

However, the assignment of the "minus" and "plus" subspectrum is not necessarily correct. By swapping signs, all values stay constant apart from D′ and J which are reversed in sign. The Sn-F dipolar coupling constant (D) has a negative value ($\gamma_{^{119}Sn}$ is-ve) and the magnitude and sign of ΔJ is unknown for such a system and so the sign of D′ cannot be assumed. However, this ambiguity can be solved by referring to the conditions concerning the order of T_{ii} (*c f.*, Chapter Two), The values in Table 6.5 show that the order is $T_1^+ > T_2^+ > T_3^+$ and $T_1^- > T_2^- > T_3^-$. This order is preserved at the limits $\phi = 0^\circ$ and 90° if $-\nu_A > |3D'|$ and also that (a) $\nu_{11} - \nu_{33} > 3D'$ and (b) that $\nu_{22} - \nu_{33} > 3D'$ (*N.B.* providing $\nu_{11} \geq \nu_{22} \geq \nu_{33}$ - which is shown to be true, see Table 6.6). Condition (a) is found to be true regardless of the sign of D′, but condition (b) can only be true if D′ is negative.

From this conclusion the absolute sign of J can be determined. In addition, from X-ray diffraction results D can be calculated and hence the anisotropy of $\underline{\underline{J}}$ is easily deduced.

$$D' = -4795\text{Hz}, \quad J = +1305\text{Hz}$$

$$D' = D - \Delta J/3.$$

r_{Sn-F} (Average value taken)[46] = 2.30Å $\quad D_{Sn,F} = -3481\text{Hz}.$

$\Delta J = 3933\text{Hz}, \quad J_{//} = 3057\text{Hz}, \quad J_{\perp} = -876\text{Hz}$

TABLE 6.6 COMPARISON OF EXPERIMENTAL VALUES AND THEORETICAL VALUES FOR Sn-F INTERACTION IN Me_3SnF

	Theory[a,b]	Experimental[a,c]	Error[a]
ν_{11}[d]	+215	235.5	20.5
ν_{22}[d]	-15	-31.4	-16.4
ν_{33}[d]	-129	-133.6	-4.6
ν_{iso}[d]	+23.7	+23.5	-0.2
ν_A	-230	-266.9	-36.9
ν_B	+200	204.1	4.1
J_{iso}[e]	+1306	1300	6

a. Values in ppm.

b. As calculated from equations (6.4) to (6.10) using sideband analysis of +/- subspectra.

c. As calculated/observed for the isotropic centrebands and middle sideband manifold.

d. As defined using resonance scale such that $\nu_{ii} = -\sigma_{ii}$, $(\nu_{iso} \equiv \delta_{iso})$.

e. In Hz

The assignments of ν_{ii} correspond to the original equations of Zilm and Grant[47] and are therefore different to those defined earlier by the Haeberlen convention.[49]

FIGURE 6.21 Direction and magnitude of NMR parameters obtained from AX_2 theory for Trimethyltin fluoride (see Table 6.6)

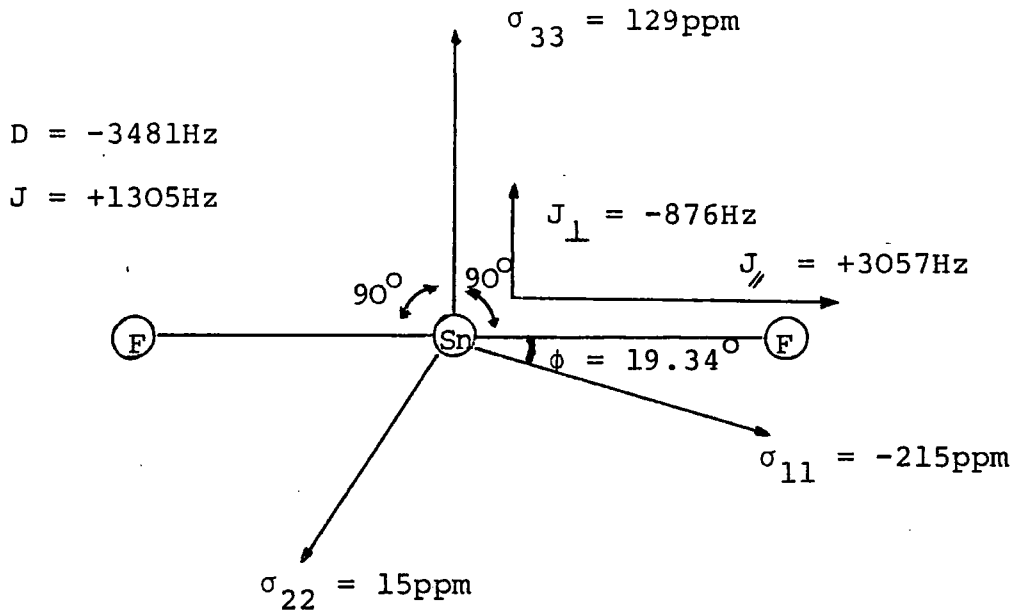

The results in Table 6.6 show that whilst the discrepancy between theory and experiment is small for ν_{33} and the isotropic NMR parameters it is quite large for ν_{11} and ν_{22}. In particular it should be noted that there is a much greater error for ν_A than ν_B. The reason for this is most likely due to the assumption of axial symmetry for $\underline{\underline{J}}$. The value of ν_A is obtained *via* equation (6.9), and thus relies on an accurate value for the effective dipolar coupling constant D'. This, in turn, depends on the asymmetry in $\underline{\underline{J}}$ (η_J) having a value of zero, which is not necessarily correct given that the system does not simply involve σ-bonding but also involves π-bonding *via* overlap of d-orbitals.[46] The other assumption which does not have a firm basis is the assignment of a shielding component perpendicular to the Sn-F axis, (see Figure 6.21).

On a purely qualitative basis, the analysis has illustrated the effects of tensorial interplay in a heteronuclear spin-½ system. The theory would perhaps be more applicable to a simpler system (*i.e.* an AX_2 system in matrix isolation) as it should be recalled that Me_3SnF is a complex polymeric network of Sn-F chains, and so intermolecular interactions will play some role as well as other complexities. Obviously, interpretation of the Me_3SnF results on a non-linear AX_2 basis is also possible, but it would need development of theory, and there is no *a priori* reason to believe such an approach would be more valid.

REFERENCES (Chap. 6)

1. "Handbook of Chemistry and Physics", 64th Edn., CRC Press (1983-4).

2. J.D. Kennedy and W. McFarlane in "NMR and the Periodic Table", Chapt.10, Academic Press, 1978.

3. P.J. Smith and A.P. Tupčiauskas, Ann.Rep.NMR Spectrosc., 1978, (8).

4. E.T. Lippmaa, M.A. Alla, T.J. Pehk and G. Engelhardt, J.Am.Chem.Soc., 1978 (100), 1929.

5. J.A. Zubieta and J.J. Zuckermann, in "Structural Tin Chemistry", Prog.Inor.Chem., (24), 251, Ed. S.J. Lippard.

6. A.G. Davies, P.G. Harrison, J.D. Kennedy, T.N. Mitchell, R.J.Puddephatt and W.McFarlane, J.Chem.Soc. (C),1969, 1136.

7. W. McFarlane, J.C. Maire, and M. Delmas, J.C.S. Dalton 1972, 1862.

8. A.P. Tupciauskas, N.M. Sergeyev and Yu.A. Ustynyuk, Org.Mag. Res. (3), 1971, 655.

9. J.D. Kennedy, W. McFarlane, G.S. Pyne, P.L. Clarke and J.D. Wardell, J.C.S. Perkin (11), 1975, 1234.

10. P.C. Chieh and J. Trotter, J.Chem.Soc. (A), 1970, 911.

11. J.D. Kennedy and W. McFarlane, J.Organomet.Chem., 1975, (94), 7.

12. E.V. van der Berghe and G.P. van der Kelen, J.Mol.Struct., 1974 (20), 147.

13. R. Okawara and K. Yasuda, J.Organomet.Chem., 1964 (1), 356.

14. N. Kasai, K. Yasuda, R. Okawara, J.Organomet.Chem., 1965, (3), 172.

15. W.P. Neumann, "The Organic Chemistry of Tin", J.Wiley,1970.

16. M.B. Houssain, J.L. Lefferts, K.C. Molloy, D. van der Helm and J.J. Zuckermann, Inorg.Chim.Acta., 1979,(36), L409.

17. J. Holecek, M. Nadvornik, K. Handlir and A. Lycka, J.Org.Met.Chem. 1983, (241), 177.

18. W. McFarlane and R.J. Wood, J.Organomet.Chem., 1974, (77), 189.

19. T.P. Lockhart and W.F. Manders (Submitted to J.Am.Chem.Soc.).

20. C. Glidewell and D.C. Liles, Acta.Cryst.1978 (B34), 129.

21. M.M. Maricq and J.S. Waugh, J.Chem.Phys. 1979, (70), 3300.

22. N.T. Bokii, G.N. Zakharova, and Y.U.T. Struchkov, Z.H.Strukt.Khim. 1970, (11), 895.

23. J.R, Lyerla, Contemp.Top.Poly.Sci., 1979, (3), 149; W.W. Fleming, C.A. Fyfe, J.R. Lyerla, H. Vanni and C.S. Yannoni, Macromolecules, 1980, (13), 460.

24. N.W. Alcock and J.F. Sawyer, J.C.S. Dalton, 1977, 1090.

25. E.O. Schlemper and W.C. Hamilton, Inorg.Chem., 1966, (5), 995.

26. A.G. Davies, H.J. Milledge, D.C. Puxley and P.J. Smith, J.Chem.Soc.(A), 1970, 2862.

27. P.T. Greene and R.F. Bryan, J.Chem.Soc. (A), 1971, 2549.

28. J.A. Lerbscher and J. Trotter, Acta.Cryst.1976, (B32), 2671.

29. T.B. Brill, R.C. Gearhart, and W.A. Welsh, J.Mag.Res., 1974, (13), 27.

30. K.B. Dillon, A. Marshall, J.Chem.Soc. Dalton Trans, 1984, 1245.

31. El Kundla and M. Alla, Proc. XX Cong. Ampere, Tallinn (1978), p.92, Published 1979 (Springer-Verlag, Berlin), Eds., E.I. Kundla, E.T. Lippmaa and T. Saluvere.

32. C.J. Groombridge, R.K. Harris, K.J. Packer, B.J. Say and S.F. Tanner, J.Chem,Soc.Commun., 1980, 175.

33. A. Naito, S. Ganapathy and C.A. McDowell, J.Chem Phys., 1981 (4), 5393.

34. M.H. Frey and S.J. Opella, J.Chem.Soc.,Chem.Comm., 1980, (11), 474.

35. D.E. Woessner and J.C. Trewella, J.Mag.Res., 1984, (59),352.

36. E.M. Menger and W.S. Veeman, J.Mag.Res., 1982 (46), 257.

37. G.E. Galimann, C.J. Groombridge, R.K. Harris, K.J. Packer, B.J. Say and S.F. Tanner, Phil.Trans.R.Soc.Lond.A. 1981, (299), 643.

38. R.J. Brown, B.K. Hunter, M. Mackowiak and J. Segel, J.Mag.Res., 1982 (50), 218.

39. H.W. Spiess, U. Haeberlen and H. Zimmermann, J.Mag.Res., 1977, (25), 55.

40. R.K. Harris, "Nuclear Magnetic Resonance", Pitman, 1983.

41. P.J. Green and J.D. Graybeal, J.Am.Chem.Soc., 1967 (89),4305.

42. P.A. Cusack, P.J. Smith, J.D. Donaldson and S.M. Grimes, "A Bibliography of X-ray Crystal Structures of Tin Compounds" (International Tin Research Institute, London),Publication No. 588.

43. E.A. Marseglia and I.D. Brown, Acta Cryst., 1973, (B29), 1352.

44. P.W. Dean and D.F. Evans, J.Chem.Soc.A, 1968, 1154. R.O. Ragsdale and B.B. Stewart, Proc.Chem.Soc.,1964, 194.

45. H.C. Clark, R.J. O'Brien and J. Trotter, J.Chem.Soc., 1964, 2232.

46. K. Yasuda, Y. Kawasaki, N. Kasai and T. Tanaka, Bull. Chem.Soc.Jap.1965, (38), 1216.

47. K.W. Zilm and D.M. Grant, J.Am.Chem.Soc., 1981 (103), 2913.

48. R.K. Harris, K.J. Packer and A.M. Thayer, J.Mag.Res., 1985 (62), 284.

49. U. Haeberlen, 'High Resolution NMR in Solids-Selective Averaging', Suppl.1, Adv.Mag.Res., 1976, Academic Press.

50. J.S. Waugh, NMR and Biochemistry, Eds., S.J. Opella & P.Lu, 1979.

51. E.R. Andrew, Int.Rev.Phys.Chem., 1981 (1), 195.

52. E.R. Andrew and L.F. Farnell, Mol.Phys., 1968, (15), 157.

ERRATUM

^{119}Sn NMR spectrum of Me_3SnOH (Chapter Six).

Further information recently received from Prof. Alwyn Davies (University College, London) reveals that the signal at -152 ppm is, in fact, due to an impurity (perhaps dimethyltin oxide or bis(trimethyltin) carbonate). Thus, there is only one genuine resonance due to Me_3SnOH at -99 ppm (and associated sideband manifold) which correlates with the findings for triphenyl tin hydroxide).